Fixed-Point Implementation of a Multistage Receiver

Rick A. Cameron

Dissertation submitted to the Faculty of the Virginia Polytechnic Institute and State University in partial fulfillment of the requirements for the degree of

Doctor of Philosophy
in
Electrical Engineering

Brian Woerner, Chair
John Kobza
Theodore Rappaport
Jeffrey H. Reed
Hugh VanLandingham

Jan. 13, 1997
Blacksburg, Virginia

Keywords: CDMA, Interference Cancellation, Synchronization, Quantization

Fixed-Point Implementation of a Multistage Receiver

Rick A. Cameron

(ABSTRACT)

This dissertation provides a study of synchronization and quantization issues in implementing a multistage receiver in fixed-point Digital Signal Processing (DSP) hardware. Current multistage receiver analysis has neglected the effects of synchronization and quantization; however, these effects can degrade system performance and therefore decrease overall system capacity.

The first objective is to analyze and simulate various effects of synchronization in a multistage system. These effects include the effect of unsynchronized users on the bit error rate (BER) of synchronized users, and determining whether interference cancellation can be used to improve the synchronization time. This information is used to determine whether synchronization will limit overall system capacity. Both analytical and simulation techniques are presented.

The second objective is to study the effects of quantization on the performance of the multistage receiver. A DSP implementation of a practical receiver will require a DSP chip with a fewer number of bits than the computer chips typically used in simulation of receiver performance. Therefore, the DSP implementation performs poorer than the simulation results predict. In addition, a fixed-point implementation is often favored over a floating-point implementation, due to the high processing requirements necessitated by the high chip rate. This further degrades performance because of the limited dynamic range available with fixed-point arithmetic. The performance of the receiver using a fixed-point implementation is analyzed and simulated.

We also relate these topics to other important issues in the hardware implementation of multistage receivers, including the effects of frequency offsets at the receiver and developing a multiuser air protocol interface (API). This dissertation represents a contribution to the ongoing hardware development effort in multistage receivers at Virginia Tech.

This work was supported by the Defense Advanced Research Projects Agency (DARPA) and the MPRG Industrial Affiliates Foundation.

Acknowledgments

First and foremost, I would like to thank Linda Maddux for her friendship, support, and endless patience and understanding as I have pursued my graduate degrees.

I owe a special thanks to my advisor, Dr. Brian Woerner, for his guidance and support throughout my graduate career. I would also like to thank my committee, Dr. John Kobza, Dr. Theodore Rappaport, Dr. Jeffrey Reed, and Dr. Hugh VanLandingham for their insights and comments during my research.

I would like to thank the sponsors of my research, DARPA and the MPRG Industrial Affiliates, for providing the equipment and support that enabled me to pursue my research.

In my many years at Virginia Tech and specifically in MPRG, I have made countless friends with the students and staff and owe them all a great deal of thanks. I would like to specifically thank all of the GloMo team for their work and support on this current project. A special thanks is owed to former MPRG'ers Prab Koushik, Yingjie Li, Bhushan Rele, Cho-Kei Sou, Graham Stead, Stavros Striglis, and Thuy Tran for their special friendship. I would like to thank Fred Bailey, Andrew Hansbrough, Andrew Predoehl, and Mark Rustin for their friendship and support over the past several years.

Finally, I would also like to thank my family who have been a constant source of encouragement and support.

Contents

List of Figures

List of Tables

Chapter 1

Introduction

A Code Division Multiple Access (CDMA) cellular system has been proposed for use as a next-generation cellular telephone system [1]. The underlying goal is to improve overall system capacity while achieving additional benefits of digital systems such as improved privacy and error correction. One of the main drawbacks to CDMA is that traditional receivers such as the correlation and Rake receivers are susceptible to the near-far problem, which occurs when one received signal is much stronger than another. Tight power control algorithms have been proposed in an attempt to overcome this problem, but even these techniques are still vulnerable [2, 3].

A great deal of research has focused on developing receiver structures that are near-far resistant. The various approaches can be divided into two general classes: single user receivers and multiuser receivers. In receivers where only a single user is demodulated (such as a mobile receiver in a cellular system), techniques based on adaptive filtering [4] can be used to combat interference and the near-far problem.

In a multiuser receiver, all of the desired users are demodulated at the same location such as the base station in a cellular system. A multiuser receiver can use all of the information about the received signals from all users to combat interference and the near-far problem. In [5], an optimum multiuser receiver for the Additive White Gaussian Noise (AWGN) channel was proposed that is ideally near-far resistant (a near-far resistance of unity). The optimum receiver structure is hopelessly complex [6], precluding the possibility of a physical implementation; however, this work did show the performance improvement which is possible with a multiuser receiver structure and spawned a considerable amount of research aimed at finding sub-optimal approaches that would retain much of the performance improvement possible with the optimum receiver, but at a greatly reduced complexity.

Two classes of sub-optimal multiuser receivers that have received a great deal of research

interest are decorrelators and interference cancellers. The decorrelators [7, 8, 9] are based upon multiplying the vector of received decision variables by the inverse of the matrix of code sequence cross-correlations, thus removing the effect of the interfering users. The interference cancellers can cancel interference either successively [10] or in parallel using multiple stages [11, 12, 13]. Other approaches exist, including hybrid approaches [14] and modifications to the receivers mentioned above [15, 16, 17]. A multistage receiver has been chosen for this work, in part because the design can be implemented in hardware due to its relatively low computational requirements and the inherent simplicity of the computational algorithms [18].

This thesis discusses research into issues that must be addressed when implementing a multistage receiver in Digital Signal Processing (DSP) hardware. A baseband multistage receiver prototype using a DSP testbed is being developed in support of an ongoing project at Virginia Tech[1]. There are two key issues that must be addressed for the physical implementation that have not been addressed in existing research: synchronization and quantization. The effects of synchronization and quantization have not been adequately addressed to date. Practical effects such as synchronization and quantization will diminish the ability of the receiver to cancel interference and thus determining the actual level of degradation is of great interest when building a receiver. In this thesis, we attempt to address these issues, as well as several other significant implementation issues.

1.1 Outline of Dissertation

There is a brief review of CDMA principles in Chapter 2. Chapter 3 provides a review of multiuser receivers. Research into multistage receivers has concentrated on analytical techniques to determine the theoretical performance of these receiver architectures. Performance was first addressed in [11, 14] and closed-form BER expressions are given in [19]. Multipath channels are addressed in [12, 20] and selective cancelation is addressed in [13, 19]. The effect of phase and timing errors has been addressed in [21].

Chapter 4 reviews spread spectrum synchronization techniques. Chapter 5 studies the synchronization process in a multistage receiver. Existing research assumes that synchronization can be achieved and that there is no unsynchronized interference. Because interferers cannot be canceled before synchronization is attained, this interference is likely to dominate the overall system interference and thus diminish the theoretical performance increase provided by the receiver. The effect of unsynchronized users on the BER of synchronized users is analyzed using an improved Gaussian approximation for all multiple access interference (MAI). The effect of the power level of the unsynchronized user is also studied,

[1] the DARPA sponsored Glomo project, formerly known as the Wamis project

as the extent to which this interference becomes dominant is related to the interfering power levels. The mean and variance of acquisition time are also studied using an improved Gaussian approximation for MAI. The multistage architecture can be used in the synchronization process, since the residual signals will be less noisy than the initial received signal. There is an associated delay with each stage, however, so the improvement must be enough to offset the increased delay. The improvement in acquisition time related to increasing the power in the unsynchronized user's signal is also studied. These issues have been studied both through analysis and simulation. A multistage receiver model has been constructed in SPW, a block diagram simulator that is based upon hardware modeling. Modeling the receiver in this fashion eases the transition to an actual hardware model. In addition, this model is digital so functions such as correlation must be done discretely and not continuously as is often done in analysis.

Chapter 6 reviews quantization analysis techniques. Chapter 7 examines the performance degradation in the multistage receiver due to quantization in a fixed-point implementation. Quantization analysis has historically proceeded along two fronts, examining the quantization deterministically and modeling the quantizer stochastically as a noise source. Although the quantizer is a deterministic process, it is a nonlinear process and difficult to analyze. Therefore, the stochastic approach is the most common. Uniform quantization noise sources are often modeled as uncorrelated uniform noise sources, and an analytic model is developed using the improved Gaussian approximation based on this assumption. While the individual quantization sources can be accurately modeled with a uniform distribution, the various noise sources are not necessarily uncorrelated. Furthermore, the uniform model can cause errors in the decision statistic that would not occur if the quantization was modeled deterministically. The overall analytic results are optimistic when compared to the simulation results. A semi-analytic technique is proposed which improves on the accuracy of the analytic model but without requiring all of the long simulation runs of the simulation model. It is shown that the multistage receiver performs well in a fixed-point implementation, assuming that the input signal has a constrained dynamic range (as would occur if power control is used).

Chapter 8 discusses the framework of the hardware development effort. System specifications and computational complexity are discussed, as well as hardware issues. The effects of frequency offsets in the oscillators of each user's transmitter are also discussed, along with a maximum likelihood phase estimator that attempts to track the frequency offsets and random phase. Since each mobile will have a different transmitting oscillator with some tolerance, the actual modulation frequency may be slightly different from those of the other users. We desire to use a single RF front-end at the multistage receiver, so the effects of frequency offsets must be accounted for. A simulation model is developed which accounts for these offsets. Chapter 9 summarizes and concludes this report.

Chapter 2

CDMA Principles

2.1 Introduction

The past decade has seen great interest in using Code Division Multiple Access (CDMA) systems for wireless systems. In [1], a CDMA system was proposed for use as the next-generation cellular telephone system. CDMA systems are also being proposed for PCS and many other wireless services [22, 23]. A key benefit of CDMA technology over more traditional multiple access techniques is the increase in total system capacity. Additional benefits include low probability of signal detection, protection against hostile and unintentional jamming, resistance to multipath fading, and graceful performance degradation in the presence of multiple access interference. Rake receivers can be used to exploit the information in multipath signals if the relative time delay of the multipath components is great enough.

There are two major spread-spectrum techniques for achieving CDMA, known as direct-sequence and frequency hopping [1, 24, 25, 26, 27, 28, 29, 30, 31, 32]. The commercial CDMA technique used in the IS-95 standard [33] is based on direct-sequence spread spectrum. In this dissertation, we will focus exclusively on the direct-sequence technique.

2.2 CDMA Characteristics

In CDMA, each user is assigned a unique pseudonoise (PN) code, a signature sequence, that is used to distinguish that user's transmission from all other users. Pseudonoise implies that the receiver knows the PN code of the desired user, but to all other users the signal will appear to be a random sequence of bits. To distinguish the bits in the PN code from the

bits of the data signal, the PN code bits are called chips. The PN code has a data rate that is much higher than the data signal. The bit and chip durations are T and T_c, respectively. The processing gain N is given by the ratio $N = T/T_c$. A simple block diagram of a binary phase shift keyed (BPSK) CDMA transmitter and correlation receiver are given in Fig. 2.1. We will denote the desired user as user 1 and assume that there are no time or phase delays for this particular user. At the transmitter, the information signal $b_1(t)$ is multiplied by the PN code $a_1(t)$. By multiplying the two signals together, the result is spread over a wide bandwidth. The result is modulated by multiplication with $\sqrt{2P}cos(\omega_c t)$, where P is the transmitted power and ω_c is the carrier frequency. The resulting transmitted signal $s_1(t)$ for user 1 is given by

$$s_1(t) = \sqrt{2P}b_1(t)a_1(t)\cos(\omega_c t) \tag{2.1}$$

All users transmit over the same frequency band and at the same time, so that the received signal $r(t)$ is given by

$$r(t) = n(t) + \sum_{k=1}^{K} s_k(t - \tau_k), \tag{2.2}$$

where $n(t)$ is noise added by the channel, k is the user index, there are K active transmitters, and τ_k is the time delay of each user k. A correlation receiver then multiplies the received signal $r(t)$ by a locally generated PN code replica $a_1(t)$, which despreads the desired signal and leaves interfering signals as wideband noise. The result is then demodulated and integrated over the bit period T, which gives the decision statistic Z,

$$Z = \int_0^T r(t)a_1(t)\cos(\omega_c t)dt \tag{2.3}$$

The bit estimate is made from the decision statistic; if Z is greater than 1, the bit estimate is a 1; otherwise, the estimate is a 0.

Many of the benefits of CDMA are derived from the properties of the PN codes. The code should have low auto-correlation values when the codes are not aligned, both to aid in synchronization and to reduce the correlation with multipath components. The code should have low cross-correlation with the other codes used in the system, to reduce the effects of the multiple access interference (MAI) [34].

Consider, for purposes of illustration, that we wish to send the bit sequence {1, 0, 0, 1} using BPSK, $N = 10$, and the PN code is {1, 1, 0, 1, 0, 1, 1, 0, 1, 0} which repeats at the bit rate. In BPSK, a 1 is transmitted with amplitude +1 and a 0 is transmitted with amplitude -1. The data waveform $b(t)$ is shown in Fig. 2.2a. The spreading signal $a(t)$ is shown in Fig. 2.2b. The spread signal $c(t)$ is shown in Fig. 2.2c. Note that the signal to be transmitted now has the same data rate as the spreading signal, which in this case is 10 times higher than the original data rate.

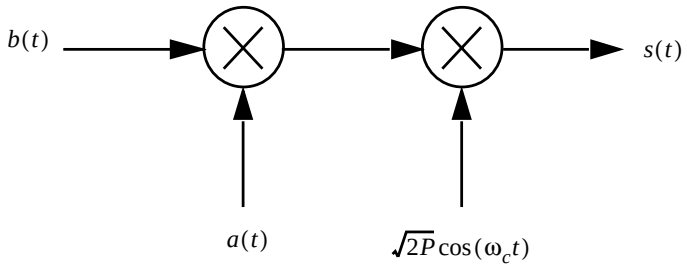

(a) CDMA Transmitter

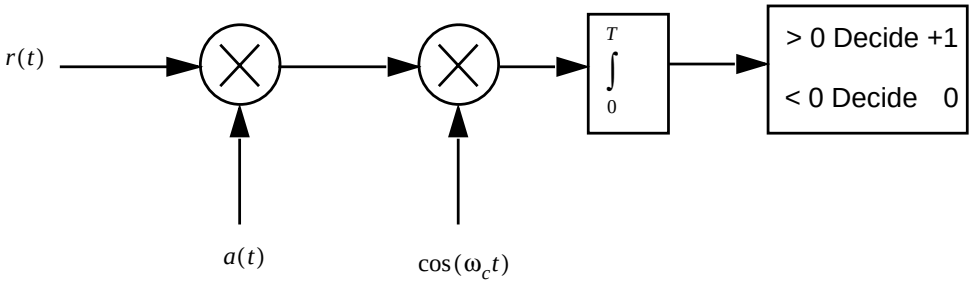

(b) Correlation Receiver

Figure 2.1: CDMA Transmitter and Correlation Receiver

Now assume that more than one user shares the communication channel. Assume that a second user simultaneously transmits a 1, and that user 2's PN code is given by {1, 0, 1, 0, 1, 0, 1, 0, 1, 0}. Finally, assume that we are trying to decode user 1's signal using a correlation receiver and that the channel is noiseless. The receiver will correlate the received signal with user 1's signature sequence over the bit period T, or over all 10 chips. The discrete correlation between the two sequences is given by summing the results of multiplying the individual chip values. The correlation with the part of the received signal due to user 1 is 10, since each multiplication will result in +1 and 10 multiplications are being summed. The discrete correlation with the desired component will always be given by N if a 1 is transmitted and by $-N$ if a 0 is transmitted. The correlation with the received signal of user 2 is 0. Therefore the total decision statistic Z is given by $Z = 0 + 10$. In this case, since $Z > 0$, we correctly decide that a 1 was sent. In this simple example, the sequences were orthogonal since user 2 did not add any multiple access interference. In practice, this is often not possible for asynchronous systems.

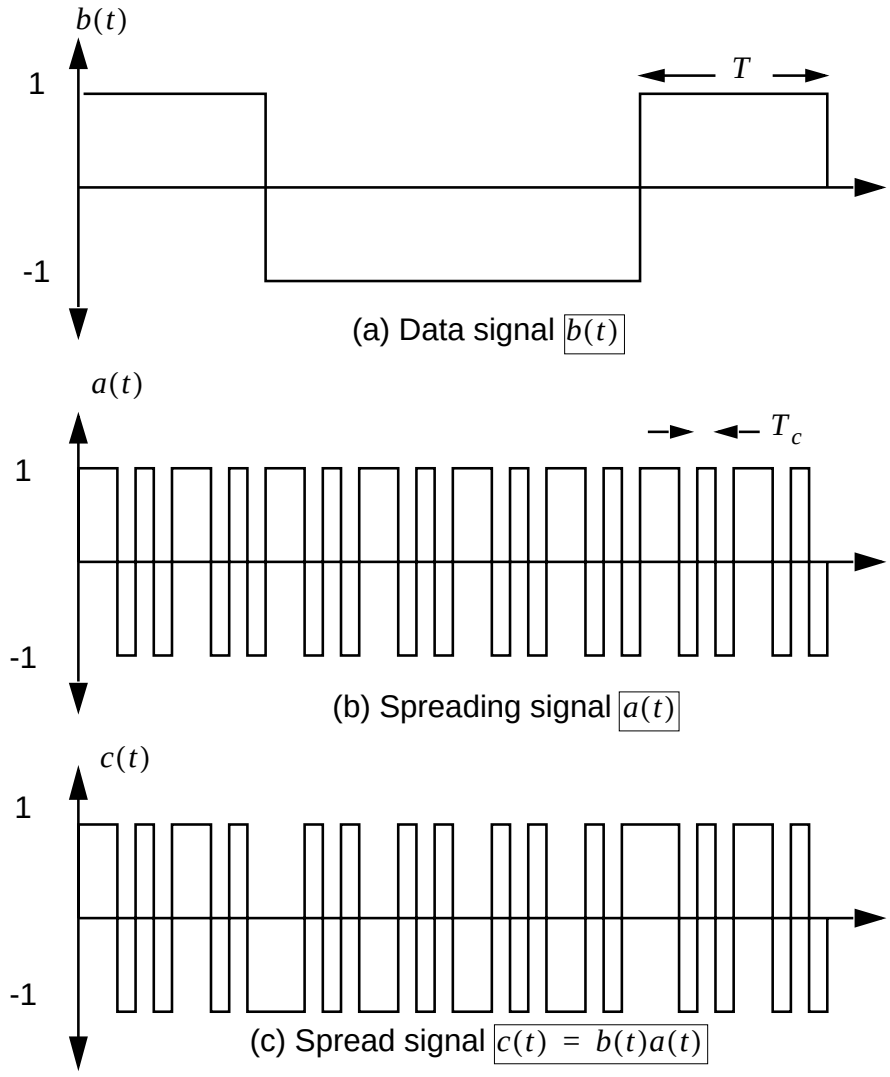

Figure 2.2: Spreading Example

Table 2.1: Capacity Loss for $E_b/N_o = 12$ dB and $BER = 10^{-3}$

σ^2 (dB)	Worst Case		Best Case	
	K_{max}	Capacity Loss (%)	K_{max}	Capacity Loss (%)
0	25	-	30	-
1	21	16	27	10
2	17	32	22	27
4	11	56	13	57

2.3 Power Control

A key requirement of the capacity improvement possible with CDMA systems, if conventional correlation receivers are used, is that the received signals of all users should have identical power levels. Disparate power levels can give rise to the near/far problem, as shown in Fig. 2.3. On the reverse channel, the increased distance of mobile 1 from the base station will cause the received signal to have a lower power than the signal from mobile 2. While mobile 2 can be received properly, the large amount of interference from mobile 2 can overcome the processing gain and cause the BER of mobile 1 to increase significantly. Other factors such as shadowing and multipath fading can cause the received power levels to vary dramatically, so power control algorithms have been proposed that attempt to adjust the transmitted power levels so that all signals are received at the same level [1, 32, 35]. An example of ideal power control is shown in Fig. 2.4, where the transmitted power is adjusted to match any fading in the channel. This cannot be done perfectly in practice, however, and even systems employing tight power control can suffer a significant capacity loss over the ideal case. Upper and lower bounds on the probability of error for systems employing imperfect power control are given in [2, 36]. A summary of the capacity loss is given in Table 2.1 based on the upper and lower bounds on the BER, where E_b/N_o is the signal-to-noise ratio of the desired user, σ^2 is the variance of the received power levels, and K_{max} is the capacity for a BER of 10^{-3}. The upper bound on the potential capacity loss from the case of ideal power control is shown in Fig. 2.5 for received power variances of 1, 2 and 4 dB if the desired user has $E_b/N_o = 12$ dB. Practical CDMA power control algorithms have been shown in field trials to have a variance of 1 to 2 dB [32]. Since capacity increase is one of the reasons for using a CDMA system, this suggests that alternate receiver structures will be required to achieve high capacity levels.

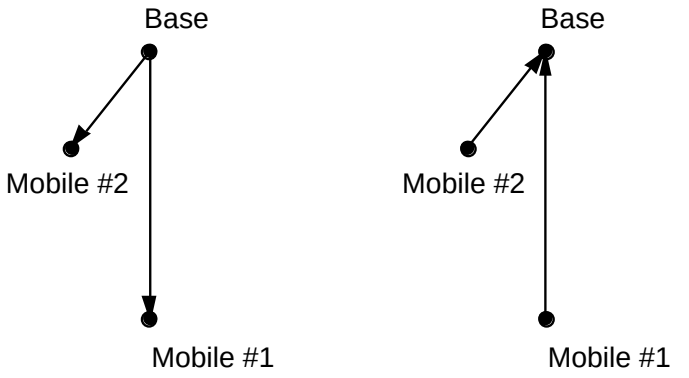

Figure 2.3: Near Far Problem

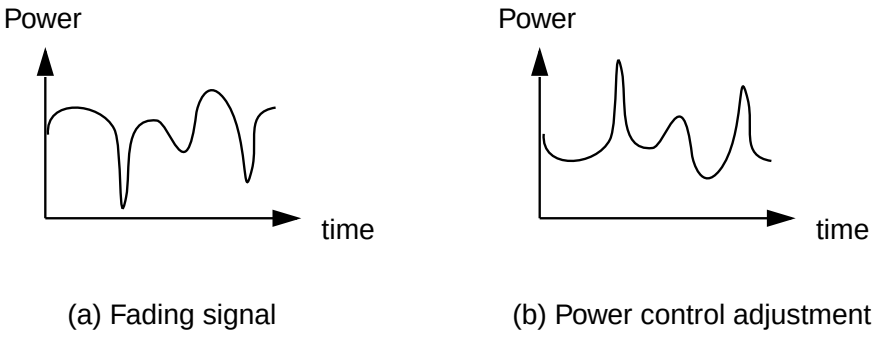

Figure 2.4: Perfect Power Control

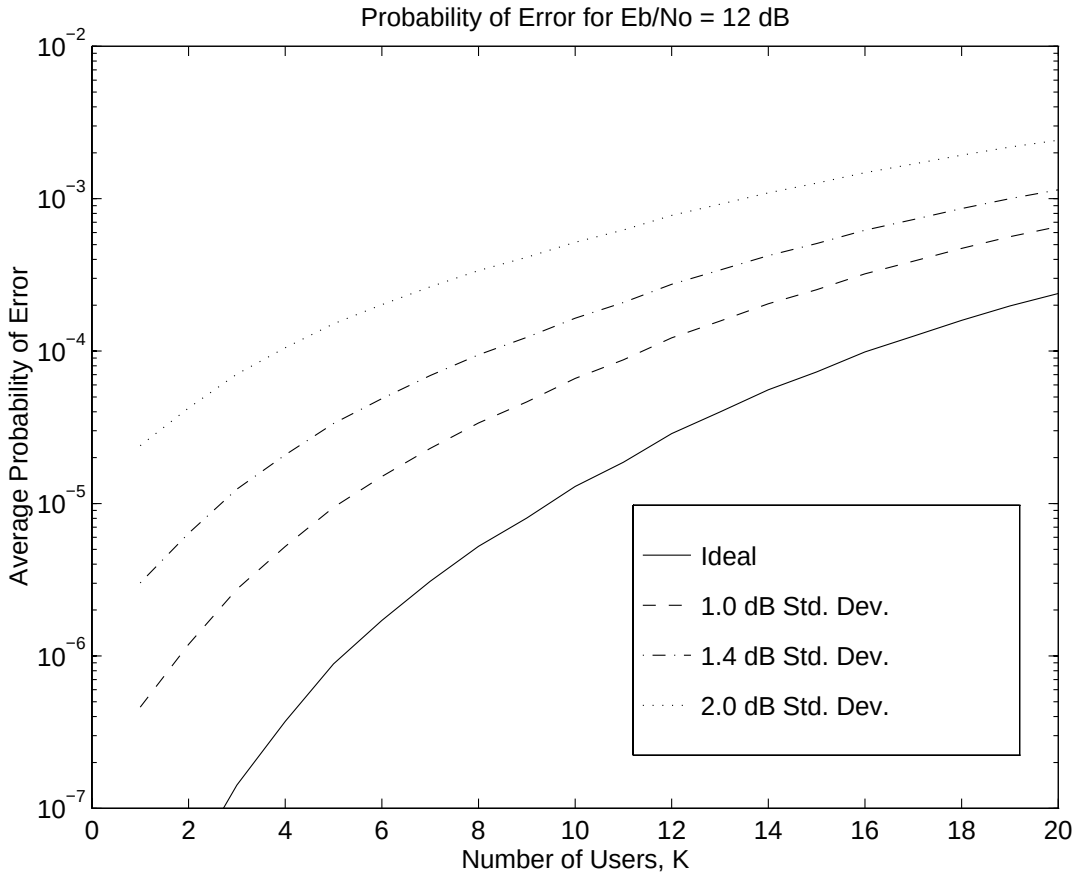

Figure 2.5: BER vs. System Capacity K, $E_b/N_o = 12$ dB

2.4 Rake Receivers

A Rake receiver weights the decision statistics of a bank of correlation receivers (fingers), each of which is matched to a multipath component of the desired user's signal [37]. A block diagram of a Rake receiver is shown in Fig. 2.6. Maximal ratio combining is typically used, which maximizes the signal-to-noise ratio (SNR) of the overall decision statistic Z. This can be closely approximated by weighting the decision statistic from finger m, Z_m, in direct proportion to its magnitude. For an M finger Rake receiver, maximal ratio combining can be achieved by computing Z using

$$Z = \sum_{m=1}^{M} |Z_m| Z_m. \tag{2.4}$$

The bit estimate is made from the overall decision statistic. In so doing, the Rake can combat multipath fading if the multipath components can be coherently resolved and thus used in the decision process. Analytic results [38, 36] show that the Rake receiver can significantly improve performance in a multipath environment, although the greatest improvement comes as E_b/N_o rises. In a low E_b/N_o environment, noise dominates the system performance and the large amount of noise in each Z_m will lead to a large amount of noise in Z. The analysis uses a channel based on measurement data, and an example of the performance improvement possible with a Rake receiver is shown in Fig. 2.7 for a particular Rayleigh fading environment. The Rake structure performed at least as well as the correlation receivers for all values of E_b/N_o. The Rake receiver is useful for combating multipath interference, but cannot combat Gaussian noise or multiple access interference.

2.5 Other Benefits and Implications of CDMA

Although high system capacity is one of the reasons that CDMA has become attractive for commercial systems, there are additional benefits provided by CDMA systems. Some of these are most beneficial to cellular telephony, whereas others are applicable to CDMA systems in general. In a cellular telephone system, one desirable feature is the reduced reliance on frequency planning. Although out-of-cell interference will keep the same cell frequencies from being used in every cell, the cellular CDMA system is not nearly as dependent upon frequency planning as is the current analog system.

Another benefit for cellular systems is the use of a soft-handoff technique, where a mobile can be simultaneously tracked by two or more base stations when it is approaching a cell boundary. In the analog system, a handoff is accomplished via a "break-before-make" technique, where once it is determined that a mobile should be handed off to another cell, the original cell stops decoding the mobile and the new cell acquires it. This can lead to dropped calls or ping-ponging, in which the mobile is handed back and forth between two cell sites. In soft-handoff, a "make-before-break" technique is used, where both cell sites decode the mobile until the mobile is clearly being received more strongly by one of the cell sites.

Another benefit when using CDMA for cellular telephony is the use of the voice activity factor. Silence occupies a significant portion of the telephone call. In a CDMA system, if the silence is detected, the power in the transmitter can be reduced, which reduces the overall interference to the system and thus allows for a higher overall system capacity. While this technique can also be used in other multiple-access schemes provided that new channels can be allocated quickly enough, it can be readily accomplished in a CDMA system.

A benefit that is more applicable to military systems is the lower probability of detection,

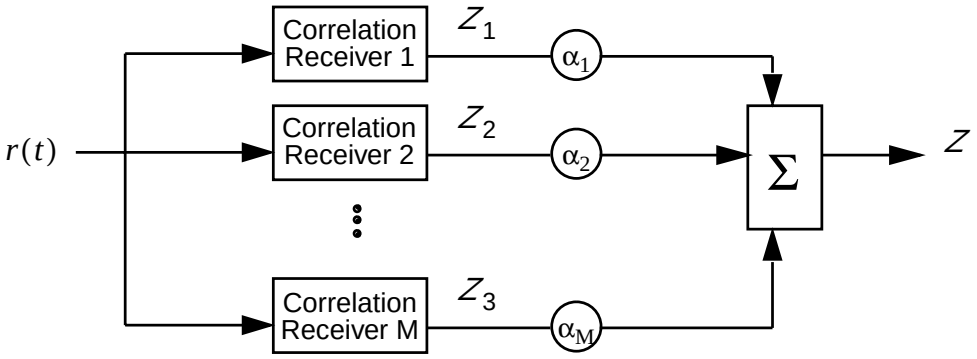

Figure 2.6: Rake Receiver Block Diagram

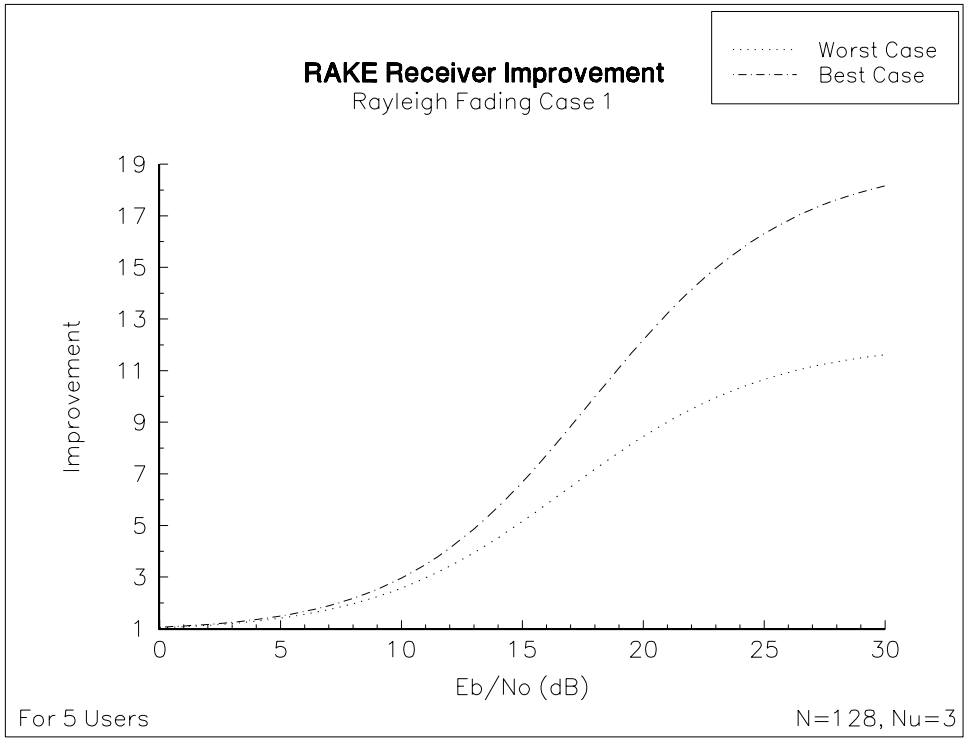

Figure 2.7: Rake Receiver Performance Improvement

since the low power, wide bandwidth signal is relatively more difficult to detect than a high power, narrow bandwidth signal. Another benefit is multipath performance. Even if a Rake receiver is not used, the low auto-correlation achieved when the PN codes are not aligned implies that multipath signals that are separated by more than 1 chip will not be coherently combined, and thus this form of fading can be reduced. In the unlicensed frequency bands, using a CDMA system can provide some protection against narrowband interferers. For most civilian systems, the interferers are not intentional but authorized users in the unlicensed bands (microwave links are one example of such an interferer).

Finally, the use of CDMA provides an inherent degree of security or privacy to the transmitted signal. In order to decode a CDMA signal, the receiver must know the PN code. Since these codes are chosen from a large set of possible codes, it would be difficult to simply 'guess' the appropriate PN code in an attempt to intercept a transmission. This degree of privacy is not on the same level of an encryption scheme, as the transmitted information is never encrypted and can be intercepted by anyone with knowledge of the PN codes being employed. It does discourage the casual eavesdropping that can occur with basic receiver designs in the current analog system.

2.6 Conclusions

CDMA systems can provide significant capacity improvements over more traditional multiple access schemes. However, if correlation receivers are used, this capacity improvement can be significantly degraded if all received power levels are not identical. While power control algorithms have been proposed to attempt to maintain identical power levels, this cannot be perfectly accomplished and thus there is a capacity drop. This suggests the need for alternative receiver structures to maximize the capacity in a practical CDMA system. Rake receivers can be employed to help combat multipath fading.

Chapter 3

Multiuser Receivers

3.1 Introduction

The vulnerability to the near-far problem is not inherent to all CDMA systems, but is dependent upon the receivers used, which has motivated the search for receiver structures that can maintain a system high capacity even in the presence of disparate received power levels. A popular approach for base station receivers is the multiuser receiver, which uses information about all received signals to improve performance.

This chapter first provides a survey of the proposed multiuser receiver structures to date. Since multiuser receivers require information about all (or many) of the received signals, they are inappropriate for scenarios where single-user receivers are required, such as on the forward link (base-to-mobile) of a cellular system. On the reverse link (mobile-to-base), the base station will be receiving all users within its cell, and therefore information from other users will be available when demodulating any particular user. This improved performance is especially important on this link, which is usually considered to be the harsher of the two links in a cellular environment. There are many reasons for this, including the limited power available at the mobile, the asynchronous nature of the transmissions (the spreading codes will not therefore be orthogonal), and since each user will be transmitting over a different channel, each received power level will be different.

3.2 Multiuser Receivers

The purpose of all multiuser receivers is to overcome the near-far problem and offer performance which approaches that of a single user system. The near-far resistance as defined in

[5, 9] is based on the asymptotic efficiency η_k, which is the limit as $\sigma \to 0$ of the ratio of the effective SNR to the actual SNR of a multiuser system (where σ is the standard deviation of the AWGN). The effective SNR is the SNR required by a single user system to achieve the same asymptotic BER as a multiuser system. The near-far resistance, then, is the minimum η_k considered over all possible interfering bit energies. The minimum allowable value of near-far resistance is zero, which implies that to achieve the BER of a single user system, the multiuser system would require an infinite SNR. The conventional correlation receiver has an efficiency of zero. The maximum allowable value of near-far resistance is one, which implies that the multiuser system is performing as well as the single user system (it cannot outperform the single user system, since completely removing all multiple access interference is equivalent to a single user system). Thus the optimum multiuser receiver will have a near-far resistance of one. A good summary of several multiuser receiver approaches is given in [39].

3.2.1 Optimum Receivers

Horwood and Gagliardi [40] analyzed a multiuser receiver for the case when all transmissions are synchronous and are passed through an encoder before transmission over the channel. An expression for the average BER was developed based on choosing an appropriate encoding function that minimizes the MAI. Van Etten [41] proposed a multiuser receiver using either a Viterbi or Ungerboeck decoding algorithm for asynchronous systems and some form of interchannel interference.

In [5], Verdú proposed an optimum multiuser receiver for asynchronous Gaussian multiple-access channels based on maximum-likelihood detection. The receiver is optimal in the sense that the performance in the absence of Gaussian noise approaches that of a single-user system. Using the near-far resistance definition given in [8], this yields a near-far resistance of one, the optimal value. In the traditional multiuser receiver, there is no interaction between the single-user receivers [5]. The optimum single-user receiver can be modeled as a bank of single-user matched filters, each of which is followed by a threshold detector. A block diagram of such a receiver is shown in Fig. 3.1, where $r(t)$ is the received signal, K is the total number of users, k is the user index and ranges from $1 \leq k \leq K$, Z_k is the decision statistic for user k, j is the bit index, and $\hat{b}_k(j)$ is the estimate of bit j for user k. Verdú's proposed receiver has a bank of single-user matched filters followed by a Viterbi decision algorithm, as shown in Fig. 3.2. Although the decision based on individual statistics may not be optimal, it is shown in [5] that the set of all decision statistics is a sufficient statistic for optimally estimating the set of data bits. In comparing the receiver structures, in can be seen that the optimal multiuser receiver is an extension of the traditional receiver. Using maximum-likelihood detection, the detector selects the

sequence that maximizes

$$P[\{r_t, t \in \Re\}|\mathbf{b}] = Cexp(\Omega(\mathbf{b})/2\sigma^2), \tag{3.1}$$

where r_t is the received signal, C is a positive scalar, $\Re$ is the set of real numbers, $\mathbf{b}$ is the vector of all K user's transmitted symbols, σ is the standard deviation of the noise, and $\Omega(\mathbf{b})$ is given by

$$\Omega(\mathbf{b}) = 2\int_{-\infty}^{\infty} S_t(\mathbf{b})dr_t - \int_{-\infty}^{\infty} S_t^2(\mathbf{b})dt. \tag{3.2}$$

The term $S_t(\mathbf{b})$ is given by

$$S_t(\mathbf{b}) = \sum_{i=-M}^{M}\sum_{k=1}^{K} b_k(i)s_k(t - iT - \tau_k). \tag{3.3}$$

This detection process chooses the sequence which minimizes the noise energy.

The optimal multiuser receiver architecture requires knowledge of all users being received by the multiuser receiver. In addition, the entire received waveform over all time must be known, since in an asynchronous system each data bit overlaps two adjacent bits from each interfering user. Any technique that only takes into account the received signal during the detection interval is inherently suboptimal. The Viterbi algorithm has 2^{K-1} states and thus a time complexity for each bit decision of $O(2^K)$. Verdú developed tight approximations to the bit error rate that, even though the complexity of the receiver structure precludes a practical implementation, demonstrated the significant performance improvements of the optimal multiuser receiver over more conventional receiver structures.

3.2.2 Suboptimum Receivers

The next stage in multiuser receiver development was to search for suboptimal techniques that approached the performance of the optimum technique, but with a much lower computational complexity and therefore were more practically implementable. There are two main classes of suboptimum receivers, linear receivers (those which implement a linear transformation of the set of decision statistics) which are largely based on decorrelation, and nonlinear receivers which are based on interference cancellation. There are two main subclasses of the interference canceler, successive cancellation and multistage cancellation. A general study of suboptimum detectors based on linear transformations is given in [42]. A simulation study of a variety of multiuser receivers is given in [18] for a variety of channels and conditions.

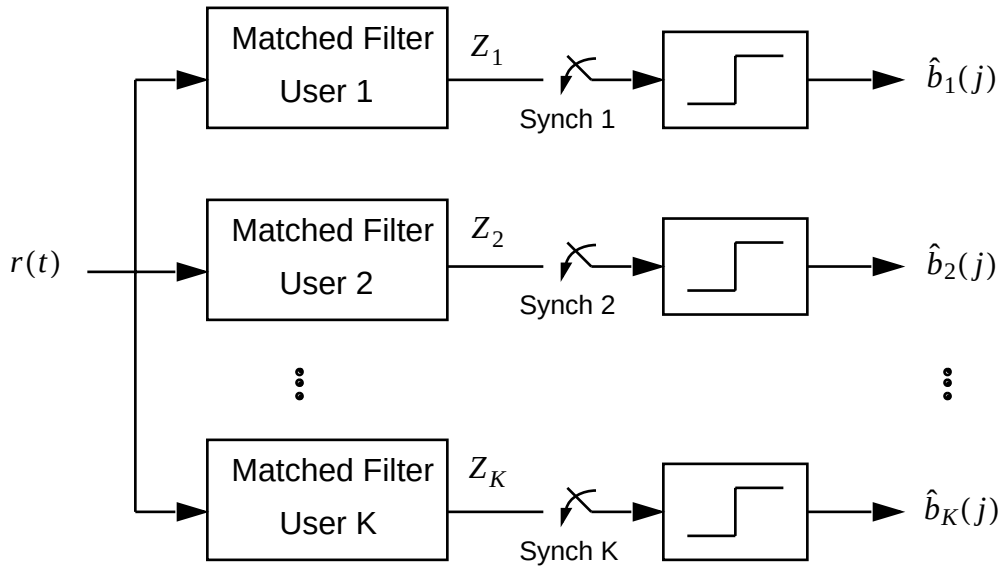

Figure 3.1: Conventional Multiuser Receiver

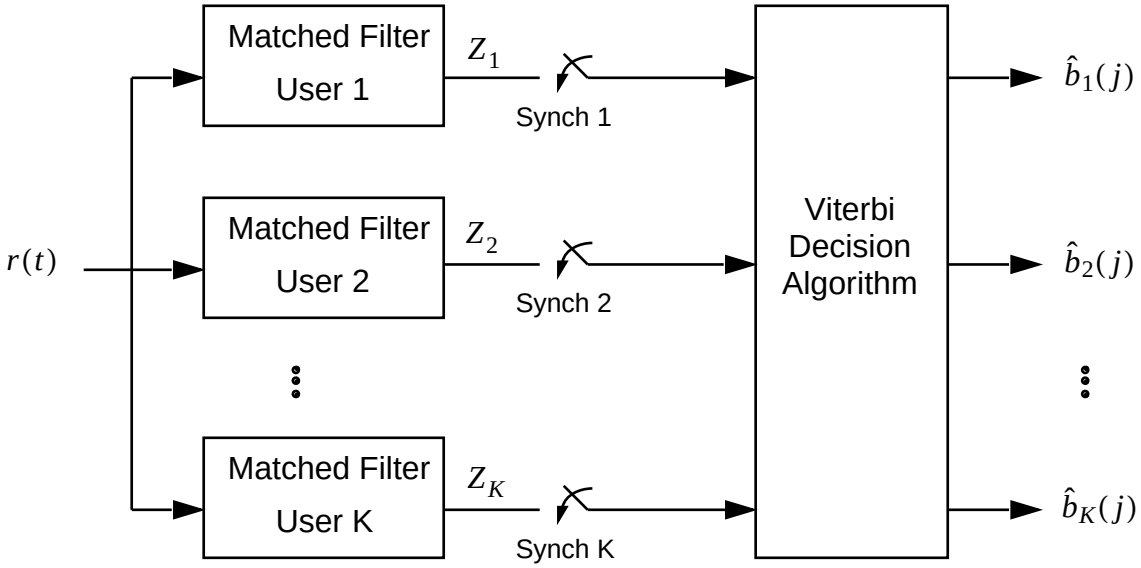

Figure 3.2: Optimum Multiuser Receiver

3.2.3 Decorrelators

A *decorrelating* receiver was initially proposed in [7], but estimates for the probability of bit error were not determined due to the complexity of the analysis. Expressions for the SNR of the decorrelator were presented in [43]. The decorrelator was extensively analyzed in [8] for the synchronous AWGN channel and in [9] for the asynchronous AWGN channel, where BER expressions were obtained. This receiver architecture computes a generalized inverse of the signal crosscorrelation matrix and uses the result to linearly transform the matched filter outputs. The resulting complexity per demodulated bit grows linearly, as opposed to the exponential growth of the optimum receiver. An advantage of this scheme over other suboptimal receivers is that the BER is independent of the received power levels, and thus estimates of the received power levels are not required.

The output of the matched filter is given by the vector

$$\mathbf{y} = \mathcal{R}\mathcal{W}\mathbf{b} + \mathbf{n}, \tag{3.4}$$

where $\mathcal{R}$ is the cross-correlation matrix for an equivalent synchronous problem, $\mathcal{W}$ is a diagonal matrix with the received signal energies from each user on the diaganol, $\mathbf{b}$ is the information sequence, and $\mathbf{n}$ is white Gaussian noise. The elements of $\mathcal{R}$ are given by

$$R_{kj}(l) = \int_{-\infty}^{\infty} \tilde{a}_k(t - \tau_k)\tilde{a}_j(t + lT - \tau_j)dt, \tag{3.5}$$

where $\tilde{a}_k(t)$ is the pseudonoise (PN) sequence of user k, τ_k is the time delay of user k, and T is the bit period.

For any linear detector, the bit estimate of user k's ith bit can be found from

$$\hat{b}_k(i) = \text{sgn}\mathbf{v}^T\mathbf{y}, \tag{3.6}$$

where $\mathbf{v}$ characterizes the detector. For a decorrelating receiver, this is given by

$$\mathbf{v} = \mathcal{R}^{-1}. \tag{3.7}$$

It is shown in [9] that this detector approaches the near-far resistance of the optimum detector in an AWGN channel. As can be seen from (3.5), the cross-correlation matrix is independent of signal energies and thus the decorrelator does not need information about received signal energies, which is a significant benefit.

One of the major drawbacks of this technique is that numerical instability can always be a problem when calculating a matrix inverse. This can be a problem even on a high-precision floating point processor, and is much more likely to be problematic on a fixed-point implementation such as those likely to be used in a practical implementation. In addition,

as can be seen from (3.5), $\mathcal{R}$ must be calculated (and therefore $\mathcal{R}^{-1}$) every time the delays τ_k change, which will occur often in a mobile environment. This must also be calculated every time any user enters or leaves the system. In addition, if the PN sequence does not repeat at the bit period, $\mathcal{R}$ must be recomputed for each new bit period. Due to the nature of the matrix inverse, the entire $\mathcal{R}^{-1}$ matrix must be recalculated even if only a few elements of $\mathcal{R}$ change. If numerical instability does occur and the receiver cannot decode the received signals, a generalized [44] (or pseudoinverse) can be calculated, but this will introduce errors and the ability to decorrelate the interference will be degraded.

Performance in the Presence of Timing, Carrier Phase, and Carrier Frequency Errors

The effects of errors in timing, carrier phase, and carrier frequency upon the performance of the decorrelator are considered in [45]. Performance is determined both in terms of the bit error rate and the near-far resistance of the receiver. The authors classify all three errors as synchronization errors, since the errors result from the imperfect estimates supplied by the synchronization routine. Performance was compared with the conventional correlation receiver.

The authors found that the decorrelator performed well in the presence of these parameter estimation errors provided that the errors were not too large. For the carrier frequency error, which is principally caused by variations in the mobile transmitters' oscillators and by Doppler shift, the authors assumed that the magnitude of this error will usually be less than 100 Hz for practical mobile communications systems. The authors do not mention what carrier frequency they assumed, as tolerances in the oscillator's carrier frequency are usually specified in parts per million, and thus are dependent upon the carrier frequency. This may be severely underestimating the magnitude of the typical carrier frequency offset (the effects of carrier frequency offsets on the multistage receiver are discussed in more detail in Section 8.3) and [46]. Assuming that the frequency offset is less than 100 Hz, the authors found that the effect on the performance of the decorrelator was negligible.

For the carrier phase error, the authors found that its effect was negligible on system performance as long as its magnitude stayed less than $\pi/30$. However, if coherent detection is assumed and the carrier phase must be estimated at the receiver in the presence of multiple access interference, the estimate of the carrier phase may well differ from the true carrier phase by more than this amount. The authors make no mention of how the carrier phase is estimated (nor do they discuss this procedure for any other parameter estimation).

For the time delay error, the authors also determined that this error had a tolerable effect on system performance for most practical applications. However, in the numerical example the authors provided, the error in estimating the true time delay was only $0.05T_c$, where

T_c is the chip period. Actual errors in estimation may yield significantly higher errors. Consider, for example, a digital receiver where the received signal $r(t)$ is oversampled by N_s samples per chip. To properly align the signature sequences with a maximum error of $0.05T_c$, this would imply that the maximum spacing between samples could be $0.1T_c$, which would require $N_s = 10$, or that the received signal be oversampled *ten times*.

The overall determination was that the decorrelator was very robust in the presence of these three estimation errors. However, the numerical examples may not in fact have been calculated using a worst case scenario, and that in fact the maximum error values assumed may be well below those of practical importance. The decorrelator's performance is not surprising given the small maximum errors that were allowed in the simulation, and thus the performance needs to be tested under more difficult conditions. This is not to imply that the decorrelator will not perform admirably in these situations as well, but simply that the results in [45] may not give an accurate accounting of the types of errors that can be expected from practical parameter estimation techniques.

In [18], the decorrelator is compared with the multistage receiver in the presence of timing errors and it is shown that, if perfect power control is assumed, then the multistage receiver is somewhat more tolerant of timing error than is the decorrelator. The decorrelator performed better with small timing errors when flat fading was assumed. Performance was nearly identical in near/far channels.

MMSE Detectors

A variation on the decorrelator is presented in [42], where a linear transformation is still used but it is now based upon minimizing the mean square error. It is shown in [42, 47, 48] that the transformation that minimizes this error is given by

$$\mathbf{v} = \left(\mathcal{R} + \frac{N_o}{2\mathcal{W}^2}\right)^{-1}. \tag{3.8}$$

A disadvantage of this technique is that we now require either knowledge of or estimates of the signal energies contained in $\mathcal{W}$. The estimate of $\mathbf{b}$, $\hat{\mathbf{b}}$, is given by

$$\hat{\mathbf{b}} = \left(\mathcal{R} + \frac{N_o}{2\mathcal{W}^2}\right)^{-1} \mathbf{y}. \tag{3.9}$$

Decision Feedback Detectors

To improve the performance of the decorrelator when decoding weaker users, a decorrelating decision-feedback (DF) detector was introduced in [16] for a synchronous CDMA system in

an AWGN channel. The receiver ranks users in order of decreasing received power, and now the decisions of previous (stronger) users are used in the decision process. Thus knowledge of stronger users is used to improve the performance of the weaker users. This structure is similar to the successive interference cancellers discussed in Section 3.2.5, although the emphasis is on optimizing the receiver filter structures. This structure outperforms the decorrelator in every case, although the gains are most significant for the weakest users. A significant drawback is that estimates of each user's power level are now strictly required by the DF process. The DF approach is extended to synchronous CDMA systems in multipath fading channels in [17] in the form of an adaptive decorrelating Rake receiver.

3.2.4 Interference Cancellers

A different approach to a suboptimal multiuser receiver is the interference canceler (IC). The idea is to subtract the interference from the received signal, thereby leaving the residual signal as essentially a single user signal in the presence of channel noise. Intuitively, if all of the multiple access interference can be perfectly canceled, the performance of the receiver will be identical to that of a conventional receiver in a single user system and the receiver will have a near-far resistance of one. In practice, the interference cannot be canceled perfectly and the efficiency will be somewhat less than one. A major drawback to these techniques is that the performance improvement is dependent upon being able to accurately estimate each user's received power level. There are two main approaches to interference cancellation: successive cancellers and parallel cancellers.

3.2.5 Successive Interference Cancellers

A successive interference cancellation architecture was proposed by Viterbi in [49] for coded systems. Patel and Holtzman developed BER expressions for uncoded systems in [10]. The motivation behind the proposed receiver is minimizing complexity, as even some suboptimal techniques in asynchronous systems have such a high complexity that a practical implementation is difficult or impossible. All successive (serial) cancellation schemes operate by subtracting users in descending order based on received power levels. This scheme achieves the power ranking by ranking the outputs of the individual correlation receivers. For asynchronous systems, this ranking occurs after averaging the correlations over n bits (the value of n must be set according to the channel to ensure that the received power ranking does not change over those n bits). A block diagram of this approach is illustrated in Fig. 3.3. The receiver lowers the BER over the conventional receiver in all cases, but performs best when there is some degree of variance in the received power levels. The BER decreases as the variance rises from zero (perfect power control), and then begins increasing again after

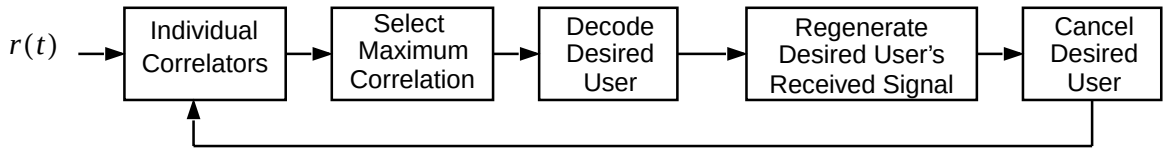

Figure 3.3: Successive Interference Canceler

the powers vary to a greater degree. This suggests that some variation in power levels is beneficial for this receiver architecture, as it allows the stronger users to be decoded well (because of the reduced MAI from the weaker users) and therefore allows their signals to be canceled effectively. If the power levels become too disparate, however, the weak users cannot be estimated properly due to noise from imperfect cancellation.

Serial Cancellation Using Walsh Transforms

A modification to the serial cancellation technique is to base the cancellation process upon Walsh transforms [15, 50, 51, 52], such as those used in the IS-95 cellular CDMA system [33]. The idea is still to successively cancel interferers from the strongest to the weakest, but the cancellation is now accomplished via the use of Walsh transforms. A given user is canceled by taking the Walsh Transform, nulling out the corresponding bin in the Walsh spectrum, and then taking the Inverse Walsh Transform. Walsh transforms have an additional benefit in that hardware implementations operate quickly [53], which is particularly important in a successive cancellation scheme where, for real time demodulation, all users must be canceled during a bit period.

Practical considerations for the Walsh serial cancellation technique were addressed in [54]. Fast Walsh Transforms were studied, since the decrease in computational complexity is significant (analogous to the decrease in moving from a Discrete Fourier Transform to a Fast Fourier Transform). Quantization was also addressed by analyzing scaling and overflow and determining accumulator lengths. A rough approximation to the level of quantization noise due to rounding is introduced based on the number of quantization bits used. A plot of the signal-to-noise ratio against the number of quantization bits is given in Fig. 3.4, where it is seen that the SNR in dB increases linearly with the number of bits used. It is shown that by choosing an appropriate number of bits to quantize the input, overflow is not a major concern with this receiver architecture. This is important, as overflow can occur for similar reasons in the multistage receiver, which suggests that the multistage receiver may be resistant to overflow as well.

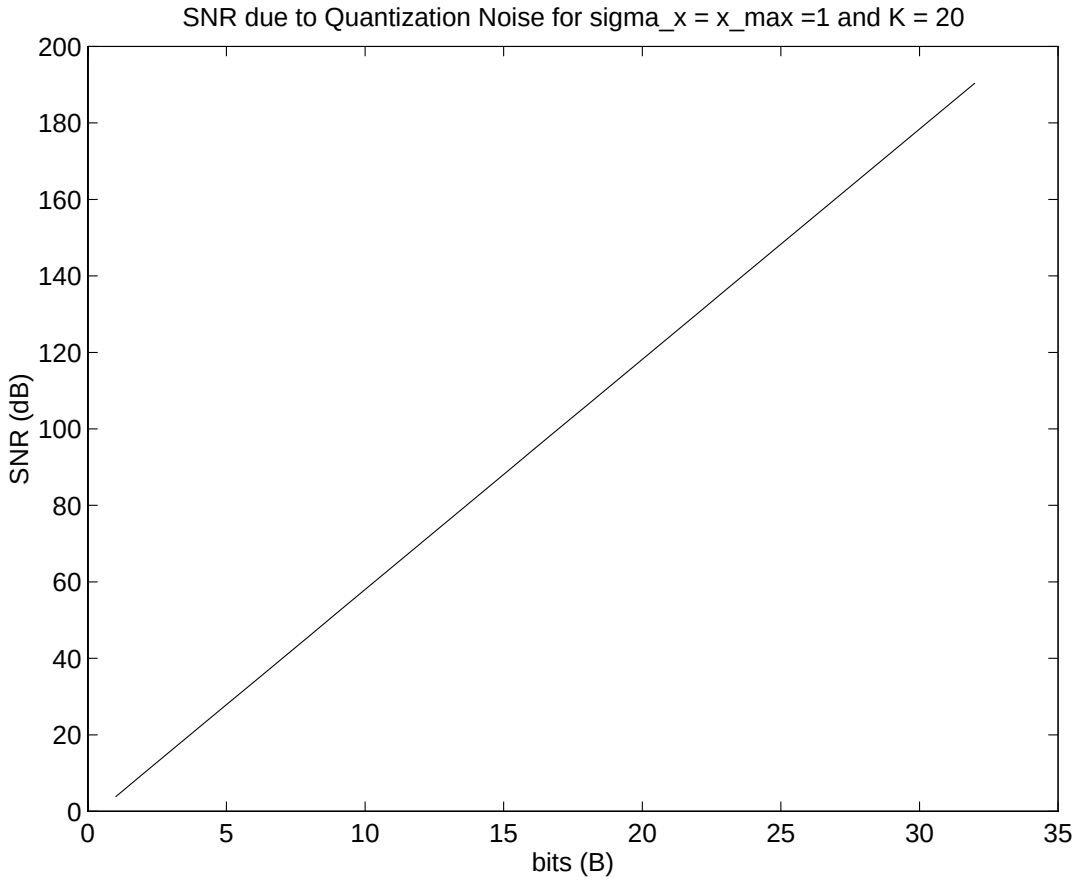

Figure 3.4: Quantization Noise for the Walsh IC

3.2.6 Parallel Interference Cancellers

An alternative to the serial cancellation schemes is parallel cancellation, in which estimates are made simultaneously for all interferers, and then subtracted from the received signal. This is repeated in multiple stages to gain better estimates of the interference, giving rise to the term *multistage* receiver. One technique was proposed by Varanasi and Aazhang in [11] using correlation receivers, where an expression for the BER of a two-stage receiver was also obtained. An alternative approach is presented by Kohno *et al* in [55] using adaptive filters, where a BER expression is obtained when the filters are in steady state (although simulations showed that for noisy, time-varying channels, stable convergence of the filter tap coefficients was difficult to obtain). The receiver used for this research is based upon the structure proposed in [11]. A block diagram of a two-stage receiver is shown in Fig. 3.5.

The first stage is essentially the traditional multiuser receiver, which is just a bank of single-user receivers. The only difference is that a bit decision is not made at this point. At the beginning of the second stage, an estimate is made of each user's received signal. These estimates are then subtracted from the received signal. The desired user's signal is then added to this residual signal, and the signal is again passed to a single-user receiver. The complexity per demodulated symbol is shown to be linear with respect to the total number of users K while maintaining a performance comparable to the optimum multiuser receiver for most practical cases.

3.2.7 Multistage Rake Receiver

In [12, 20], the concepts of a Rake receiver and a multistage receiver are combined. By replacing the bank of correlation receivers with a bank of Rake receivers, the multistage architecture can be used to combat fading and MAI in a multipath environment. Closed form expressions are presented for BER using the Gaussian approximation for MAI in [56, 19], which for any user k in an AWGN channel, if all received power levels are the same, is for stage $s+1$

$$P_b^{(s+1)} = Q\left\{\left[\frac{1}{2(PT/N_o)}\left(\frac{1-(\frac{K-1}{3N})^{s+1}}{1-(\frac{K-1}{3N})}\right)+\left(\frac{K-1}{3N}\right)^{s+1}\right]^{-1/2}\right\}, \tag{3.10}$$

where there are K total active users in the system, P is the power level of the received signal from user k, T is the bit period, the Gaussian noise has two-sided power spectral density $N_o/2$, and N is the processing gain of the CDMA system. A plot of improvement possible with the multistage receiver is shown in Fig 3.6 for an AWGN with identical receiver power levels, $N = 128$, and $K = 32$. This simple estimate becomes optimistic at low BER and more elaborate BER estimation techniques have been developed [57]. There is a significant performance improvement when going from a one stage to two stages, and a somewhat smaller improvement when moving to three stages. There is little improvement in going to a four stage receiver for this channel, and therefore much of performance improvement can be gained with a small number of stages. The largest improvement comes as E_b/N_o, as better estimates can be obtained with less noise and thus the cancellation improves, resulting in lower BER. Cancellation will be beneficial if the E_b/N_o is given by

$$E_b/N_o > \frac{1}{2\left(1-\frac{K-1}{3N}\right)} \tag{3.11}$$

and if $(K-1)/3N < 1$. A plot of the minimum E_b/N_o required for the cancellation to be beneficial is shown in Fig. 3.7.

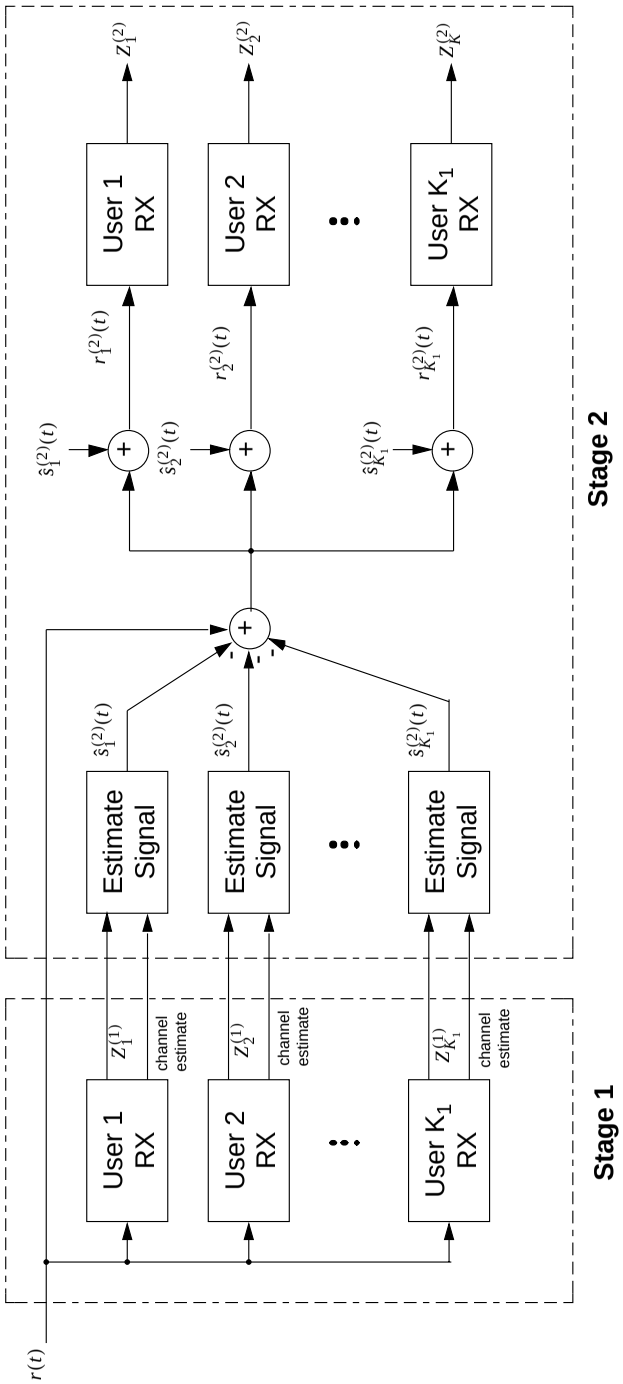

Figure 3.5: Two-Stage Multistage Receiver

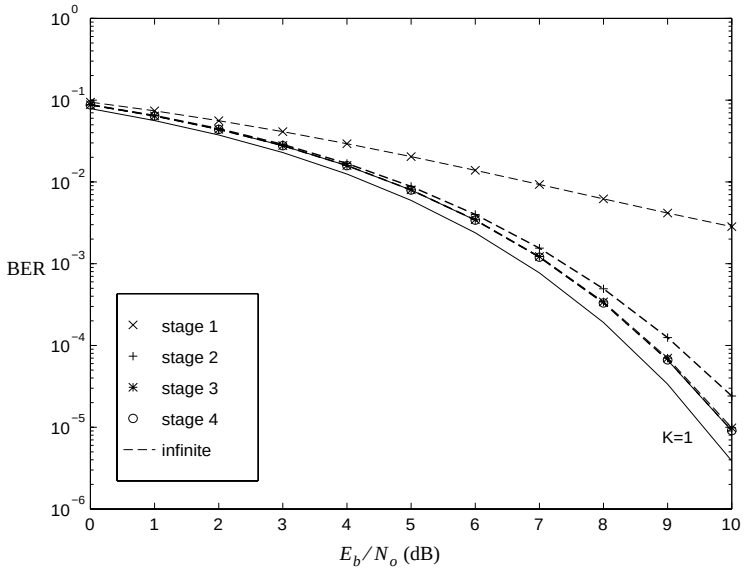

Figure 3.6: Analytic BER vs. E_b/N_o for up to four stages of interference cancellation in AWGN channel with perfect power control for $N = 128$ and $K = 32$

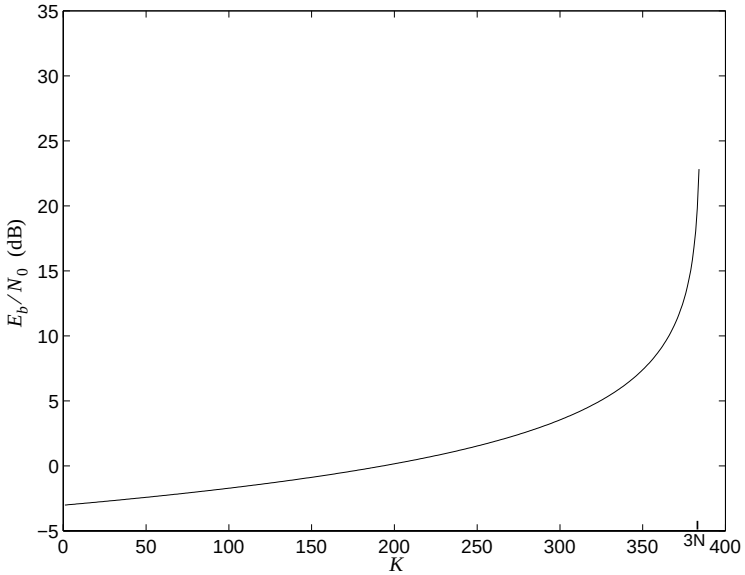

Figure 3.7: Minimum E_b/N_o required for beneficial interference cancellation vs. total number of users, K, for $N = 128$

Near-Far Resistance of the Multistage Receiver

Using the closed-form expression for the BER, we can determine the near-far resistance of an infinite stage multistage receiver. If the received power levels are not identical, the BER (assuming we are decoding user 1) of a finite stage receiver is given by [56]

$$P_b^{(s+1)} = Q\left\{\left[\frac{1}{2(P_1T/N_o)}\left(\frac{1-(\frac{K-1}{3N})^{s+1}}{1-(\frac{K-1}{3N})}\right)+\left(\frac{1}{3N}\right)^{s+1}\right.\right. \left.\left.\left(\frac{(K-1)^{s-1}-(-1)^{s+1}}{K}\left(\frac{\sum_{k=2}^{K}P_k}{P_1}+1\right)+(-1)^{s+1}\right)\right]^{-1/2}\right\}, \tag{3.12}$$

where P_k is the received power of user k's signal. For a receiver with infinite stages ($s=\infty$), if $(K-1)/3N<1$, this reduces to

$$\lim_{s\to\infty} P_b^{(s+1)} = Q\left\{\left[2(P_1T/N_o)\left(1-\left(\frac{K-1}{3N}\right)\right)\right]^{1/2}\right\}. \tag{3.13}$$

Using the near-far definition given in [5, 9], we must first compute the asymptotic efficiency η_k, which is the limit as $\sigma\to 0$ of the ratio of the effective SNR to the actual SNR of a multiuser system. The effective SNR is the SNR required by a single user system to achieve the same asymptotic BER as a multiuser system. The near-far resistance is the minimum η_k considered over all possible interfering bit energies. The single user equivalent for the system considered here is a simple BPSK system, in which the asymptotic BER is given by [58]

$$P_b = Q\left(\sqrt{\frac{2E_b}{N_o}}\right). \tag{3.14}$$

Therefore, the effective E_b/N_o will be the E_b/N_o of (3.14) required to give an identical BER for (3.13) under the limit as $N_o\to 0$. By equating (3.13) and (3.14), we find that the effective E_b/N_o is given by

$$\left(\frac{E_b}{N_o}\right)_{\text{eff}} = (E_b/N_o)\left[1-\left(\frac{K-1}{3N}\right)\right]. \tag{3.15}$$

The asymptotic efficiency can then be found via

$$\begin{aligned}\eta_k &= \lim_{N_o\to 0}\frac{(E_b/N_o)_{\text{eff}}}{E_b/N_o} \\ &= 1-\left(\frac{K-1}{3N}\right).\end{aligned} \tag{3.16}$$

Since this is independent of the interfering bit energies, we have shown that the near-far resistance $\overline{\eta_k}$ of an infinite stage multistage receiver is given by

$$\overline{\eta_k} = 1 - \left(\frac{K-1}{3N}\right). \tag{3.17}$$

By a parallel analysis, it can be shown that the near-far resistance of a finite stage multistage receiver is $\overline{\eta_k} = 0$. This implies the E_b/N_o of a multiuser system would have to be infinite to match the BER of a single user system. This occurs because there will always be some residual signal that cannot be canceled in a finite number of stages, and this residual signal will cause some degradation in the BER of the multistage receiver. Thus, at high E_b/N_o, a finite stage multistage receiver cannot achieve *exactly* the BER of a single user system, although as shown in Fig. 3.6, it can come close. This implies that, even though it has a near-far resistance of zero according to the above definition, the finite stage receiver is still quite useful at combatting the near-far problem.

The Improved Gaussian Approximation

The Gaussian approximation is known to be optimistic under certain conditions [59], particularly for low BER and low number of users. The Gaussian approximation also assumes that no particular variable dominates the performance of the overall system. If one interferer is not canceled effectively in a multistage system, that user may dominate the interference and the Gaussian approximation may be increasingly less accurate. An improved form of the Gaussian approximation was first introduced in [59], and a further simplified (but still accurate) approximation in [60]. This was further modified by Liberti in [61] to allow for disparate received power levels (whether random or constant). Buehrer [21] applied this form of the improved Gaussian approximation to develop a more accurate expression for BER in a multistage receiver.

Selective Cancellation

The cancellation process can actually *increase* the noise in the multiple access interference if a user's received power falls below a certain threshold [13, 19]. This occurs because an accurate estimate of the received signal cannot be obtained and the ineffective cancelation increases the overall noise. The technique of *selective* cancellation has been introduced to only cancel users whose received powers are above a set threshold. For the AWGN channel, it is only beneficial to cancel the interference from user k if the received power P_k is given by

$$P_k > \frac{N_o}{2T} + \frac{1}{3N}\sum_{j=1, j\neq k}^{K} P_j. \tag{3.18}$$

In a cellular CDMA system, a large amount of MAI comes from out-of-cell interference [62, 63]. These interfering users are often received with low powers due to the longer distances from the base station. While attempting to cancel all users improves the BER over using traditional receivers, even lower BER can be achieved by selectively canceling the interferers. It is shown in [63] that averaging the received power estimate over several bit periods can improve the estimate if the power does not change significantly during that time.

Parameter Estimation

The preceding analysis of the multistage analysis has assumed that we can perfectly estimate the carrier phase and the time delay of each user k's received signal. In practice, however, the receiver will have to estimate these parameters and then use these parameter estimates when calculating the interference estimates. The fact that we are using estimates and not the actual parameters will introduce noise into the cancellation process and thus degrade the overall bit error rate performance. A study of how the receiver performs in the presence of this additional noise is given in [18].

The use of averaging to reduce the variance in the parameters is also studied [18]. The average is taken using the traditional sample average over N_b bits, given by

$$\hat{A}_k = \frac{1}{N_b} \sum_{n=1}^{N_b} \hat{A}_{k,i}, \tag{3.19}$$

where $\hat{A}_{k,i}$ is the parameter estimate of user k during bit interval i and $\hat{A}_k$ is the average of that estimate over N_b bits. This technique can be used to decrease the variance of the estimates *provided* that the estimate does not vary significantly during the N_b bits used in the averaging process. Results show that averaging over a small number of bits can reduce the variance in the estimates in both static and time-varying channels. Methods of estimating the amplitude, time delay, and carrier phase are provided.

Numerical results were generated for varying levels of phase estimation and time delay estimation (the amplitude estimation errors are already accounted for in the multistage model) [18]. It was shown that the multistage receiver still outperforms the conventional receiver for reasonable levels of estimation (although there is noticeable degradation as the estimation error increases), and furthermore that the receiver is more sensitive to timing errors than to phase errors.

3.2.8 Other Approaches

There are other approaches to multiuser receivers, including hybrid combinations. In [14], Varanasi and Aazhang note that the first stage which determines the initial bit estimate need not be a bank of correlation receivers, but can instead be any receiver structure. One possibility suggested in [14] is to use the decorrelating receivers proposed by Lupas and Verdú. The complexity remains linear with respect to the number of users K, but the multistage architecture now allows for bit estimates to be formed on less noisy signals. A drawback of this approach is that the use of decorrelators implies that this hybrid receiver will still be vulnerable to numerical instabilities caused by computing the inverse of the correlation matrix. The computational complexity has also increased over a receiver employing conventional receivers.

Another approach combines the interference canceler with adaptive antenna arrays [64]. An adaptive array attempts to combat interference by nulling out signals that do not arrive at the same angle of arrival as the desired signal. Drawbacks to using the arrays by themselves is that interference with the same angle of arrival cannot be nulled, and the degree to which interference can be nulled is restricted by the number of elements used in the array, as this determines what type of antenna pattern can be generated. By using an adaptive array in conjunction with interference cancellation, the array can be used to limit the number of users that must be cancelled (and thereby limit the complexity of the required interference canceler), and the interference canceler can combat the interference that cannot be reduced by the array alone. Information from the IC process can be used in updating the taps of the array. In the cancellation process, the algorithm must know which interferers arrived at the same angle of arrival, since only these interferers will be canceled. This technique observes the correlator outputs, and assumes that strong outputs indicate same angle of arrival, since the array will null to some degree the other interferers. The reduction in complexity of the IC scheme is therefore dependent upon the number of interferers that can be adequately nulled by the array, which is in turn dependent upon the number of elements in the array.

3.3 Conclusions

In this chapter, we have summarized the various approaches that have been taken in multiuser receiver design. The optimum receiver in the AWGN channel is too complex for practical implementation, and so sub-optimum techniques have been developed that retain much of the optimum receiver's performance but at a linear complexity. The two main classes are the linear receivers based on decorrelation, and the non-linear receivers based on interference cancellation. Cancellation can be performed either in serial or parallel.

Parallel cancellation has been shown through analysis and simulation to provide an attractive combination of performance robustness and complexity [65]. So we will pursue parallel cancellation in this thesis. We will address some practical considerations of multistage performance. First, we will address synchronization, with a discussion of spread spectrum synchronization techniques in Chapter 4 and an examination of synchronization effects in the multistage receiver in Chapter 5. First, we consider the effect the unsynchronized users will have upon the BER of synchronized users. This can be significant since we cannot cancel the unsynchronized users. Next, we will use the multistage architecture to improve the acquisition time. An analytic and simulation model is presented in each case.

The next topic that we address is quantization, with a discussion of quantization analysis technique in Chapter 6 and an examination of the effects of quantization in the multistage receiver in Chapter 7. The hardware prototype that is being developed requires a fixed-point implementation because of cost and speed considerations. Fixed-point systems have limited dynamic range, and we investigate the performance degradation caused by quantization noise. An analytic, simulation, and semi-analytic model is presented.

Finally, carrier phase offsets and phase estimation are considered in Chapter 8, along with the computational complexity and other issues related to the hardware prototype being developed. Each mobile will have a carrier frequency slightly different from the other's due to tolerances in the oscillators. Many conventional phase tracking techniques are closed-loop approaches, but the cancellation process requires open-loop approaches. A simulation model of a maximum likelihood phase estimator is presented.

Chapter 4

Synchronization Techniques for CDMA

4.1 Introduction

In this chapter, a survey of the various synchronization schemes for CDMA systems is presented. Many early spread spectrum systems did not require multiple access and therefore not all of the spread spectrum synchronization techniques are suitable for a CDMA environment. Synchronization is critical when using multiuser receivers for several reasons. First, as in all CDMA systems, it is important to synchronize as quickly as possible so that a user may begin transmitting with little noticeable delay. Second, in a multiuser receiver, since the unsynchronized user's signal is unknown, that signal cannot be used to combat the interference due to that user and thus it will increase the BER of all other users.

4.2 Synchronization

In order for a spread spectrum signal to be despread, the locally generated replica of the spreading sequence at the receiver must be aligned with the desired user's spreading sequence in the received signal. Various synchronization schemes have been proposed to accomplish this. Synchronization generally occurs in two stages, acquisition and tracking. In acquisition, an attempt is made to align the sequences within some degree of tolerance, typically a chip period [66]. Once it is determined that the sequences have been aligned properly, tracking mode is entered, which maintains the alignment with the received signal. Acquisition is often considered the most difficult aspect of synchronization, and as such

has received the greatest amount of research interest. Only acquisition is considered in this thesis.

The metric used to compare synchronization techniques varies with the intended use of the spread spectrum system. Two important criteria are the probability of false alarm and the probability of detection. These terms are sometimes defined in two different ways, so care must be taken to ensure that the proper definition is used for the case being studied. Historically, the probability of false alarm is the probability that synchronization is detected when the desired signal is not actually present [67, 68]. The probability of detection is the probability that synchronization is detected when the desired signal is present. This was applicable to early spread spectrum systems like range finding systems, where the receiver was trying to detect a pulse, not decode any information. The important criteria in such a system is whether the signal is present or not.

For continuous communication systems where the signal is continuously transmitted until the signal is acquired and the message completed, the desired signal is always present, although the code phase is unknown. Since the signal is present, it makes little sense to calculate the probability that synchronization is detected when it is not present. Instead, the probability of false alarm is defined as the probability that synchronization is detected when the two PN codes are not properly aligned [69]. The probability of detection is the probability that synchronization will be detected when the codes are properly aligned. Since the spread spectrum communication systems considered here, including the cellular CDMA system, are continuously transmitting systems, this definition is used throughout this thesis.

Regardless of how they are defined, the probabilities of false alarm and detection are most useful as a measure of performance in bursty communications, where the transmitter sends a short signal and then is silent for a longer period of time [70]. For continuously transmitting systems, a more useful measure of system performance is acquisition time. The acquisition time is a random variable because of the random components of the received signal, and therefore must be characterized according to its probability distribution. Since this is very difficult to achieve for any case of practical interest, the mean and variance of acquisition time are usually derived instead [69].

4.2.1 Matched Filters

The first serial synchronization technique was proposed by Sage [67] using matched filters and threshold detection in a single user spread spectrum system operating in Gaussian noise. Matched filters have the benefit of being straightforward to implement and rapid acquisition, although they are often impractical for long chip sequences [71]. Passive matched

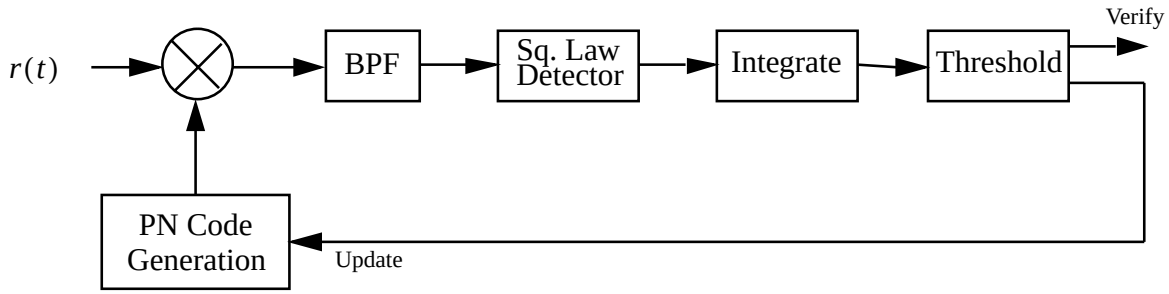

Figure 4.1: Single Dwell Time System Model

filters are often constructed using a tapped delay line [72]. Since the tap structure in the tapped delay line changes as the signature sequences change, this structure must be adaptable if decoding more than one possible signature sequence is required [71].

4.2.2 Active Correlators

Single Dwell Time Acquisition

In [69], the single dwell time acquisition technique is presented, which derives its name from the fact that a single integration time is used in determining whether synchronization has been achieved for a particular code alignment. The model assumes a single spread spectrum user in Gaussian noise and a receiver using noncoherent detection. The received signal is multiplied by the locally generated PN code and then passed through a bandpass filter (BPF). The output is then passed through a square-law detector (an envelope detector followed by a square-law device). The output is then integrated and passed to a threshold device, whereupon tracking mode is entered if the output crossed the threshold, and the PN code replica is shifted in phase if not. A block diagram of this system is shown in Fig. 4.1. Expressions for the mean and variance of acquisition time are presented (assuming no Doppler shift). First approximations to the mean and variance of acquisition time are presented if Doppler shift is present. In [73], an expression for the probability of successful synchronization is given for single dwell time systems.

Double Dwell Time Acquisition

A double dwell time technique is also presented in [69], in which two integration times are used. In the initial search, a short integration time is used to try and quickly find

the correct code phase. If the threshold is crossed after the shorter integration, a longer integration takes place and the result is compared to a second threshold. If this threshold is crossed, the output is passed to the tracking routine, otherwise the code phase is updated and the process begins again (using the shorter integration period). Approximations to the mean and variance of acquisition time are given for both the case of no Doppler shift and the case of Doppler shift. Analysis of multiple dwell time techniques is presented in [74], where it is shown that double dwell time techniques show a significant improvement over single dwell time techniques, and that further improvement can be obtained using multiple dwell times but that the improvement is marginal. The enhancement possible in acquisition time is particularly noticeable as the penalty time increases.

Variable Dwell Time Acquisition

Variable dwell time schemes also exist, which are based on the sequential analysis presented in [75]. The output of the integrator is continuously compared to a variable threshold, and if at any time the output falls below this threshold, then the code phase is updated and the search begins again. In this fashion, a given code phase does not have to be searched for a long time if it is readily apparent that the integrator output is well below the expected level. Determining appropriate values for the variable threshold are critical in maintaining acceptable levels for the probabilities of detection and false alarm.

Expanding Window Search Strategy

An expanding window strategy is applied to fixed and variable dwell time schemes in [76], where an approximation is introduced for the cumulative probability distribution of the acquisition time. In some cases, the code phase will not be uniform over the dwell time, but will have some other probability distribution. This is the case when some *a priori* knowledge is known of the code phase. This can occur, for example, if synchronization has just been lost and is trying to be re-established or if the code phase is based on the time of day and some information is known about the distance of the transmitter from the receiver. Since the phase is known to most likely be within some subset of the total uncertainty region, an expanding window strategy begins by searching that most likely region, and, if synchronization is not achieved, gradually expands the search until eventually the whole uncertainty region is swept.

4.2.3 Sequential Estimation

An alternative to the active correlation approach is sequential estimation, in which a small number of bits are examined and the state of the received PN code is estimated [77]. A locally generated PN code is still used, although instead of multiplying the received signal by the PN code, the local PN code is set to the state of the estimated received signal. A statistical decision is then made to determine if the codes are in alignment. This process can greatly reduce the acquisition time compared to the serial search techniques, but has significant limitations. First, the technique performs well only in the presence of Gaussian noise. If other forms of interference are present, the algorithm performs very poorly and therefore is not applicable to systems where multiple access is desired or where severe jamming is expected. In addition, the algorithm assumes that the received PN signal is at baseband, which implies that some form of coherent demodulation must be done prior to PN code acquisition.

4.2.4 Acquisition using Interference Cancellation

Acquisition in an interference cancellation receiver has been studied in [78]. Two methods are studied, based essentially on a serial and parallel cancellation approach. The model assumes that the receiver is attempting to acquire K users in an AWGN channel. In the first approach, the assumption is made that users will synchronize according to their power ranking (strongest to weakest). As soon as a user synchronizes, the received signal from that user is estimated and subtracted from the signal. This process repeats until the weakest user is synchronized. In the second approach, a bank of matched filters attempts to acquire all users at once. As each user is synchronized, an estimate is made of the corresponding received signal and subtracted from the overall received signal. Unsynchronized users continue attempting to synchronize on the residual signal until all users are synchronized. The approach assumes a Gaussian approximation for all correlator outputs and develops an expression for the probability of detection. The acquisition method is known as automatic threshold control and is discussed in [79]. While extensive results were not given, the parallel scheme was observed to synchronize all users faster than the serial approach, at the cost of increased hardware complexity.

The results of [78] do not address the effects of the unsynchronized users on the bit error rates of the synchronized users, nor the mean or variance of acquisition time. The results best describe the case of when a system is being initialized and *all* users are unsynchronized. The results then stress which of the cancellation techniques will acquire all K users the fastest. This approach does not attempt to analyze a system that is already operating with some number of synchronized users already present. In addition, no attempt is made to

characterize the performance of each user with respect to acquisition; the techniques are judged solely on how long it would take to acquire all K users. Finally, the multiple access is always modeled using a Gaussian approximation, which is known to be optimistic under certain conditions [30].

4.2.5 Other Techniques

Hybrid acquisition schemes are also possible. For example, a hybrid scheme is proposed in [80] which uses both matched filters and active correlators. This scheme was mainly proposed to counteract jamming, not multiple access interference. At the beginning of each transmission, a short prefix is attached which is detected by the matched filter architecture. The shortness of the prefix (which is repeated a set number of times) allows for a matched filter with a reduced complexity. If the output of the matched filters exceeds some threshold, an active correlation scheme is begun to attempt to reliably acquire the full signal. If the output of the correlator exceeds a different threshold, then acquisition is assumed. This scheme attempts to combine the rapid search capabilities of the matched filters with the reliable detection of long sequences with active correlators.

A verification mode may follow the main acquisition mode and precede the tracking mode [72]. In verification mode, if the acquisition loop detects acquisition when the correlator output crosses the set threshold, the signal is passed to a coincidence detector. Here, the locally generated and received PN sequences are correlated in a series of independent trials, and the results are compared to a threshold. If a certain majority of the correlator outputs do not exceed the threshold, the estimated code phase is incremented by one interval and acquisition begins again. If that majority does cross the threshold, the tracking mode is entered where a fine alignment is maintained between the two PN sequences. Such systems are sometimes referred to as two-dwell systems. Verification is used to reduce the likelihood of a false alarm and the associated penalty time before the acquisition process can begin anew. The penalty for using a verification mode is that the mean acquisition time is increased due to the increased time spent in verifying the code phase.

A modification of the straight serial search of the single dwell time approach is the Z search [66, 72]. Using this technique, the region of code phase uncertainty is searched. If the search is unsuccessful, the estimate of the code phase is reset and the search begins again. Resetting the code phase takes a set period of time known as the reset time. An alternative to resetting the code phase is to begin the search in the opposite direction of the previous search, so that the code phase sweep will proceed backwards from the previous sweep. There is no associated reset time with this technique.

A way of greatly reducing the mean acquisition time is to use a parallel architecture, where

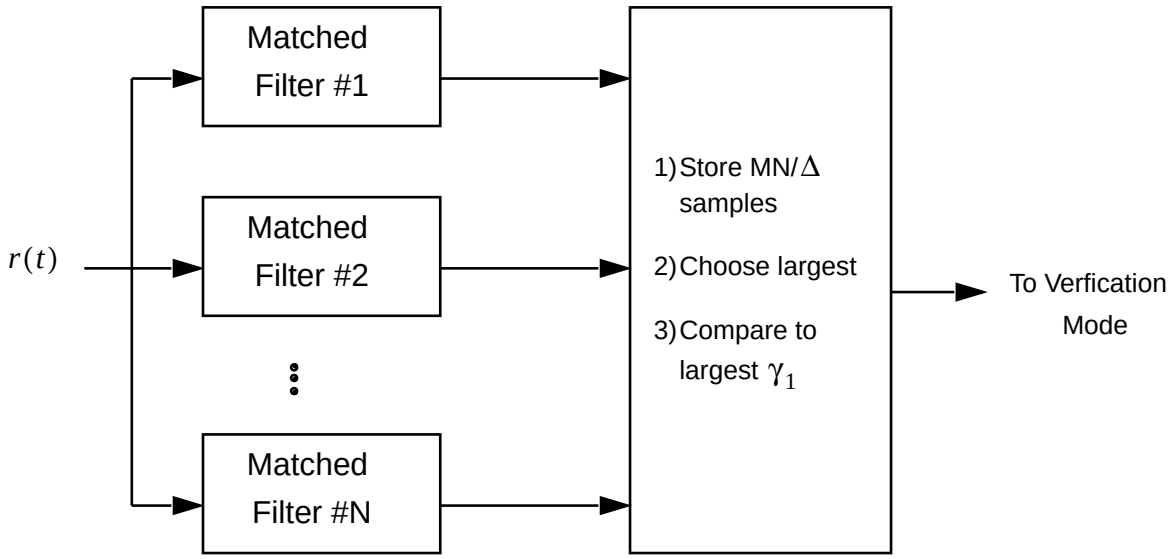

Figure 4.2: Parallel Acquisition Model

multiple code phases are searched at the same time as shown in Fig. 4.2. In the extreme case, an acquisition loop can be used for every code phase uncertainty. Alternatively, a subset of the phase uncertainties can be searched at any given time. The obvious drawback to this technique is the increase in hardware required to achieve the parallel architecture. These structures are very useful when acquisition time must be kept to an absolute minimum. A comparison of several parallel schemes in conjunction with verification is given in [81]. Parallel schemes have also been analyzed in Rayleigh fading [82], nonselective and frequency-selective Rician fading [83], and non-fading channels [82].

4.2.6 Conclusions

A wide variety of techniques are available for acquiring a signal in an interference cancellation receiver. The initial synchronization results presented in the next chapter are for the single dwell technique system with coherent demodulation. This is a widely applicable technique that can operate in the presence of interference. The matched filter approach is not adopted because it can only be used in systems with short spreading codes. Estimation techniques are not used because they perform poorly in the presence of interference, and multiple access interference is an inherent part of multiuser systems. Methods to improve acquisition time such as using special PN codes or preambles are not used because they

add significantly to the complexity of the analysis, and it is expected that the benefits provided by these techniques will provide a similar level of performance improvement in a multistage receiver as they do in single user receivers.

Chapter 5

Synchronization Issues for the Multistage Receiver

The purpose of synchronization in a spread spectrum system is to align the spreading code of the received signal with the locally generated replica of the spreading code at the receiver [70]. The synchronization routine attempts to resolve the uncertainty in the received timing and phase information. Synchronization is usually accomplished in two stages: acquisition and tracking. Acquisition is used to initially acquire a signal within some degree of tolerance. Tracking is used to maintain the alignment between the spreading codes after the signal has been acquired. Uncertainty in timing and phase will occur after initial acquisition due to effects such as clock misalignment, multipath, and Doppler shift. This chapter deals only with acquisition. The effect on performance of timing errors and phase jitter in the course of normal tracking is dealt with in [18].

There are two main effects of synchronization that we wish to study. The first is the effect of unsynchronized users on the BER of synchronized users. The second is the improvement in the mean acquisition time when using the multistage architecture in the synchronization process.

5.1 Analyzing the Effect of Unsynchronized Users on Synchronized Users

Any CDMA system will have a mix of synchronized and unsynchronized users. Both user types will act as multiple access interference (MAI) to the desired user. For one stage receivers (no interference cancellation), there will be no difference in the effect of

interference caused by unsynchronized and synchronized users. However, for stages 2 and beyond, interference cancellation can be performed upon the synchronized users, but not the unsynchronized users. The unsynchronized interference will affect the BER in two ways. First, the uncancelled interference will appear directly at the output of the last stage of the receiver, and will likely dominate if the power is significantly greater than the residual power of the synchronized users after cancellation. The unsynchronized interference will also appear at each decision stage in the receiver, degrading the estimation of synchronized interference. This will increase the noise in the cancellation process and increase the BER at the output.

A closed form expression for BER for any arbitrary number of stages and any number of synchronized users is given in [13, 19]. This analysis relies upon the Gaussian approximation to model the MAI. The approximation, when compared to simulation results, is shown to be valid for BER above 10^{-3}. The Gaussian approximation cannot be used to model the unsynchronized users, however. These users, particularly when they have power levels that are greater than the synchronized users, will dominate system performance since their interference cannot be canceled. The Gaussian approximation assumes that no residual interference source dominates. Since a fundamental assumption of the approximation has been violated, we must look for a more accurate technique to model the MAI.

In [59], Morrow and Lehnert presented an improved Gaussian approximation for modeling multiple access interference when using the conventional correlation receiver. This technique closely models the exact interference levels, although the complexity is much greater than that of the standard Gaussian approximation. Holtzman presented a modification to the improved Gaussian approximation in [60], which has a high degree of accuracy but now with a computational simplicity approaching that of the standard approximation. Liberti then extended this technique [61] to allow the power of the received signal from each user to be modeled independently of all others, either as a constant or a random variable.

This form for the improved Gaussian approximation has been extended to the multistage receiver structure by Buehrer [21, 18]. This model assumes that all users are synchronized, so the following analysis extends the model to allow MAI due to unsynchronized users as well. Since the MAI is not affected by the method of synchronization used, this analysis may be applied regardless of how synchronization is actually achieved.

5.2 System Model

We consider a DS/SS multiple access system with binary phase shift keyed (BPSK) signaling and a multistage receiver. Since the multistage receiver requires knowledge of all synchronized users' spreading codes, and since only the base station will have access to

these codes, the reverse link (mobile to base station) is modeled. There are K_1 synchronized users and K_2 unsynchronized users in the system, with a total of $K = K_1 + K_2$ users. Any arbitrary user k's received signal is represented by

$$s_k(t) = \sqrt{2P_k} b_k(t - \tau_k) a_k(t - \tau_k) \cos\{\omega_c(t - \tau_k) + \phi_k\} \tag{5.1}$$

where k is the number of the user, P_k is the power of the signal, $b_k(t - \tau_k)$ represents the data signal, $a_k(t - \tau_k)$ represents the spreading signal, and $\cos\{\omega_c(t - \tau_k) + \phi_k\}$ represents the modulating waveform. The random phase ϕ_k is uniformly distributed over $[0,\ 2\pi)$, while the random delay τ_k is uniformly distributed over $[0, T)$, where T is the bit period. We assume that P_k is independent for each user and also independent of the phase ϕ_k and the delay τ_k. We assume, without loss of generality, that the phases and delays of user k are relative to the desired user d, so that $\phi_d = 0$ and $\tau_d = 0$.

The data signal $b_k(t)$ is given by

$$b_k(t) = \sum_{i=-\infty}^{\infty} b_{k,i} p_T(t - iT), \tag{5.2}$$

where $b_{k,i} \in \{+1, -1\}$ is an infinite sequence of data bits and $p_T(t)$ is a rectangular pulse with unity amplitude and duration T. The spreading code $a_k(t)$ is given by

$$a_k(t) = \sum_{i=-\infty}^{\infty} a_{k,i} p_{T_c}(t - iT_c), \tag{5.3}$$

where the chip values are given by $a_{k,i} \in \{+1, -1\}$ and T_c is the chip duration. The total number of chips per bit, N, is given by $T = NT_c$. When a single propagation path is present, the received signal at the base station is given by

$$r(t) = n(t) + \sum_{k=1}^{K} s_k(t - \tau_k), \tag{5.4}$$

where $n(t)$ is additive white Gaussian noise (AWGN) with two-sided power spectral density $N_o/2$.

The first stage of the multistage receiver is a bank of correlation receivers, as shown in Fig 3.5. Each of these receivers recovers the transmitted data bit by correlating the received signal $r(t)$ with the signature sequence of user k, $a_k(t)$, to form a decision statistic $Z_{k,i}^{(1)}$, given by

$$Z_{k,i}^{(1)} = \int_{iT+\tau_k}^{(i+1)T+\tau_k} r(t) a_k(t - \tau_k) \cos(\omega_c t + \phi_k) dt. \tag{5.5}$$

The next step, for each stage $s+1$, is to make an estimate $\hat{s}_k^{(s+1)}(t)$ of each synchronized user k's received signal $s_k(t)$ given by

$$\hat{s}_k^{(s+1)}(t) = \sqrt{2\hat{P}_k}\hat{b}_k(t-\hat{\tau}_k)a_k(t-\hat{\tau}_k)\cos(\omega_c t + \hat{\phi}_k). \tag{5.6}$$

We will assume that the estimates of the delay and phase, $\hat{\tau}_k$ and $\hat{\phi}_k$, can be obtained perfectly from the synchronization routine. Therefore, for any data bit i, the only remaining unknown portion of (5.6) is given by $\sqrt{\hat{P}_k}\hat{b}_{k,i}$. We can obtain this estimate by weighting the decision statistic from the previous stage, using

$$\sqrt{\hat{P}_k}\hat{b}_{k,i} = \frac{\sqrt{2}}{T}Z_{k,i}^{(s)}. \tag{5.7}$$

By substituting (5.2) and (5.7) into (5.6), we obtain

$$\hat{s}_k^{(s+1)}(t) = \frac{2}{T}a_k(t-\tau_k)\cos(\omega_c t + \phi_k)\sum_{i=-\infty}^{\infty} Z_{k,i}^{(s)}p_T(t-iT). \tag{5.8}$$

Now that we have constructed estimates of each synchronized user's received signal, we perform interference cancellation by subtracting all synchronized interfering signals from the desired user's signal. It is computationally more efficient to accomplish this by first subtracting all estimates from the received signal, and then adding back the desired user before detection by the next receiver stage. This process is illustrated in Fig. 3.5.

By subtracting out the interference estimates, we form a new received signal $r_j^{(s)}(t)$ at each stage s for each user j, $1 \le j \le K_1$, given by

$$\begin{aligned} r_j^{(s)}(t) &= r(t) - \sum_{k=1,k\neq j}^{K_1} \hat{s}_k^{(s)}(t-\tau_k) \\ &= n(t) + s_j(t) + \sum_{k=1,k\neq j}^{K_1}[s_k(t-\tau_k) - \hat{s}_k^{(s)}(t-\tau_k)] + \sum_{k=K_1+1}^{K_2} s_k(t-\tau_k). \end{aligned} \tag{5.9}$$

The first term is the Gaussian noise, the second term is the desired user's signal, the third term is the residual after the interference estimates have been subtracted out, and the final term is the MAI due to the unsynchronized users.

The received signal for each user j given by (5.9) is then passed to the next bank of correlation receivers, as shown in Fig. 3.5. A new decision statistic is formed at stage s during bit i by correlating $r_j^{(s)}(t)$ with user j's spreading code,

$$Z_{j,i}^{(s)} = \int_{iT+\tau_j}^{(i+1)T+\tau_j} r_j^{(s)}(t)a_k(t-\tau_j)\cos(\omega_c t + \phi_j)dt. \tag{5.10}$$

This decision statistic is then passed on to the next stage until the final stage of the receiver has been reached. At the last stage, an estimate is made of the desired user d's transmitted bit. The estimate of data bit i from user d, $\hat{b}_{d,i}$, is determined from $Z_{d,i}^{(s)}$ by

$$\hat{b}_{d,i} = \begin{cases} 1, & Z_{d,i}^{(s)} \geq 0 \\ -1, & Z_{d,i}^{(s)} < 0 \end{cases} . \tag{5.11}$$

5.3 Analysis Using an Improved Gaussian Approximation

This section develops an expression for the BER based on the decision statistic given in (5.10). The improved Gaussian approximation uses the mean and variance of the variance of MAI to determine BER [60], so we must determine these variables based on the characteristics of the interference. The analysis of [18] will be extended to allow for unsynchronized users, since the characteristics of the MAI at stages $s = 2$ and above will differ for synchronized and unsynchronized interferers.

Analysis for the First Stage

To obtain an expression for the decision statistic that is dependent upon the MAI, we substitute (5.9) into (5.10) and obtain

$$Z_{j,i}^{(s)} = \eta + \sqrt{\frac{P_j}{2}} T b_{j,i} + \sum_{k=1, k\neq j}^{K} I_{k,j}^{(s)}, \tag{5.12}$$

where η is a zero mean Gaussian random variable with variance $N_o T/4$ representing the correlated noise, the second term represents the desired component, and $I_{k,j}^{(s)}$ is the residual after interference cancellation for the total MAI (the unsynchronized interference cannot be cancelled and so this term will reflect the total interference from that user).

In [59], it is shown that the MAI terms of the first stage, $I_{k,j}^{(1)}$, are conditionally independent given B, the number of zero crossings during a bit interval in the spreading code. We define a random variable, Ψ, to be the conditional variance of the total multiple access interference as [59]

$$\Psi = E\left[\left(\sum_{k=1, k\neq d}^{K} I_{k,d}^{(1)} \right)^2 \mid \{\phi_k\}, \{\tau_k\}, \{P_k\}, B \right]. \tag{5.13}$$

To compute the BER directly using Ψ, the probability density function of Ψ must be computed. Since this greatly increases the computational complexity of the analysis, Holtzman introduced the improved Gaussian approximation [60], which only requires the mean and variance of Ψ to compute BER. This derivation relies on using a Taylor series expansion based on differences instead of derivatives. Allowing for random power levels as given in [61], it is shown that the mean of Ψ, μ_Ψ, is given by

$$\mu_\Psi = \frac{T_c^2 N}{6} \sum_{k=1,k\neq d}^{K} \mu_{P_k}, \tag{5.14}$$

where μ_{P_k} is the mean of the received power P_k of user k. The variance of Ψ, σ_Ψ^2, is given by

$$\begin{aligned} \sigma_\Psi^2 &= \frac{T_c^4}{4}\left[\frac{23N^2+18N-18}{360}\sum_{k=1,k\neq d}^{K}\mu_{P_k}^2 + \frac{7N^2+2N-2}{40}\sum_{k=1,k\neq d}^{K}\sigma_{P_k}^2 \right. \\ &\quad \left. + \frac{N-1}{36}\sum_{k=1,k\neq d}^{K}\sum_{j=1,j\neq k\neq d}^{K}\mu_{P_k}\mu_{P_j}\right], \end{aligned} \tag{5.15}$$

where $\sigma_{P_k}^2$ is the variance of the received power of user k. If constant received powers are desired, the mean is set to the desired power level for user k and the variance is set to zero. An accurate approximation for the probability of error for user d can then be determined using [61]

$$\begin{aligned} P_{b,d}^{(1)} &\approx \frac{2}{3}Q\left(\sqrt{\frac{P_d T^2}{2\left(\mu_\Psi + \frac{N_o T}{4}\right)}}\right) + \frac{1}{6}Q\left(\sqrt{\frac{P_d T^2}{2\left(\mu_\Psi + \sqrt{3}\sigma_\Psi + \frac{N_o T}{4}\right)}}\right) \\ &\quad + \frac{1}{6}Q\left(\sqrt{\frac{P_d T^2}{2\left(\mu_\Psi - \sqrt{3}\sigma_\Psi + \frac{N_o T}{4}\right)}}\right), \end{aligned} \tag{5.16}$$

where $Q(\cdot)$ is the standard Q function defined by

$$Q(x) = \frac{1}{\sqrt{2\pi}}\int_x^\infty e^{-\frac{u^2}{2}}du. \tag{5.17}$$

Analysis for Stages 2 and Above

The above results apply only to the first stage of the receiver, which is identical to a bank of correlation receivers. It is shown in [18] that if we define an *effective* power at each stage s of the receiver, we can derive an expression for the mean and variance of this effective

power, $\mu_{P_k}^{(s)}$ and $(\sigma_{P_k}^{(s)})^2$. We can then use $\mu_{P_k}^{(s)}$ and $(\sigma_{P_k}^{(s)})^2$ instead of μ_{P_k} and $\sigma_{P_k}^2$ when computing the mean and variance of the total conditional MAI Ψ given by (5.14) and (5.15). The goal is to develop expressions for $\mu_{P_k}^{(s)}$ and $(\sigma_{P_k}^{(s)})^2$ based on the effective power in the interference at each stage of the receiver. Since interference cancellation can only be performed on synchronized users, we must develop separate expressions for $\mu_{P_k}^{(s)}$ and $(\sigma_{P_k}^{(s)})^2$ based on whether user k is synchronized or not.

5.3.1 First Stage Multiple Access Interference

The interference characteristics of the MAI due to synchronized and unsynchronized users will be the same at the first stage, since there has been no interference cancellation at this point. Since cancellation is not performed on unsynchronized interference at later stages, the unsynchronized interference at future stages will be the same as at stage 1.

Using (5.10) and (5.12), we can solve for the interference caused by user k ($1 \leq k \leq K$) to user j ($1 \leq j \leq K_1$) during the bit interval i as

$$I_{k,j}^{(1)} = \sqrt{\frac{P_k}{2}} \cos(\phi_k - \phi_j) \int_{iT+\tau_j}^{(i+1)T+\tau_j} b_k(t-\tau_k) a_k(t-\tau_k) a_j(t-\tau_j) dt. \tag{5.18}$$

Since users k and j will in general not be bit-aligned, the integral of (5.18) can be rewritten in terms of the two bits of user k (bit $i-1$ and bit i) that overlap bit i of user j as

$$\begin{aligned} I_{k,j}^{(1)} &= \sqrt{\frac{P_k}{2}} \cos(\phi_k - \phi_j) \left\{ \int_{iT+\tau_j}^{iT+\tau_k} b_{k,i-1} a_k(t-\tau_k) a_j(t-\tau_j) dt \right. \\ &\quad \left. + \int_{iT+\tau_k}^{(i+1)T+\tau_j} b_{k,i} a_k(t-\tau_k) a_j(t-\tau_j) dt \right\}. \end{aligned} \tag{5.19}$$

In [60], it is shown that this can be reduced to

$$I_{k,j}^{(1)} = T_c \sqrt{\frac{P_k}{2}} \cos(\phi_k - \phi_j) W_k, \tag{5.20}$$

where W_k is defined in [60] and it is shown that $E[W_k] = 0$ and $E[W_k^2] = 2N/3$.

To compute the total multiple access interference, we need to know the mean and variance of the power of the interference, $\mu_{P_k}^{(1)}$ and $(\sigma_{P_k}^{(1)})^2$, respectively. Since there has been no interference cancellation at this point, these are simply the mean and variance of each individual power level P_k. Using (5.14) and (5.15), μ_Ψ and σ_Ψ can be computed and used to compute the BER via (5.16).

5.3.2 Synchronized MAI for Stages 2 and Higher

While the MAI due to unsynchronized users remains constant throughout the multistage receiver, the MAI of synchronized users will change due to interference cancellation. We can write the interference for a synchronized user j caused by synchronized user k at stages 2 and higher by

$$I_{k,j}^{(s+1)} = I_{k,j}^{(1)} - \hat{I}_{k,j}^{(s+1)}, \tag{5.21}$$

where $\hat{I}_{k,j}^{(s+1)}$ represents the MAI caused by the estimates $\hat{s}_k^{(s+1)}(t)$. Therefore, the MAI at stage $s+1$ is given by the original MAI minus the estimate of the original MAI, so that $I_{k,j}^{(s+1)}$ represents the residual MAI after interference cancellation. Using (5.6), (5.7), and (5.10), we can write $\hat{I}_{k,j}^{(s+1)}$ as

$$\begin{aligned}\hat{I}_{k,j}^{(s+1)} &= \frac{1}{T}\cos(\phi_k - \phi_j)\left\{\int_{iT+\tau_j}^{iT+\tau_k} Z_{k,i-1}^{(s)} a_k(t-\tau_k)a_j(t-\tau_j)dt \right. \\ &\quad \left. + \int_{iT+\tau_k}^{(i+1)T+\tau_j} Z_{k,i}^{(s)} a_k(t-\tau_k)a_j(t-\tau_j)dt\right\}. \end{aligned} \tag{5.22}$$

We can further simplify this expression for the interference estimate *provided* that we make the assumption that the decision statistic $Z_{k,i}^{(s)}$ can be pulled outside of the integral, which the definition of (5.10) will not strictly allow. Much of the prior research into multistage receivers has simply assumed that this could be done. However, doing so in effect ignores any portion of $Z_{k,i}^{(s)}$ that is correlated with user j's PN code. Since the interference of user j to user k is embedded in $Z_{k,i}^{(s)}$, there will be some correlation present. It is this term that makes the expected value of the interference estimates non-zero and introduces a bias (non-zero mean) into the decision statistic of user j, as will be discussed in more detail in Section 5.4.6.

For now, however, we will assume that the decision statistic can be pulled out of the integral without repercussion. In that case, the expression for the interference estimate reduces to

$$\begin{aligned}\hat{I}_{k,j}^{(s+1)} &= \frac{1}{T}\cos(\phi_k - \phi_j)\left\{Z_{k,i-1}^{(s)} \int_{iT+\tau_j}^{iT+\tau_k} a_k(t-\tau_k)a_j(t-\tau_j)dt \right. \\ &\quad \left. + Z_{k,i}^{(s)} \int_{iT+\tau_k}^{(i+1)T+\tau_j} a_k(t-\tau_k)a_j(t-\tau_j)dt\right\}. \end{aligned} \tag{5.23}$$

By substituting (5.19) and (5.23) into (5.21), we obtain

$$I_{k,j}^{(s+1)} = \cos(\phi_k - \phi_j)\left\{\left[\sqrt{\frac{P_k}{2}}b_{k,i-1} - \frac{Z_{k,i-1}^{(s)}}{T}\right]\int_{iT+\tau_j}^{iT+\tau_k} a_k(t-\tau_k)a_j(t-\tau_j)dt\right.$$

$$+\left[\sqrt{\frac{P_k}{2}}b_{k,i}-\frac{Z_{k,i}^{(s)}}{T}\right]\int_{iT+\tau_k}^{(i+1)T+\tau_j}a_k(t-\tau_k)a_j(t-\tau_j)dt\Bigg\}. \tag{5.24}$$

To put (5.24) into the form of (5.19), we define $\nu_{k,i}^{(s+1)}$ to be

$$\begin{aligned}\nu_{k,i}^{(s+1)} &= 2\left[\sqrt{\frac{P_k}{2}}b_{k,i}-\frac{Z_{k,i}^{(s)}}{T}\right]^2 \\ &= P_k-\sqrt{8P_k}b_{k,i}\frac{Z_{k,i}^{(s)}}{T}+2\left(\frac{Z_{k,i}^{(s)}}{T}\right)^2.\end{aligned} \tag{5.25}$$

Thus $\nu_{k,i}^{(s+1)}$ can be interpreted as the effective power in the interference from synchronized user k during bit interval i after $s+1$ stages. We can now rewrite (5.24) in the form of (5.20) as

$$I_{k,j}^{(s+1)}=T_c\sqrt{\frac{\nu_{k,i}^{(s+1)}}{2}}\cos(\phi_k-\phi_j)W_k. \tag{5.26}$$

The overall MAI at stage $s+1$, $\Psi^{(s+1)}$, can be found by modifying (5.13) to account for the interference cancellation process,

$$\Psi^{(s+1)}=E\left[\left(\sum_{k=1,k\neq j}^{K}I_{k,j}^{(s+1)}\right)^2\mid\{\phi_k\},\{\tau_k\},\{P_k\},B\right]. \tag{5.27}$$

Since all K users contribute to $\Psi^{(s+1)}$, the terms $I_{k,j}^{(s+1)}$ must be defined appropriately based on whether the interfering user k is synchronized or not. For synchronized users, (5.26) should be used. For unsynchronized users, the interference will not change from stage to stage and (5.20) should be used.

5.3.3 Derivation of Mean of Effective Signal Power

In this section, we calculate the mean of the effective signal power $\nu_{k,i}^{(s+1)}$. The mean can be found directly from (5.25) by taking the expectation as

$$\mu_{P_k}^{(s+1)}=E[\nu_{k,i}^{(s+1)}]=E\left[P_k-\sqrt{8P_k}b_{k,i}\frac{Z_{k,i}^{(s)}}{T}+2\left(\frac{Z_{k,i}^{(s)}}{T}\right)^2\right]. \tag{5.28}$$

Using the expression for the decision statistic given by (5.12), the mean can be rewritten as

$$\begin{aligned}\mu_{P_k}^{(s+1)} &= E\left[P_k - \sqrt{8P_k}\frac{b_{k,i}}{T}\left(\eta + \sqrt{\frac{P_k}{2}}Tb_{k,i} + \sum_{l=1,l\neq k}^{K} I_{l,k}^{(s)}\right)\right. \\ &\quad \left. + \frac{2}{T^2}\left(\eta + \sqrt{\frac{P_k}{2}}Tb_{k,i} + \sum_{l=1,l\neq k}^{K} I_{l,k}^{(s)}\right)^2\right] \\ &= 2E\left[\left(\frac{\eta}{T}\right)^2\right] + \frac{2}{T^2}E\left[\left(\sum_{l=1,l\neq k}^{K} I_{l,k}^{(s)}\right)^2\right], \end{aligned} \tag{5.29}$$

using $E[\eta] = 0$ and assuming that $E[I_{l,k}^{(s)}] \approx 0$. Again, the mean is not identically zero due to the correlated terms in the decision statistic. The true value of $E[I_{l,k}^{(s)}]$ is discussed in more detail in Section 5.4.6. We may often assume it has zero mean, particularly if the system is not heavily loaded (a large number of active users) or if there are other significant factors contributing to the noise in the decision statistic (this can be channel noise, fading, quantization noise, interference from unsynchronized users or other uncanceled components, etc.) For this analysis we will assume $E[I_{l,k}^{(s)}] = 0$. Since we are assuming that the terms $I_{l,k}^{(s)}$ are uncorrelated, we have

$$E\left[\left(\sum_{l=1,l\neq k}^{K} I_{l,k}^{(s)}\right)^2\right] = E\left[\sum_{l=1,l\neq k}^{K}\left(I_{l,k}^{(s)}\right)^2\right]. \tag{5.30}$$

We can then solve for the variance of the multiple access interference from the previous stage s as

$$\begin{aligned}\frac{1}{T^2}E\left[\sum_{l=1,l\neq k}^{K}\left(I_{l,k}^{(s)}\right)^2\right] &= \frac{1}{T^2}E\left[\sum_{l=1,l\neq k}^{K} T_c^2\cos^2(\phi_l - \phi_k)\frac{\nu_{l,i}^{(s)}}{2}W_k^2\right] \\ &= \frac{1}{6N}\sum_{l=1,l\neq k}^{K}\mu_{P_k}^{(s)}, \end{aligned} \tag{5.31}$$

where we have used $E[\cos^2(\phi_l - \phi_k)] = 1/2$. Using $E = [(\eta/T)^2] = N_o/(4T)$ and (5.31), we can solve (5.29) to be

$$\mu_{P_k}^{(s+1)} = \frac{N_o}{2T} + \frac{1}{3N}\sum_{l=1,l\neq k}^{K}\mu_{P_l}^{(s)}, \qquad 1 \le k \le K_1. \tag{5.32}$$

We now have a recursive definition for the mean of the effective interference power.

5.3.4 Variance of Effective Signal Power

In this section, we develop a definition for the variance of the effective interference power, $(\sigma_{P_k}^{(s+1)})^2$. The variance by definition is given by

$$(\sigma_{P_k}^{(s+1)})^2 = E\left[\left(\nu_k^{(s+1)}\right)^2\right] - \left(\mu_{P_k}^{(s+1)}\right)^2. \tag{5.33}$$

Since we found $\mu_{P_k}^{(s+1)}$ in Section 5.3.3, we need to find an expression for $E[(\nu_k^{(s+1)})^2]$. Because of the mathematical nature of the derivation, the explicit derivation is given in Appendix A. The expression for the variance of the effective interference power at stage $s+1$ caused by user k, $1 \le k \le K_1$, is shown to be

$$\begin{aligned}(\sigma_{P_k}^{(s+1)})^2 &= \frac{N_o^2}{2T^2} + \frac{4N_o}{T^3}\mu_\psi^{(s)} - \frac{4}{T^4}\left(\mu_\Psi^{(s)}\right)^2 + \frac{9(4N^2-3N)}{40N^4}\sum_{l=1,l\neq k}^{K}\left[(\sigma_{P_l}^{(s)})^2 + \left(\mu_{P_l}^{(s)}\right)^2\right] \\ &\quad + \frac{4N^2-9N+13}{12N^4}\sum_{l=1,l\neq k}^{K}\sum_{m=1,m\neq l\neq k}^{K}\mu_{P_l}^{(s)}\mu_{P_l}^{(s)}. \end{aligned}\tag{5.34}$$

5.3.5 Calculating BER for Stages 2 and Beyond

Once the mean and variance of the effective interference power is known, calculating the BER is a straightforward process. First, we must find the mean and variance of the overall MAI at stage s. The mean is given by (A.15), and the variance is a straightforward extension of (5.15) given by

$$\begin{aligned}\left(\sigma_\Psi^{(s)}\right)^2 &= \frac{T_c^4}{4}\left[\frac{23N^2+18N-18}{360}\sum_{k=1,k\neq j}^{K}\left(\mu_{P_k}^{(s)}\right)^2 + \frac{7N^2+2N-2}{40}\sum_{k=1,k\neq j}^{K}\left(\sigma_{P_k}^{(s)}\right)^2\right. \\ &\quad \left. + \frac{N-1}{36}\sum_{k=1,k\neq j}^{K}\sum_{l=1,l\neq k\neq j}^{K}\mu_{P_k}^{(s)}\mu_{P_j}^{(s)}\right]. \end{aligned}\tag{5.35}$$

The appropriate expressions for $\mu_{P_k}^{(s)}$ and $\sigma_{P_k}^{(s)}$ must be used, depending on whether the interfering user is synchronized or not. For synchronized users, $1 \le k \le K_1$, equations (5.32) and (5.34) should be used. For unsynchronized users, $K_1+1 \le k \le K_2$, these values will always be the mean and standard deviation of the received power P_k.

The improved Gaussian approximation to the BER can then be calculated by modifying (5.16) to account for the multiple receiver stages,

$$P_{b,d}^{(s)} \approx \frac{2}{3}Q\left(\sqrt{\frac{P_d T^2}{2\left(\mu_\Psi^{(s)} + \frac{N_o T}{4}\right)}}\right) + \frac{1}{6}Q\left(\sqrt{\frac{P_d T^2}{2\left(\mu_\Psi^{(s)} + \sqrt{3}\sigma_\Psi^{(s)} + \frac{N_o T}{4}\right)}}\right)$$

$$+\frac{1}{6}Q\left(\sqrt{\frac{P_d T^2}{2\left(\mu_\Psi^{(s)} - \sqrt{3}\sigma_\Psi^{(s)} + \frac{N_o T}{4}\right)}}\right). \tag{5.36}$$

5.3.6 Numerical Results

This section discusses numerical results based on the analytical model presented in the previous section. The analytical model has been verified through simulation, which is discussed in detail in Section 5.4.

A spreading code length of $N = 128$ is used. A constant signal-to-noise ratio is maintained with respect to the desired user, where $E_b/N_o = 12$ dB is used. The bit energy is given by $E_b = PT$, and the noise power is defined in the system model of Section 5.2. The synchronized users are assumed to have constant power with $P_k = 1$ and E_b/N_o is measured with respect to this power level. There is a single unsynchronized user ($K_2 = 1$) whose power level varies about the synchronized user's power.

The first set of plots compares the BER vs. capacity for a multistage receiver (with between 1 and 4 stages) with a given unsynchronized interference level. Capacity refers to the number of synchronized users (K_1). In Fig. 5.1, there is no unsynchronized interference. In Fig. 5.2, the unsynchronized interferer is 6 dB below the synchronized users (the unsynchronized user has $E_b/N_o = 6$ dB). In Fig. 5.3, the unsynchronized user has the same power level as the other users ($E_b/N_o = 12$ dB). In Fig. 5.4, the unsynchronized user is 6 dB above the other users ($E_b/N_o = 18$ dB). These plots show the improvement possible by adding stages to the multistage receiver to overcome the effects of the interference.

The second set of plots compares the BER vs. capacity with varying levels of unsynchronized interference power for a given stage in the receiver. These plots show the increase in BER caused by a single unsynchronized user as his received power increases. Plots are shown for 1, 2, 3, and 4 stage receivers in Figs. 5.5, 5.6, 5.7, and 5.8 respectively. For a small number of users, increasing the power in the unsynchronized interferer has a stronger influence than if there are a large number of synchronized users. The results make intuitive sense, as the large number of users will cause the synchronized MAI to dominate instead of the MAI due to the unsynchronized user.

These results have two key implications. The first is that some form of power control is still necessary, to ensure that when a user first begins transmitting, the power is set as low as possible to still allow for a rapid acquisition. The second is that the acquisition process needs to be as short as possible, to minimize the amount of time that the MAI of that user cannot be canceled.

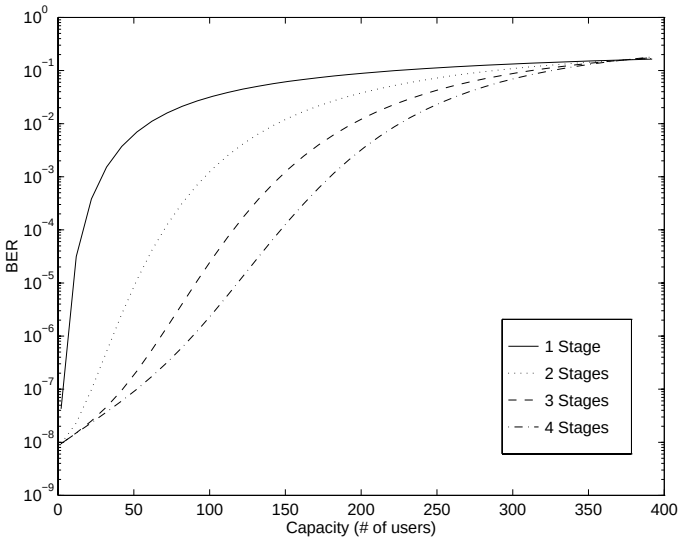

Figure 5.1: BER for No Unsynchronized Interference and Synchronized Users with $E_b/N_o =$ 12 dB

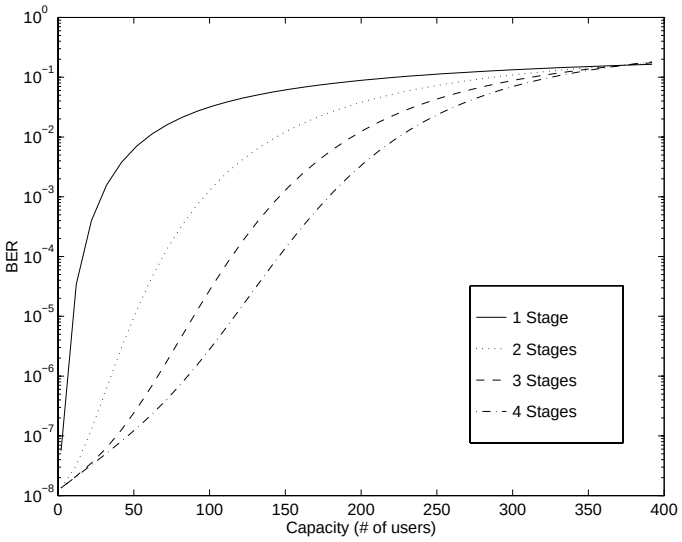

Figure 5.2: BER for Unsynchronized Interferer with $E_b/N_o = 6$ dB and Synchronized Users with $E_b/N_o = 12$ dB

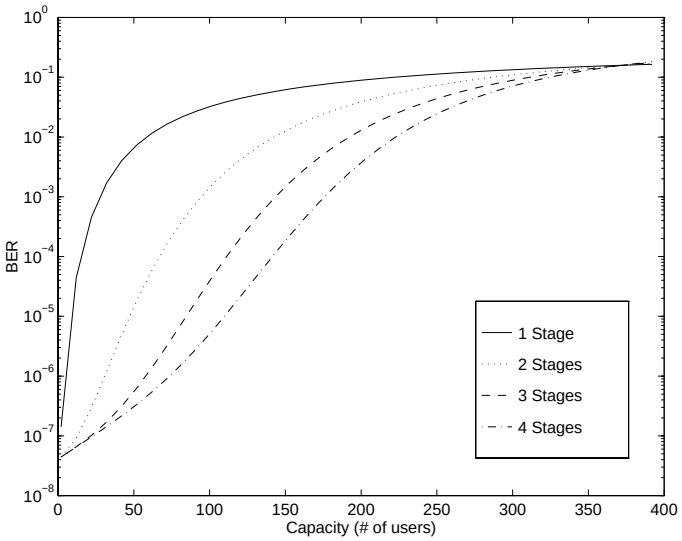

Figure 5.3: BER for Unsynchronized Interferer with $E_b/N_o = 12$ dB and Synchronized Users with $E_b/N_o = 12$ dB

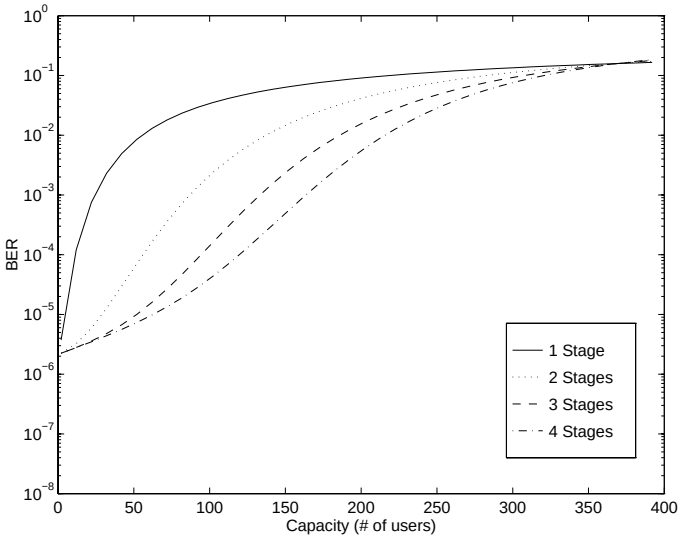

Figure 5.4: BER for Unsynchronized Interferer with $E_b/N_o = 18$ dB and Synchronized Users with $E_b/N_o = 12$ dB

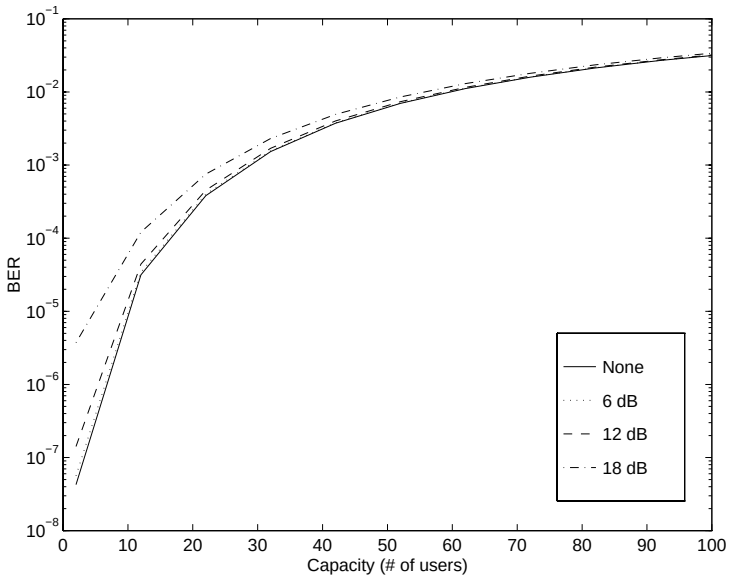

Figure 5.5: BER for Unsynchronized Interference and 1 Stage Receiver

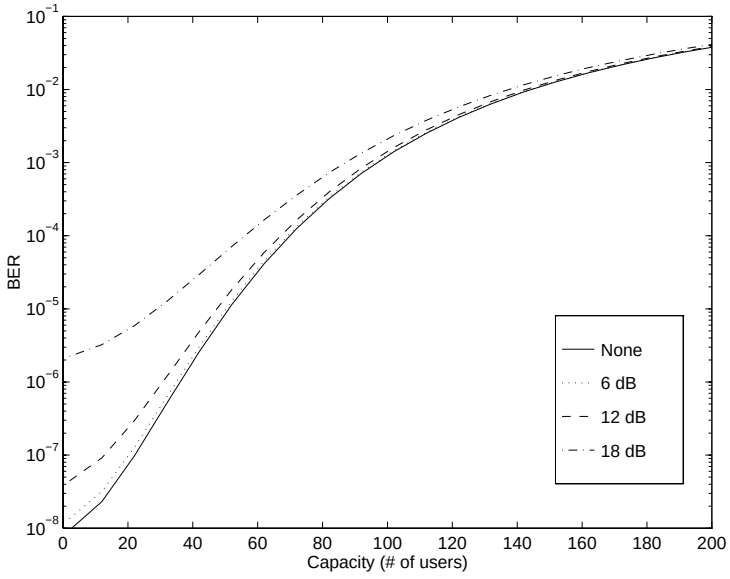

Figure 5.6: BER for Unsynchronized Interference and 2 Stage Receiver

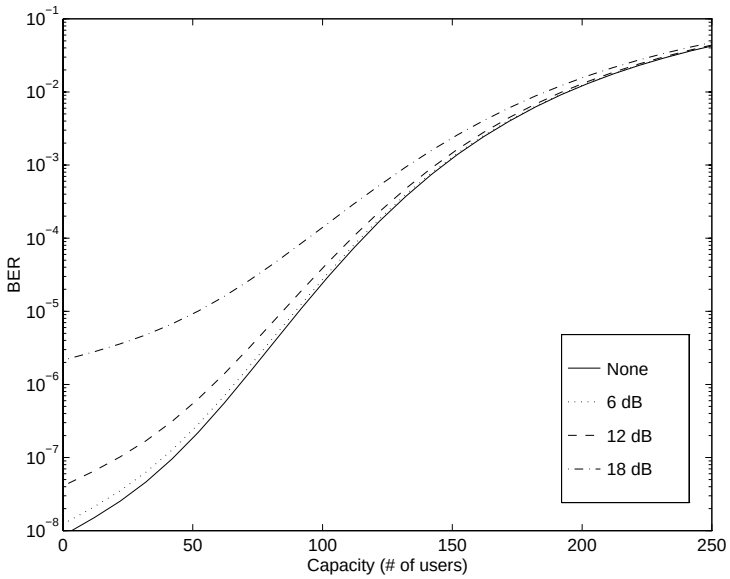

Figure 5.7: BER for Unsynchronized Interference and 3 Stage Receiver

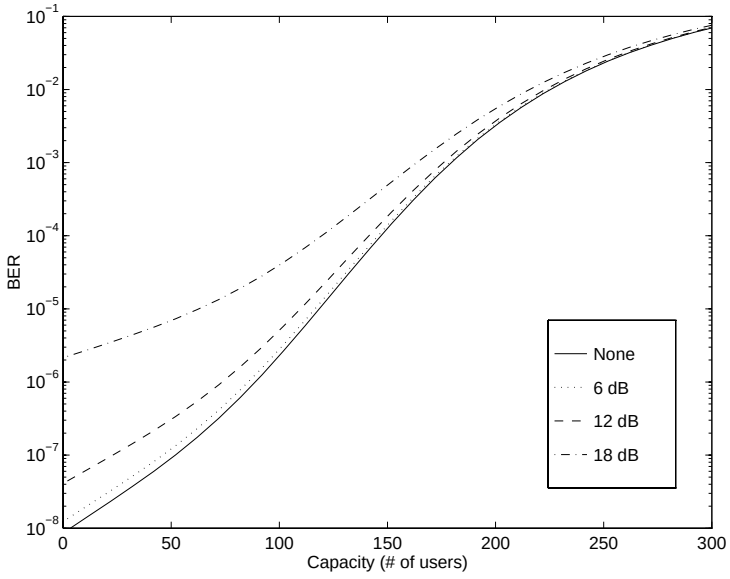

Figure 5.8: BER for Unsynchronized Interference and 4 Stage Receiver

5.4 Simulation Model with Unsynchronized Interference

A simulation model was constructed using the Signal Processing Workstation (SPW) 3.1 to verify the analytical results obtained in the previous section. SPW is a block diagram editor for communications systems, with the models typically based on hardware implementations. This emphasis on hardware-based modeling (as opposed to mathematically-based models) makes the transition from software model to DSP testbed more straightforward. The DSP testbed approach is discussed in more detail in Chapter 8. The nature of SPW requires that many issues such as timing and component interaction be explicitly defined.

5.4.1 System Model

A multistage receiver using one or two stages has been modeled in SPW for an AWGN channel. The filenames are *synch1a1* and *synch1a2* for systems employing the one and two stage receivers, respectively. The SPW block diagrams are shown in Figs. 5.9 and 5.10. There are 7 synchronized users ($K_1 = 7$) in each CDMA system, with one unsynchronized user ($K_2 = 1$). The spreading code has 31 chips per bit ($N = 31$) and the codes are generated randomly and do not repeat. The data rate is 9600 bps and the number of samples per chip, N_s, is 4. For the one stage system, the bank of transmitters is on the left side of the diagram, including the desired and unsynchronized interfering users. Each transmitted signal is passed through the channel, and then the desired user (user 1) is recovered at the receiver. For the two stage system, the received signal is passed to a bank of correlation receivers, then estimates of the interference are made and subtracted out, then user 1 is recovered. There are signal sinks at various places in the system model so that key signals can be plotted in SPW's Signal Calculator, if so desired.

5.4.2 Transmitter Model

The transmitter model is called *ss_tx_iq* and is shown in Fig. 5.11. The random time delay for each transmitter is modeled at the system level, not in the transmitter block itself. User 1 is considered the desired user and has $\tau_1 = 0$ and a random phase that is uniform over $[0, 2\pi)$ and changes after every bit period. All other users have a discrete delay that is uniform over $[0, NN_s - 1]$ samples, which changes at each bit transition. The discrete phase at the transmitter is generated randomly from a uniform distribution over $[0, 2\pi)$. The phase is also allowed to change once per bit at the bit transition period. All users have the same amplitude. Since the simulation uses a baseband model of a bandpass system,

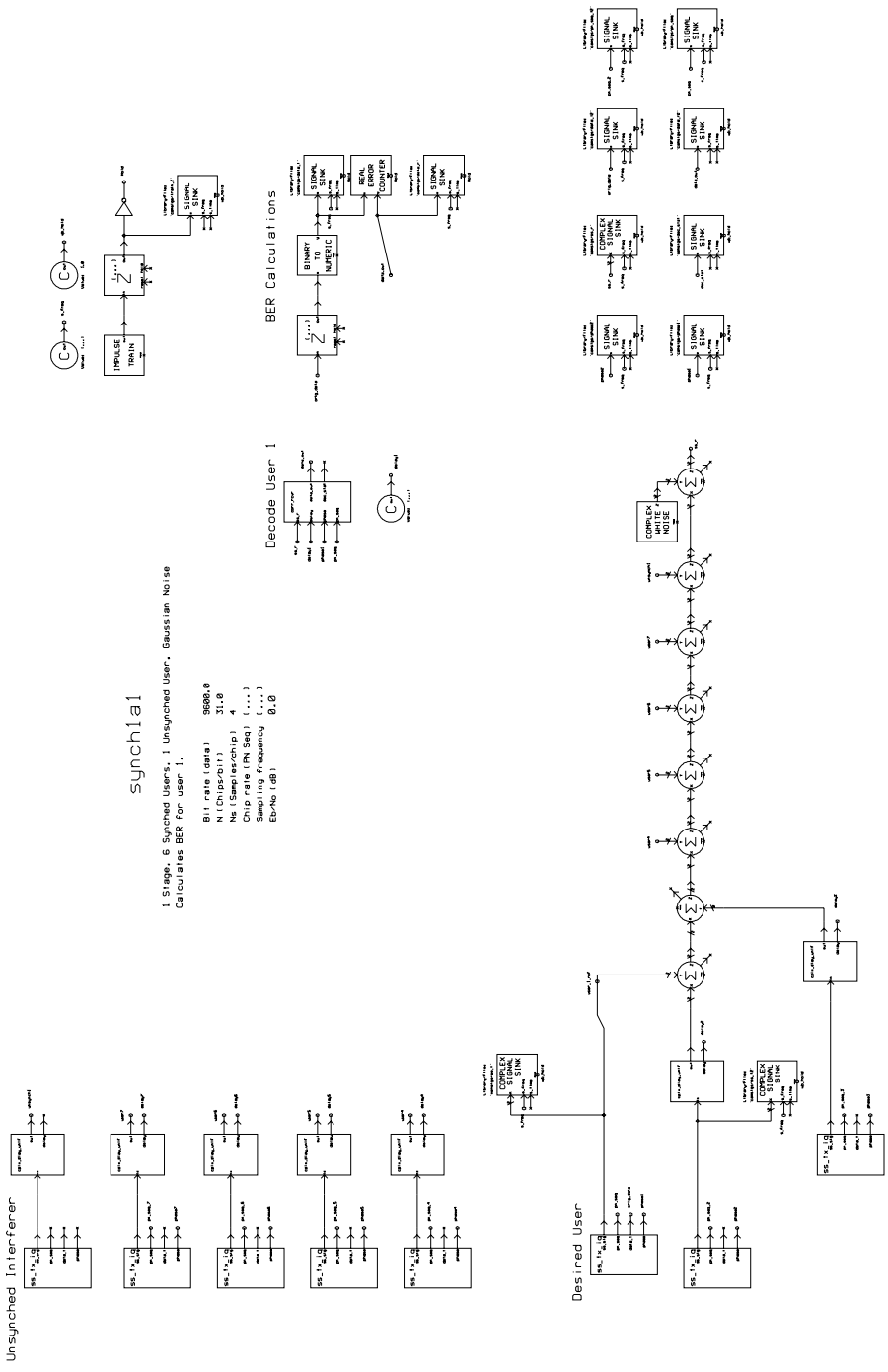

Figure 5.9: SPW One Stage Receiver

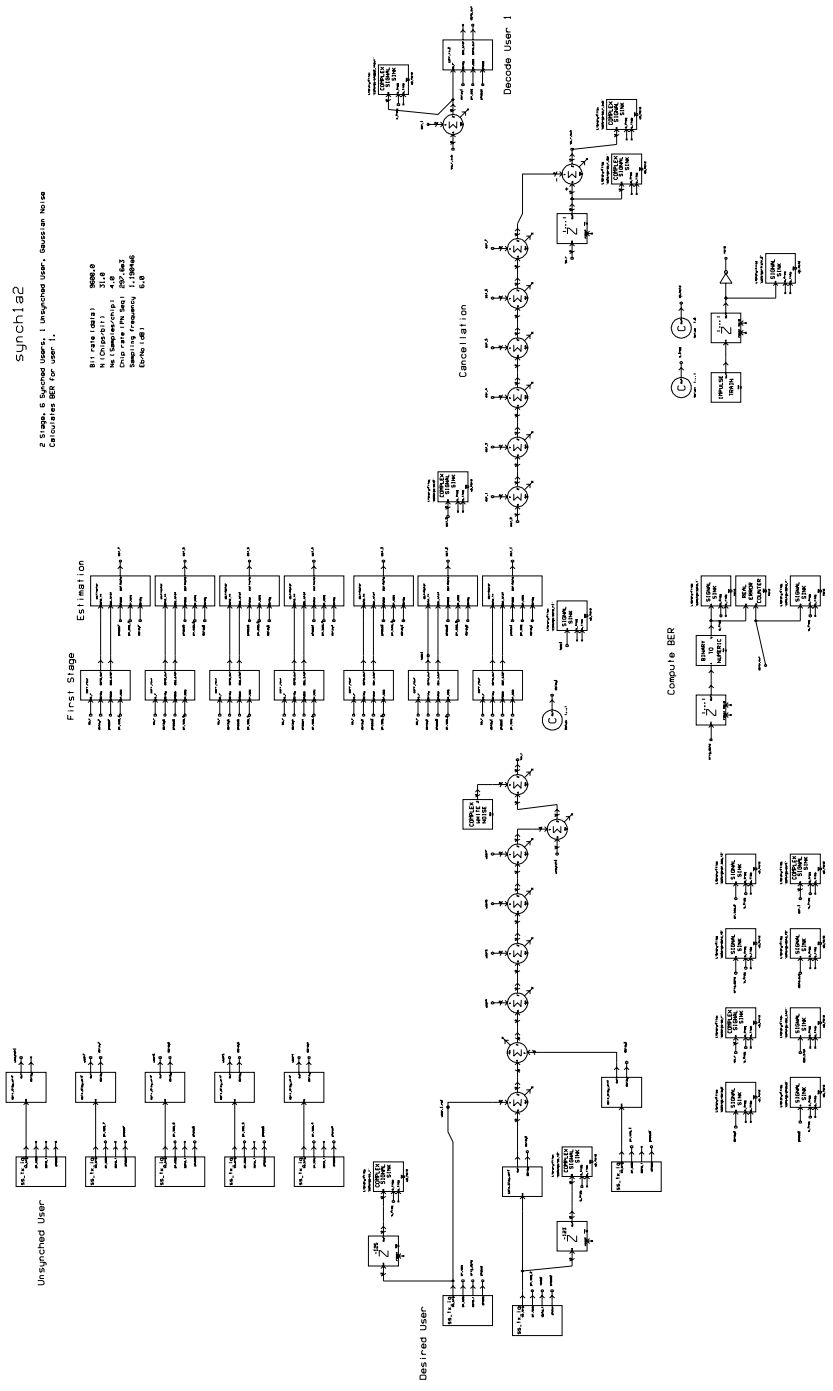

Figure 5.10: SPW Two Stage Receiver

in-phase (I) and quadrature (Q) channels are maintained at each point in the simulation. There are no filters at the transmitter. The PN code is generated randomly and does not repeat. The I and Q channels are formed by multiplying the data bit by $\cos(\phi_k)$ and $\sin(\phi_k)$ respectively, then multiplying each by the PN code. The transmitted power level can be adjusted by changing the amplitude block.

5.4.3 Channel Model

The channel is part of the system block diagrams and consists of summing all of the users together, to provide the multiple access interference, and the addition of AWGN. The amount of noise injected is dependent upon the desired ratio of bit energy to noise energy, E_b/N_o, which is a parameter that is set before simulation begins. The noise is calculated using a Gaussian noise source with

$$\sigma^2 = \frac{N_o f_s}{2}. \tag{5.37}$$

5.4.4 Receiver Model

The receiver itself is part of the system block diagram, but some of the subsystems are individual blocks. The receiver can have one or two stages. The one stage receiver consists of a single correlation receiver, to decode user 1. In an actual implementation, there will be $K_1 = 7$ receivers to recover the bits of all synchronized users. For the results needed from the simulation, however, only the desired user's BER is required, and so only that receiver is modeled to keep simulation runtime to a minimum. The first stage correlation receiver block is called *corr_rcvr_a* and is shown in Fig. 5.12. The receiver is passed the time and phase delay information, as it is assumed that a synchronization routine is perfectly estimating the delay and phase of that user's desired signal. The I and Q versions of the locally generated PN code replica are created by multiplying the PN code by $\cos(\phi_k)$ and $\sin(\phi_k)$ respectively, then delaying the result by τ_k. This is then correlated with the received signal and a bit estimate is made, which is passed to the BER calculator.

The first stage of the two stage receiver is a bank of $K_1 = 7$ correlation receivers, which have a decision statistic at the output that is used to determine the estimate of the power level. The signal estimate is then formed by attempting to reconstruct the received signal of user k, $r_k^{(s)}(t)$. The estimation block is called *estimator* and is shown in Fig. 5.13. A replica of user k's spreading code is delayed by the amount user k's transmitted signal has been delayed, τ_k, plus the delay caused by the initial correlation process, $NN_s - 1$. This delay occurs because each correlation requires NN_s samples, so after the initial sample

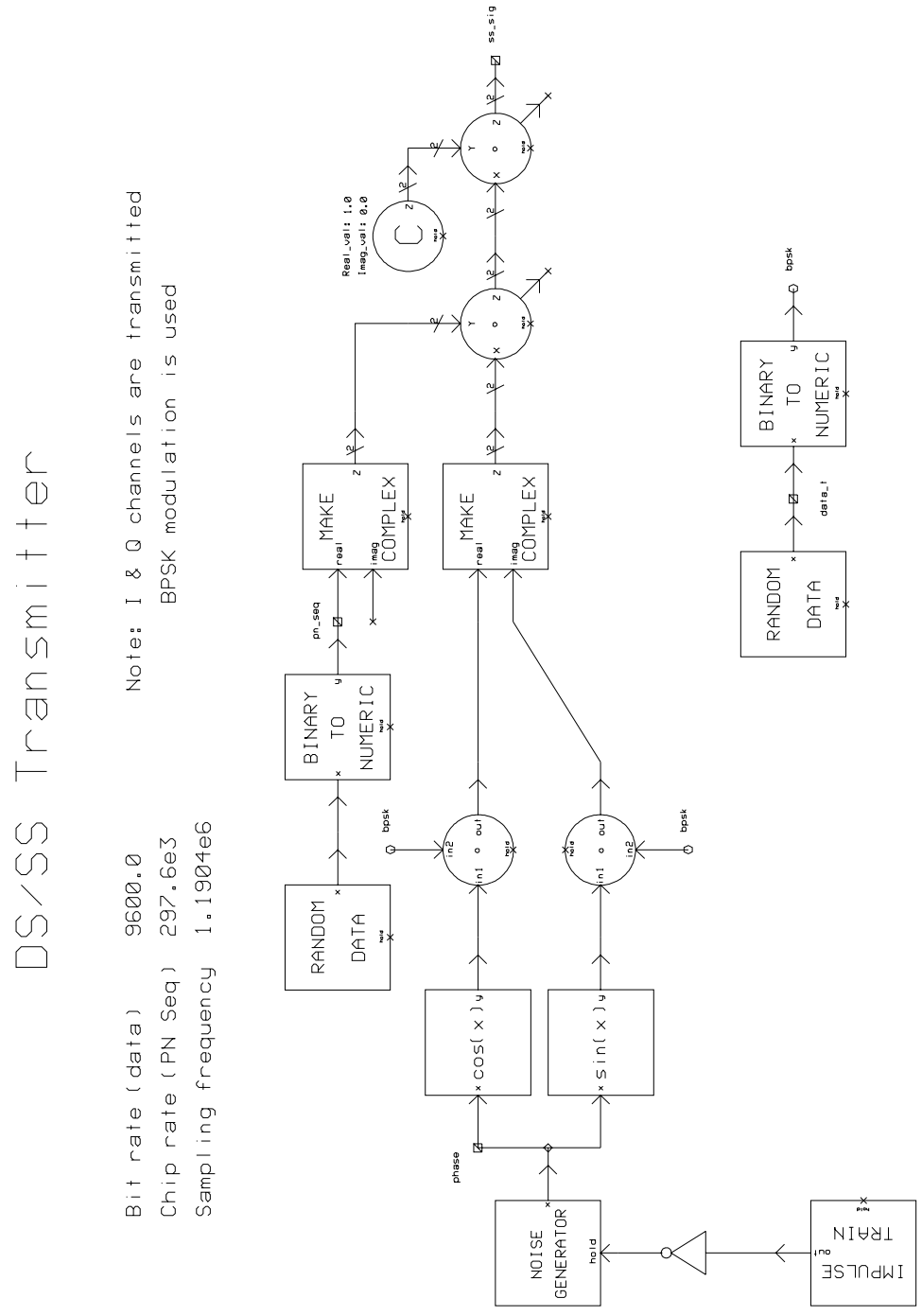

Figure 5.11: SPW CDMA Transmitter

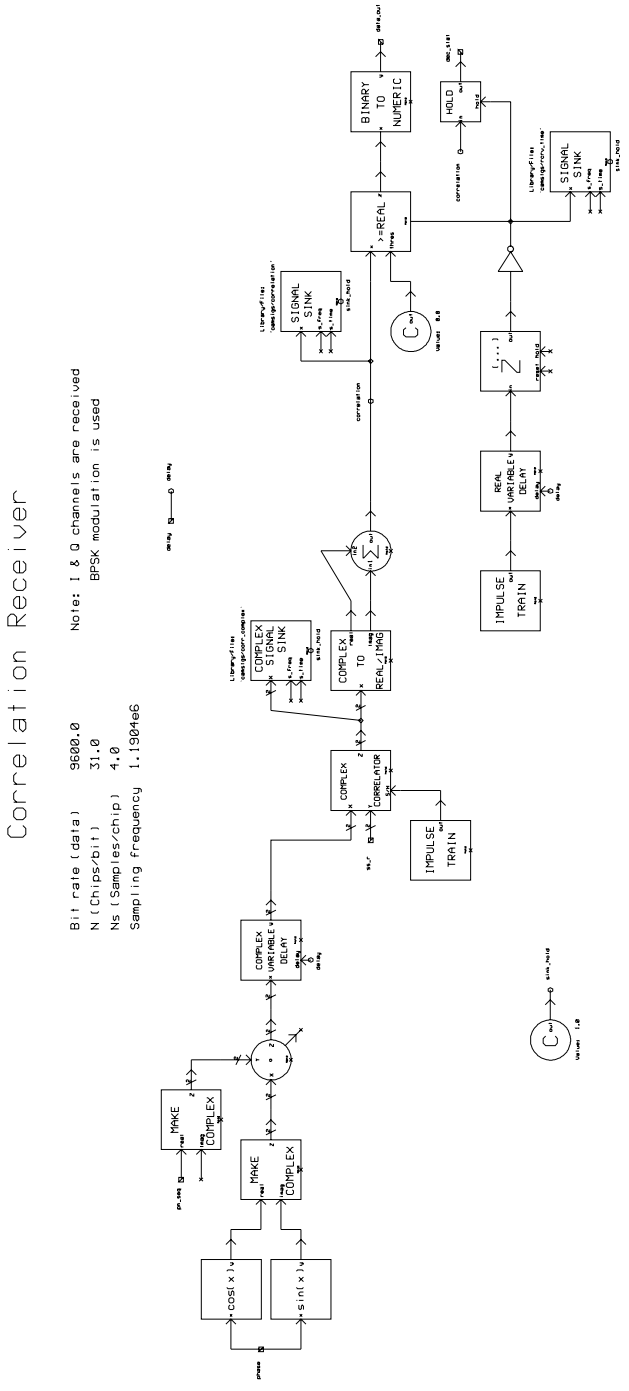

Figure 5.12: SPW Correlation Receiver (Stage 1)

arrives, the correlation process is not completed until the other $NN_s - 1$ samples arrive. This delayed PN replica is then multiplied by the data estimate for bit i at stage 2, $b_{k,i}^{(2)}$. This product is then multiplied by the estimate of the power level during bit interval i, which can be found from

$$\hat{P}_k^{(2)} = \frac{|Z_{k,i}^{(2)}|}{NN_s}. \tag{5.38}$$

This estimate is then multiplied by $\cos(\phi_k)$ and $\sin(\phi_k)$ to form I and Q estimates respectively, which form the output of the block.

At the system block level, all estimates are then subtracted from a delayed version of the received signal (it must be delayed to keep the resulting signal time aligned with the estimates, which are delayed due to the inherent delay of the correlation process). Since user 1 is again the desired user, the estimate of user 1's signal is then added back to the residual signal and this is passed to a second stage correlation receiver, which makes the bit decision. The second stage correlation receiver block is called *corr_rx_2* and is shown in Fig. 5.14. The only difference between the first and second stage correlation receivers is that an additional delay of $NN_s - 1$ samples is required in the second stage when constructing the locally generated PN code, to account for the delay in the residual signal caused by the initial correlation process. The bit estimate is made, which is passed to the BER calculator.

5.4.5 Comparison with Analytical Results

A plot of BER vs. E_b/N_o is given in Fig 5.15 for both analytical and simulation results, which was also published in [3]. The results are shown to be in close agreement for all values of E_b/N_o considered. The match is particularly close for the case of the single stage receiver, while there is some small deviation at lower BER for the two stage receiver. Therefore, the analytical results presented for the improved Gaussian approximation to BER for a multistage receiver with unsynchronized interference present have been validated by simulation results.

5.4.6 The Bias in the Decision Statistic

As noted in Section 5.4.5, there is some deviation in the analytic and simulation results for the two stage receiver. As discussed in [18], this occurs because we have assumed that $E[I_{l,k}^{(s)}] \approx 0$, when in fact this may not always be a valid approximation. We know that $E[I_{l,k}^{(1)}] = 0$, but the mean of the interference estimates $\hat{I}_{l,k}^{(s)}$ may not be zero (although it has been assumed by most previous researchers to be zero). There is actually a mean that increases as the number of synchronized (and thus canceled) users K_1 increases, and

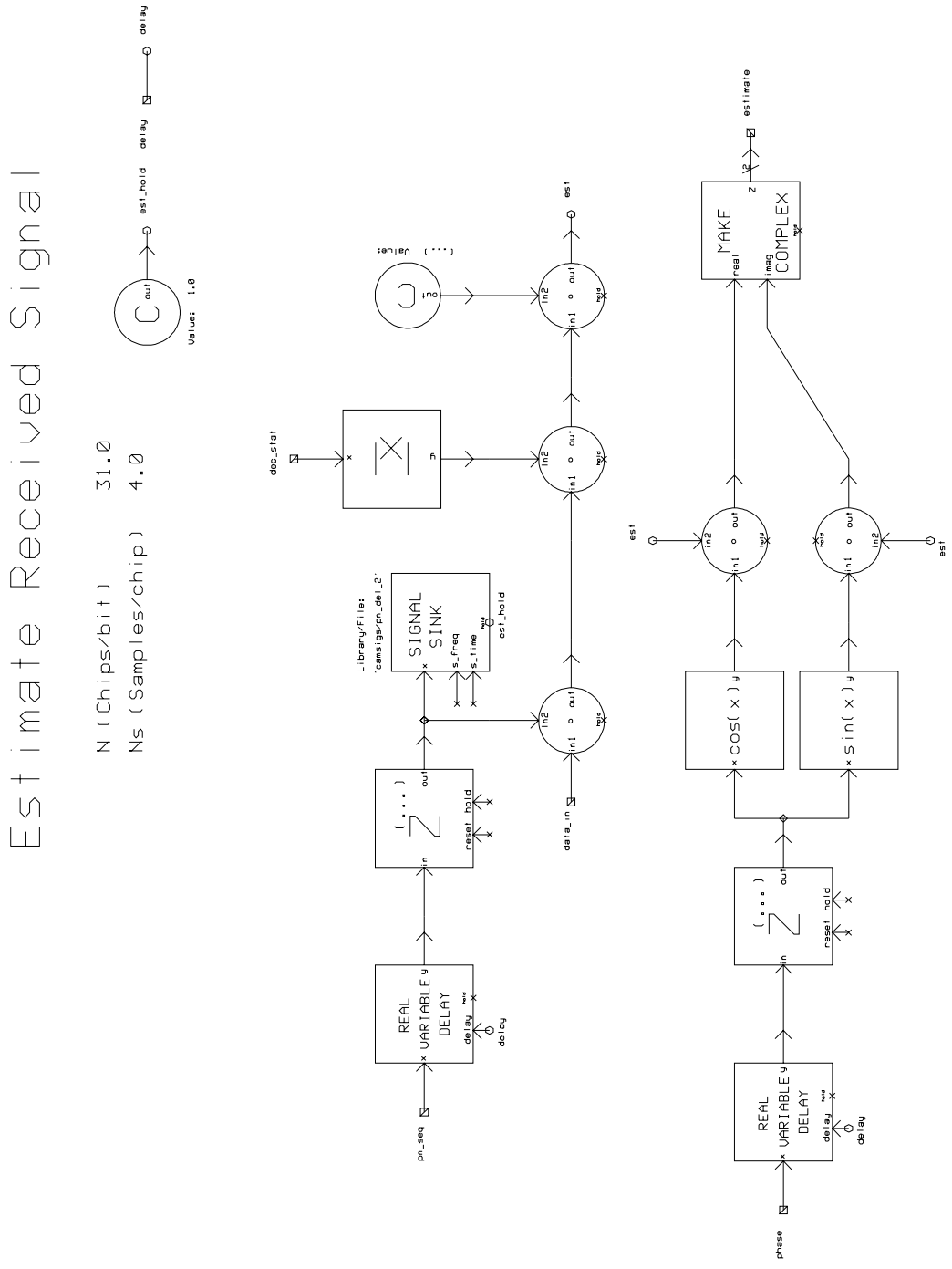

Figure 5.13: SPW Estimation Block

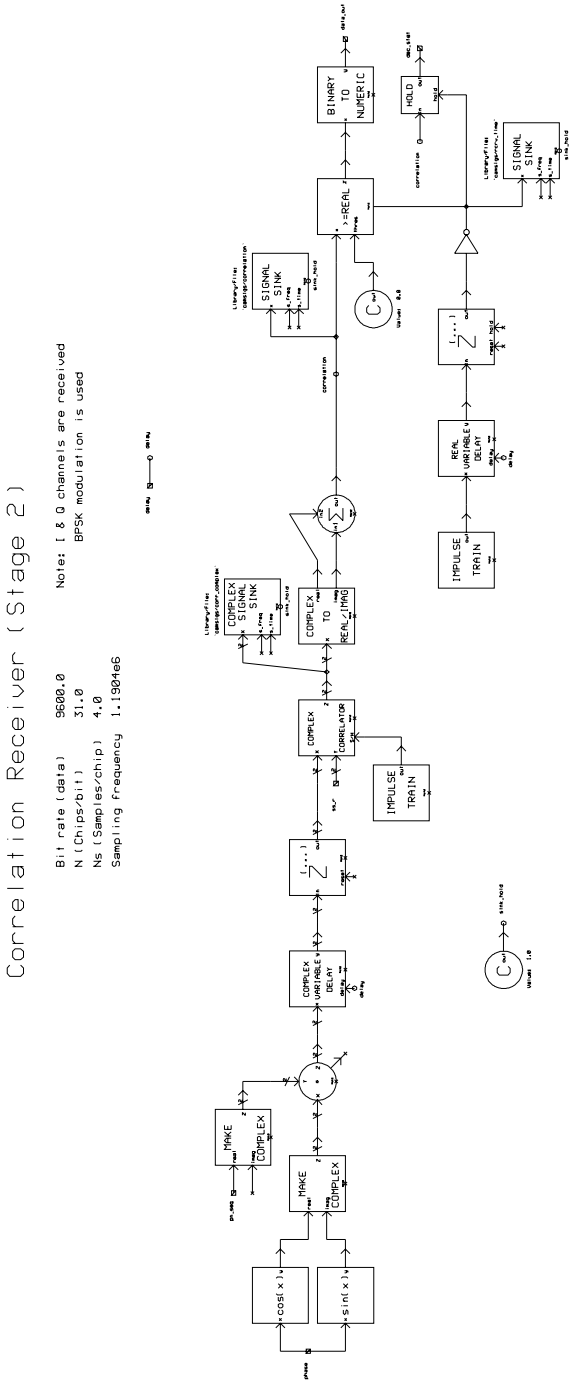

Figure 5.14: SPW Correlation Receiver (Stage 2)

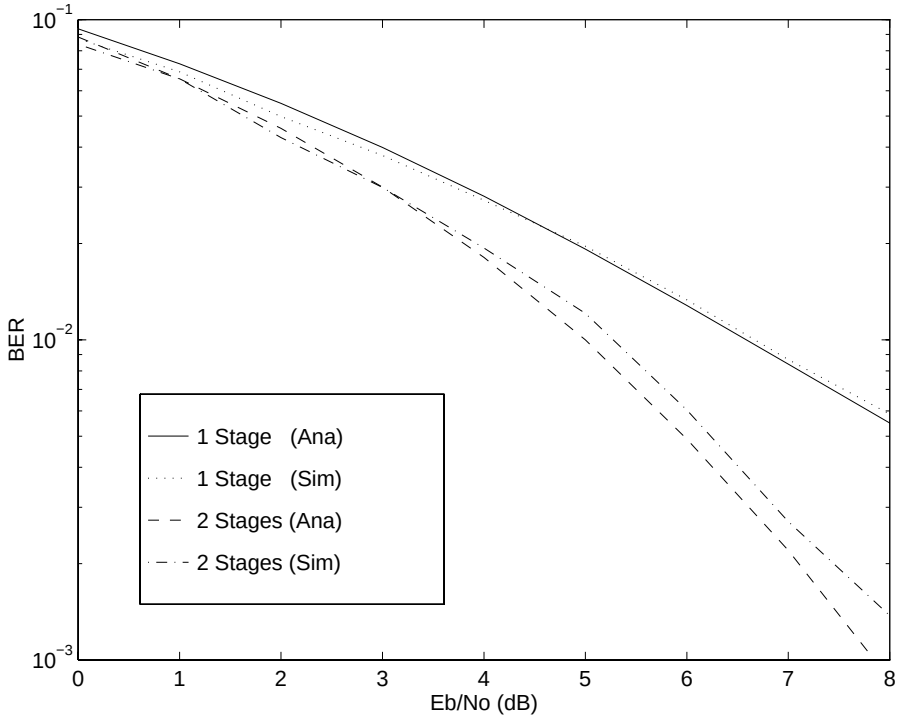

Figure 5.15: Analysis and Simulation Comparison

therefore this mean (bias) will be most evident when the number of active users is large, and when this bias forms a significant portion of the noise in the decision statistic (which in turn implies that it will significantly affect the overall BER of the receiver).

To see how this bias occurs, we need to look at the definition of the interference estimate $\hat{I}_{k,j}^{(s)}$ given in (5.24) (for now, we will assume that there are no unsynchronized users and that the total number of users is given by K). By substituting in the value of the decision statistic given in (5.12), we can rewrite (5.23) as

$$\begin{aligned}\hat{I}_{k,j}^{(s+1)} &= \cos(\phi_k - \phi_j)\left\{\int_{iT+\tau_j}^{iT+\tau_k}\left[\frac{\eta + \sqrt{\frac{P_k}{2}}Tb_{k,i-1} + \sum_{l=1,l\neq k}^{K} I_{k,l}^{(s)}}{T}\right]\right. \\ &\quad \cdot a_k(t-\tau_k)a_j(t-\tau_j)dt + \int_{iT+\tau_k}^{(i+1)T+\tau_j}\left[\frac{\eta + \sqrt{\frac{P_k}{2}}Tb_{k,i} + \sum_{l=1,l\neq k}^{K} I_{k,l}^{(s)}}{T}\right] \\ &\quad \left.\cdot a_k(t-\tau_k)a_j(t-\tau_j)dt\right\}. \end{aligned} \tag{5.39}$$

Note that the term due to the decision statistic is not pulled out of the integral. We can not automatically do this since embedded in the estimates at stage s, $\hat{I}_{k,j}^{(s)}$, are the decision statistics from stage $s-1$, $Z_{l,i}^{(s-1)}$, which are in turn dependent upon the estimates from that stage, $\hat{I}_{k,j}^{(s-1)}$. These estimates are in turn dependent upon the decision statistics from the previous stage $s-2$, $Z_{k,i}^{(s-2)}$, and so forth until we reach the decision statistic at stage $s=1$ and the first interference estimates at stage $s=2$. Therefore, for any arbitrary stage s, the interference estimate is related in this complex fashion to all of the preceding interference estimates and decision statistics. When we consider the additional complexity caused by sources such as channel noise, unsynchronized interference, quantization noise (as we shall see in Chapter 7), and other sources of degradation to the decision statistic, calculating the expected value (mean) of this term for any arbitrary stage is extremely difficult, and no closed-form expression exists due to this recursive nature.

To gain some insight into the nature of this bias, however, we shall simplify the problem and only consider the expected value of the first stage of interference estimates, $\hat{I}_{k,j}^{(2)}$, or the estimates that we make in stage 2 of the receiver. These estimates are given by

$$\begin{aligned}\hat{I}_{k,j}^{(2)} &= \frac{\cos(\phi_k-\phi_j)}{T}\left\{\int_{iT+\tau_j}^{iT+\tau_k}\left[\eta+\sqrt{\frac{P_k}{2}}Tb_{k,i-1}+\sum_{l=1,l\neq k}^{K}I_{k,l}^{(1)}\right]\right.\\ &\quad\cdot a_k(t-\tau_k)a_j(t-\tau_j)dt+\int_{iT+\tau_k}^{(i+1)T+\tau_j}\left[\eta+\sqrt{\frac{P_k}{2}}Tb_{k,i}+\sum_{l=1,l\neq k}^{K}I_{k,l}^{(1)}\right]\\ &\quad\left.\cdot a_k(t-\tau_k)a_j(t-\tau_j)dt\right\}. \qquad (5.40)\end{aligned}$$

If we take the mathematical expectation of this estimate, we get

$$\begin{aligned}E\left[\hat{I}_{k,j}^{(2)}\right] &= E\left[\frac{\cos(\phi_k-\phi_j)}{T}\left\{\int_{iT+\tau_j}^{iT+\tau_k}\left[\sqrt{\frac{P_k}{2}}Tb_{k,i-1}+\sum_{l=1,l\neq k}^{K}I_{k,l}^{(1)}\right]a_k(t-\tau_k)a_j(t-\tau_j)dt\right.\right.\\ &\quad\left.\left.+\int_{iT+\tau_k}^{(i+1)T+\tau_j}\left[\sqrt{\frac{P_k}{2}}Tb_{k,i}+\sum_{l=1,l\neq k}^{K}I_{k,l}^{(1)}\right]a_k(t-\tau_k)a_j(t-\tau_j)dt\right\}\right], \qquad (5.41)\end{aligned}$$

where we have used $E[\eta]=0$.

By looking at the expectation of the interference estimates at stage 2 as given in (5.42), we can see where the bias comes from. The estimate of user k's interference to user j, since it is based on the decision statistic from stage 1, is itself based on the actual interference from user j in stage 1. Thus, when we are calculating the residual interference estimate from user k's to user l, there is a component of this residual interference which is *correlated* with j. The rest of the terms in the summation will have a mean of zero. Therefore, (5.42)

reduces to

$$E\left[\hat{I}_{k,j}^{(2)}\right] = E\left[\frac{\cos(\phi_k-\phi_j)}{T}\left\{\int_{iT+\tau_j}^{iT+\tau_k}\left[\sqrt{\frac{P_k}{2}}Tb_{k,i-1}+I_{k,j}^{(1)}\right]a_k(t-\tau_k)a_j(t-\tau_j)dt + \int_{iT+\tau_k}^{(i+1)T+\tau_j}\left[\sqrt{\frac{P_k}{2}}Tb_{k,i}+I_{k,j}^{(1)}\right]a_k(t-\tau_k)a_j(t-\tau_j)dt\right\}\right]. \quad (5.42)$$

The term involving P_k is simply the interference from user k to user j, or $I_{k,j}^{(1)}$. This term is known to have $E[I_{k,j}^{(1)}]=0$, so we are left with only the term related to $I_{k,j}^{(1)}$, which is what will introduce the bias into the decision statistic. Therefore, (5.42) reduces to

$$E\left[\hat{I}_{k,j}^{(2)}\right] = E\left[\frac{\cos(\phi_k-\phi_j)}{T}\int_{iT+\tau_j}^{(i+1)T+\tau_j} I_{k,j}^{(1)}a_k(t-\tau_k)a_j(t-\tau_j)dt\right]. \quad (5.43)$$

We know from (5.19) the definition of $I_{k,j}^{(1)}$, so we can evaluate (5.43) by direct substitution,

$$E\left[\hat{I}_{k,j}^{(2)}\right] = E\left[\sqrt{\frac{P_k}{2}}\frac{\cos^2(\phi_k-\phi_j)}{T}\int_{iT+\tau_j}^{(i+1)T+\tau_j}\left\{\int_{iT+\tau_j}^{iT+\tau_k} b_{k,i-1}a_k(t-\tau_k)a_j(t-\tau_j)dt + \int_{iT+\tau_k}^{(i+1)T+\tau_j} b_{k,i}a_k(t-\tau_k)a_j(t-\tau_j)dt\right\}a_k(t-\tau_k)a_j(t-\tau_j)dt\right], \quad (5.44)$$

which reduces to [18]

$$E\left[\hat{I}_{k,j}^{(2)}\right] = -\frac{2}{3}\frac{T}{N}\sqrt{2P_k}. \quad (5.45)$$

If we assume that the interference estimates are independent, then the total bias in the sum of the $K-1$ interference estimates is just $K-1$ times this value, or

$$E\left[\sum_{k=1,k\neq j}^{K}\hat{I}_{j,k}^{(2)}\right] = -\frac{2}{3}\frac{(K-1)T}{N}\sqrt{2P_k}. \quad (5.46)$$

There is a negative mean to the interference estimates that is directly proportional to K and inversely proportional to N. Thus we would expect the bias to be most significant when K is large and N is relatively small, and when this negative mean will cause enough errors to be a relatively dominant source of errors in the receiver.

5.4.7 Using a Backoff Factor

The use of a backoff factor has been proposed [18] as a means of reducing the negative effects of the non-zero mean of the interference estimates. Instead of attempting to cancel

the interference based on the entire interference estimate, we instead only cancel a portion of that estimate. The decision statistic is now given by

$$Z_{j,i}^{(s)} = \eta + \sqrt{\frac{P_j}{2}} T b_{j,i} + \sum_{k=1,k\neq j}^{K} I_{k,j}^{(1)} - c\hat{I}_{k,j}^{(s)}, \tag{5.47}$$

where c is the backoff factor and is defined over the range $[0, 1]$. The backoff factor as presented in [18, 65] is used to reduce the mean of the interference estimates, and a performance evaluation in [18] shows that the backoff factor can indeed improve performance in heavily loaded systems. This improvement is attributed to the reduction of this mean. The performance improvement is in fact only partially due to the reduction of the mean, as the backoff factor is accomplishing more than a simple mean reduction.

Basic stochastic theory states that if we multiply a random variable x by a constant c, then the result cx will have a mean of $c\mu_x$ and a standard deviation of $c\sigma_x$, where μ_x and σ_x are the mean and standard deviation of x, respectively. Therefore, when we multiply the interference estimates by c, we are not only reducing the mean by a factor of c, but we are also reducing the standard deviation as well. This has several key implications for the performance of the multistage receiver.

First, some of the performance improvement observed when using a backoff factor is due to reducing the standard deviation, not just the mean. Reducing the mean of the estimates implies that we will reduce the amount which the estimates bias the decision statistic away from the desired value. Reducing the standard deviation implies that we are reducing the spread of the noise values about the mean. Thus we are less likely to have, if the decision statistic should be positive, a large noise component that will cause it to be negative.

Second, the use of a backoff factor is desirable *even if there is no mean present in the interference estimates*. Even if the receiver could perfectly compensate for the mean of the estimates by adding back in the appropriate offset, using a backoff factor will still reduce the standard deviation and thus can improve BER performance.

Third, all bit errors in the cancelation process do not have the same effect. In a traditional receiver, if the decision statistic is supposed to be positive, it does not matter if the receiver determines a decision statistic of -0.0001 or -1000. In either case, an error will be made and it will have the same effect on the BER. In a multistage receiver, however, that decision statistic will be used to compute the interference estimate in the next stage. Since we are making the wrong bit decision, we are not subtracting interference but in fact adding it. In this case, if the decision statistic is -0.0001, the amplitude of the estimate will be correspondingly small and we will not add much interference. If the decision statistic is -1000, the estimate will have a large amplitude and we will add a significant amount of interference. Thus we have made it more difficult for all of the other users to make the

proper bit estimate. It is therefore most important that we not only reduce the probability of making the wrong bit estimate, but reducing the probability that, given that the bit estimate is in fact wrong, that we are confident that the bit estimate is correct.

Finally, it implies that the backoff factor can be used to compensate for *any* degradation in the interference estimates, whether the problem is due to the mean of the interference estimates, unsynchronized interference, quantization noise, fading, power control, or any other factor. There is an optimum value of the backoff factor that will allow the receiver to subtract as much interference as possible without actually adding any interference. Research in [18] focused on determining a backoff factor for a given system loading (an appropriate assumption in that case since the only source of degradation considered was the heavy system loading). From a practical standpoint, however, it does not matter what causes the degradation in the decision statistic and therefore the interference estimates. The key parameters that determine the appropriate backoff factor are the moments of the interference estimates. These moments will not be available to a practical receiver; however, an estimate of the BER can be gained by a quality indicator in the receiver. The mobiles will transmit a known pattern with some regularity, and the receiver can decode those patterns and compare them to their true values and make an estimate of the BER. This quality indicator can then be used as an estimate of the confidence in the interference estimates at the next stage of the receiver, so that we can base the backoff factor on the overall noise in the interference estimates. This is not an entirely satisfactory solution since there are factors degrading the decision statistic other than the interference estimates; however, whatever degrades the decision statistic inherently degrades the interference estimates, so we would expect that determining the backoff factor in this manner should provide a reasonable value. In addition, this allows the backoff factor to be dynamic and change as the decision statistic degrades and improves over time. Finally, it allows a backoff factor to be chosen for each user, so that we can cancel any particular user based on our confidence in the interference estimate for that user. In this fashion, the use of the backoff factor can be thought of as an extension of selective cancellation, where instead of simply allowing $c \in \{0, 1\}$, we allow c to range anywhere from $[0, 1]$.

In conclusion, we have seen that the backoff factor is in fact not simply reducing the mean of the interference estimates, but reducing the standard deviation as well. Thus the backoff factor is a means of expressing our confidence in the interference estimates. Using a backoff factor is appropriate as long as there is any significant degradation in the decision statistic, regardless of the cause. Because the degradation is not simply caused by system loading, the backoff factor should be based on the overall noise in the decision statistic, not the ratio of users to spreading code length. This also allows the backoff factor to vary over time and to be assigned differently for each user.

5.5 Analysis of Single Dwell Acquisition

A metric must be chosen to evaluate a given synchronization technique. One commonly used for systems that continuously transmit data is the mean time of acquisition, which is the average time required to successfully search the region of uncertainty and acquire the signal [70]. For bursty transmissions where acquisition is not a necessary requirement, a comparison of detection probability against false alarm probability is a more suitable metric. Since the mobile communication systems considered here use continuously operating links, mean acquisition time will be studied. Expressions for the probabilities of detection and false alarm must still be derived as they are parameters of the mean acquisition time.

5.5.1 Single Dwell System Model

One common form of acquisition is the single dwell time system [69], where a single integration is used in the search process. The single dwell technique operates by searching q cells, where q is some integer multiple of the PN code length. If the code acquisition loop is updated in quarter chip increments, then there will be $q = 4N$ cells to be searched. If the output of the integration crosses some set threshold, then a verification mode is entered (in which either a longer dwell time is used in the integration process, or the code tracking mode is entered). If a false alarm occurs, when the routine detects a signal when the desired signal is not present, there will be some penalty time $K_p\tau_D$ seconds that must pass before the routine can attempt to acquire the true signal. The acquisition time is a random variable, although explicitly determining its probability distribution function is quite difficult in practice. Therefore, the mean and variance are usually determined.

The search algorithm of the single dwell technique can be well understood in terms of a flow diagram [69]. For notational simplicity, the standard unit of time will be the dwell time, τ_D, and all delays will be in units of dwell time. If we determine that acquisition has been achieved for a given cell, this is referred to as a hit. Consider the flow graph shown in Fig. 5.16. The probability that the two PN codes are properly phase aligned, P_1, is given by

$$P_1 = \frac{1}{q} \tag{5.48}$$

since there are q cells to be searched and it is equally probable that the true code phase could lie in any of the q cells. For any node i, $1 \leq i \leq q$, if we have not discovered the correct cell, the probability that the true code phase is in cell i is given by

$$P_i = \frac{1}{q+1-i}. \tag{5.49}$$

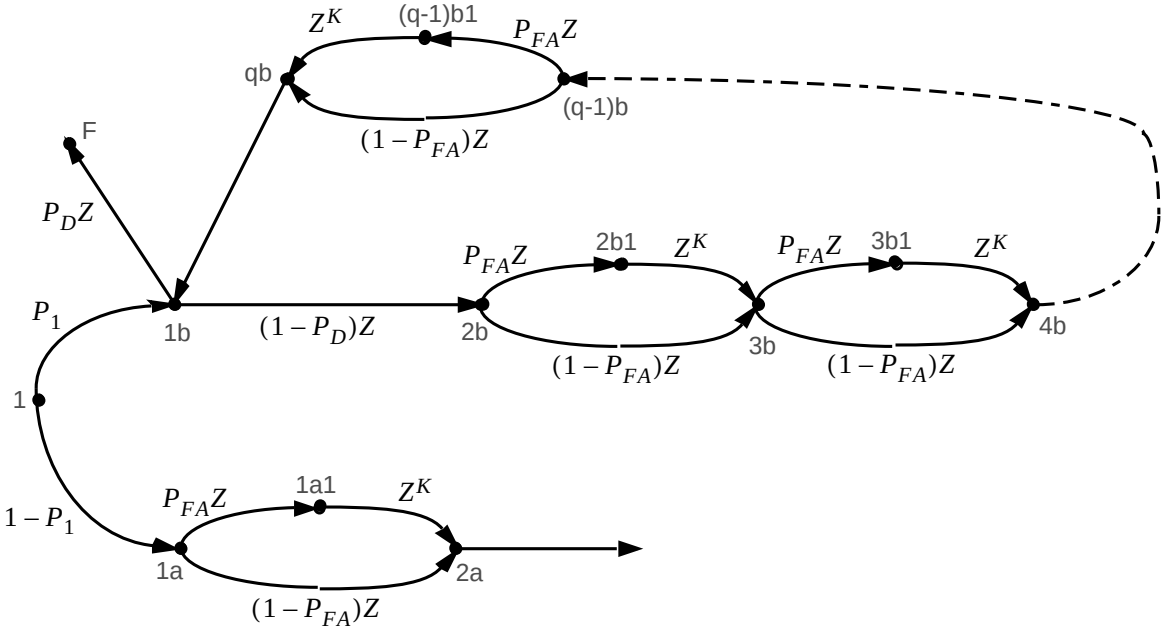

Figure 5.16: Flow Diagram for Single Dwell Time Acquisition

If we begin at node 1, then there are two possible transitions. Either the two PN codes are properly aligned with probability P_1, or they are not with probability $1-P_1$. First, assume that the correct cell is not being searched. This occurs with probability $1-P_1$ and we transition to node 1a. There is no delay associated with this transition, since this is solely a probabilistic decision. At node 1a, two events can occur. First, we can falsely determine that we have found the correct cell (a false alarm). This occurs with probability P_{FA} and we advance to node 1a1. Since it will take one dwell time to (incorrectly) determine that the correct code phase has been achieved, there is a unit delay associated with this transition. Since there is a penalty time associated with each false alarm, the transition from node 1a1 to node 2a takes K_p units of time ($K_p\tau_D$ seconds). If we correctly determine that the correct cell is not being searched, we transition directly from node 1a1 to node 2a with probability $1-P_{FA}$. Since a dwell time is required for this determination, there is a unit delay associated with this transition. At node 2a, the search begins anew with the next cell.

Now assume that the correct cell is being searched at node 1. This occurs with probability P_1 and we transition to node 1b. As before, since this is a probabilistic decision only, there is no associated delay. At node 1b, one of two events can occur: either the correct code phase is chosen and the search ends (a hit), or if a hit does not occur, q cells must be searched before the correct cell can be searched again. A hit will occur with probability P_D,

the probability of detection, and we advance to the final node, node F. Since it will take one dwell time to determine that this is the correct node, there is a unit delay associated with this transition. At this point, acquisition is finished and either verification or tracking mode is entered. If the correct code phase is not chosen at node 1b, which occurs with probability $1 - P_D$, we advance to node 2b, where we will have to search through q cells before returning to node 1b, the correct cell location. At each of the q cells between nodes 2b and 1b, the same transitions can occur as at node 1a: either a false alarm (with a unit delay and then the penalty time) or a miss (with unit delay). Obviously, there is a large delay if we reach node 2b, since we must perform a long search with many possibilities of false alarm before being allowed to search the correct cell again.

5.5.2 Determining the Mean and Variance of Acquisition

Based on the flow graphs [69], the mean acquisition time (in seconds) is then found to be

$$\mu_a = \frac{2 + (2 - P_D)(q - 1)(1 + K_p P_{FA})}{2P_D} \tau_D. \tag{5.50}$$

This can be approximated, if the number of cells to be searched q is much greater than 1, as

$$\mu_a = \frac{(2 - P_D)(1 + K_p P_{FA})}{2P_D} q\tau_D. \tag{5.51}$$

While this approximation does not provide a great deal of computational simplicity compared to the explicit calculation, it does aid in the determination of the variance of acquisition time.

The variance of the acquisition time, σ_a^2, can be found from the generating function defined in [69]. For the case of $q >> 1$, the variance is given by

$$\begin{aligned} \sigma_a^2 &= \tau_D^2 \left\{ (1 + K_p P_{FA})^2 q^2 \left(\frac{1}{12} - \frac{1}{P_D} + \frac{1}{P_D^2} \right) + 6q[K_p(K_p + 1)P_{FA}(2P_D - P_D^2) \right. \\ &\quad \left. + (1 + K_p P_{FA})(4 - 2P_D - P_D^2)] + \frac{1 - P_D}{P_D^2} \right\}. \end{aligned} \tag{5.52}$$

If we further stipulate that $K_p << q$, the variance can be approximated by

$$\sigma_a^2 = \tau_D^2 (1 + K_p P_{FA})^2 q^2 \left(\frac{1}{12} - \frac{1}{P_D} + \frac{1}{P_D^2} \right). \tag{5.53}$$

We now must solve for P_{FA} and P_D. These terms are dependent upon the receiver type being used. In [68], P_{FA} and P_D are found for a single user system using noncoherent

detection. In this case, the probability of false alarm assumes that the desired signal is not present. The received signal is multiplied by the locally generated PN sequence, passed through a bandpass filter, passed through a square law detector, and then integrated and passed to a threshold device. A block diagram of this system is shown in Fig. 4.1. These results do not hold for multiple access systems, and in particular for multiuser receivers.

If we assume that the phase ϕ_d of user d is known, then we can perform coherent demodulation. While the reverse link in a CDMA system will often require noncoherent demodulation due to the lack of a transmitted reference, more complicated detection schemes can be used to perform the acquisition. To gain insight into how the multiuser receiver can improve the acquisition process, we will assume that the received signal can be coherently demodulated, and therefore the results of the preceding sections can be applied in finding P_{FA} and P_D for the multistage receiver. Since we are modeling a continuously transmitting communications system, we will assume that when calculating P_{FA} that the desired signal is present, but that the correct code phase is not being searched.

5.5.3 Numerical Analysis of Probabilities of False Alarm and Detection

Probability of False Alarm

The probability of false alarm is the probability that the acquisition routine acquires the signal when in fact the correct code phase has not been chosen. This will occur when, based on the partial correlation and the values of the noise and interference, the magnitude of the decision statistic crosses a set threshold. Therefore, we need to develop an expression for the MAI when the local replica of the PN sequence of the desired user d is not properly aligned with the received signal of user d. For simplicity, we will model the partial correlation from the non-aligned sequences as though it were the MAI from another unsynchronized user and that there is no desired signal component. The partial correlation levels for the most part will resemble levels of interference from another user. This model can break down near the peak of the autocorrelation function, where there will be some finite rise time from the noise level to the peak correlation level. If enough samples are used in the acquisition process, it is possible that several samples will fall on the curve above the noise level. This possibility is not taken into account in the following analysis. If this were to occur in practice, the verification mode might be able to determine that the correct phase is nearly chosen and let the tracking mode actually determine the exact phase.

If we add an additional unsynchronized user to the system to model the self-interference from user d, we now have K_2+1 unsynchronized users, where user K_2 (the self-interference) has power P_d and user K_2+1 (the desired component) has a power of zero. Therefore, the

decision statistic in the acquisition loop after s stages of cancellation and for bit i is given by

$$Z_{d,i}^{(s)} = \eta + \sum_{k=1,k\neq d}^{K+1} I_{k,d}^{(s)}. \tag{5.54}$$

The decision statistic consists of the Gaussian noise, the residue of the interference from the synchronized users, and the interference from the other unsynchronized users. There is no desired component. The variance of η is known to be $N_oT/4$ and the conditional variance of the MAI, ψ, is given in (5.13). Both the noise and the variance have a mean of zero. If we denote the threshold as η_T, then the probability that the decision statistic exceeds this threshold is given by

$$P_{FA} = Q\left(\frac{\eta_T}{\sqrt{\psi + \frac{N_oT}{4}}}\right). \tag{5.55}$$

If we apply Holtzman's improved Gaussian approximation, we find that P_{FA} is approximately given by

$$\begin{aligned} P_{FA} \approx\ & \frac{2}{3}Q\left(\frac{\eta_T}{\sqrt{\mu_\psi + \frac{N_oT}{4}}}\right) + \frac{1}{6}Q\left(\frac{\eta_T}{\sqrt{\mu_\psi + \sqrt{3}\sigma_\psi + \frac{N_oT}{4}}}\right) \\ & + \frac{1}{6}Q\left(\frac{\eta_T}{\sqrt{\mu_\psi - \sqrt{3}\sigma_\psi + \frac{N_oT}{4}}}\right). \end{aligned} \tag{5.56}$$

Probability of Detection

Now we need to develop an expression for the probability of detection, P_D. This is simply the probability that the decision statistic exceeds the threshold when user d's signal is present and the correct code phase has been chosen. In this case, we have the original system model of K_1 synchronized users and K_2 unsynchronized users. By applying (5.10), we find that the decision statistic for user d after s stages of interference cancellation and during bit i is given by

$$Z_{d,i}^{(s)} = \eta + \sqrt{\frac{P_d}{2}}Tb_{d,i} + \sum_{k=1,k\neq d}^{K} I_{k,d}^{(s)}. \tag{5.57}$$

Therefore, using the improved Gaussian approximation, we can approximate the probability that the decision statistic is greater than the threshold by

$$P_D \approx \frac{2}{3}Q\left(\frac{\eta_T - \sqrt{\frac{P_d}{2}}T}{\sqrt{\mu_\psi + \frac{N_oT}{4}}}\right) + \frac{1}{6}Q\left(\frac{\eta_T - \sqrt{\frac{P_d}{2}}T}{\sqrt{\mu_\psi + \sqrt{3}\sigma_\psi + \frac{N_oT}{4}}}\right)$$

$$+\frac{1}{6}Q\left(\frac{\eta_T - \sqrt{\frac{P_d}{2}}T}{\sqrt{\mu_\psi - \sqrt{3}\sigma_\psi + \frac{N_o T}{4}}}\right). \tag{5.58}$$

We now have all of the terms necessary to solve for the mean and variance of acquisition time given in (5.50) and (5.52) respectively.

5.5.4 Numerical Results

Numerical results have been calculated for $N = 128$ with the number of samples per chip $N_s = 4$. Up to 4 stages are considered. The data rate is assumed to be 9600 bps. The E_b/N_o of all synchronized users is 12 dB with power $P_k = 1$. There is a single unsynchronized user, whose power varies with respect to the synchronized users' power. The number of synchronized users varies from $1 \leq K_1 \leq 400$. The threshold is set at

$$\eta_T = \frac{100}{124}\sqrt{\frac{P_d}{2}}T. \tag{5.59}$$

This is equivalent to having a threshold of 100 in a discrete system where an ideal correlation would yield $NN_s = 124$. A penalty time of $K_p = 3$ is used for all cases.

In Figs. 5.17-5.19, the probability of detection is plotted against the system capacity (in terms of synchronized users). The unsynchronized user's power level is -6, 0, and +6 dB with respect to the synchronized users in Figs. 5.17, 5.18, and 5.19 respectively. As expected, the probability of detection decreases as more users are added, since the power in the interference is increased. Here, as in all of the cases below, there is a noticeable improvement when adding an additional stage to the receiver. The difference is largest when going from 1 to 2 stages, although there is still a noticeable difference between 3 and 4 stages if the system is heavily loaded.

In Figs. 5.20-5.22, the probability of false alarm is plotted against the system capacity. The unsynchronized user's power level is -6, 0, and +6 dB with respect to the synchronized users in Figs. 5.20, 5.21, and 5.22 respectively. The probability of false alarm rises as the number of users increases as expected.

In Figs. 5.23-5.25, the mean acquisition time is plotted against the system capacity. The unsynchronized user's power level is -6, 0, and +6 dB with respect to the synchronized users in Figs. 5.23, 5.24, and 5.25 respectively. The mean acquisition time rises as users are added to the system, which is a direct result of P_D falling and P_{FA} increasing. These graphs do *not* reflect, however, the inherent delay due to the processing in each stage. This is directly determined by how fast the DSP hardware can perform the estimation and cancellation, and thus will be specific to each hardware design. Therefore, it will only be

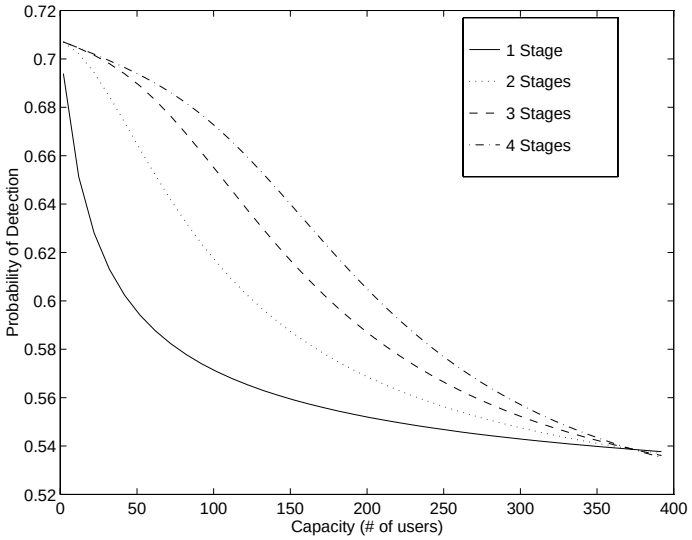

Figure 5.17: Detection Probability for Unsynchronized $E_b/N_o = 6$ dB and Synchronized $E_b/N_o = 12$ dB

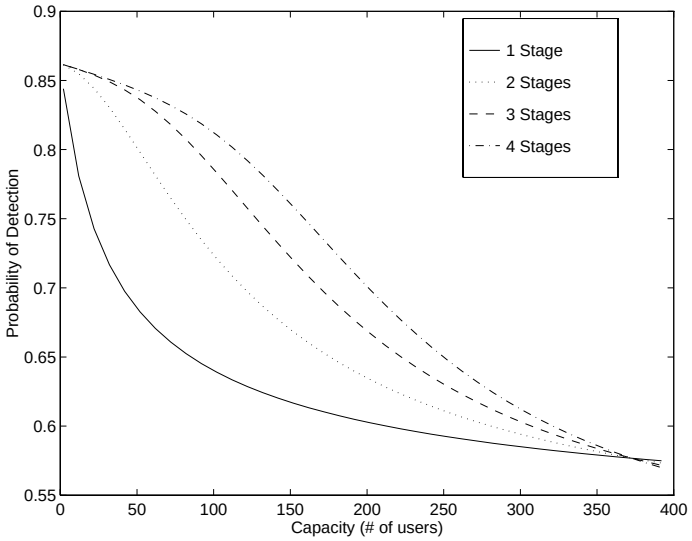

Figure 5.18: Detection Probability for Unsynchronized $E_b/N_o = 12$ dB and Synchronized $E_b/N_o = 12$ dB

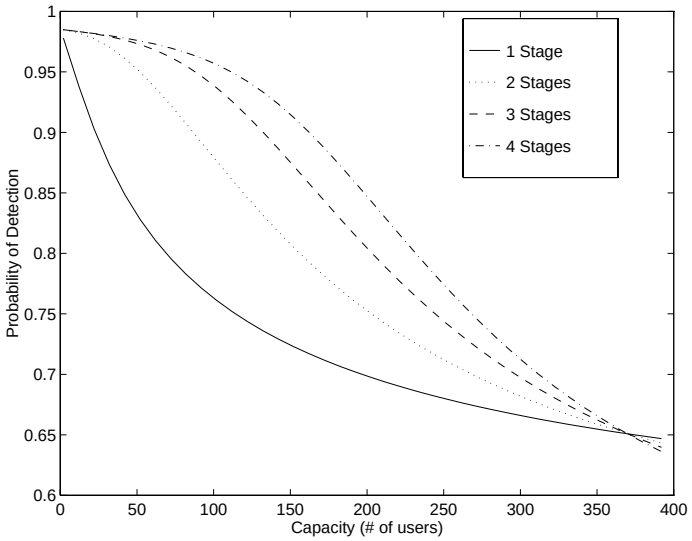

Figure 5.19: Detection Probability for Unsynchronized $E_b/N_o = 18$ dB and Synchronized $E_b/N_o = 12$ dB

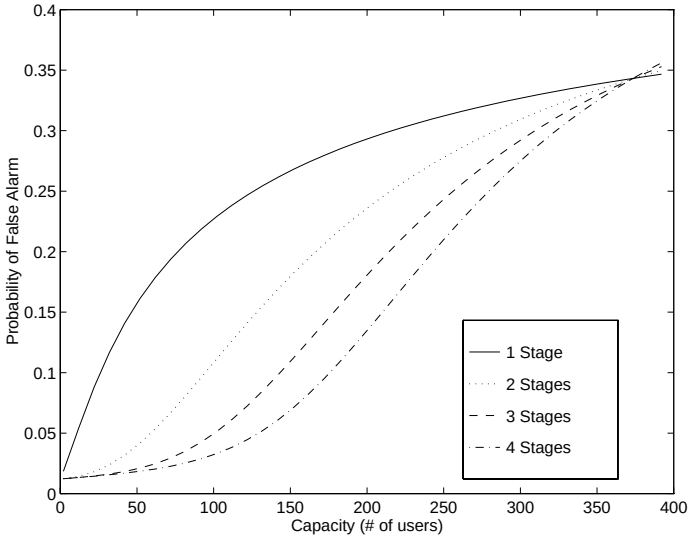

Figure 5.20: False Alarm Probability for Unsynchronized $E_b/N_o = 6$ dB and Synchronized $E_b/N_o = 12$ dB

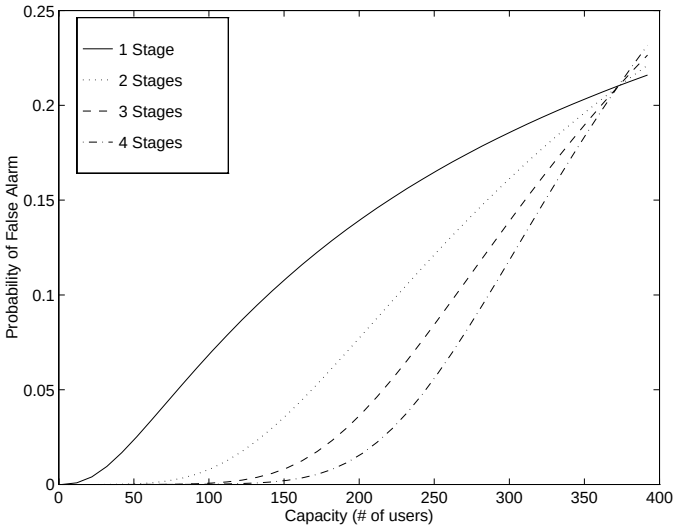

Figure 5.21: False Alarm Probability for Unsynchronized $E_b/N_o = 12$ dB and Synchronized $E_b/N_o = 12$ dB

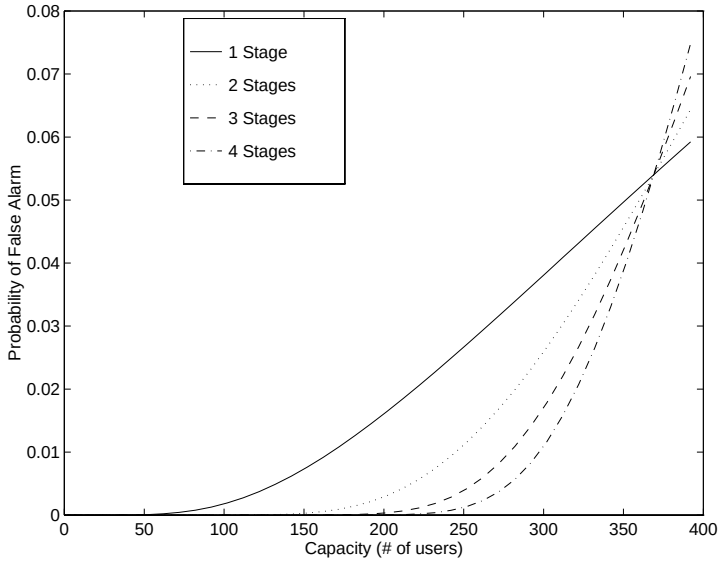

Figure 5.22: False Alarm Probability for Unsynchronized $E_b/N_o = 18$ dB and Synchronized $E_b/N_o = 12$ dB

worthwhile to add an extra stage if the extra processing delay is less than the decrease in acquisition time.

In Figs. 5.26-5.28, the variance of acquisition time is plotted against the system capacity. The unsynchronized user's power level is -6, 0, and +6 dB with respect to the synchronized users in Figs. 5.26, 5.27, and 5.28 respectively. The variance of acquisition time rises as users are added to the system, which is also a direct result of P_D falling and P_{FA} increasing.

Next, the power in the unsynchronized user is held constant at $E_b/N_o = 12$ dB for all users and the threshold is allowed to vary. In Fig. 5.29, the original penalty time remains the same at $K_p = 3$. In Fig. 5.30, the penalty time is increased to $K_p = 10$, which implies that false alarms will have a greater impact and increase μ_a. Regardless of K_p, for this value of E_b/N_o, moving to two stages provides a dramatic decrease in μ_a. The values of η_T that optimize μ_a are nearly the same for all stages when $K_p = 3$, although there is a slight increase as the stages increase. For $K_p = 10$, however, there is a dramatic drop in the optimum threshold (particularly from stage 1 to stage 2), which implies that not only does using the multistage architecture in the acquisition process allow for faster synchronization, but it also allows for a lower threshold to be set, which implies that weaker signals can be acquired than if conventional receivers were used. This is of great importance in a multistage receiver system, since this allows users to use less power when attempting to synchronize, which will lower the unsynchronized interference to the existing synchronized users. This is a major benefit, since we have already seen that unsynchronized interference can dominate system performance, particularly as the interference levels rise.

5.6 Acquisition Simulation Model

The simulation model for acquisition is based on the SPW model presented earlier. Here, though, there are only 6 synchronized users ($K_1 = 6$) and one unsynchronized user, the user we are trying to acquire. The one stage model is called *synch2a* and the two stage model is called *synch2a2*. Acquisition is accomplished via the *synchbox* block, which replaces the correlation receiver in *synch1a1* and *synch1a2*. All users have the same power level and $E_b/N_o = 12$ dB. The threshold settings were 100 and 115. While the synchronized users had random delays and phases that changed with the bit period, the unsynchronized user had a constant delay but a randomly changing phase. To model the randomness of the delay, 9 uniformly spaced values were chosen for simulation purposes (delays of 1, 15, 31, 46, 62, 78, 93, 108, and 123 samples). Ideally, all 124 possible delays should have been tested, but this was not done in the interests of time. Since the acquisition time is a random variable even with a constant delay, multiple simulation runs for a single delay were required to obtain an average acquisition time for that delay value. The number of runs was typically

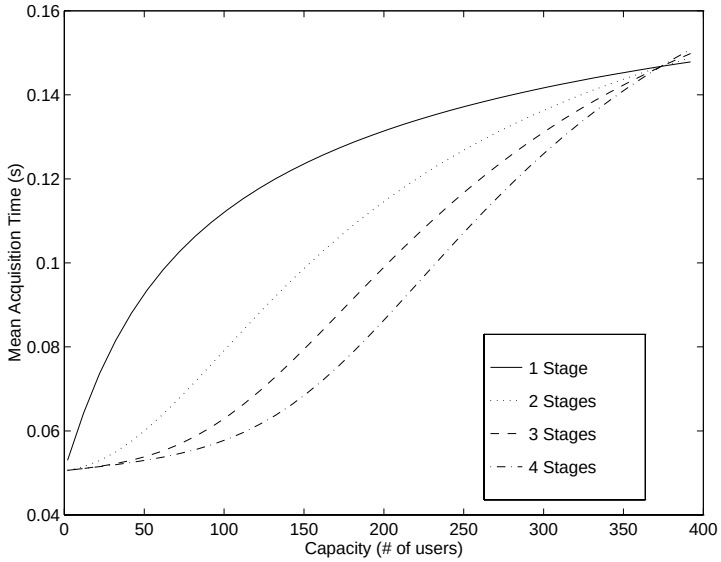

Figure 5.23: Mean Acquisition Time for Unsynchronized $E_b/N_o = 6$ dB and Synchronized $E_b/N_o = 12$ dB

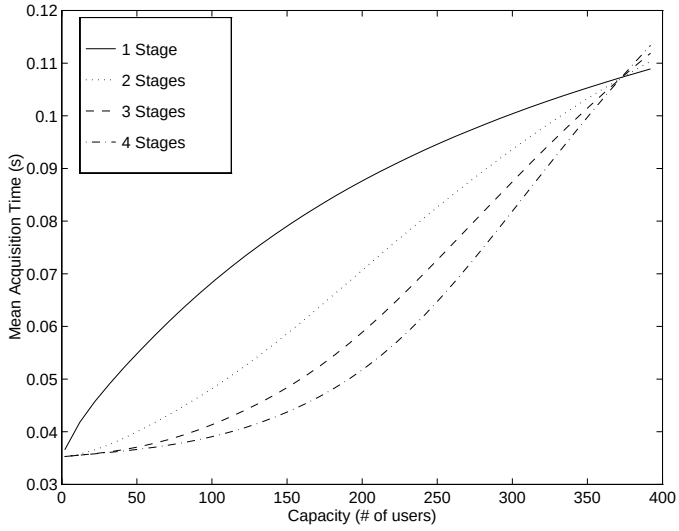

Figure 5.24: Mean Acquisition Time for Unsynchronized $E_b/N_o = 12$ dB and Synchronized $E_b/N_o = 12$ dB

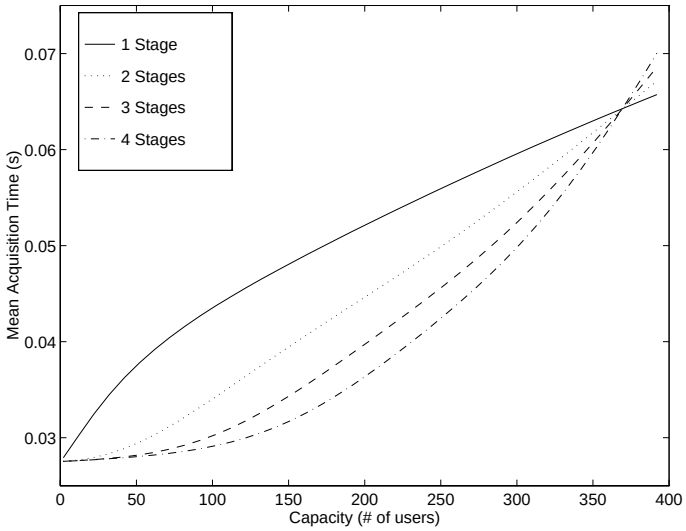

Figure 5.25: Mean Acquisition Time for Unsynchronized $E_b/N_o = 18$ dB and Synchronized $E_b/N_o = 12$ dB

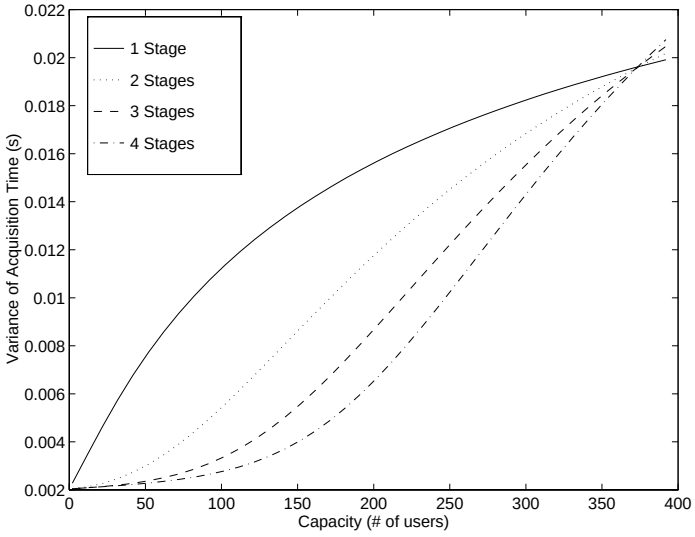

Figure 5.26: Acquisition Time Variance for Unsynchronized $E_b/N_o = 6$ dB and Synchronized $E_b/N_o = 12$ dB

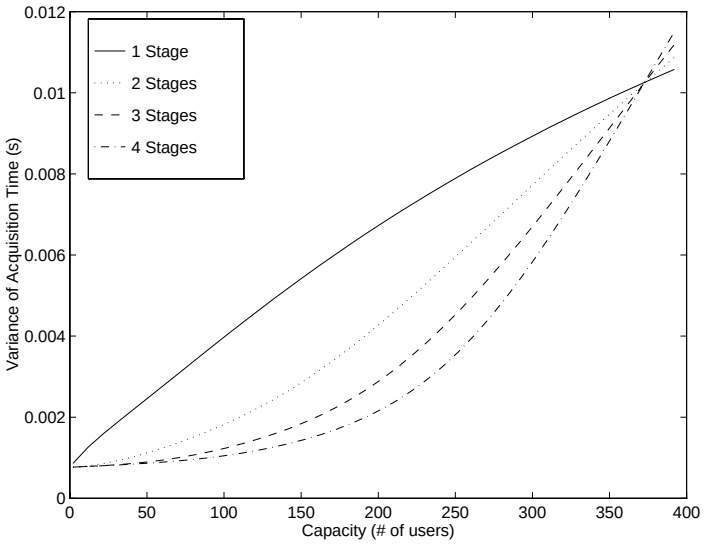

Figure 5.27: Acquisition Time Variance for Unsynchronized $E_b/N_o = 12$ dB and Synchronized $E_b/N_o = 12$ dB

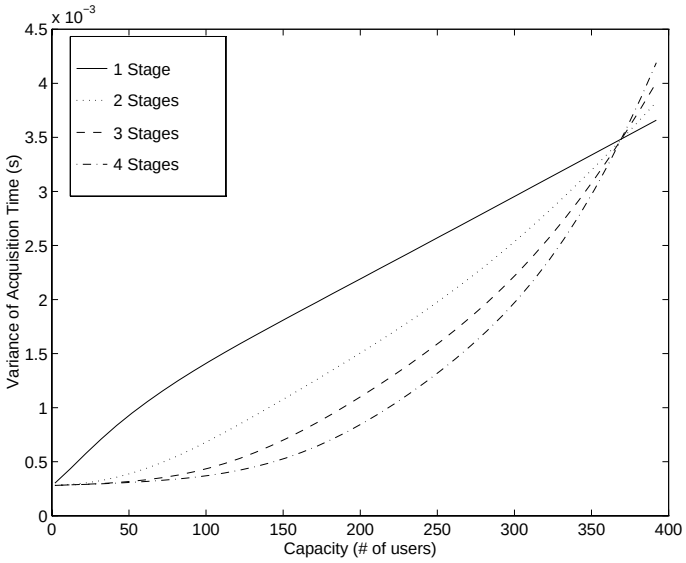

Figure 5.28: Acquisition Time Variance for Unsynchronized $E_b/N_o = 18$ dB and Synchronized $E_b/N_o = 12$ dB

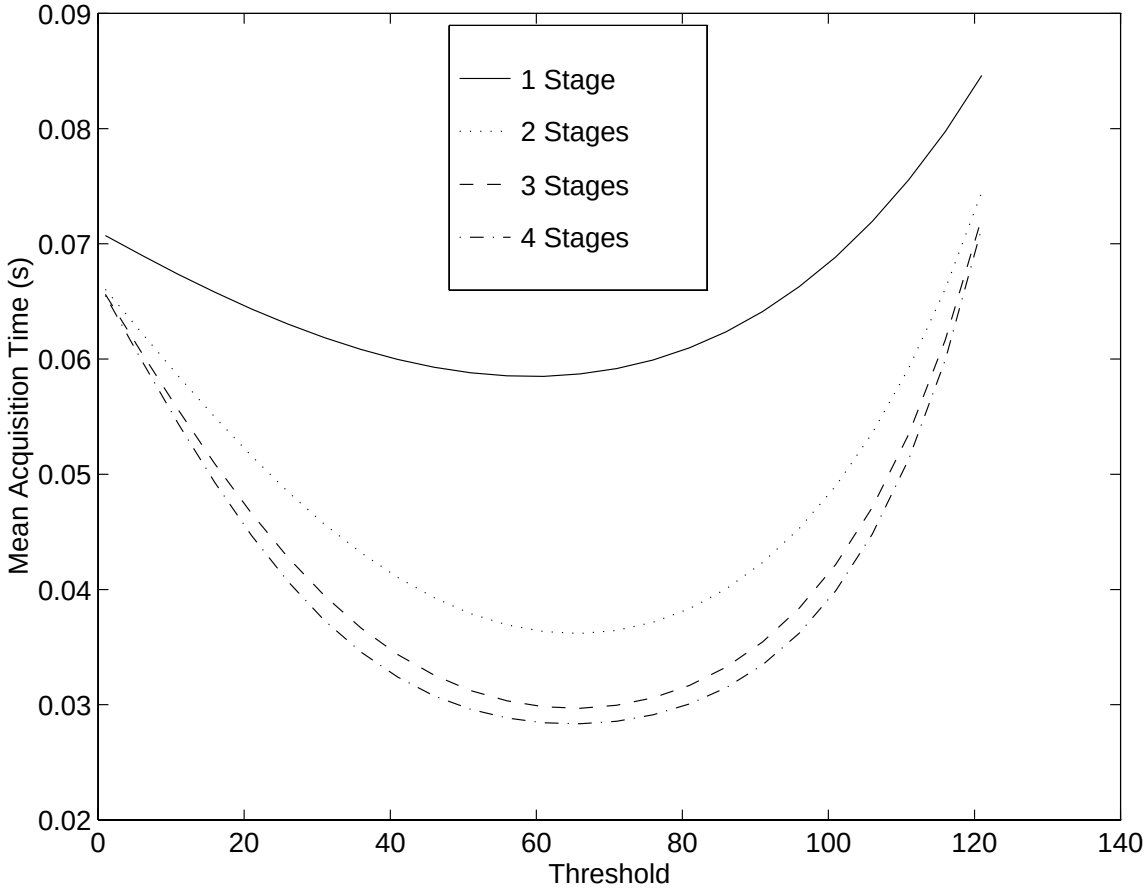

Figure 5.29: Mean Acquisition Time for $K_p = 3$

between 20 and 40. The acquisition times for these select delay values were then averaged to determine an overall mean acquisition time.

The acquisition block *synchbox* is shown in Fig. 5.31. The routine starts with a delay estimate of 0 and increments this by 1 sample *regardless* of whether acquisition is detected or not. This avoids designing a feedback loop to increment the delay estimate only if synchronization was not detected. SPW requires a delay in the feedback loop, so this simplified the design considerably. The parameter *update* determines when acquisition is accomplished, as this will have value 1 whenever the correlation output crosses the threshold; it will be 0 otherwise. Thus, if *update* goes high, acquisition has been detected. By observing *update* and the delay estimate parameter *delay_est* in the Signal Calculator, it can be determined

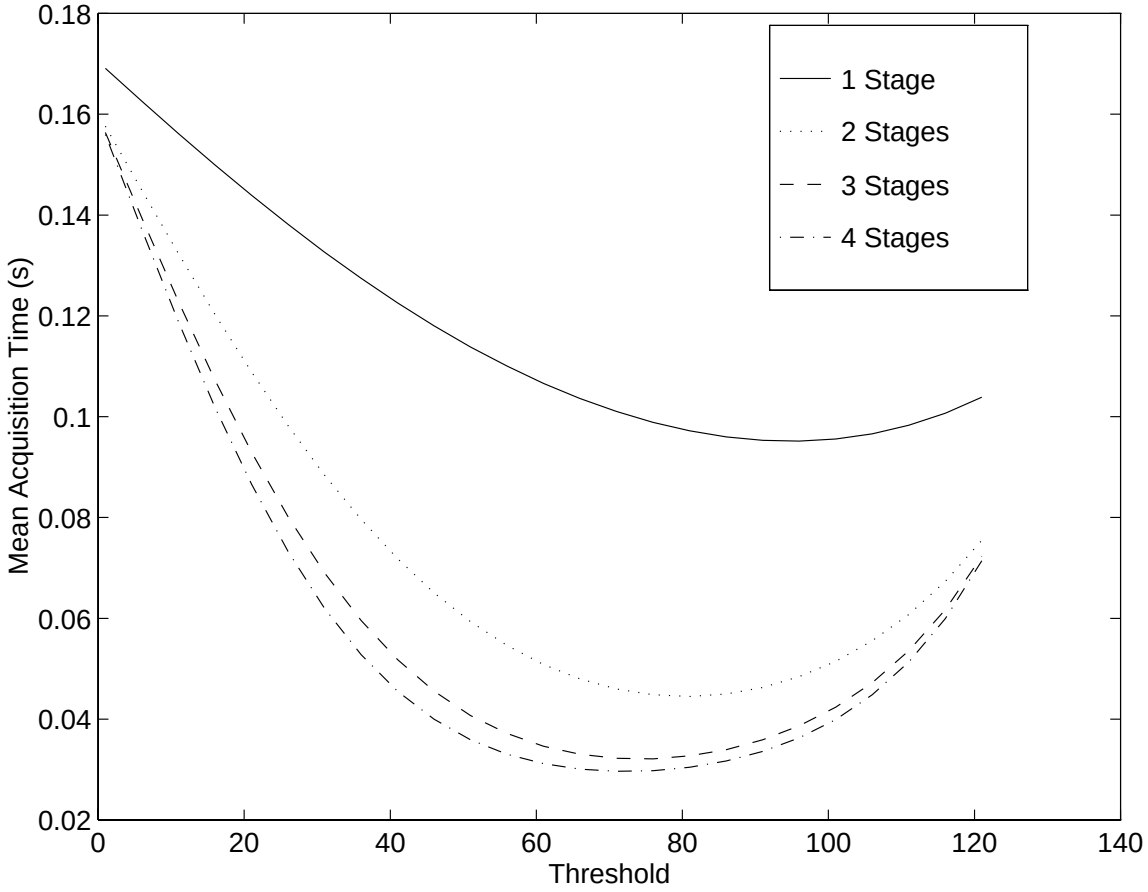

Figure 5.30: Mean Acquisition Time for $K_p = 10$

if the acquisition determination was correct. If not, a penalty time can be added to the true acquisition time for each false alarm. This allows a single set of simulation runs to be used for multiple penalty times. This relies on the noise being uniformly distributed across the samples, so that the probabilities of false alarm and detection do not change if a penalty time is physically inserted into the simulation or not.

A summary of the simulation results are given in Table 5.1 and compared with the analytical prediction. In all cases, the simulated time was worse than the analytical time. There are several possible reasons for this. First, as noted in Sec. 5.4.5, the simulation model had a slightly higher BER than the analytical model, suggesting a slightly higher noise level. The simulated acquisition times are heavily dependent not only on the false alarms, but

Table 5.1: Analytical and Simulated Mean Acquisition Times (ms)

	$\eta_T = 100$		$\eta_T = 115$	
	One Stage	Two Stage	One Stage	Two Stage
Analytical	11.4	9	15.6	13.6
Simulated	15.6	11.6	18.2	17.9

especially upon misses when the correct phase is being searched, due to the length of time before the correct phase is searched again. Although the routine usually acquired on the first or second try, occasionally the correct code phase was missed on multiple consecutive attempts; these multiple misses produced lengthy acquisition times which significantly increased the overall average time. There were occasional times when the correct phase was missed on multiple occasions, which tended to skew the average even if the routine usually acquires on the first or second try. Therefore, if there is destructive interference that is causing misses in the acquisition routine, this will cause the overall mean acquisition time to rise. It is also possible that more delay values are necessary to get a reasonable profile of the individual acquisition times, or that more simulation runs are required for a particular delay value to ensure that the result is accurate. The model was initially tested by removing all noise and interference, with the result that the routine acquired the signal perfectly every time and with the ideal correlation value.

Despite the differences in analysis and simulation, the pattern of results is the same. The second stage generally allowed for faster synchronization. Based on the simulation results, this is partially due to the increase in hits on the first or second try, and due to the decrease in false alarms caused by the decrease in interference levels. Therefore, the improvement in acquisition time will become more dramatic as the penalty time increases.

5.7 Conclusions

The synchronization performance of multistage receivers has been analyzed and simulated. We have studied two key issues: what effect the unsynchronized users have on synchronized users, and how the multistage receiver itself can be used to allow for a more rapid acquisition.

Unsynchronized interference increases the BER of synchronized users, and can drastically decrease performance when the interference levels are strong. The multistage receiver provides *no* near-far resistance against these unsynchronized users, and thus some form of

power control is recommended to try and limit the transmit power of unsynchronized users as low as possible and still allow for rapid acquisition. The system provider will have to provide a trade-off between allowing the unsynchronized user a higher transmit power in an attempt to acquire faster, but limiting the power to reduce the substantial interference that user can cause to the synchronized users. If a substantial number of users are trying to acquire at once, this could limit the system capacity since the multistage receiver cannot cancel this interference.

We have also shown how the multistage architecture can be used both to reduce the acquisition time and to allow for lower threshold settings as the penalty time increases. We can accomplish this by acquiring the residual received signal instead of the initial received signal. Because the residual signal will have reduced levels of multiple access interference, this will reduce the probability of false alarm and increase the probability of detection, which will in turn decrease the mean acquisition time. In addition, we have shown that the optimum threshold setting may decrease as the number of stages increases. This will allow unsynchronized users to transmit at lower power levels and thus decrease the amount of interference to the synchronized users.

A flexible simulation model has been developed in SPW that models both the effect of unsynchronized interference and the single dwell time acquisition scheme. The simulation results verify the analytical results.

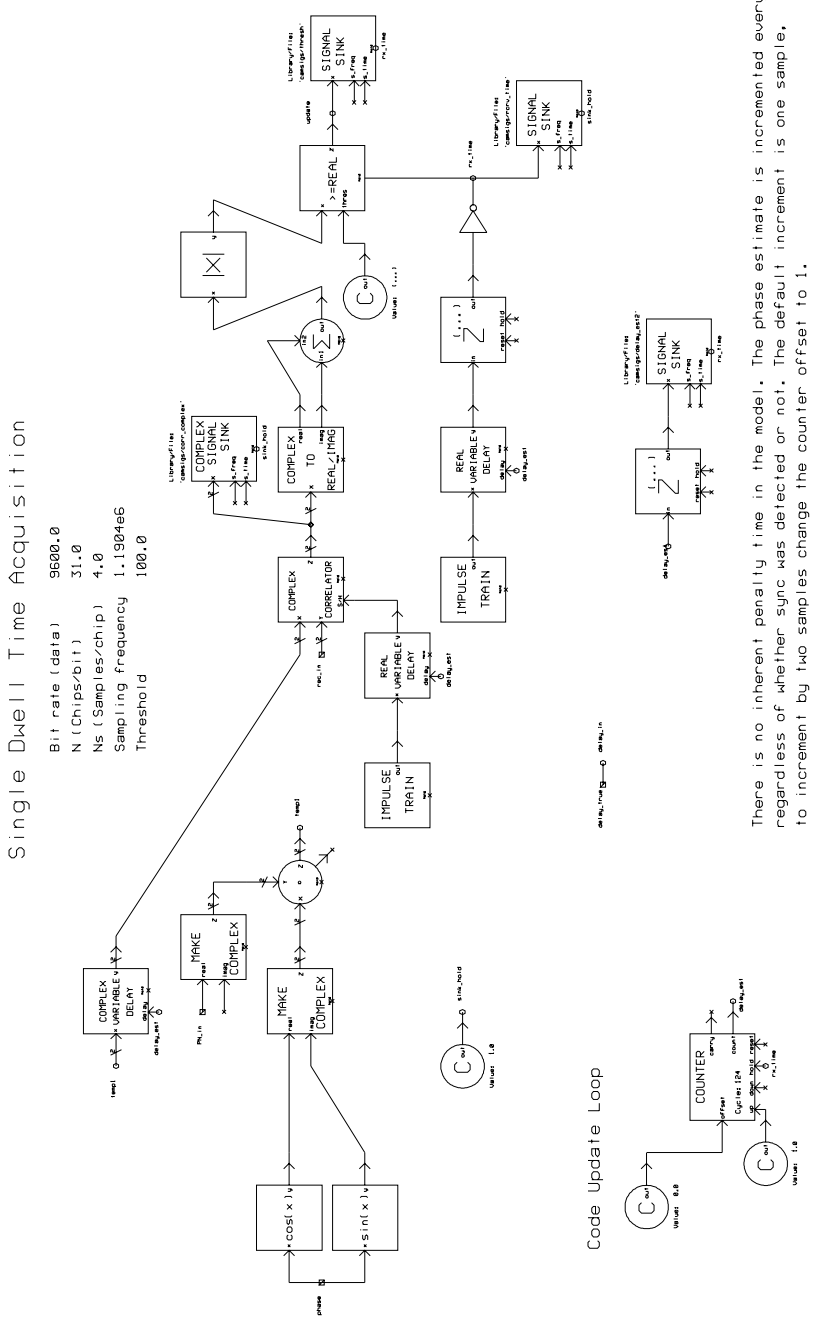

Figure 5.31: SPW Single Dwell Time Acquisition Model

Chapter 6

Quantization Effects

6.1 Introduction

When performing a theoretical analysis, numbers can be represented as real or complex numbers with infinite precision. In a computer or DSP chip, a number must be represented with some finite numerical precision [84]. The process of converting a continuous amplitude signal into a discrete amplitude signal is known as *quantization*. In the process of quantizing any given number, there are two main effects that determine the precision with which that number can be discretely represented: the number of bits used for quantization and whether fixed or floating point representation is used. There are additional techniques that can be used to improve the accuracy with which a signal is quantized over time, including companding (compression and expansion) and non-uniform quantization. These techniques are useful if the probability distribution of the signal waveform is non-uniform.

The use of quantized signals can cause additional errors in a DSP system. In a mathematical operation such as addition or multiplication, it is possible for the result to be larger than either of the inputs. Since the result must be quantized to the number of bits used in the rest of the system, the result must be either truncated or rounded-off to the nearest level. Finally, if the magnitude of the result of a mathematical operation becomes too large, overflow (or underflow) will result. This can cause serious errors, and scaling is sometimes used to ensure that this condition does not occur.

In this chapter, we will first discuss the nature of quantization and fixed-point representations. We will then discuss the uniform quantization model. We will then focus on the efforts of past researchers on studying the effects of quantization. The operation of the uniform quantizer is straightforward and deterministic. The analysis of this device can prove complex however, due to the nonlinearity of the quantization process. There have been two

main thrusts of research in this area: a deterministic examination of the output based on a deterministic input [85, 86], and approximating the quantizer with a uniform noise source based upon a stochastic description of the input signal [87]. The fact that the noise model is dependent upon the input implies that, when studying the effects of quantization in a given receiver design, a model designed for one set of input constraints may not accurately model the same receiver design with a different set of inputs. The difficulty in accurately modeling quantization has led many researchers to use the uniform noise model without first determining whether or not it is appropriate [88], even though conditions for applying the model were specified in the initial analysis by Bennett [87].

6.1.1 Fixed-Point Representation

We can represent any number using base a (also known as radix a) by [89]

$$(\ldots b_2 b_1 b_0 . b_{-1} b_{-2} \ldots)_a = \ldots + b_2 a^2 + b_1 a + b_0 + b_{-1} a^{-1} + b_{-2} a^{-2} + \ldots, \qquad (6.1)$$

where the b's are referred to as digits. For a binary (base 2) system, these are usually referred to as bits. If $i > j$, then digit a_i is *more significant* than digit a_j. The digit with the highest index for a given representation is the most significant bit; the bit with the lowest index is the least significant bit. The period between b_0 and b_{-1} is the radix point, which in base 10 is usually called the decimal point and in base 2, the binary point.

Since the mathematical operations in most DSP chips are based on the binary number system, a number is generally represented as being quantized in binary form [84]. While there are a number of ways to represent a binary number, the most common form is known as two's complement, which will be the method used here. The difference in representations is the way in which negative numbers are represented. In *signed magnitude*, the leftmost bit position is used to indicate the sign (a 0 for a positive number, a 1 for a negative number) [90]. An advantage of this technique is that it is symmetric, so that the largest number that can be represented, for n bits, is $2^{n-1} - 1$ and the most negative number is $-(2^{n-1} - 1)$. Thus, changing the sign of the number cannot result in overflow. A disadvantage is that the number 0 can be represented as +0 and -0, even though they are the same. Another problem is that when two numbers of opposite sign are added, the magnitudes of each must be compared to determine the sign of the result. In *one's complement*, negative numbers are represented by taking the magnitude of the number, representing it binary, and then complementing each bit (changing 1's to 0's and vice versa). Thus, for $n = 3$, we would represent -2 by taking the representation for 2, 010, and inverting each bit, or 101. There is still a dual representation for 0 in one's complement, which is why *two's complement* is often used. In two's complement, a negative number is represented by adding 1 to the one's complement representation. Therefore, -2 would be represented as 110. There is only one

representation for zero, since the one's complement representation of 0 is 111, and adding 1 will give 000. Addition and subtraction are also straightforward since, even if the numbers have different signs, the result will always be the correct representation. The drawback is that the range is from -2^{n-1} to $2^{n-1}-1$, so that if the sign changes on the most negative number, overflow will occur.

Using an infinite number of bits, a real number x can be perfectly represented using fractional two's complement notation as

$$x = X_m \left(-b_0 + \sum_{i=1}^{\infty} b_i 2^{-i} \right), \tag{6.2}$$

where X_m is a scaling factor and $b_i \in \{0, 1\}$. If $b_0 = 0$, then x is positive; otherwise, x is negative. If we quantize x using $B+1$ bits, then the quantized version of x, $\hat{x}$, is given by

$$\hat{x} = X_m \left(-b_0 + \sum_{i=1}^{B} b_i 2^{-i} \right) = X_m \hat{x}_B. \tag{6.3}$$

There are B bits used to represent $\hat{x}_B$ and 1 bit for the sign bit b_0. Since the scaling factor determines the maximum magnitude of x, the range of x is given by $-X_m \leq x \leq X_m$. In hardware implementations, X_m is usually represented in the form

$$X_m = 2^c, \tag{6.4}$$

where c is called the characteristic. The fractional part of x, $\hat{x}_B$, is known as the mantissa. If $X_m > 1$, then x can be greater than 1.

There are two ways of defining X_m in a hardware system, either using fixed-point or floating-point representation. In fixed-point, c is fixed and need not be explicitly represented in the hardware architecture. Since c cannot change, it is possible that very large numbers cannot be represented in the set range, and that very small numbers will be quantized to zero. In floating-point, c can vary with x and therefore must be explicitly represented in hardware. Since c can increase (and decrease) as the magnitude of x increases (and decreases), very small numbers can be represented with a great deal of precision, and very large numbers can be represented without increasing the number of bits. While floating-point is desirable for its numerical accuracy, the hardware tends to be slower and more expensive due to the requirement that c be represented in binary form in the hardware.

A comparison of fixed-point fractional, fixed-point integer, and floating-point implementations is given in Table 6.1. Floating-point is desirable due to its high dynamic range, low possibility of overflow, and limited roundoff noise. The major drawback in terms of the multistage DSP implementation is the relative slow speed when compared to the fixed point implementations.

Table 6.1: Comparison of Binary Implementations

Feature	Fixed-Point Fractional	Fixed-Point Integer	Floating Point
overflow, addition	yes	yes	unlikely
overflow, multiplication	no	yes	unlikely
roundoff error, addition	no	no	yes
roundoff error, multiplication	yes	no	yes
dynamic range	modest	modest	high
hardware implementation	simple	simple	difficult, slow

6.1.2 Quantization Error

The most basic quantizer is shown in Fig. 6.1, where x is the input, x_ϵ is the quantized output, and there are 8 possible bins (quantization levels) [88]. Although the quantizer shown here is centered about zero, this need not be the case [91]. The only requirement for a uniform quantizer is that the bin width Δ be uniform (the same) for all bins. In this manner, no part of the input signal is quantized more accurately than another part of the signal. This is appropriate when no *a priori* knowledge is known of the input signal. For signals such as voice, where the signal may be known to be more likely to be in a certain region, a non-uniform quantizer will allow more bins to be concentrated in the areas where the signal is most likely to appear [87].

The quantization error is given by

$$e = q(x) = x_\epsilon - x. \tag{6.5}$$

If we use uniform quantization (uniform spacing of quantization levels) and $B + 1$ bits, then the minimum spacing between levels is given by

$$\Delta = X_m 2^{-B}. \tag{6.6}$$

Another common (and equivalent representation) is to calculate the bin width Δ based on the number of bits and the quantization range. If we assume the range is given by $[L_l, L_u]$, then the bin width is given by

$$\Delta = \frac{L_u - L_l}{2^B}. \tag{6.7}$$

The characterization of e depends upon whether rounding or truncation is used. In rounding, a number is rounded off to the nearest quantization level. In truncation, any portion

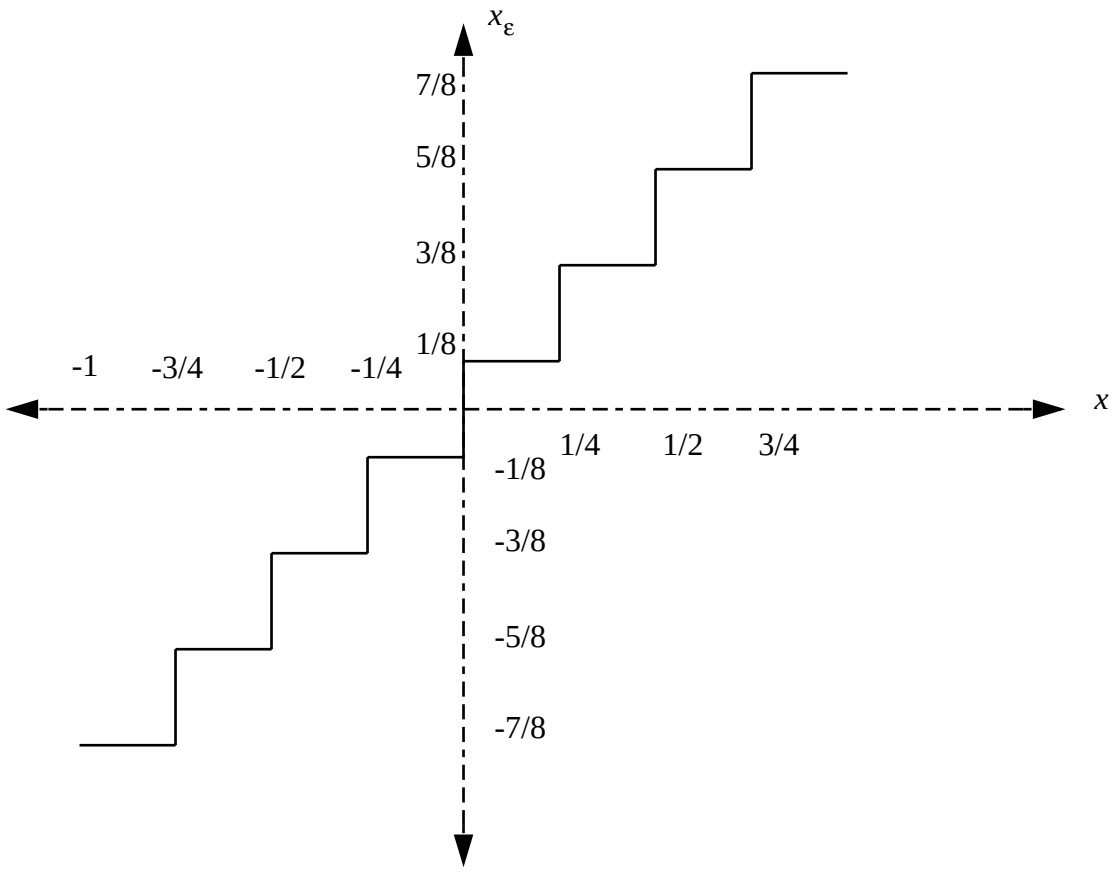

Figure 6.1: Uniform Quantizer

of $\hat{x}_B$ that requires greater than B bits is simply truncated. Regardless of the technique, however, quantization is a nonlinear memoryless operation. The range of the error is $-\Delta/2 \leq e \leq \Delta/2$ for rounding and $-\Delta \leq e \leq 0$ for truncation.

Overflow can occur if a number to be quantized is larger than the scaling factor X_m (underflow if the number is less than $-X_m$). This error can be a serious one, as illustrated by the following example. In 5 bit two's compliment notation, the number 15 would be represented as 01111. If we add 1 to this (00001), the result is 10000, or -16. In this case, a simple addition caused a severe error. One method of counteracting this problem, which is often used in analog-to-digital converters, is to clip the result so that when we add anything to 15, we still get 15 (the maximum representable positive number). A benefit of using two's complement notation is that, if two numbers when added together do not cause overflow, then the result is correct even if an intermediate sum caused overflow. This can

easily be illustrated by an example. First, assume that $n = 4$. Next assume that we want to add $4 + 4 = 8$ to $-2 - 2 = -4$ to get $8 - 4 = 4$. In two's complement notation we add 0010+0010 = 1000 (overflow) to 1110+1110 = 1100 to get 1000+1100 = 0100, or 4. Thus the result is correct, even though overflow occurred at the first addition. This property will not hold if clipping has occurred. A method of combating overflow is scaling, which is discussed in more detail in Section 6.3.3.

Some form of quantization is also necessary when multiplying two numbers. If two $B + 1$ bit numbers are multiplied together, the result will be a $2B + 1$ number that must be either truncated or rounded back to $B + 1$ bits. Overflow is quite possible if the numbers being multiplied are greater than one. For example, the multiplication of 4x5=20 would cause overflow in a 5 bit system, where the largest number that can be represented without overflow is 15.

Analyzing quantization error exactly is difficult due to the nonlinear operation of the quantizer, the possibility of overflow, and the numerous points that rounding or truncation can occur. Since the exact nature of the error is dependent upon the input, it is impossible in general to quantify the exact nature of the error. Modeling quantization using linear noise sources does provide a reasonable approximation; if exact results are needed, simulation is required. The linear model has been shown to provide accurate predictions of statistical averages when the input is a widely varying signal (such as speech) [84].

Modeling quantization with a linear noise source $e[n]$ relies on several key assumptions [84]:

1. The noise has a uniform distribution of amplitudes over one quantization period
2. The noise source is a wide-sense stationary white-noise process
3. There is no correlation between the noise source and the input to the quantizer, all other quantization noise sources, and the system input.

A block diagram of a linear noise model is shown in Fig. 6.2. Since the noise amplitude is modeled as uniform over the allowable range, the mean and variance for rounding are

$$\begin{aligned} \mu_e &= 0 \\ \sigma_e^2 &= \frac{\Delta^2}{12} \end{aligned} \tag{6.8}$$

and for truncation are

$$\begin{aligned} \mu_e &= -\frac{\Delta}{2} \\ \sigma_e^2 &= \frac{\Delta^2}{12}. \end{aligned} \tag{6.9}$$

The nonlinearity of the quantization process can lead to zero-input limit cycles, which are oscillations at the output even when there is no input to the system. Quantization (particularly if it exists in a feedback loop) and overflow can both lead to limit cycles. This is a strictly nonlinear process that cannot be modeled using linear noise sources.

6.2 Deterministic Analysis

Although Bennett's stochastic approach [87] has been the approach followed by most researchers, the first research done in uniform quantization (equivalent to Pulse Count Modulation, or PCM) was actually that of Clavier, Panter, and Grieg [85, 86] in 1947. Although often overlooked by modern researchers, these authors were the first to show the effect of quantizing the amplitude to a discrete number of levels. The authors considered the case of single frequency input, two frequency input, and continuous frequency input.

For the simpler cases such as the sinusoidal tones, the effects of the resulting distortion caused by quantization are studied through the use of the Fourier series representation. A periodic input is represented as a Fourier series and then compared with the Fourier series representation of the output (which can be determined exactly due to the deterministic operation of the quantizer, assuming the number of quantization levels and the dynamic range of the input is known).

For more complicated inputs where the signal has a continuous frequency spectrum, the Fourier series approach is quite complicated and a Fourier transform approach is adopted instead. Here, the Fourier transform of the input is taken and then multiplied by the transform of the pulse spectrum, and then the inverse transform could be taken on the result. The motivation of this research was to investigate the properties of crosstalk in a PCM system, not to characterize the quantization process as a noise source.

This analysis is only applicable for a single, deterministic input, and does not provide a

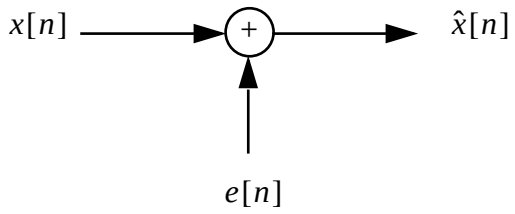

Figure 6.2: Linear Quantization Noise Model

way of analyzing systems where the input can be defined stochastically but not deterministically (since the operation of the quantizer is dependent upon the input, the Fourier transform of the quantizer cannot be determined unless the input is known). In analyzing communication systems, we would like to have a quantizer model that is not dependent upon the input and can thus be applied to a wide range of inputs. This will also allow for noise sources to be used in analyzing communication systems, where calculating Fourier transforms may be exceedingly complicated.

6.3 Stochastic Analysis

Bennett's paper in 1948 [87] was the first paper to examine the uniform quantizer from a stochastic perspective. Bennett began by noticing that, if no overflow occurred (or equivalently, there were an infinite number of steps), and if there were a large number of small steps, then the error signal (the difference between the quantized version of a signal and the original version) is composed of a series of very nearly straight lines with varying slope. Bennett based his analysis upon a staircase transducer, a physical device which operates as a quantizer. Thus his results are based upon the step size in voltage E_o instead of the bin width Δ as used in Chapter 7.

If we analyze the error signal and assume that the individual sections are indeed straight lines, than the error voltage ϵ is given by

$$\epsilon = sl, \quad -\frac{E_o}{2s} < l < \frac{E_o}{2s}, \tag{6.10}$$

where s is the slope of the line and l is time referenced to the midpoint of the interval (such that the midpoint then becomes the origin). The mean square error of the error voltage can then by found via

$$\begin{aligned} \overline{\epsilon^2} &= \frac{s}{E_o}\int_{-E_o/2s}^{E_o/2s} \epsilon^2 dl \\ &= \frac{E_o^2}{12}. \end{aligned} \tag{6.11}$$

Bennett also notes that the output signal-to-noise ratio D can be determined when the input is a test tone, and that a simple expression results for D based on the number of bits. If we assume that the input tone has a maximum amplitude of E (and thus mean square value of $E^2/2$), then the total quantizer range must be $2E$ to ensure that overflow does not occur (since the input tone will swing from $-E$ to E). The ratio of the mean square value

Table 6.2: Signal-to-noise Ratio vs. No. of Quantization Bits

Number of Bits N	**Number of Bins** r	**Signal-to-Noise Ratio** D
3	8	21
4	16	27
5	32	33
6	64	39
3	128	45
3	256	51

of the input tone voltage to the mean square value of the quantizing noise voltage is given by

$$\frac{E^2/2}{E_o^2/12} = \frac{3r^2}{2}, \tag{6.12}$$

where r is the ratio of the total quantizer range to the bin width given by $2E/E_o$. The ratio r is by definition the number of bins used in the uniform quantizer. If we assume that the sampling frequency is f_s, then the bandwidth required would be rectangular to $f_s/2$. However, a practical system cannot have a perfectly rectangular shape, because some transition period is necessary between the passband corner frequency and the cutoff frequency. Thus a factor κ is introduced which is the ratio of the equivalent rectangular noise band to $f_s/2$. Since the noise power gets multiplied by κ, D (in dB) is given by

$$D = 10 \log_{10} \frac{3r^2}{2\kappa} \text{ dB}. \tag{6.13}$$

Bennett found a value of $\kappa = 3/4$ to be a good practical result, which simplifies (6.13) to

$$D = 20 \log_{10} r + 3 \text{ dB}. \tag{6.14}$$

Results for the signal-to-noise ratio D are given in Table 6.2 for several values of the number of bits N (where $r = 2^N$) if we assume that $\kappa = 3/4$. The signal-to-noise ratio increases by about 6 dB with the addition of each bit.

Bennett also notes that uniform quantization is not optimum for some signals such as speech and discusses methods of analyzing systems using non-uniform quantizers (no single noise model can be given since it will vary as the non-uniform spacing varies).

6.3.1 The Quantization Theorem

Widrow provided a thorough stochastic examination of the uniform quantizer in 1956 [91]. He determined a measure of determining when the uniform model was appropriate for a given input; this rule came to be known as the Quantization Theorem. This model is most useful when the probability distribution function of the input signal x can be determined, and is not as useful when analyzing complex systems such as the multistage receiver.

The One-Dimensional Quantization Theorem

Widrow's theorem is based on the use of characteristic functions and assumes that the input signal to be quantized can be modeled as a random variable. If a continuous random variable x has a probability density function $f_x(X)$, then its corresponding characteristic function $\phi_x(\omega)$ is given by

$$\phi_x(\omega) = E\left[e^{j\omega x}\right], \tag{6.15}$$

where $j = \sqrt{-1}$ and $E[\cdot]$ denotes the expectation given by

$$E[y] = \int_{-\infty}^{\infty} Y f_y(Y) dY. \tag{6.16}$$

We can rewrite (6.15) as

$$\phi_x(\omega) = \int_{-\infty}^{\infty} f_x(X) e^{j\omega X} dX. \tag{6.17}$$

Note that this is nearly identical to the expression for the Fourier Transform of x, with the exception that there is no negative sign in the exponent. If we define the quantization error ϵ as

$$\epsilon = x_q - x \tag{6.18}$$

where x_q is the quantized version of x, then the Quantization Theorem then states that the distribution of the quantization error e will be uniform over $[-\Delta/2, \Delta/2]$ if

$$\phi_x(\omega) = 0 \quad \text{for all} \quad |\omega| \geq \frac{2\pi}{\Delta}. \tag{6.19}$$

Thus if the characteristic function is band-limited in this fashion, the quantization noise will have a uniform distribution over time.

The Two-Dimensional Quantization Theorem

To examine the second-order statistics of the quantization noise, the two-dimensional Quantization Theorem may be used. If we define two random variables x_1 and x_2 which occur

at time instants n and m respectively, then a two-dimensional form of the quantization theorem may be developed [91].

6.3.2 A Necessary and Sufficient Condition for Uniform Noise

Although Widrow [91] provided conditions under which the uniform noise model was appropriate, his conditions were sufficient but not necessary (meeting those conditions guaranteed the appropriateness of the uniform noise model, but did not imply that only these situations were appropriate). Sripad and Snyder presented a paper which provided a necessary and sufficient condition for modeling quantization noise with a uniform noise model [92].

The Extended Quantization Theorem

Sripad and Snyder also provided a means of determining the probability density function of the quantization error even if the uniform model was not appropriate, which therefore provides a means of determining how much the true distribution varies from the uniform distribution and how much error will be introduced if the uniform model is used.

The probability density function of the quantization error is shown to be

$$f_\epsilon(E) = \begin{cases} \frac{1}{\Delta} + \frac{1}{\Delta}\sum_{n\neq 0}\phi_x\left(\frac{2\pi n}{\Delta}\right)\exp\left(\frac{-j2\pi nE}{\Delta}\right), & -\Delta/2 \leq E < \Delta/2 \\ 0, & \text{otherwise} \end{cases} . \tag{6.20}$$

It can also be shown that

$$\phi_x(2\pi n/\Delta) = 0 \quad \text{for all} \quad n \neq 0 \tag{6.21}$$

holds if and only if the probability density function of the quantization error is uniform, or

$$f_\epsilon(E) = \begin{cases} \frac{1}{\Delta}, & -\Delta/2 \leq E < \Delta/2 \\ 0, & \text{otherwise} \end{cases} . \tag{6.22}$$

By comparing (6.19) and (6.21), we see that (6.19) is a specific case of (6.21). Thus (6.21) is an expanded form of the Quantization Theorem which expands the class of input signals whose quantization error will have a uniform distribution.

Consider an example of a signal which meets (6.21) but not (6.19), yet does have a quantization error that is uniform. If the signal x itself is uniform, it will have probability density function

$$f_x(X) = \begin{cases} \frac{1}{\Delta}, & -\Delta/2 \leq X < \Delta/2 \\ 0, & \text{otherwise} \end{cases} \tag{6.23}$$

and characteristic function

$$\phi_x(\omega) = \frac{\sin(\Delta\omega/2)}{\Delta\omega/2}. \tag{6.24}$$

This characteristic function is not appropriately band-limited and thus does not satisfy the conditions of (6.19) but does satisfy (6.21) since

$$\phi_x\left(\frac{2\pi n}{\Delta}\right) = \frac{\sin \pi n}{\pi n} = 0 \quad \text{for all} \quad n \neq 0. \tag{6.25}$$

Thus for this case, the quantization error associated with the uniform random variable x is uniform. If we compare the probability density function of the quantization error in (6.20) with the uniform density function of (6.22), we see that the error that will be introduced if the true density function is not uniform is given by

$$f_e(E) = \frac{1}{\Delta} \sum_{n \neq 0} \phi_x\left(\frac{2\pi n}{\Delta}\right) \exp\left(\frac{-j2\pi n E}{\Delta}\right), \quad -\Delta/2 \leq E < \Delta/2. \tag{6.26}$$

If we wish to use the uniform model even though the quantization noise is not strictly uniform, we can use this term to determine how significant the difference will be between the true density function and the uniform density function.

The Two-Dimensional Extended Quantization Theorem

In a similar fashion, we can extend the two-dimensional Quantization Theorem of [91] to account for the necessary and sufficient condition given in (6.21) [92]. This form is useful when determining the appropriateness of the uniform noise model as it relates to the second-order statistics of the quantization noise.

Gaussian Input Signals

Finally, Sripad and Snyder consider the case when the input signal to be quantized is Gaussian, since this covers a large range of signals of practical interest. If x is a zero-mean Gaussian random variable, its probability density function is given by

$$f_x(X) = \frac{1}{\sqrt{2\pi}\sigma_x} e^{-X^2/2\sigma_x^2}, \tag{6.27}$$

where σ_x is the standard deviation of x. The corresponding characteristic function is given by

$$\phi_x(\omega) = e^{-\omega^2\sigma_x^2/2}. \tag{6.28}$$

This characteristic function *does not* meet the restrictions of (6.21) and thus the density function of the quantization error will not be strictly uniform. The actual density function of the quantization error can be shown to be

$$f_\epsilon(E) = \begin{cases} \frac{1}{\Delta}\left[1 + 2\sum_{n\neq 0}\cos\left(\frac{2\pi nE}{\Delta}\right)\exp\left(-\frac{2\pi^2 n^2\sigma_x^2}{\Delta^2}\right)\right], & -\Delta/2 \leq E < \Delta/2 \\ 0, & \text{otherwise} \end{cases} . \quad (6.29)$$

We can use the density function of (6.29) to determine how well the quantization error can be approximated with a uniform error source. It can be shown that the mean μ_ϵ and variance σ_ϵ^2 of the quantization error is given by

$$\mu_\epsilon = 0 \quad (6.30)$$

$$\sigma_\epsilon^2 = \frac{\Delta^2}{12}\left[1 + \frac{12}{\pi^2}\sum_{n=1}^{\infty}\frac{(-1)^n}{n^2} exp\left(-\frac{2\pi^2 n^2\sigma_x^2}{\Delta^2}\right)\right]. \quad (6.31)$$

Both the uniform mean and the true mean are zero, so the means match exactly. The variance of the uniform distribution is $\Delta^2/12$, so the true variance deviates from this by a summation term which is dependent upon the ratio σ_x/Δ. Thus the accuracy of the uniform noise model will depend upon the ratio of the variance of the input Gaussian signal to the bin width of the uniform quantizer. As this ratio increases, the overall summation term decreases and thus the difference between the true and uniform densities decreases. Sripad and Snyder found that if $\Delta = 1$, the uniform model provides a close match for $\sigma_x \geq 1$. If $\Delta \neq 1$, then the uncorrelated uniform model is generally appropriate if $\sigma_x > \Delta$.

Sripad and Snyder also discuss the second order properties of the quantization noise resulting from a Gaussian input using the two-dimensional extended Quantization Theorem, but the results are not so easily classified as in the one-dimensional case and thus the results are not discussed here.

6.3.3 Scaling

To avoid the large errors overflow can create in a fixed-point system, scaling can be used to reduce or eliminate the possibility of overflow [93]. Scaling implies that, before quantization, a signal is scaled by some factor s_L that reduces the signal energy and thus reduces the possibility of overflow. A block diagram of the effect upon SNR is shown in Fig. 6.3, where $x(n)$ is the input, s_L is the scale factor, and SNR is the signal-to-noise ratio at the output. The downside to scaling is that the output SNR is reduced by s_L^2 (for scaling, $s_L < 1$). This occurs because the scaling occurs on the input (reducing its energy) before quantization, and thus before the quantization noise is added. Thus the signal is reduced while the noise

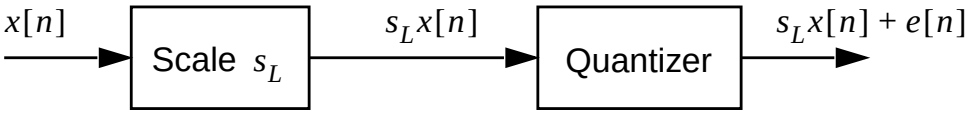

Figure 6.3: Scaling Model

is not. There are three common approaches to this problem: sum scaling, L_2 scaling, or L_∞ scaling.

The first technique is the most conservative and guarantees no overflow, the second is the least conservative, and the third is moderately conservative. An alternative is to design s based on allowing overflow to occur a certain percentage of the time. Since precise scaling can only be done if the impulse response $h[n]$ is known, it is especially useful for digital filter design. For complex systems such as the digital multistage receiver where a single-input single-output impulse response cannot be derived, an exact scaling technique cannot be developed. The alternative is to set the quantization range $[L_l, L_u]$ so that overflow is minimized based on a typical signal level (which may be most easily observed through simulation).

In sum (or L_1) scaling, s_L is set to ensure that overflow cannot occur at some node k. If we define $w_k(n)$ as the kth node variable and $h_k(n)$ as the impulse response between $x(n)$ and $w_k(n)$, then $w_k(n)$ is given by

$$w_k(n) = \sum_{m=-\infty}^{\infty} x(n-m)h(m). \tag{6.32}$$

A limit on the magnitude of $w_k(n)$ can be found via

$$\begin{aligned} |w_k(n)| &= |\sum_{m=-\infty}^{\infty} x(n-m)h_k(m)| \\ &< x_{max} \sum_{m=-\infty}^{\infty} |h_k(m)|, \end{aligned} \tag{6.33}$$

since x_{max} is the maximum possible value of $x(n)$ and a sum's magnitude is bounded by the sum of the individual magnitudes. To ensure that no overflow occurs, we must ensure that $|w_k(n)| < 1$, therefore

$$x_{max} < \frac{1}{\sum_{m=-\infty}^{\infty} |h_k(m)|}. \tag{6.34}$$

If we assume a fractional representation that $x_{max} < 1$ (X_m can still be greater that one so that the overall quantized number can be greater than one), then to ensure that overflow

does not occur, we must scale the input by

$$s_L = \frac{1}{\max_k \left[\sum_{m=-\infty}^{\infty} |h_k(m)|\right]}. \tag{6.35}$$

so that $s_L x_{max} < 1$ and no overflow occurs. Ensuring no overflow is as conservative a scaling technique as possible. The major drawback to this approach is that, because it is reduced by s_L^2, the output SNR may be degraded beyond acceptable limits.

The second approach, L_2 scaling, is the least conservative approach. This approach sets the scale factor to ensure that the energy in $w_k(n)$ is less than or equal to the energy of the input $x(n)$. If we assume that the energy of the input signal is bounded (which it will be for a physically realizable system), the magnitude of $w_k(n)$ is bounded by

$$|w_k(n)| \leq \sqrt{\sum_{n=-\infty}^{\infty} |h_k(n)|^2 \sum_{n=-\infty}^{\infty} |x(n)|^2}. \tag{6.36}$$

Since the energy of the input signal $x(n)$ is bounded, we know that

$$\sum_{n=-\infty}^{\infty} |x(n)|^2 \leq 1 \tag{6.37}$$

and therefore we can choose our scaling factor s as

$$s_L = \frac{1}{\sqrt{\sum_{n=-\infty}^{\infty} |h_k(n)|^2}}. \tag{6.38}$$

This form is commonly used and degrades SNR the least of the three proposals.

The third technique, L_∞ scaling, only ensures that there will be no overflow if a sine wave is applied to the input. This scaling factor is derived from the frequency response of the impulse response, $H_k(e^{j\omega})$, where ω is the frequency in rad/s. To ensure that the frequency response of $w_k(n)$ does not exceed 1 given a sinusoidal input, we can set s_L to be

$$s_L = \frac{1}{\max_k |H_k(e^{jw})|}. \tag{6.39}$$

An alternative to these approaches is to allow overflow to occur a given percentage of the time, and to set s_L so that the output SNR is maximized given this overflow percentage.

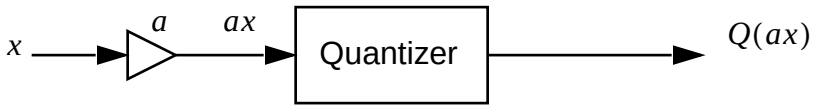

Figure 6.4: Roundoff Noise Model

6.3.4 Roundoff Error

In [94], Barnes *et al.* analyze the statistics of roundoff error, which is similar to but somewhat different from the error from quantizing a continuous amplitude signal. The roundoff error model is shown in Fig. 6.4, where x is a discrete input, a is the multiplicative constant, and $Q(\cdot)$ is the quantization function. The roundoff error e is given by $e = Q(ax) - ax$. This paper examines the conditions under which the uncorrelated white noise model is appropriate for roundoff error, and the statistical behavior of the noise when the conditions are not met.

The difference between roundoff error and the quantization error studied previously is that the input signal x is discrete in amplitude, not continuous (it has already been quantized), and the multiplicative constant a is discrete (there was no multiplication in the previous model). The result of the multiplication, ax, is then quantized. While a similar process to the quantization of a continuous-amplitude signal, the requirements for the white noise model are somewhat different. The term roundoff error is universally used regardless of whether the quantizer performs rounding or truncation.

We begin by assuming that x has been quantized uniformly with bin width Δ and can thus be represented in the form $x = n\Delta$. Furthermore, we assume that the multiplication output ax will also be quantized uniformly with bin width Δ [94]. As with the previous case of quantization, the error produced by roundoff is a deterministic process. This implies that if x is deterministic, then the roundoff error e will be deterministic as well. However, to aid in the analysis of communication systems, we will make a similar assumption as in our previous model and allow x to be a random variable, so that the error e will be random as well. Barnes assumes that x is a discrete, zero-mean Gaussian random variable with standard deviation σ_x. All of the following results regarding the appropriateness and characterization of the roundoff noise model are based on this assumption and will not apply in general if x has a different distribution.

The remaining assumption involves the constant a. We will assume that a can be expressed by $a = N/M$, where N is some integer, M is a positive integral power of two, and that their ratio N/M is irreducible [94]. Since N/M is irreducible and M is a power of two, this implies that N must be an odd integer (although it may be positive or negative).

While this implies that the constant a is rational, the constraints on the noise model are dependent upon M and thus it is assumed that most constants of practical interest can be represented in this fashion. What we seek, then, is to examine the statistics of the roundoff error based on a (in the form of N/M), and on the ratio of the input standard deviation to the bin width σ_x/Δ, which provides a measure of the dynamic range if x is random.

Since x is a discrete random variable, we represent it with the probability mass function $p_x(n\Delta)$, where [95]

$$p_x(n\Delta) = Pr[x = n\Delta] \tag{6.40}$$

where n is some integer. The characteristic function of x, $\phi_x(\omega)$, is given by [94]

$$\phi_x(\omega) = \sum_n \exp(j\omega n\Delta) p_x(n\Delta). \tag{6.41}$$

Probability Mass Function of Roundoff Error

We know that, since x has been quantized uniformly with bin spacing Δ, that it can be represented in the form [94]

$$x = n\Delta \tag{6.42}$$

where n is an integer. It is shown in [94] that if the approximation

$$\phi_x\left(\frac{2\pi m}{M\Delta}\right) \approx 0, \quad m \not\equiv 0 \mod M, \tag{6.43}$$

holds, then the density function of the roundoff error is approximately

$$p_e\left(\frac{l\Delta}{M}\right) \approx \frac{1}{M}, -\frac{M}{2} < l \leq \frac{M}{2}. \tag{6.44}$$

In general, the uniform noise model is a valid approximation if

$$\sigma_x \geq \frac{M\Delta}{2} \tag{6.45}$$

(note that for the original quantization case, the uniform noise model was a valid approximation if $\sigma_x \geq \Delta/2$).

Roundoff Error Statistics

We now wish to, in general, stochastically characterize the roundoff error by solving for its mean and variance [94]. It is shown via a Discrete Fourier Transform analysis that, for signals with large dynamic range, we can approximate ϕ_x as

$$\phi_x(2\pi k/M\Delta) \approx 0, \quad k \not\equiv 0 \bmod M. \tag{6.46}$$

For this specific case, we can approximate the mean and variance of the roundoff error sequence as

$$\mu_e \approx \frac{\Delta}{2M} \tag{6.47}$$

and

$$\sigma_e^2 \approx \frac{\Delta^2}{12}\left(1 - \frac{1}{M^2}\right). \tag{6.48}$$

In this case, the roundoff error sequence can be modeled as uniformly distributed white noise.

Numerical Examples

Barnes *et al.* then proceed to consider a number of numerical examples, including the case when the discrete random variable x is modeled with a Gaussian probability mass function [94]. The conclusions of these results are that the uniform model is appropriate for roundoff noise if the input signal has a large dynamic range and bandwidth. In general, however, the stochastic characterization of the roundoff error is a function of the multiplicative constant a and of the discrete input x (in terms of its dynamic range and bandwidth). The roundoff error will differ most from the uniform noise model when the input signal is narrowband and a low-noise environment is being considered.

6.3.5 Roundoff Error for Continuous Amplitude Multiplier Coefficients

The work of Barnes *et al.* [94] was extended by Tokaji and Barnes [96] to allow the multiplier coefficient a to be a continuous random variable (in the earlier analysis, a had to be discrete and put in the form $a = N/M$, where N was an odd integer, M was a power of two, and the ratio N/M was irreducible). For this case, if a is rational and in the form of $a = N/M$, the only restriction on N and M is that their ratio N/M be irreducible, which implies that the greatest common divisor of N and M is 1, or

$$GCD(N, M) = 1. \tag{6.49}$$

This considerably complicates the analysis over the previous discussion.

If a is rational and the characteristic function of the input x is approximately given by

$$\phi_x\left(\frac{2\pi m}{M}\right) \approx 0, \qquad m = 1, 2, \cdots, M-1 \tag{6.50}$$

then the characteristic function of the roundoff error is approximately given by

$$\phi_e(\omega, N/M) \approx \phi_0(\omega) \tag{6.51}$$

where $\phi_0(\omega)$ is the characteristic function of the roundoff error if it is uniformly distributed, or

$$\phi_0(\omega) = \frac{1}{M} \sum_{m \in I} \exp(j\omega m/M), \tag{6.52}$$

where I is given by

$$I = \{-(M-1)/2, -(M-3)/2, \cdots, (M-1)/2\} \tag{6.53}$$

if M is even and by

$$I = \{-M/2 + 1, -M/2 + 2, \cdots, M/2\} \tag{6.54}$$

if M is odd. The probability density function of the roundoff error is approximately given by

$$p_e(m/M) \approx p_0(m/M). \tag{6.55}$$

where $p_0(m/M)$ is the probability mass function of a uniform discrete variable given by

$$p_0(m/M) = \begin{cases} \frac{1}{M}, & m \in I \\ 0, & m \notin I \end{cases} . \tag{6.56}$$

Thus if (6.50) holds, then the roundoff error can be approximated with a uniform noise model.

Tokaji and Barnes then proceed to develop expressions for the first, second, and joint moments associated with the roundoff error. These expressions are dependent upon using a Fourier series representation and specific to each case studied. After examining a number of numerical cases and showing that the distribution of the roundoff error may not be uniform in some cases, the authors conclude that the true error distribution will vary from the uniform distribution the most when the input signal levels are low and when the multiplier coefficient a is either in the neighborhood of an integer or if it is rational and the denominator M is relatively small. Thus, as with the other types of errors that have been studied, we see that the uniform model is an accurate way to model the distribution of the quantization error for a wide variety of cases of practical interest, but that there are significant cases where the model is not accurate.

6.3.6 Roundoff Error for Continuous Amplitude Multiplier Coefficients and Continuous Input Signals

Wong introduced a model in 1990 [97] in which both the input signal x and the multiplication coefficient a are continuous. While the analysis is considerably more complex than

in previous cases and thus is not discussed here, the reader is referred to Wong's paper if more detail is required. Wong presents conditions upon which the uniform, white, and uncorrelated noise model is appropriate for the quantization and roundoff error (based on the first and second order moments of the noise). There are now two noise sources here, first for the quantization of x and then the roundoff error after x is multiplied by a. Thus the overall quantization noise e is defined to be

$$e = q(aq(x)) - ax, \tag{6.57}$$

where $q(\cdot)$ is the uniform quantization operation. The noise from quantizing x is now itself quantized after being multiplied by a.

The limits placed on a assume that it is either an integer or that it is a rational number (the case of a being an integer is treated separately from other rational numbers because different assumptions may be used). Although irrational forms of a are not considered, it is not expected that irrational coefficients will be used in most fixed-point systems and thus this case is not of as much practical importance.

Wong also considers the case when the input x has a Gaussian distribution and the conditions are not met for using the uniform noise model. As in previous cases, the uniform model does in fact provide a very good approximation to the actual noise distribution if the ratio of the standard deviation of the input x is large when compared with the bin width of the uniform quantizer, Δ. Wong also considers the effects of dithering.

6.3.7 Quantization Noise in Analog-to-Digital Converters

Gray provided a broad survey of analytic techniques for the uniform quantizer in 1990 [88], and specifically applied the results of these efforts to oversampled analog-to-digital converters (ADC's) such as Sigma-Delta modulators (a thorough treatment of the operation of Delta modulators was provided by Slepian in 1972 [98]). The difficulty in modeling the effects of quantization noise in oversampled ADC's is that the quantization noise exists in feedback loops. These ADC's operate by using low-rate quantizers in feedback loops and filtering, and in doing so attempt to mimic the performance of ADC's using a much higher rate (higher resolution) quantizer. The goal behind this technique is to use the much cheaper low-rate quantizers and use better timing circuits to achieve a low-cost ADC with the performance of its more expensive brethren (these types of ADC's are common in the industry today and have become standard in modern compact disc players). The exact nature of the ADC can vary significantly, but the most common variants are Sigma-Delta modulation, dithered Sigma-Delta modulation, two-stage Sigma-Delta modulation, and second-order Sigma-Delta modulation. These modulators can be cascaded to form even higher order modulators.

In the study of these complex systems (and other complex systems), it can be difficult to use the analysis of the preceding sections to determine whether or not the uniform noise model is appropriate. Simply characterizing the signal to be quantized stochastically, and then determining if the associated characteristic function meets the requirements of the extended Quantization Theorem can be a daunting if not outright impossible task, particularly when the systems are non-linear. Simulation can be a valuable tool in determining the validity of various noise models in these cases. While some researchers have simply used the uniform noise models because of their simplicity, without first applying any criterion for determining the validity of those models, it is important (as has been noted in several of the preceding sections) to ensure that the noise model being used is appropriate, because there are a number of instances in which the uncorrelated uniform noise model may not be appropriate. This is particularly true of ADC's employing low-rate quantizers in feedback loops, since there are not many quantization levels and the bin width is relatively large.

One approach taken by modern authors in analyzing cases such as these particular ADC's where the uniform model is not appropriate is to combine the deterministic and stochastic approaches in one unified model. The deterministic approach is commonly referred to as describing function analysis, a term borrowed from control theory. In this approach, the performance of the quantizer is examined for a specific input such as a DC signal or a sinusoid (as used in the 1947 paper by Clavier *et al.* [85, 86]. However, instead of actually applying the quantization process as did Clavier, in describing function analysis the quantizer is replaced by a linear gain so that the output is a weighted version of the input. The gain is determined by minimizing the mean-squared error between this sinusoidal output and the true output of the quantizer. In the unified approach, the describing function analysis is used to generate the fundamental component of the quantizer noise, and then an additive white noise process is added to that component to account for the stochastic behavior. This noise must also be determined in a least squares sense since it is no longer the same as the noise sources used in purely white noise approaches. This approach is more difficult than either of the two separate approaches and thus is typically used to analyze common ADC structures.

6.3.8 Minimizing the Quantization Error

Max showed in 1960 that if we either know the input to a quantizer or know the distribution of the input, we can optimize the levels of the quantizer in such a way as to minimize the error caused by quantization by minimizing the mean-square error [99]. Lloyd further refined this technique in 1982 [100], and the resulting algorithm has come to be known as the Lloyd-Max algorithm [101] and is used to set the optimum quantization levels for a given quantizer (again, we are assuming *a priori* knowledge of the input signal). The

algorithm is iterative and thus requires a numerical solution, so the optimum levels are typically generated on computer when the number of quantization bins is significant. The Lloyd-Max algorithm is not used in this research because the signal to be quantized at the input to the digital receiver, $r(t)$, does not have a known distribution. Similarly, we do not know the distribution of the amplitudes of the interference estimates that will be quantized. Finally, we assume for simplicity that the same type of quantizer is being used both for the received signal and the interference estimates, and thus a quantizer that is optimized in the Lloyd-Max sense for the received signal will not be optimized for the interference estimates. Thus, we simply use uniformly spaced levels in all of the quantizers.

6.3.9 Dithering

Although it is not germane to the research presented in this report, it is worthwhile to make mention of the use of dithering in the quantization process. The use of a dither signal is an old technique that can be used to make the output of the quantizer white even if it would not be so otherwise [102]. This is a common approach in systems such as voice telephony where the human listener will be making a subjective judgment on the quantized signal. Since the human mind prefers the sounds of white noise to periodic or noise with abrupt spikes, it is desirable to have the quantizer output white quantization noise at all times, regardless of what the input signal is. Thus, even if the input is a DC tone, the dither signal can be added to the tone before quantization and the resulting output will have white quantization noise (instead of a constant quantization error). Thus if we have an input signal x and a dither signal d, the summed signal that will be quantized is given by

$$y = x + d. \tag{6.58}$$

The dither signal d is itself a random, independent and identically distributed random process that is *also independent* of the input signal x. This is an important property, since if x and d are correlated, the quantization noise will not necessarily be white. It should be stressed that dithering is used to improve the *subjective* quality of the noise, not to diminish it. Since we will be evaluating the performance of the multistage receiver based on the bit error rate (an objective measure), there is no need for dithering in our approach.

6.4 Conclusions

The noise caused by uniform quantization is often modeled stochastically as a uniform noise source. The Quantization Theorem has been developed to determine when this model may be strictly applied, and to determine the error if the conditions are not met. Models

have been developed both for quantizing a continuous amplitude signal and for multiplying a discrete amplitude signal by a constant coefficient. These methods assume that the probability distribution function of the input is known, and provide a characterization of the error at the output of the quantizer.

Part of the difficulty in quantization analysis lies not just in modeling the noise at the output of the quantizer, but in modeling how this noise interacts with the rest of the system. We will study the effect of quantization in the multistage receiver in the next chapter. Here, we will be most interested in the characteristics of the quantization noise not at the output of the quantizer, but after it has been correlated with the desired PN code in the correlation receiver. In addition, since there are multiple quantization sources in the receiver, we shall see that modeling all of the sources as being uncorrelated may lead to an underrepresentation of the overall quantization noise, which in this case will lead to an optimistic bit error rate prediction.

Simulation is often used to verify the accuracy of the quantization model, and we will use a sample simulation run to characterize the correlated quantization noise. Next, we will model all of the quantization noise as a lumped noise source, which inherently accounts for the correlation amongst the various quantization noise sources. Finally, we will turn to a semi-analytic technique in which the power in the quantization noise is set to match the BER curves of the simulation and semi-analytic models. Using a semi-analytic approach will also allow for compensation of other inaccuracies in the analytic model, such as the unaccounted for mean in the interference estimates.

Chapter 7

Quantization In the Multistage Receiver

7.1 Introduction

The prototype multistage receiver being developed at Virginia Tech is a completely digital design. Given the nature of the specifications (which are discussed, along with the associated computational complexity, in Chapter 8), this places extreme demands upon the computational abilities of the microprocessors being used. Regardless of whether we are developing the receiver based on a traditional DSP architecture or using the new reconfigurable computing platform, the high computational demands and high operating speeds imply that we will need to use fixed-point arithmetic with as few bits as possible. Thus we need to determine how the use of fixed-point arithmetic will affect the ability of the multistage receiver to cancel interference. As we shall see later, spread spectrum systems employing correlation receivers enjoy an inherent advantage over more traditional designs in regards to quantization noise, since this noise is passed through the correlator and thus some processing gain is achieved on this noise as well as the interference and channel noise.

The rest of the chapter is organized in the following manner. First, the modeling of the quantization noise sources is discussed. Next, an analytical framework for evaluating the BER is developed based on the improved Gaussian approximation. Numerical case studies are then presented and compared with simulation results. A semi-analytic technique is then presented which improves upon the accuracy of the analytic model, which is pessimistic under certain conditions. Finally, conclusions are presented.

7.2 Quantization Errors in a Multistage Receiver

It is assumed that, for reasons of implementation, the speed and low cost of a fixed-point implementation will be desirable for a DSP implementation of a multistage receiver. The simplicity of the algorithms in the multistage architecture allows a close examination of where potential quantization problems are likely to occur. Fixed-point quantization can then be simulated in SPW through the addition of quantization blocks and compared to the original SPW simulations, which are themselves calculated using the 32 bit floating-point notation of the SUN Sparc platform. The SPW system model is shown in Fig. 7.1 and discussed in detail in section 7.5.

The received signal at the input of the receiver, $r(t)$, must be quantized, so there will be an associated quantization error. Overflow is also possible, so care must be taken in choosing X_m so that overflow does not occur at the input. From this stage forward, every number will be quantized with $B+1$ bits, since the rest of the receiver architecture is digital.

The received signal is then passed to the correlation receiver, where various additions and multiplications take place, so each operation must be analyzed to determine where errors will most likely be introduced. If we ignore the effects of the coherent demodulation (multiplication of the received signal by the cosine and sine of the known phase), the first multiplication takes place during the discrete correlation process, which is given by

$$Z_{k,i}^{(s)} = \sum_{i=1}^{NN_s} r_{k,i}^{(s)} a_{k,i} p_{T_s}(t - iT_s), \tag{7.1}$$

where $r_{k,i}^{(s)}$ is the sampled version of $r_k^{(s)}(t)$ at sample i and $a_{k,i}$ is the chip value of user k's PN sequence during sample i. Since $a_{k,i} \in \{1, -1\}$, the multiplications in the correlation process amount to a possible sign change of the received signal sample, and thus no overflow is possible and no truncation or rounding is required. There is, therefore, no noise introduced at this point. There is a possibility of overflow in the summation term, although the result is not likely to significantly exceed the desired threshold value, and so an appropriate scaling term can be chosen. In addition, overflow is not a concern in the intermediate additions because two's complement notation is being used. Since the correlation value will be used both in determining the bit value and the estimate of the received power level, if overflow does occur, clipping is probably the best approach to ensure that the result remains as close to the original value as possible.

The next stage where quantization errors can occur is in the estimation stage. The initial multiplication is of the data bit estimate $\hat{b}_{k,i}$ with a locally generated PN sequence replica. This is a trivial multiplication in that $\hat{b}_{k,i} \in \{-1, 1\}$, and so the result is a possible sign change of the chip values. Since there is no possible overflow and truncation or rounding

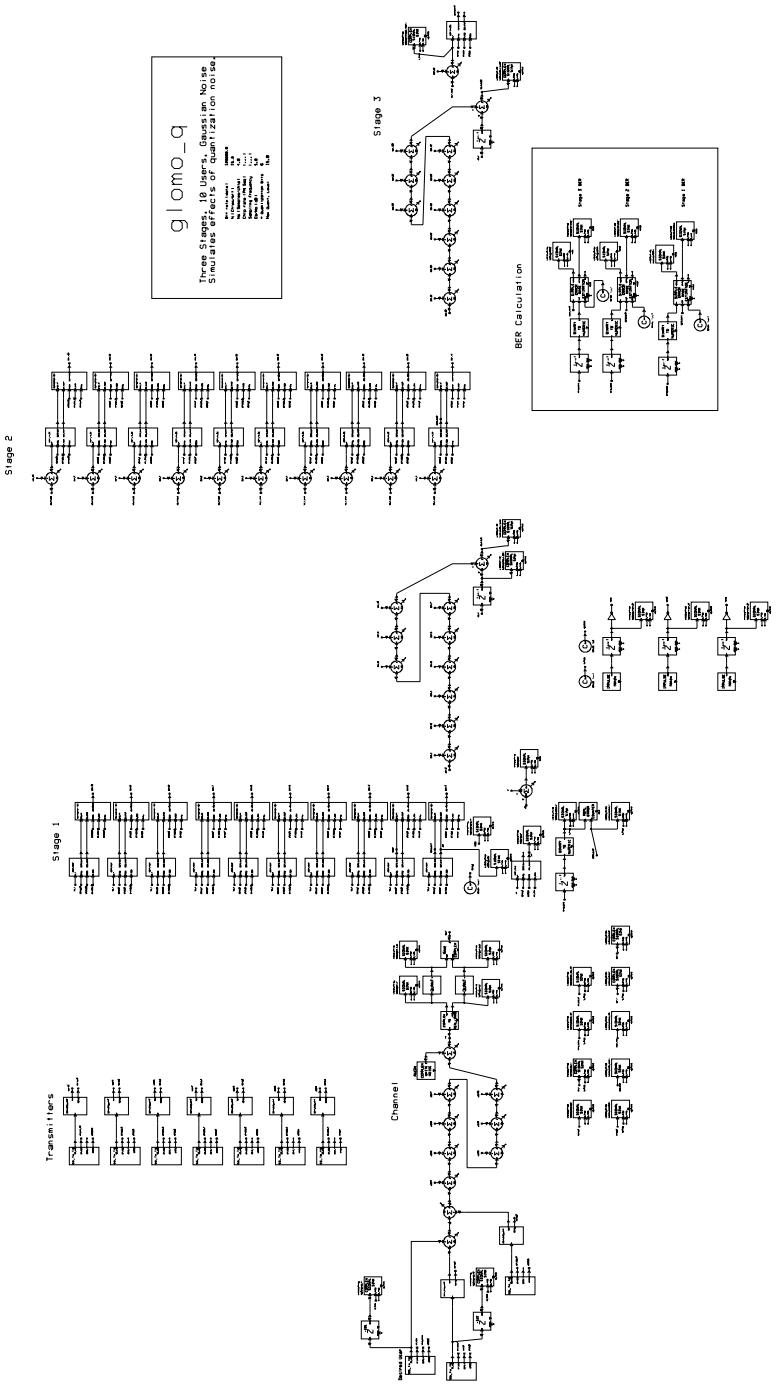

Figure 7.1: SPW Fixed-Point Multistage Receiver Model

is not necessary, no noise is introduced at this point. The next step is to multiply by the magnitude of the decision statistic. Since the chip values are in the set $\{-1, 1\}$, this multiplication can also only be a sign change and no noise is introduced. The next step is the multiplication by the constant term $1/(NN_s)$, which must be quantized and therefore there will be accompanying quantization noise. Since this is a known term, the amount of noise will be known (and constant over time). The multiplication will not result in overflow since this constant is less than one. Truncation or rounding will be necessary so noise may be introduced here as well. The next step is to multiply this result by the cosine and sine of the phase term ϕ_k. Since each of these terms is less than one, overflow is not a concern, but truncation or rounding will be necessary. At this point, the I and Q portion of the reconstructed signal $\hat{s}_k^{(s)}$ are completed.

Next, all signal estimates are summed together as shown in Fig. 7.1. Overflow is theoretically possible at this point, although this summation should have a magnitude near that of the original received signal, and therefore if the initial received signal did not overflow, the reconstructed estimate should not as well. As before, overflow is not a concern for the intermediate additions because of the use of two's complement notation. Each of these summations will require truncation or rounding. The next step is to subtract the reconstructed estimates from the received signal itself. Overflow (and underflow) is not likely to be a problem since the two terms have similar magnitudes. Truncation or rounding will be necessary since this residual signal should ideally be close to zero. The next stage is to add back in the estimate of the desired user's signal, which has already been truncated or rounded when the estimates were originally summed. This signal is passed to the next correlation receiver, which has been discussed in a preceding paragraph.

This concludes the preliminary analysis of sources of error in the multistage receiver. Overflow is not likely to be a problem as long as the initial received signal values can be quantized without overflow. There are a number of areas where noise due to truncation or rounding is introduced. Scaling may help to minimize the noise at certain points, since the approximate range of values of the resulting summation may be known.

7.3 System Model

The system model is based upon the improved Gaussian approximation model presented in Chapter 4, but with modifications to account for the effects of quantization. The transmitted system model is the same (with the exception that all K users are now assumed to be synchronized), but the receiver model differs both because the received signal $r(t)$ is quantized at the input to the digital receiver and because the amplitudes of the interference estimates will be quantized.

The received signal $r(t)$ is quantized at the input to the digital receiver with B bits, resulting in the quantized signal

$$r_\epsilon(t) = n_c(t) + e_r(t) + \sum_{k=1}^{K} s_k(t - \tau_k), \tag{7.2}$$

where $n_c(t)$ represents the AWGN channel noise (this was just $n(t)$ in the synchronization model) and $e_r(t)$ represents the quantization noise. The decision statistics in the first stage of receivers are made based on this quantized form of the received signal. For a user k during bit interval i, this decision statistic is given by

$$Z_{k,i}^{(1)} = \int_{iT+\tau_k}^{(i+1)T+\tau_k} r_\epsilon(t) a_k(t - \tau_k) \cos(\omega_c t + \phi_k) dt. \tag{7.3}$$

The next step is to form the interference estimates, but the amplitude estimates will have to be quantized before they can be used in the digital receiver. We will be quantizing the amplitude estimate $2Z_{k,i}^{(s)}/T$, so the estimate of user k's received signal is given by

$$\hat{s}_k^{(s+1)}(t) = a_k(t - \tau_k) \cos(\omega_c t + \phi_k) \sum_{i=-\infty}^{\infty} \left\{ \frac{2}{T} Z_{k,i}^{(s)} + e_k^{(s)}(t) \right\} p_T(t - iT), \tag{7.4}$$

where $e_k^{(s)}(t)$ is the quantization error for user k's estimate at stage s. Because the linear noise model assumes that there is no correlation of this error from user to user and from stage to stage, and because the stochastic representation of the model will not change from user to user or from stage to stage, we will denote this error as e_s and assume that it is the same for each user k at each stage s.

We now form the new received signal $r_{j,\epsilon}^{(s)}(t)$ at each state s for each user j, $1 \le j \le K$, by subtracting out the interference estimates, yielding

$$\begin{aligned} r_{j,\epsilon}^{(s)}(t) &= r_\epsilon(t) - \sum_{k=1,k\neq j}^{K} \hat{s}_k^{(s)}(t - \tau_k) \\ &= n_c(t) + e_r(t) + s_j(t) + \sum_{k=1,k\neq j}^{K} \left[s_k(t - \tau_k) - \hat{s}_k^{(s)}(t - \tau_k) \right]. \end{aligned} \tag{7.5}$$

The first term is the Gaussian channel noise, the second term is the quantization noise due to quantizing the received signal, the third term is the desired user's signal, and the final term is the residual multiple-access interference. This received signal is then passed to the next bank of correlation receivers. At each stage s, a new decision statistic $Z_{j,i}^{(s)}$ is obtained during bit interval i by correlating $r_{j,\epsilon}^{(s)}(t)$ with user j's spreading code,

$$Z_{j,i}^{(s)} = \int_{iT+\tau_j}^{(i+1)T+\tau_j} r_{j,\epsilon}^{(s)}(t) a_j(t - \tau_j) \cos(\omega_c t + \phi_j) dt. \tag{7.6}$$

The decision statistic is then passed onto the next stage for use in interference estimation until the final stage of the receiver has been reached. At the final stage, the estimate of bit i from user d, $\hat{b}_{d,i}$, is determined from $Z_{d,i}^{(s)}$ by

$$\hat{b}_{d,i} = \begin{cases} 1, & Z_{d,i}^{(s)} \geq 0 \\ -1, & Z_{d,i}^{(s)} < 0 \end{cases} . \tag{7.7}$$

Note that although the decision statistic itself may need to be quantized in the digital receiver before the bit decision is made, the quantization process itself *cannot* change the sign of the decision statistic, and thus it does not add any noise to the bit estimation process. Therefore, we do not need to account for the quantization of $Z_{j,i}^{(s)}$ before the bit estimation in the bit error rate calculation.

7.4 Analysis Using an Improved Gaussian Approximation

As in the previous chapter, we wish to model the multiple access interference using an improved Gaussian approximation. The key difference here is that the ability to cancel interference is degraded by the effects of quantization and not by unsynchronized interference. We begin with an expression for the decision statistic $Z_{j,i}^{(s)}$ by substituting (7.5) into (7.6) to obtain

$$Z_{j,i}^{(s)} = \eta_c + \epsilon_r + \sqrt{\frac{P_j}{2}} T b_{j,i} + \sum_{k=1,k\neq j}^{K} I_{k,j}^{(s)}, \tag{7.8}$$

where η_c is a zero mean Gaussian random variable with variance $N_o T/4$ representing the correlated channel noise, ϵ_r is the correlated noise associated with quantizing the input signal $r(t)$, the third term represents the desired component, and the final term is the residual MAI after interference cancellation (the quantization noise due to the quantization of the interference estimates is embedded in this term).

Analyzing the Correlated Quantization Noise

While e_r is uniform over $[-\Delta/2, \Delta/2]$, we do not know the distribution of the correlated version ϵ_r. For any random variable X, we can find the distribution of the random variable Y where $Y = g(X)$ via [103]

$$f_Y(y) = \sum_{i=1}^{k} \frac{f_X(x^{(i)})}{|g'(x^{(i)})|}, \tag{7.9}$$

where $g'(x)$ is the first-order derivative of $g(x)$ with respect to x and i represents the k roots of $g(x)$. Thus to solve for the distribution of the correlated quantization noise ϵ_r, we need to analyze $\epsilon_r = g(e_r)$, which is, at the output of user k's correlation receiver,

$$\epsilon_r = \int_{iT+\tau_k}^{(i+1)T+\tau_k} e_r(t) a_k(t-\tau_k) \cos(\omega_c t + \phi_k) dt. \tag{7.10}$$

This presents a distinct problem, since the derivative of this function (a definite integral) is not defined. This implies that we cannot explicitly solve for the distribution of ϵ_r using analytical techniques.

In the simulation section, we shall see that we can approximate the distribution of ϵ_r quite well using a zero-mean Gaussian random variable whose standard deviation can be obtained from a short simulation run. This standard deviation will be appropriate for a specified number of bits B and a given quantizer range.

Analyzing the Conditional Variance of the Total MAI

As before, we wish to analyze the distribution of the conditional variance of the total MAI, Ψ, which is given by

$$\Psi = E\left[\left(\sum_{k=1,k\neq d}^{K} I_{k,d}^{(1)} \right)^2 \mid \{\phi_k\}, \{\tau_k\}, \{P_k\}, B \right]. \tag{7.11}$$

There is no change in the way μ_Ψ and σ_Ψ are defined based on the mean and the variance of the effective signal powers,

$$\mu_\Psi^{(s)} = \frac{T_c^2 N}{6} \sum_{k=1,k\neq d}^{K} \mu_{P_k}^{(s)}, \tag{7.12}$$

and

$$\begin{aligned} \left(\sigma_\Psi^{(s)}\right)^2 &= \frac{T_c^4}{4} \left[\frac{23N^2+18N-18}{360} \sum_{k=1,k\neq d}^{K} \left(\mu_{P_k}^{(s)}\right)^2 + \frac{7N^2+2N-2}{40} \sum_{k=1,k\neq d}^{K} \left(\sigma_{P_k}^{(s)}\right)^2 \right. \\ &\quad \left. + \frac{N-1}{36} \sum_{k=1,k\neq d}^{K} \sum_{j=1,j\neq k\neq d}^{K} \mu_{P_k}^{(s)} \mu_{P_j}^{(s)} \right]. \end{aligned} \tag{7.13}$$

Determining the Probability of Bit Error

The form of the improved Gaussian approximation for the probability of bit error has changed due to the addition of the error source ϵ_r in the decision statistic of (7.8), since

$Z_{k,i}^{(s)}$ is not necessarily a Gaussian random variable (if we do not assume that ϵ_r has a Gaussian distribution). We can envision this decision statistic as the sum of two random variables, the decision statistic we used previously plus the correlated quantization noise ϵ_r. In general, the probability distribution function of Z where $z = g(x, y)$ is given by [95]

$$F_Z(z) = \int_{(x,y)\in C_z} \int f_{XY}(x, y)dxdy, \tag{7.14}$$

where C_z is the point set determined from $g(x, y) \leq z$ and $f_{XY}(x, y)$ is the joint density function of x and y. For the case where $z = x + y$, the density function $p_Z(z)$ is given by

$$f_Z(z) = \int_{-\infty}^{\infty} f_{XY}(z - y, y)dy. \tag{7.15}$$

If x and y are independent random variables, then (7.15) can be shown to be

$$f_Z(z) = \int_{-\infty}^{\infty} f_X(z - y)f_Y(y)dy \tag{7.16}$$

$$= \int_{-\infty}^{\infty} f_X(x)f_Y(z - x)dx. \tag{7.17}$$

Thus the new density function is the convolution of the two individual density functions, or

$$f_Z(z) = f_X(x) * f_Y(y) = f_Y(y) * f_X(x). \tag{7.18}$$

We can use (7.16) or (7.17) to solve for the probability of error, based on the density function of the decision statistic. Once we have this density function, we can calculate the probability that $Z_{k,i}^{(s)} < 0$ given that the bit sent during interval i is a 1.

If we model ϵ_r as a Gaussian random variable (as discussed in Section 7.6.1), then the resulting expression for the probability of bit error simplifies to a form similar to that of the case when quantization is not used. Using the improved Gaussian approximation, the bit error probability can be closely approximated by

$$P_{b,d}^{(1)} \approx \frac{2}{3}Q\left(\sqrt{\frac{P_d T^2}{2\left(\mu_\Psi^{(s)} + \frac{N_o T}{4} + \sigma_{\epsilon_r}^2\right)}}\right) + \frac{1}{6}Q\left(\sqrt{\frac{P_d T^2}{2\left(\mu_\Psi^{(s)} + \sqrt{3}\sigma_\Psi^{(s)} + \frac{N_o T}{4} + \sigma_{\epsilon_r}^2\right)}}\right)$$
$$+\frac{1}{6}Q\left(\sqrt{\frac{P_d T^2}{2\left(\mu_\Psi^{(s)} - \sqrt{3}\sigma_\Psi^{(s)} + \frac{N_o T}{4} + \sigma_{\epsilon_r}^2\right)}}\right), \tag{7.19}$$

where σ_{ϵ_r} is the standard deviation of the correlated quantization noise source ϵ_r.

The next step is to determine $\mu_\Psi^{(s)}$ and $\sigma_\Psi^{(s)}$ at each stage s so that we can properly characterize the multiple access interference. As before, we must do this separately for stage 1 and for stages 2 and beyond, since there is no interference cancellation in stage 1. This also implies that there is no interference estimation in stage 1, and thus no quantization noise due to the quantization of the interference estimate.

7.4.1 First Stage Multiple Access Interference

Since there is no interference cancellation in the first stage of the multistage receiver, there is no interference estimation and thus no quantization of the interference estimate. Therefore, there is no change in the way we characterize the first stage multiple access interference, and the interference caused by user k to user j is still given by

$$\begin{aligned} I_{k,j}^{(1)} &= \sqrt{\frac{P_k}{2}}\cos(\phi_k - \phi_j)\left\{\int_{iT+\tau_j}^{iT+\tau_k} b_{k,i-1}a_k(t-\tau_k)a_j(t-\tau_j)dt \right. \\ &\quad \left. + \int_{iT+\tau_k}^{(i+1)T+\tau_j} b_{k,i}a_k(t-\tau_k)a_j(t-\tau_j)dt\right\}. \end{aligned} \tag{7.20}$$

As before, this can be reduced to

$$I_{k,j}^{(1)} = T_c\sqrt{\frac{P_k}{2}}\cos(\phi_k - \phi_j)W_k, \tag{7.21}$$

where W_k is defined in [60] and it is shown that $E[W_k] = 0$ and $E[W_k^2] = 2N/3$.

7.4.2 MAI For Stages 2 and Higher

The residual interference at stage s from user k to user j is still given by

$$I_{k,j}^{(s+1)} = I_{k,j}^{(1)} - \hat{I}_{k,j}^{(s+1)}, \tag{7.22}$$

but now the interference estimate $\hat{I}_{k,j}^{(s+1)}$ contains the quantization noise caused by quantizing the estimate $2Z_{k,i}^{(s)}/T$. By applying (7.4) and (7.6), we obtain

$$\begin{aligned} \hat{I}_{k,j}^{(s+1)} &= \cos(\phi_k - \phi_j)\left\{\int_{iT+\tau_j}^{iT+\tau_k}\left[\frac{Z_{k,i-1}^{(s)}}{T} + \frac{e_s}{2}\right]a_k(t-\tau_k)a_j(t-\tau_j)dt \right. \\ &\quad \left. + \int_{iT+\tau_k}^{(i+1)T+\tau_j}\left[\frac{Z_{k,i}^{(s)}}{T} + \frac{e_s}{2}\right]a_k(t-\tau_k)a_j(t-\tau_j)dt\right\}. \end{aligned} \tag{7.23}$$

As in Chapter 5, we can further simplify this expression for the interference estimate *provided* that we make the assumption that the decision statistic $Z_{k,i}^{(s)}$ can be pulled outside of the integral, which the definition of (7.6) will not strictly allow. This in effect ignores any portion of $Z_{k,i}^{(s)}$ that is correlated with user j's PN code. However, since the interference of user j to user k is embedded in $Z_{k,i}^{(s)}$, there will be some correlation present. It is this

term that makes the expected value of the interference estimates non-zero and introduces a bias into the decision statistic of user j, as was discussed in detail in Section 5.4.6.

For now, however, we will make the assumption that $Z_{k,i}^{(s)}$ can be pulled outside the integral, so that the interference estimate can be rewritten as

$$\begin{aligned}\hat{I}_{k,j}^{(s+1)} &= \cos(\phi_k - \phi_j)\left\{\left[\frac{Z_{k,i-1}^{(s)}}{T} + \frac{\epsilon_s}{2}\right]\int_{iT+\tau_j}^{iT+\tau_k} a_k(t-\tau_k)a_j(t-\tau_j)dt \right. \\ &\quad \left. + \left[\frac{Z_{k,i}^{(s)}}{T} + \frac{\epsilon_s}{2}\right]\int_{iT+\tau_k}^{(i+1)T+\tau_j} a_k(t-\tau_k)a_j(t-\tau_j)dt\right\}, \end{aligned} \tag{7.24}$$

where ϵ_s is the quantization noise e_s when correlated with the PN sequence of user j. By substituting (7.20) and (7.24) into (7.22), we obtain

$$\begin{aligned} I_{k,j}^{(s+1)} &= \cos(\phi_k - \phi_j)\left\{\left[\sqrt{\frac{P_k}{2}}b_{k,i-1} - \left(\frac{Z_{k,i-1}^{(s)}}{T} + \frac{\epsilon_s}{2}\right)\right]\int_{iT+\tau_j}^{iT+\tau_k} a_k(t-\tau_k)a_j(t-\tau_j)dt \right. \\ &\quad \left. + \left[\sqrt{\frac{P_k}{2}}b_{k,i} - \left(\frac{Z_{k,i}^{(s)}}{T} + \frac{\epsilon_s}{2}\right)\right]\int_{iT+\tau_k}^{(i+1)T+\tau_j} a_k(t-\tau_k)a_j(t-\tau_j)dt\right\}. \end{aligned} \tag{7.25}$$

To put (7.25) into the form of (7.20), we define $\nu_{k,i}^{(s+1)}$ to be

$$\begin{aligned}\nu_{k,i}^{(s+1)} &= 2\left[\sqrt{\frac{P_k}{2}}b_{k,i} - \left(\frac{Z_{k,i}^{(s)}}{T} + \frac{\epsilon_s}{2}\right)\right]^2 \\ &= P_k - \sqrt{8P_k}b_{k,i}\left(\frac{Z_{k,i}^{(s)}}{T} + \frac{\epsilon_s}{2}\right) + 2\left(\frac{Z_{k,i}^{(s)}}{T} + \frac{\epsilon_s}{2}\right)^2. \end{aligned} \tag{7.26}$$

Thus, as before, $\nu_{k,i}^{(s+1)}$ can be interpreted as the effective power in the interference from user k during bit interval i after $s+1$ stages, but with the key difference in that now noise has been added to the cancellation process due to the quantization of the amplitude estimate. We can now rewrite (7.25) in the form of (7.21) as

$$I_{k,j}^{(s+1)} = T_c\sqrt{\frac{\nu_{k,i}^{(s+1)}}{2}}\cos(\phi_k - \phi_j)W_k, \tag{7.27}$$

which is the same form as before since the quantization noise is embedded in the effective power $\nu_{k,i}^{(s+1)}$.

The next step is to determine expressions for the mean and variance of this effective power so that we may use (7.12) and (7.13) to solve for the mean and variance of the conditional variance of the MAI, Ψ. Once these two parameters are known, we can solve for the probability of bit error using (7.19).

7.4.3 Derivation of Mean of Effective Signal Power

In this section, we calculate the mean of the effective signal power $\nu_{k,i}^{(s+1)}$. The mean can be found directly from (7.26) by taking the expectation as

$$\mu_{P_k}^{(s+1)} = E[\nu_{k,i}^{(s+1)}] = E\left[P_k - \sqrt{8P_k}b_{k,i}\left(\frac{Z_{k,i}^{(s)}}{T} + \frac{\epsilon_s}{2}\right) + 2\left(\frac{Z_{k,i}^{(s)}}{T} + \frac{\epsilon_s}{2}\right)^2\right]. \tag{7.28}$$

Using the expression for the decision statistic given by (7.8), the mean can be rewritten as

$$\begin{aligned}\mu_{P_k}^{(s+1)} &= E\left[P_k - \sqrt{8P_k}b_{k,i}\left\{\frac{1}{T}\left(\eta_c + \epsilon_r + \sqrt{\frac{P_k}{2}}Tb_{k,i} + \sum_{l=1,l\neq k}^{K} I_{l,k}^{(s)}\right) + \frac{\epsilon_s}{2}\right\}\right. \\ &\quad \left. + \frac{2}{T}\left\{\frac{1}{T}\left(\eta_c + \epsilon_r + \sqrt{\frac{P_k}{2}}Tb_{k,i} + \sum_{l=1,l\neq k}^{K} I_{l,k}^{(s)}\right) + \frac{\epsilon_s}{2}\right\}^2\right] \\ &= 2E\left[\left(\frac{\eta_c}{T}\right)^2\right] + \frac{2}{T^2}E[\epsilon_r^2] + \frac{1}{2}E[\epsilon_s^2] + \frac{2}{T^2}E\left[\left(\sum_{l=1,l\neq k}^{K} I_{l,k}^{(s)}\right)^2\right], \end{aligned} \tag{7.29}$$

using $E[\eta_c] = 0$, $E[\epsilon_r] = 0$, and where we have assumed that $E[I_{l,k}^{(s)}] = 0$ (we are ignoring the bias term that is discussed in Section 5.4.6), and we have assumed that all of the random variables are uncorrelated. Since the terms $I_{l,k}^{(s)}$ are still uncorrelated, we have

$$E\left[\left(\sum_{l=1,l\neq k}^{K} I_{l,k}^{(s)}\right)^2\right] = E\left[\sum_{l=1,l\neq k}^{K}\left(I_{l,k}^{(s)}\right)^2\right]. \tag{7.30}$$

Because the quantization noise from the estimation process is embedded in the $I_{l,k}^{(s)}$ terms, we still have that

$$\begin{aligned}\frac{1}{T^2}E\left[\sum_{l=1,l\neq k}^{K}\left(I_{l,k}^{(s)}\right)^2\right] &= \frac{1}{T^2}E\left[\sum_{l=1,l\neq k}^{K} T_c^2\cos^2(\phi_l - \phi_k)\frac{\nu_{l,i}^{(s)}}{2}W_k^2\right] \\ &= \frac{1}{6N}\sum_{l=1,l\neq k}^{K}\mu_{P_k}^{(s)}, \end{aligned} \tag{7.31}$$

where we have used $E[\cos^2(\phi_l - \phi_k)] = 1/2$. Using $E = [(\eta_c/T)^2] = N_o/(4T)$ and (7.31), we can solve (7.29) to be

$$\mu_{P_k}^{(s+1)} = \frac{N_o}{2T} + \frac{2}{T^2}E[\epsilon_r^2] + \frac{1}{2}E[\epsilon_s^2] + \frac{1}{3N}\sum_{l=1,l\neq k}^{K}\mu_{P_l}^{(s)}, \tag{7.32}$$

for $1 \leq k \leq K$. It is worthwhile noting where the effects of quantization appear in the mean of the effective powers: the ϵ_r term is due to the initial quantization of the received signal $r(t)$, the ϵ_s term is due to the quantization of the amplitude estimate of user k for stage $s+1$, and the quantization noise from the other users is embedded in the mean of the effective powers of those users, which is accounted for in the summation term.

Therefore we now have a recursive definition for the mean of the effective interference power that accounts for the quantization that occurs at the input of the digital receiver and during the amplitude estimation process for each stage and for each user.

7.4.4 Variance of Effective Signal Power

In this section, we develop a definition for the variance of the effective interference power, $(\sigma_{P_k}^{(s+1)})^2$. The variance by definition is given by

$$(\sigma_{P_k}^{(s+1)})^2 = E\left[\left(\nu_k^{(s+1)}\right)^2\right] - \left(\mu_{P_k}^{(s+1)}\right)^2, \tag{7.33}$$

where both $\nu_k^{(s+1)}$ and $\mu_{P_k}^{(s+1)}$ contain quantization noise. Since we found $\mu_{P_k}^{(s+1)}$ in Section 7.4.3, we need to find an expression for $E[(\nu_k^{(s+1)})^2]$. Because of the mathematical nature of the derivation, the explicit derivation is given in Appendix B. The expression for the variance of the effective interference power at stage $s+1$ caused by user k, $1 \leq k \leq K$, is shown to be

$$\begin{aligned}
(\sigma_{P_k}^{(s+1)})^2 \;=\; & \frac{N_o^2}{2T^2} + 4\frac{E[\epsilon_r^4]}{T^4} + \frac{E[\epsilon_s^4]}{4} + \frac{N_o E[\epsilon_s^2]}{T} + 4\frac{E[\epsilon_r^2]E[\epsilon_s^2]}{T^2} + 4\frac{N_o E[\epsilon_r^2]}{T^3} \\
& + \left(\frac{4N_o}{T^3} + 16\frac{E[\epsilon_r^2]}{T^4} + 4\frac{E[\epsilon_s^2]}{T^4}\right)\mu_\psi^{(s)} - 4\frac{E^2[\epsilon_r^2]}{T^4} - \frac{E^2[\epsilon_s^2]}{4} \\
& - \frac{4}{T^4}\left(\mu_\Psi^{(s)}\right)^2 + \frac{9(4N-3)}{40N^3}\sum_{l=1,l\neq k}^{K}\left[(\sigma_{P_l}^{(s)})^2 + \left(\mu_{P_l}^{(s)}\right)^2\right] \\
& + \frac{4N^2-9N+13}{12N^4}\sum_{l=1,l\neq k}^{K}\sum_{m=1,m\neq l\neq k}^{K}\mu_{P_l}^{(s)}\mu_{P_m}^{(s)}.
\end{aligned} \tag{7.34}$$

We now have the required terms to calculate the probability of bit error as expressed in (7.19), where we are assuming that the distribution of the correlated quantization noise sources ϵ_r and ϵ_s are Gaussian and that the sample standard deviations can be obtained via a sample simulation run or by some either means.

Bit rate (data)	128000.0
N (Chips/bit)	15.0
Ns (Samples/chip)	4.0
Chip rate (PN Seq)	(...)
Sampling frequency	(...)
Eb/No (dB)	5.0
# Quantization Bits	12
Max Quant. Level	20.0

Figure 7.2: The System and Simulation Parameters

7.5 The Simulation Model

The SPW system model is shown in Fig. 7.1 and is stored as filename *glomo_q*. The multistage receiver has a total of three stages (two stages of cancellation), and 10 users are modeled. Additive white Gaussian noise (AWGN) is the only degradation caused by the channel. The phase and delay at each transmitter are random and uniformly distributed over $[0, 2\pi)$ and $[0, NN_s - 1]$ respectively, where N is the number of chips per bit and N_s is the number of samples per chip. Bit error rates are calculated at each stage of the receiver. Because it is difficult to view particular parts of the system as shown in Fig. 7.1, the various pieces of the design are discussed in more detail with magnified figures in the following sections.

7.5.1 System Parameters

The system and simulation parameters are set in *glomo_q* as shown in Fig. 7.2. The parameters used for these fixed-point simulations are based upon the current hardware prototype specifications as they existed when the simulations were begun, although these specifications are subject to change and discussed in more detail in Chapter 8. The bit rate is set at $r_b = 128$ kbps and the number of chips per bit is $N = 15$, yielding an overall chip rate of $r_c = 1.92$ Mcps. With $N_s = 4$ samples per bit, this gives an overall sample rate of $r_s = 7.68$ Msps. The value of E_b/N_o is allowed to vary, and the typical range for these simulations is 0 to 10 dB. The number of quantization bits ranges from 4 to 12 and the typical quantization range is $[-20, 20]$, although $[-15, 15]$ is also used.

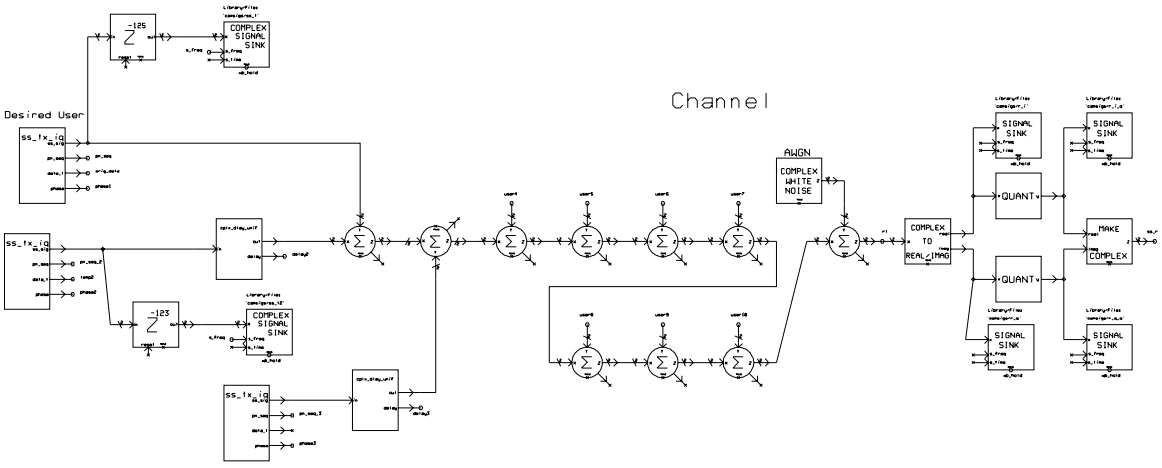

Figure 7.3: Quantizing the Received Signal

7.5.2 Quantizing the Received Signal

One of the primary differences between the fixed-point model and the SPW model used in previous sections is that the received signal $r(t)$ is now quantized as shown in Fig. 7.3. On the left are three of the transmitters, including the desired users. Next all 10 users are summed together (the other 7 transmitters are not shown here), and the AWGN is added to simulate the channel. In previous simulations, this constituted the received signal that the multistage receiver processed. Here, this signal is split into its I and Q portions, and then each of these channels is quantized using a uniform quantizer with the number of bits and the quantization range being taken from the system parameters. The signal is then re-combined into a single complex, baseband signal that models the quantized received signal $r_\epsilon(t)$.

7.5.3 Quantizing the Interference Estimates

The other significant feature that has been added to the fixed-point SPW model is the quantization of the amplitudes of the interference estimates. In Fig. 7.4, the correlation receiver used in the first stage and the interference estimator used in the second stage are shown. This particular plot shows the blocks for user 10. The correlation receiver is identical to the one used previously; its outputs are the decision statistic and the bit estimate. The block that calculates the interference estimate is different, however, as it quantizes the calculated interference estimate. The block is stored as *estimator_q* and its

block diagram is shown in Fig. 7.5.

The inputs to the estimation block are the decision statistic, the bit estimate, the PN sequence of that particular user, the time delay, and the phase delay. It is assumed that the time delay has been provided by a synchronization routine and that the phase is provided either through a coherent source or through a phase estimation routine (one method for estimating the phase is discussed in Chapter 8). The decision statistic is normalized and then quantized with a uniform quantizer. This quantized result is the new amplitude estimate and it is multiplied by the bit estimate (with the appropriate phase and delay). The output is the overall interference estimate, which is a complex signal.

The interference estimates are then summed and subtracted from the *quantized* received signal $r_\epsilon(t)$, not the actual received signal. The rest of the receiver proceeds along similar lines, the estimate of the desired user is added to the residual signal and then this signal is passed to the correlation receiver. In stage 3, another quantized interference estimate is generated, the estimates are summed and subtracted from the quantized received signal, and then the results are passed to the final bank of correlation receivers.

7.5.4 Miscellaneous Files

The final portion of the system block diagram is the bit error rate calculation as shown in Fig. 7.6. Since all three stages are being simulated at once, we must calculate three separate bit error rates. Each bit error rate calculator is supplied a delayed version of the original data stream (each must be delayed by a different amount) and the bit estimate from the appropriate bank of correlation receivers. Both the bit error rate and the number of errors are saved in separate data files.

The system block *int_q_calc2* is similar to *glomo_q*, but it is used to calculate the mean and variance of the quantization noise from the summed quantized interference estimates for use in the analytical model (the mean and variance of the quantization noise from the quantized received signal are calculated using *glomo_q*. The key differences are that the received signal is not quantized here (to eliminate the quantization noise it causes) and that there are now two parallel calculations, one where the estimates are quantized and one where they are not. This allows for a comparison between quantized and unquantized versions so that the noise may be analyzed. The block diagram is not shown here because of its similarity to the previous system model.

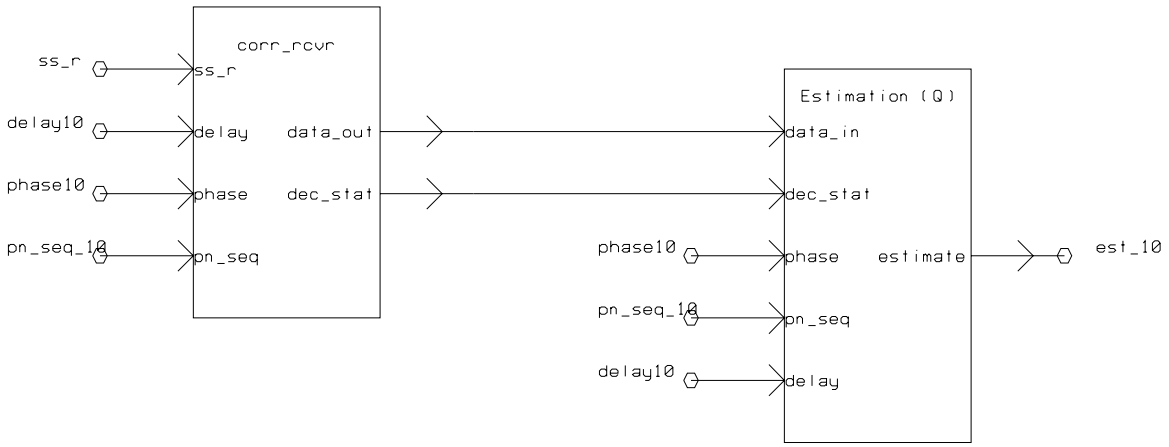

Figure 7.4: Quantizing the Interference Estimates

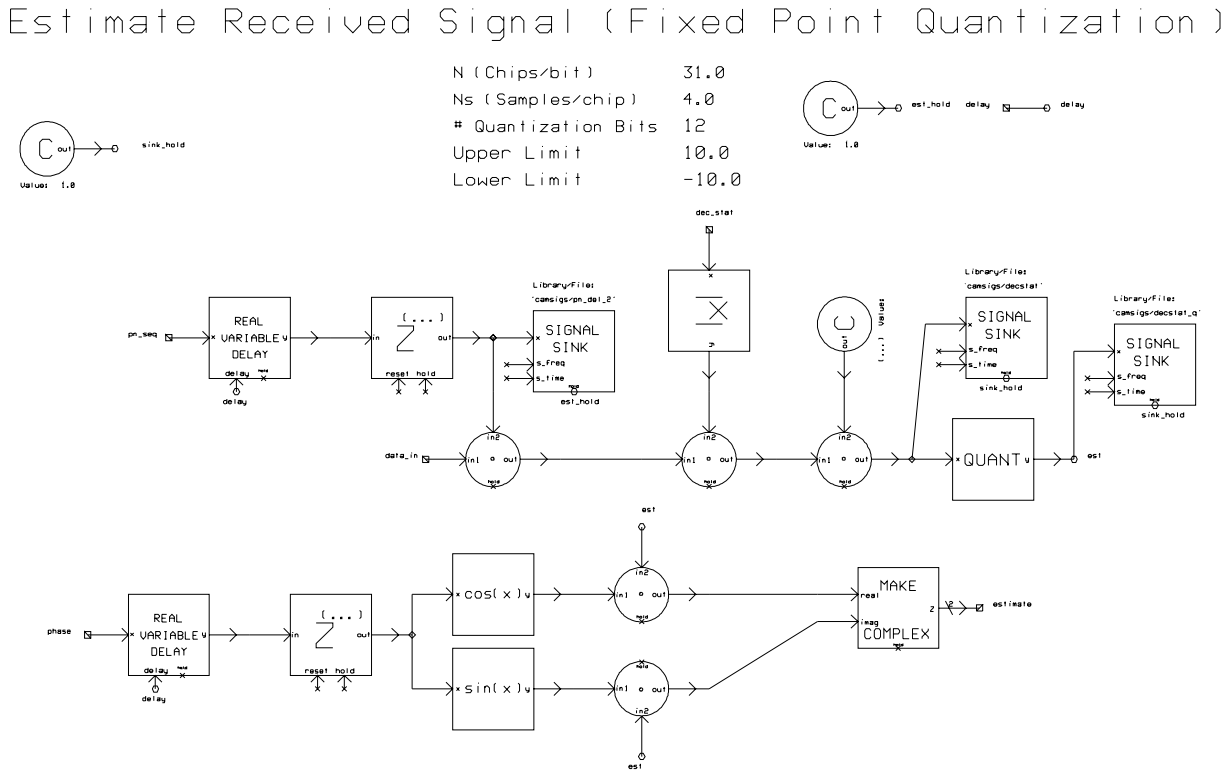

Figure 7.5: Fixed-Point Interference Estimation

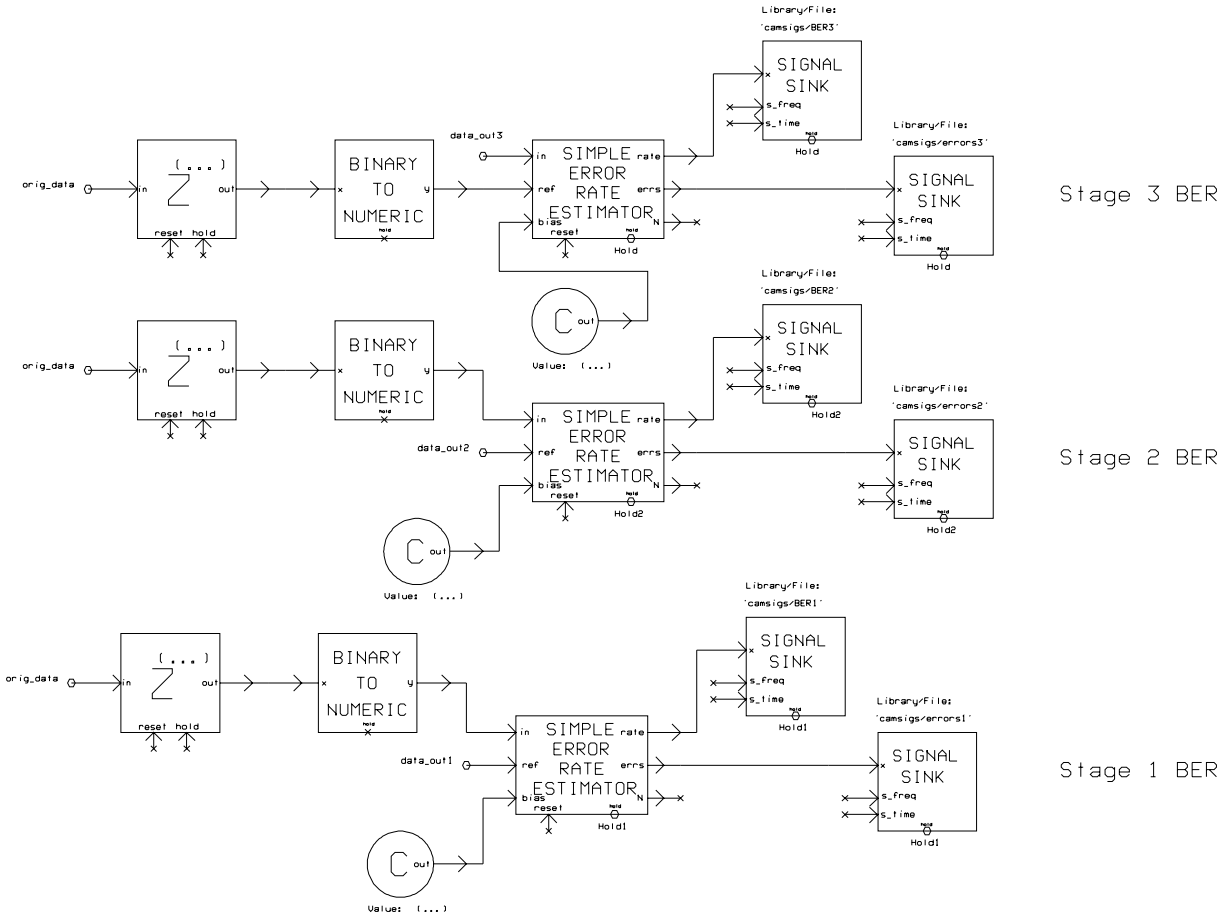

Figure 7.6: Calculating the Bit Error Rate

7.6 Numerical Results

Simulation results have been generated and compared to the analytical model for 12, 8, 6, and 4 bits, a quantization range from -20 to 20, and a range on E_b/N_o from 0 to 10 dB. Overflow occurred rarely between values of E_b/N_o of 0 to 4 dB, but never at higher signal levels. Before discussing the overall results, however, we first need to examine the characteristics of the quantization noise.

7.6.1 Examining the Quantization of the Received Signal

The input signal to the multistage receiver $r(t)$ is quantized at the input to the digital multistage receiver, resulting in the addition of the quantization error signal $e_r(t)$. An example of the difference between the true received signal $r(t)$ and its quantized equivalent $r_\epsilon(t)$ is shown in Fig. 7.7 for the I channel, where 60 samples (1 bit of data) are shown and 4 bits were used in the quantization process. In the analytical model, the error signal $e_r(t) = r_\epsilon(t) - r(t)$ is modeled as a random variable with a uniform distribution over $[-\Delta/2, \Delta/2]$, which has zero mean and variance of $\Delta^2/12$. At the output of the correlator, this quantization noise has a new distribution and is represented by the random variable ϵ_r. As discussed in Section (7.4), there is no direct analytical solution to the new distribution. Therefore we turn to simulation to provide a semi-analytic solution to the input quantization noise source.

Quantization Noise e_r

A plot of 60 samples (1 bit) of the quantization noise e_r resulting from quantizing the I portion (of the I and Q portions) of the received signal $r(t)$ is shown in Fig. 7.8, where the simulation run length was 100,000 samples, and the simulation parameters were set for 8 quantization bits, quantization range of [-20, 20], and $E_b/N_o = 5$ dB. A histogram of e_r is shown in Fig. 7.9 for the same simulation run. It is clear that the distribution is uniform as predicted. The uniform quantizer in the SPW simulation model uses truncation and not rounding, which is why the range of sample values is from $[-\Delta, 0]$ instead of $[-\Delta/2, \Delta/2]$. The predicted characterization of a uniform noise source when using truncation is given in Sec. 6.1.2 as

$$\begin{aligned} \mu_e &= -\frac{\Delta}{2} \\ \sigma_e^2 &= \frac{\Delta^2}{12}. \end{aligned} \tag{7.35}$$

Using 8 bits over the range [-20, 20] yields $\Delta = 0.15625$. Thus the uniform noise model would predict a mean of -0.07813 and a standard deviation of 0.04511. For the sample run above, the sample mean was -0.07817 and the sample standard deviation was 0.04504. These results are tabulated in Table 7.1. Clearly, the distribution of the quantization noise is well matched to a uniform noise model, although it is important to again note that the quantization noise is not a random variable but deterministic, and that a uniform model does not predict the noise for a given sample (i.e., a given input), but instead accounts for the distribution of the noise over time.

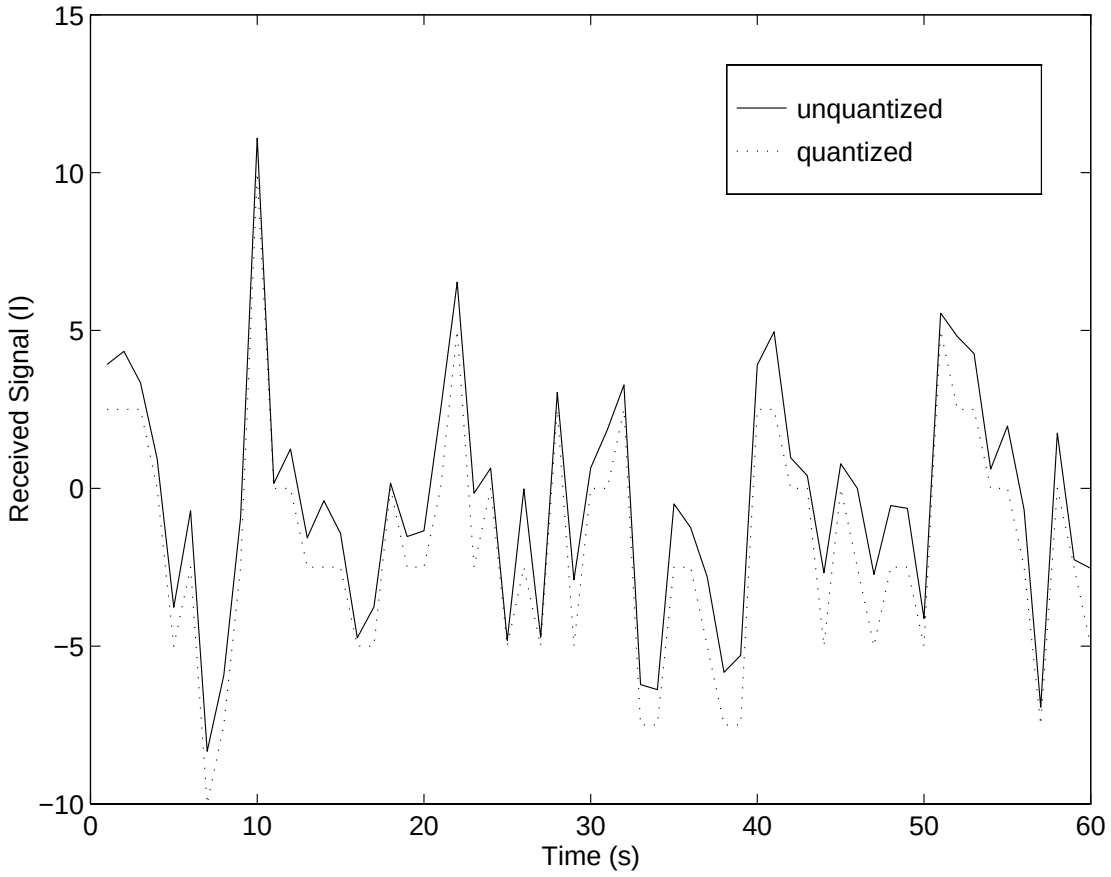

Figure 7.7: Received Signal (Actual and Quantized Versions) When Using 4 Bits

Correlated Quantization Noise ϵ_r

We now turn our attention to the correlated version of e_r, ϵ_r, since we cannot readily derive an analytic model to represent it. A plot of 60 samples (1 bit of data) of ϵ_r is shown in Fig. 7.10 when using 8 bits in the quantization process, a quantization range of [-20, 20], an E_b/N_o of 5 dB, and a simulation run length of 100,000 samples. A histogram of the correlated noise is plotted in Fig. 7.11 for the same simulation run. The sample mean is -0.009875 and the sample standard deviation is 1.2321. The distribution is clearly no longer uniform, and looks roughly Gaussian. A normal probability plot is shown in Fig. 7.12, where the pdf of the sample data is compared to the pdf of a Gaussian (normal) distribution. If the sample data were truly Gaussian in nature, the plot would be linear and follow that

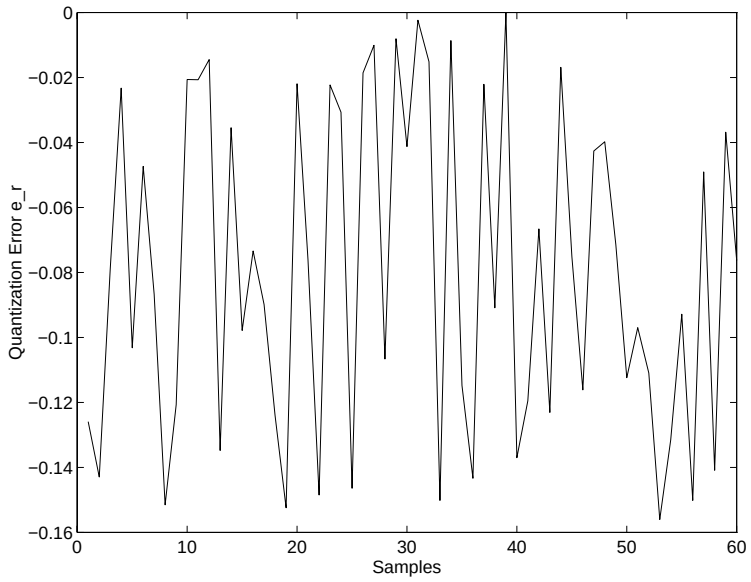

Figure 7.8: Quantization Noise e_r When Using 8 Bits

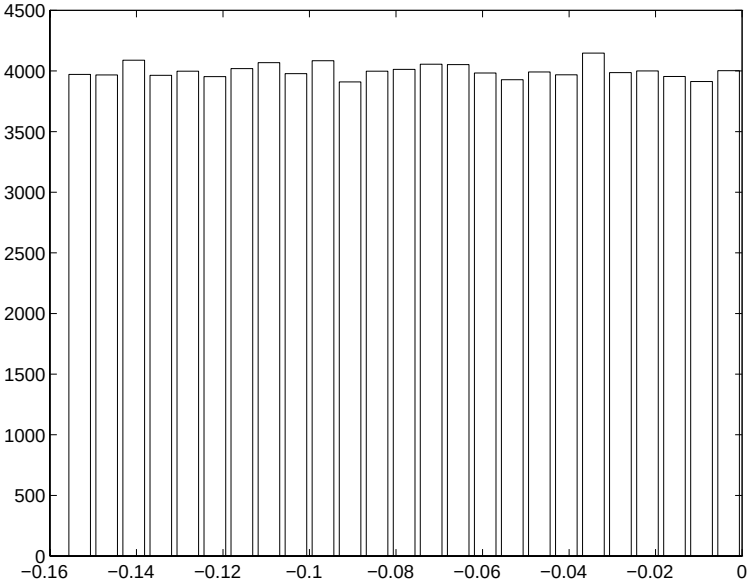

Figure 7.9: Histogram of Received Signal Quantization Noise e_r

Table 7.1: Characterization of e_r

	Predicted	**Simulation**
μ_{e_r}	-0.07813	-0.07817
σ_{e_r}	0.04511	0.04504

Table 7.2: Sample Mean and Standard Deviation of ϵ_r

# of Bits	μ_{ϵ_r}	σ_{ϵ_r}
4	-0.1080	19.6732
6	-0.0356	4.9120
8	-0.009875	1.2321
12	-0.001103	0.07721

of the dashed line. Any deviation from this linear ideal indicates that the sample data is not strictly Gaussian for that range of data. From the plot, it is clear that the sample data is reasonably Gaussian, with a very close match in the center of the data range and some divergence at the tails of the distribution. From a modeling standpoint, if there is to be some divergence from a true Gaussian distribution, we would prefer that it be in the tails since these data values will occur with the lowest probability. Thus we would expect that, given the close match for the most common data values, that the correlated input quantization noise source can be modeled with a Gaussian distribution with zero mean and standard deviation based on the sample standard deviation taken from a representative simulation run.

The sample mean and standard deviation of ϵ_r is tabulated in Table 7.2 for bit levels of 4, 6, 8, and 12. The simulation parameters used E_b/N_o of 5 dB and a 100,000 sample run length. The values follow the expected pattern, with the variance in the noise rapidly decreasing as we increase the number of bits in the quantization process (and thus more accurately quantize the amplitude of the estimate). These results were used in developing the semi-analytic model for ϵ_r used in the analytical results. The validity of this model is borne out by the close match between the analytic and simulation models for the 1 stage receiver, where ϵ_r is the only quantization noise source.

It is worth remembering that the reason that ϵ_r has a different distribution than the uniform distribution of e_r is entirely a result of the correlation properties of the correlation receiver, and thus this will hold for any spread spectrum system that employs correlation receivers.

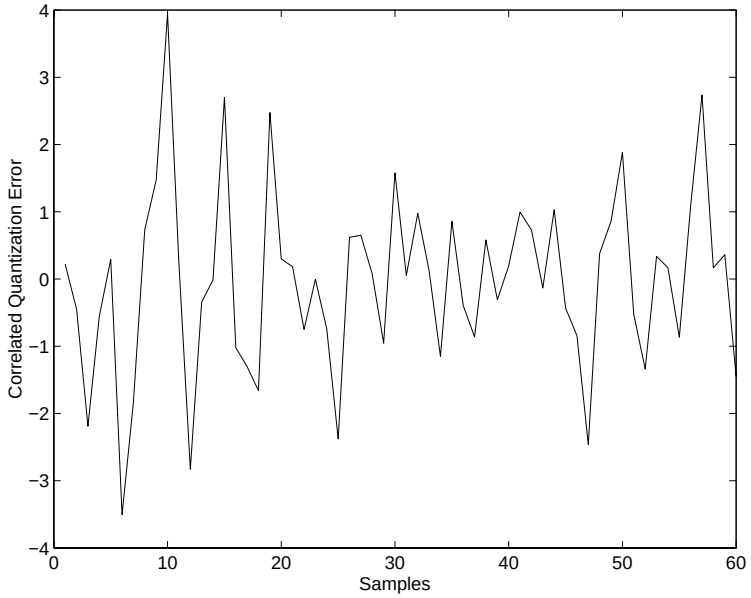

Figure 7.10: Correlated Quantization Noise ϵ_r

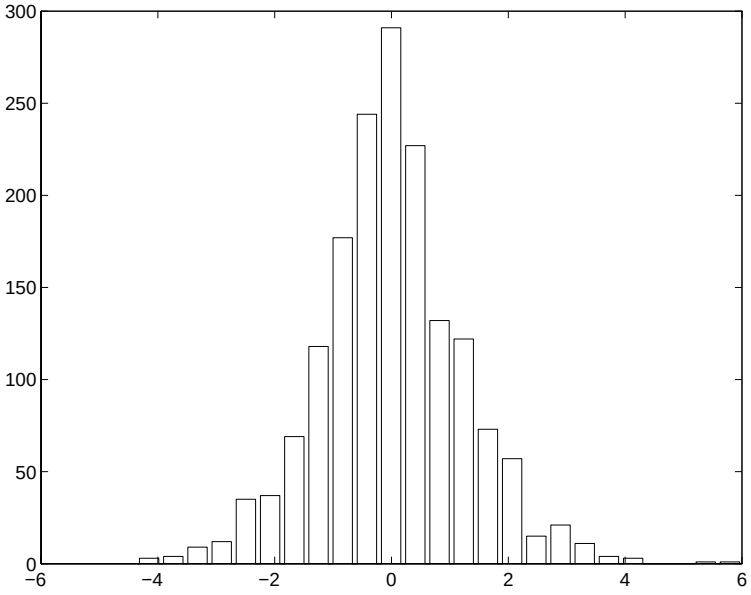

Figure 7.11: Histogram of Correlated Quantization Noise ϵ_r

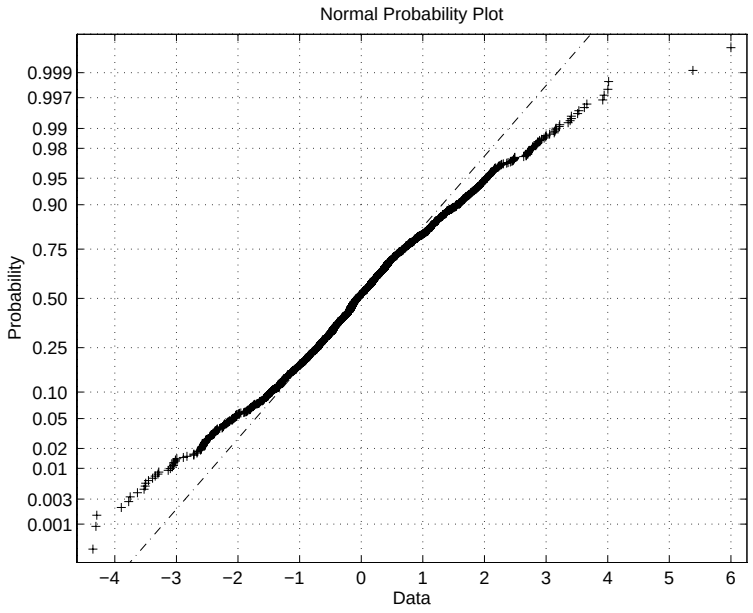

Figure 7.12: Normal Probability Plot for Correlated Quantization Noise ϵ_r

The processing gain of the system applies to the quantization noise of the received signal as well as to the channel noise and interference, as this quantization noise goes through the correlation process as well. Thus the noise that appears in the decision statistic has been processed by the correlator and is less severe than at the output of the uniform quantizer. The practical result of this is that a lower number of bits may be required for quantization than in a similar non-spread system receiver. Thus all spread spectrum systems benefit from the use of the correlator, not just systems employing multistage receivers.

Using this sample standard deviation and assuming a Gaussian distribution allows us to use a very practical semi-analytic technique in which the analytic model developed previously can still be used, but with the noise source ϵ_r being characterized based on parameters taken from simulation. To see how well this technique holds, we can look at the receiver performance for just the first stage, where no interference cancellation has taken place and the only quantization source is ϵ_r. By looking at Figs. 7.18-7.23, we see that the semi-analytic and simulation results match very closely for the first stage, implying that this Gaussian model for ϵ_r is indeed appropriate and accurate.

Table 7.3: Characterization of e_s

	Predicted	**Simulation Stage 2**	**Simulation Stage 3**
μ_{ϵ_s}	-0.07813	-0.07824	-0.07825
σ_{ϵ_s}	0.04511	0.04484	0.04501

7.6.2 Examining the Quantization of the Interference Estimates

We now turn our attention to examining the characteristics of the noise from quantizing the interference estimates, e_s. An example of the quantization process is shown in Fig. 7.13 for the estimate of user 1's signal in stage 3 over a single bit period, where the first plot is of the original (unquantized) estimate of user 1's signal, the second plot is the quantized version of that estimate, and the third plot is the actual quantization noise signal. There are 8 bits used for quantization and the E_b/N_o was 5 dB. Because the decision statistic estimate is constant over a bit period, the quantization error will have a constant magnitude as well. The error signal is essentially this magnitude modulated by the signature sequence. This is notably different from the quantization noise signal e_r, which varies from sample to sample due to the nature of the received signal $r(t)$.

The distribution of a simulation run of 100,000 samples is shown in Fig. 7.14, where the quantizer in question is from user 2's estimation block in stage 2 of the receiver and 8 bits are used in the quantization process. While still approximately uniform, the pdf is not nearly as flat as it was for the quantization of the received signal. This is to be expected, since we are now accumulating samples that have been modulated by a signature sequence, and thus the magnitude of the error will not change over a bit period (here, 60 samples). It will thus take more samples for the overall noise distribution to appear uniform. The sample mean was -0.07824 and the sample standard deviation was 0.04484. A comparison of the sample simulation values of the mean and standard deviation for stages 2 and 3 with the predicted values for a uniform noise source is tabulated in Table 7.3. Thus the first and second moments are still near the predicted values for each stage, and so we expect that, since the sample pdf fairly closely follows the uniform pdf, the uniform noise source should be a good model for the quantization of the interference estimates. The histogram of the quantization noise at stage 3 for user 2 is shown in Fig. 7.15. The sample mean was -0.07825 and the sample standard deviation was 0.04501. As at stage 2, the quantization noise is fairly uniform.

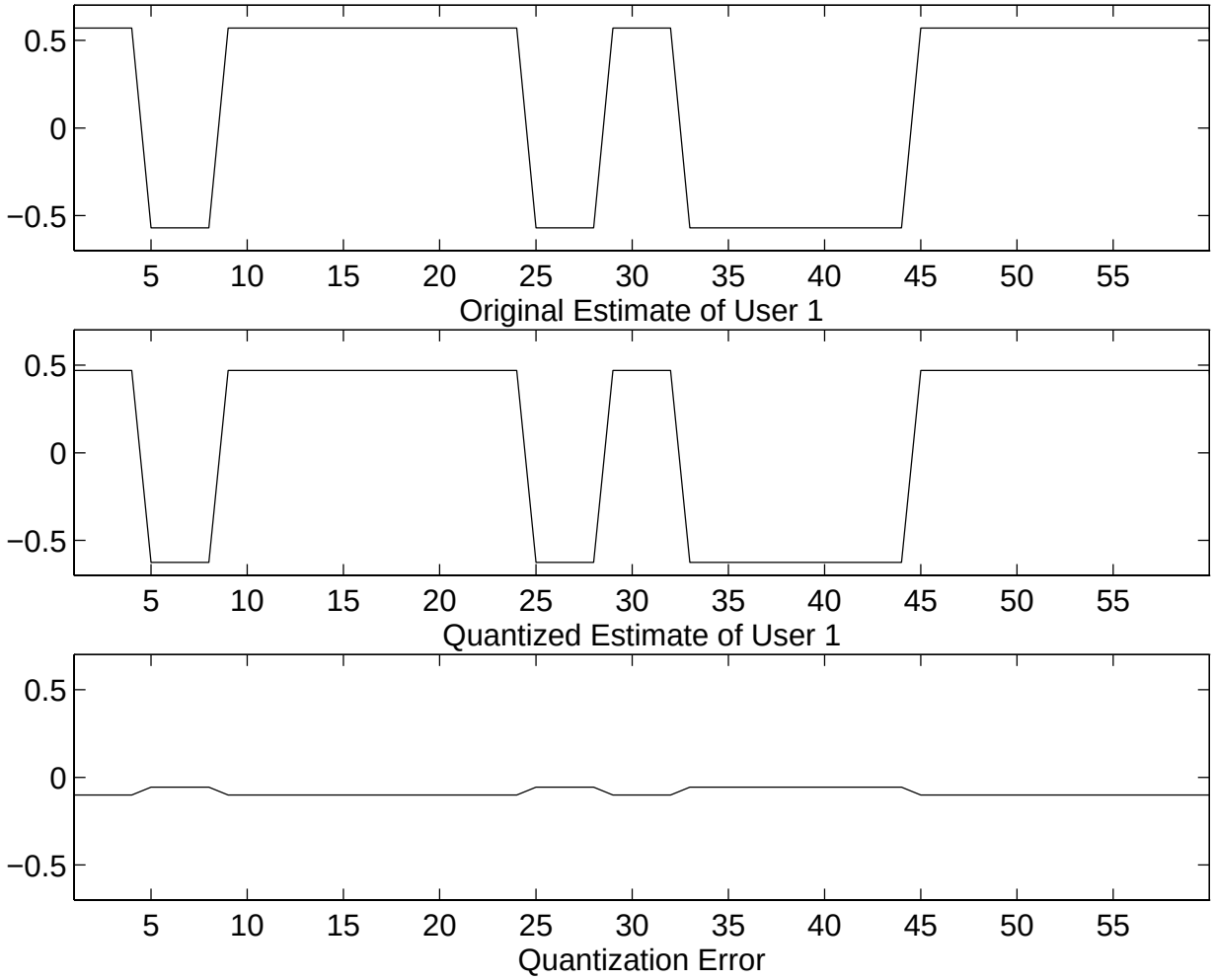

Figure 7.13: Original Estimate, Quantized Estimate, and Quantization Noise for User 1's Estimate in Stage 3

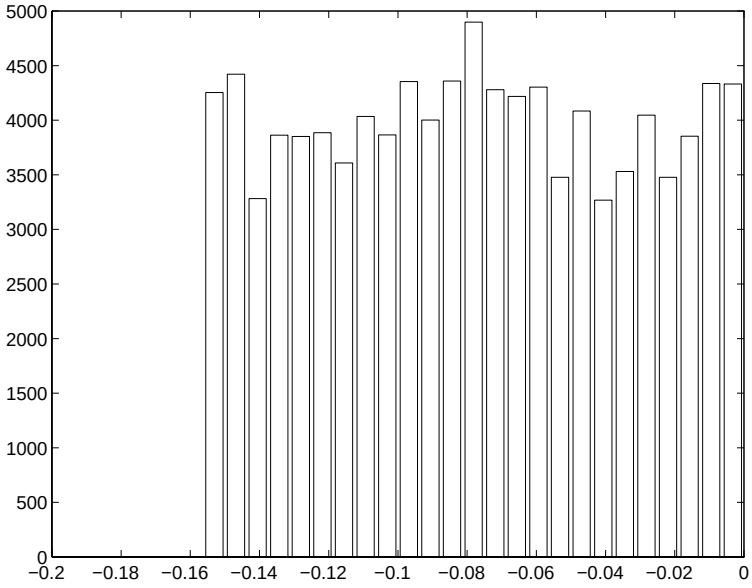

Figure 7.14: Histogram of Estimation Quantization Noise e_s in Stage 2 for User 2

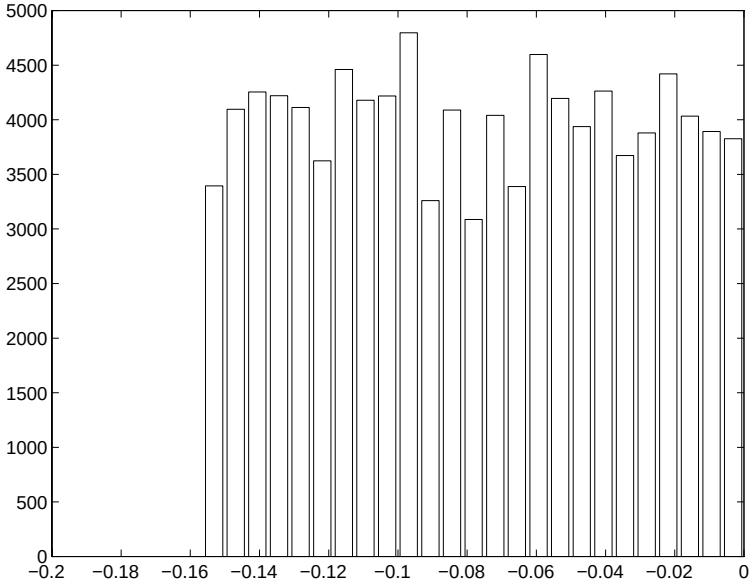

Figure 7.15: Histogram of Estimation Quantization Noise e_s in Stage 3 for User 2

Table 7.4: Sample Mean and Standard Deviation of ϵ_s

# of Bits	μ_{ϵ_r}	σ_{ϵ_r}
4	-0.1080	19.6732
6	-0.0275	3.8417
8	-0.008604	0.9509
12	-0.0003261	0.0587

7.6.3 Examining the Correlated Quantization Noise of the Interference Estimates

Although the distribution of e_s is uniform, the distribution of the correlated noise ϵ_s will not be. As is the case with e_r and ϵ_r, there is no exact analytic expression for the distribution of ϵ_s. We again turn to simulation to parameterize the stochastic model for ϵ_s.

A histogram of the correlated noise from stage 2 is plotted in Fig. 7.16 for the same simulation run. The sample mean is -0.008604 and the sample standard deviation is 0.9509. The distribution is clearly no longer uniform, and looks roughly Gaussian. A normal probability plot is shown in Fig. 7.17. From the plot, it is clear that the sample data is reasonably Gaussian, with a very close match in the center of the data range and some divergence in the tails. Again, it is most important that we accurately model the central portion of the distribution since these events occur with the highest probability. Thus we would expect that, given the close match for the most common data values, that the correlated input quantization noise source can be modeled with a Gaussian distribution with zero mean and standard deviation based on the sample standard deviation taken from a representative simulation run. The same parameters are used for stages 2 and 3. The sample parameters are summarized in Table 7.4 for the various number of bits used in the quantizer.

7.6.4 Examining the Bit Error Rate Performance

Now that we have verified the accuracy of each quantization noise source, we examine the bit error rate curves and both compare the analytic and simulation results and examine the degradation as fewer bits are used in the quantization process. A summary of the bin widths when using 12, 8, 6, and 4 bits is given in Table 7.5, where it is assumed that the quantization range is over [-20, 20].

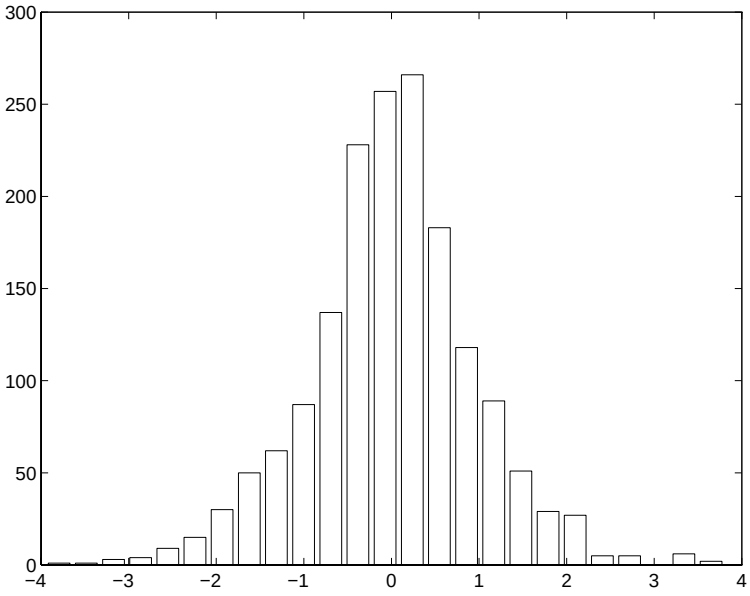

Figure 7.16: Histogram of Correlated Quantization Noise ϵ_s in Stage 2 for User 1

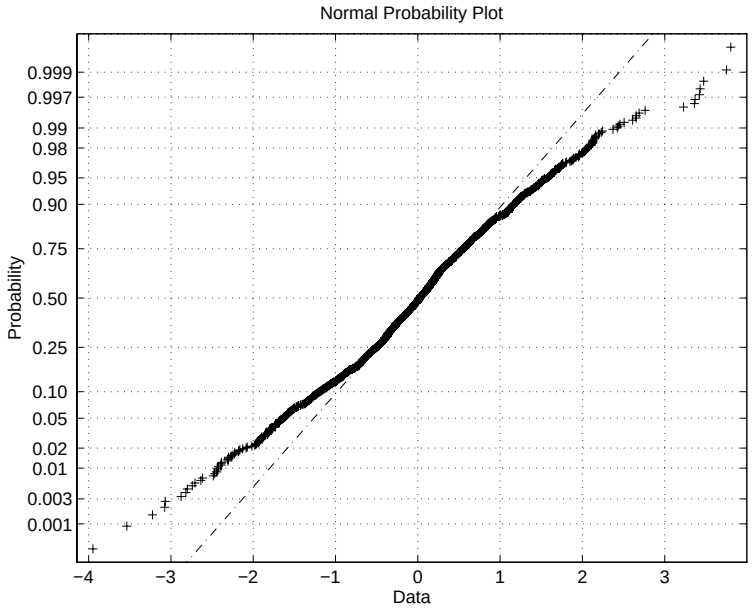

Figure 7.17: Normal Probability Plot for Correlated Estimation Quantization Noise ϵ_s

Table 7.5: Quantization Bin Width Δ

# of Bits	# of Levels	Bin Width	Maximum Error
12	4096	0.009765625	0.0048828125
8	256	0.15625	0.078125
6	64	0.625	0.3125
4	16	2.5	1.25

Comparing the Analytic and Simulation Results

In Figs. 7.18-7.23, the BER is plotted against E_b/N_o for quantization bit levels of 12, 8, 6, and 4 bits. Several key observations can be made from these BER curves by comparing the accuracy of the analytic model with the simulation model.

First, consider the case of 12 bits (Fig. 7.18). As noted in Section 7.6.1, the analytic and simulation models are in close agreement for stage 1 for the entire range of E_b/N_o. The analytic results for the stages employing interference cancellation get optimistic (lower BER than simulation) as E_b/N_o increases, which is due to the bias inherent in the estimation process discussed in Section 5.4.6. A comparison of the performance of receivers employing no quantization and quantization levels of 12, 8, 6, and 4 bits are shown in Fig. 7.19 and Fig. 7.20 for a 1 stage and 3 stage receiver, respectively. The results for 12 bits are nearly identical to the case when quantization is not used, which is not surprising. Using 12 bits means that we are quantizing with $2^{12} = 4096$ levels. Since our range is from -20 to 20, this implies that each bin has width

$$\begin{aligned} \Delta_{12} &= \frac{20-(-20)}{4096} \\ &= 0.009765625. \end{aligned} \tag{7.36}$$

Therefore the maximum error that can occur due to quantization is $\Delta/2 = 0.0048828125$. This fine bin spacing yields an ability to accurately quantize each interference estimate, as well as the initial received signal. Thus we expect to see almost no noticeable degradation over the case when quantization is not used, and this is indeed the case.

Next, consider the case of 8 bits (Fig. 7.21). As before, the stage 1 results are accurate across the range of E_b/N_o. For stages 2 and 3, however, the analysis again becomes optimistic (predicts too low of a BER) as E_b/N_o increases above 5 dB. Again, this is due to the bias in the decision statistic, as the quantization noise is still not significant enough to degrade performance notably over the ideal case. The simulation results show that there is almost no noticeable degradation when using 8 bits over the non-quantized case. The bin width

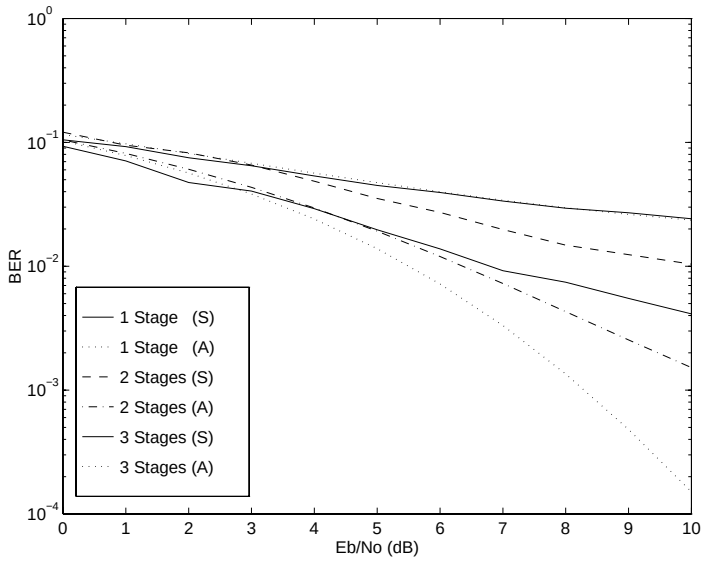

Figure 7.18: BER vs. E_b/N_o for 12 bits and Limit=20

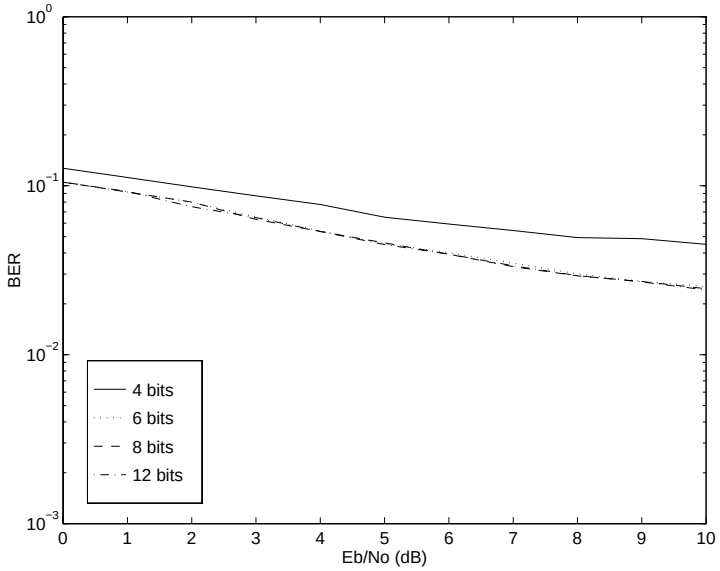

Figure 7.19: 1 Stage RX Comparison with Varying Levels of Quantization

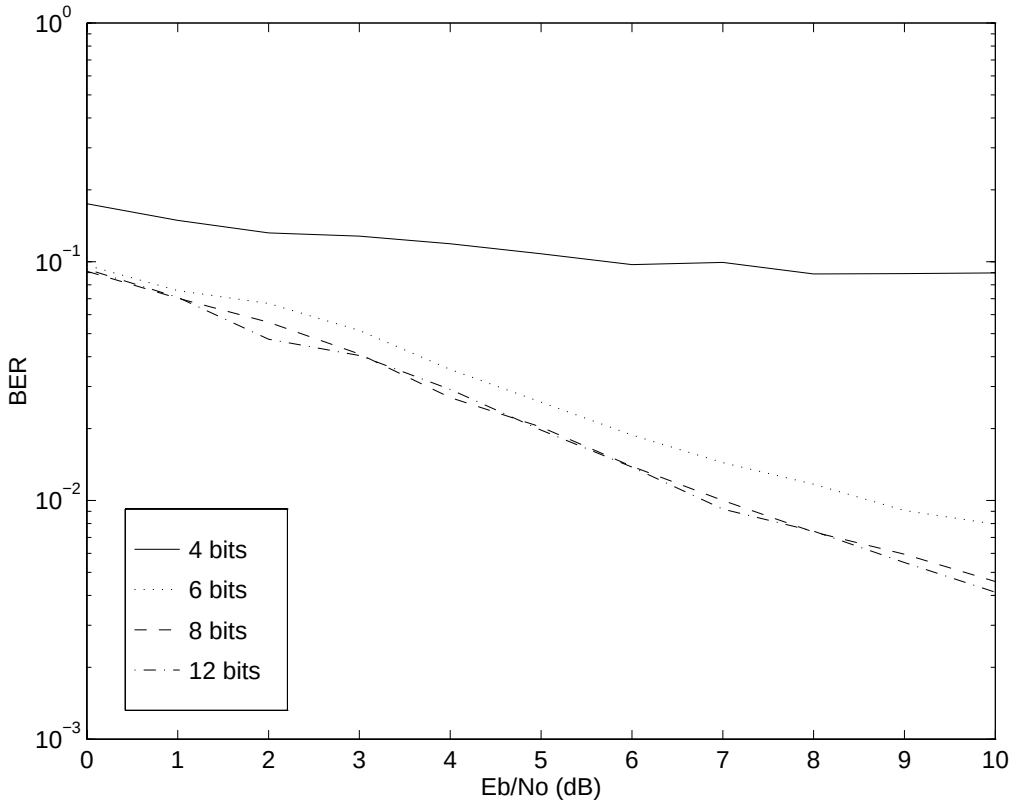

Figure 7.20: 3 Stage RX Comparison with Varying Levels of Quantization

for this case is no longer nearly as fine as the case for 12 bits, and is given by

$$\begin{aligned} \Delta_8 &= \frac{20-(-20)}{256} \\ &= 0.15625. \end{aligned} \tag{7.37}$$

The maximum error due to quantization is thus $\Delta/2 = 0.078125$. Since the amplitude of each user's transmitted signal is 1, this still provides a suitable degree of accuracy and, as can be seen from the comparisons in Figs. 7.19 and 7.20, there is almost no noticeable degradation from the ideal case. Thus the performance of the receiver is nearly the same regardless of whether 8 or 12 bits is used (there is some degradation when going to 8 bits, but it is not significant for the case studied here).

Next, consider the case of 6 bits (Fig. 7.22). Again, using the Gaussian noise model for the

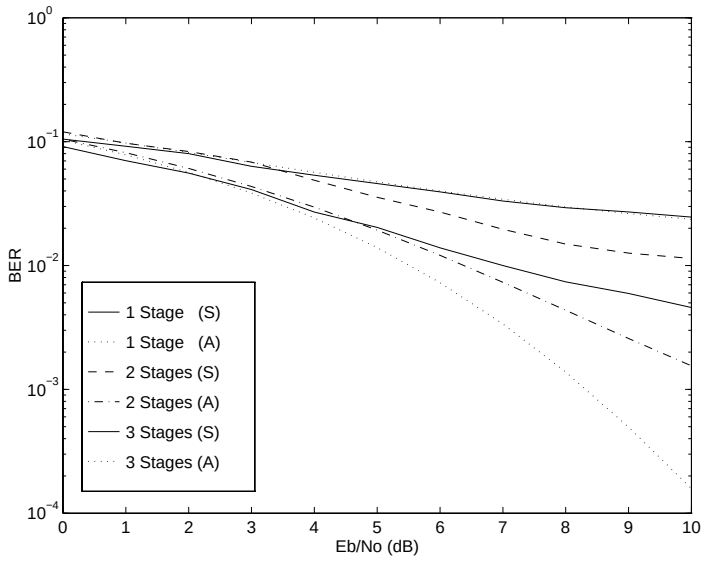

Figure 7.21: BER vs. E_b/N_o for 8 bits and Limit=20

correlated quantization noise ϵ_r, the stage 1 results are accurate across the range of E_b/N_o. For stages 2 and 3, however, the analysis becomes more optimistic than before (predicts too low of a BER) for values of E_b/N_o above 5 dB. This optimism cannot be entirely explained by the bias in the decision statistic. The bin width for this case is given by

$$\begin{aligned} \Delta_6 &= \frac{20-(-20)}{64} \\ &= 0.625. \end{aligned} \tag{7.38}$$

The maximum error due to quantization is thus $\Delta/2 = 0.3125$. Since the amplitude of each user's transmitted signal is 1, the maximum error can now be an appreciable portion of the estimate. We know from simulation that we are accurately modeling the performance of a single quantization source, which implies that the optimistic results are partially a result of modeling the quantization noise sources as independent, when in fact they become less independent as the bin width increases. This effect is discussed in more detail in Section 7.6.5.

As can be seen from the comparisons in Figs. 7.19 and 7.20, there is noticeable degradation when performing interference cancellation, but the performance of the first stage remains similar to the cases of 8 and 12 bits. This is because the maximum error is not nearly as significant compared to the maximum value of the received signal as compared to the

interference estimates, which have a much smaller amplitude. The degradation visible at stage 3 may be acceptable as a tradeoff in the lower number of bits that are required, depending on whether higher capacity (or alternatively a lower BER) is more important than a smaller number of bits.

Finally, we examine the case when only 4 bits are used in the quantization process (Fig. 7.23). As in the previous cases, the analytic and simulation models yield nearly identical results for the one stage receiver. For stages 2 and 3, the analysis is again severely optimistic, predicting that the two stages perform significantly better than the one stage receiver. The simulation results show that attempting to cancel the interference with such a low degree of numerical precision degrades performance to the point that stages 2 and 3 actually perform worse than stage 1. The wide disparity between the predicted and simulated results again implies that the bias is not accounting for all of the optimism in the predicted BER. The non-independence of the quantization sources is again the culprit, as demonstrated and explained in Section 7.6.5.

The bin width for this case is given by

$$\begin{aligned} \Delta_4 &= \frac{20-(-20)}{16} \\ &= 2.5. \end{aligned} \tag{7.39}$$

The maximum error due to quantization is thus $\Delta/2 = 1.25$. Since the amplitude of each user's transmitted signal is 1, the maximum error can now be an appreciable portion of the estimate. All stages show a severe degradation from the non-quantized case, indicating that using 4 bits will not provide acceptable performance in any circumstance.

7.6.5 Sources of Error in the Analytic Model

As we have seen, the accuracy of the analytic model degrades as the number of bits decreases, and can degrade as E_b/N_o increases. There are two main factors that are contributing to the pessimistic predictions of the BER.

Stochastic Modeling of a Deterministic Process

First, the uniform noise model allows for noise to be added to the signal in ways that it would not be added in the actual receiver. For example, consider the decision statistic. The receiver makes a bit estimate as to whether a +1 or -1 was sent based on whether the decision statistic is greater than or less than zero. Quantization will not affect this decision; if the signal is greater than zero before quantization, then the quantized version

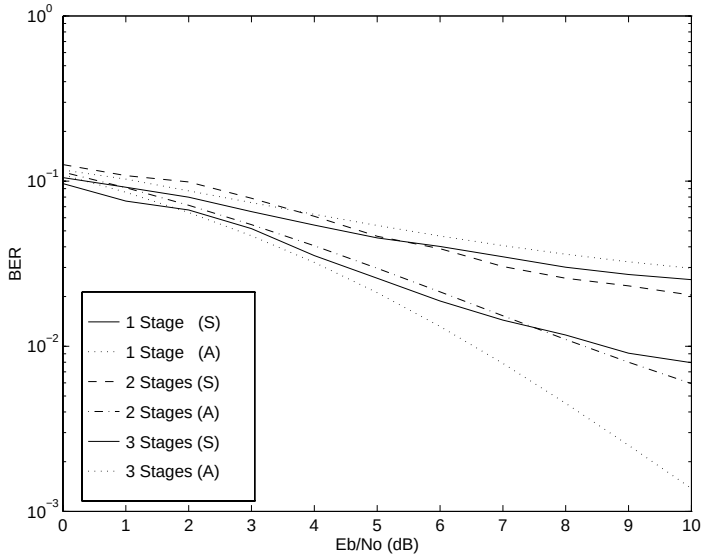

Figure 7.22: BER vs. E_b/N_o for 6 bits and Limit=20

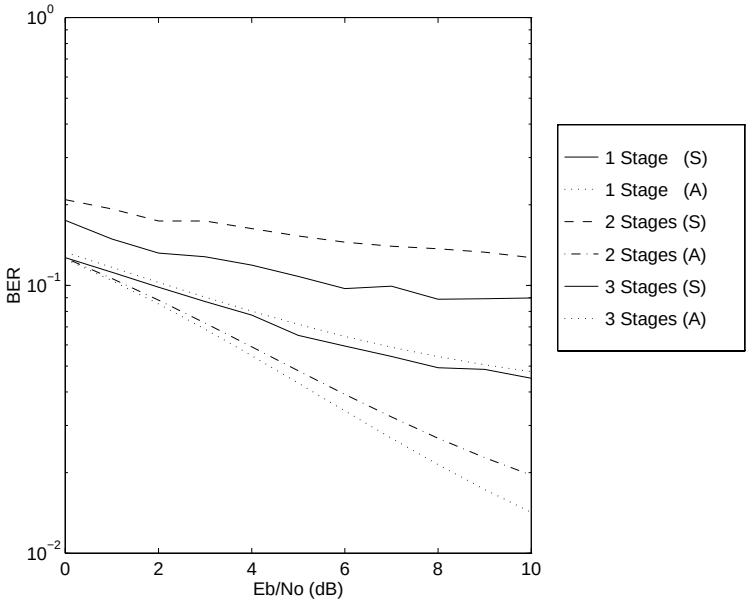

Figure 7.23: BER vs. E_b/N_o for 4 bits and Limit=20

will also be greater than zero. In a similar fashion, if the decision statistic is less than zero, the quantized result will also be less than zero. The uniform noise model does not make this distinction however, since it is independent of the input to the quantizer.

Consider the case when the decision statistic is within half a bin's width of zero as shown in Fig. 7.24. The uniform noise model would suggest that the quantized result could be $\pm\Delta/2$ about the true value. If an error occurs in possible error region # 1, the model will allow the quantized result to be less than zero even though in reality it would be quantized above zero. The wrong bit estimate will be made in the analysis, whereas an error would not have been made in an actual system. Conversely, there may be cases where the decision statistic is slightly less than zero (possible error region #2) when a +1 has been set, and the uniform noise model will incorrectly allow the quantized result to be greater than zero. In this case, the analytic model will not predict an error when the actual system would make the incorrect bit estimate. Since the probability is greater that, given a +1 was sent, the decision statistic will be in region #1 rather than region #2, analysis based on the uniform noise model will overestimate the number of errors being made and lead to a pessimistic bit error rate estimation. However, this effect may be very small in many cases and as we have seen previously, the analysis is actually optimistic and thus this effect has little overall impact on the BER determination. However, it is important in that it shows how modeling the deterministic quantization error with a random process can lead to errors.

This effect will be more noticeable as the number of quantization bits decreases. Consider the case of 12 bits. The area where the analytic model will allow errors to occur where they should not, $0 \leq Z_{k,i}^{(s)} \leq \Delta/2$, is between 0 and 0.0048828125. The probability that $Z_{k,i}^{(s)}$ will be in this region is very small, and thus we do not expect it to significantly impact the overall BER. Next, at 8 bits, the possible error region is between 0 and 0.078125. The probability that we will be in this region is still small, but greater than before. Thus we would expect that its effect will only be noticeable when the power in the channel noise decreases and overall errors are more infrequent, and this is also seen. Next, at 6 bits, the possible error region is from 0 to 0.3125, and the probability that we will be in this region is much higher. At 4 bits, the region grows to 0 to 1.25, allowing for significant overestimation of the BER. There is no simple or practical way to accurately model this phenomenon, however, since we wish to avoid modeling the quantization noise based on the input to the quantizer.

Non-independence of Quantization Noise Sources

A second source of error in our assumptions is that all of the K quantization noise sources in any stage s are independent, and further that the quantization noise sources associated with user k are independent from stage s to stage $s+1$. Both of these situations can be

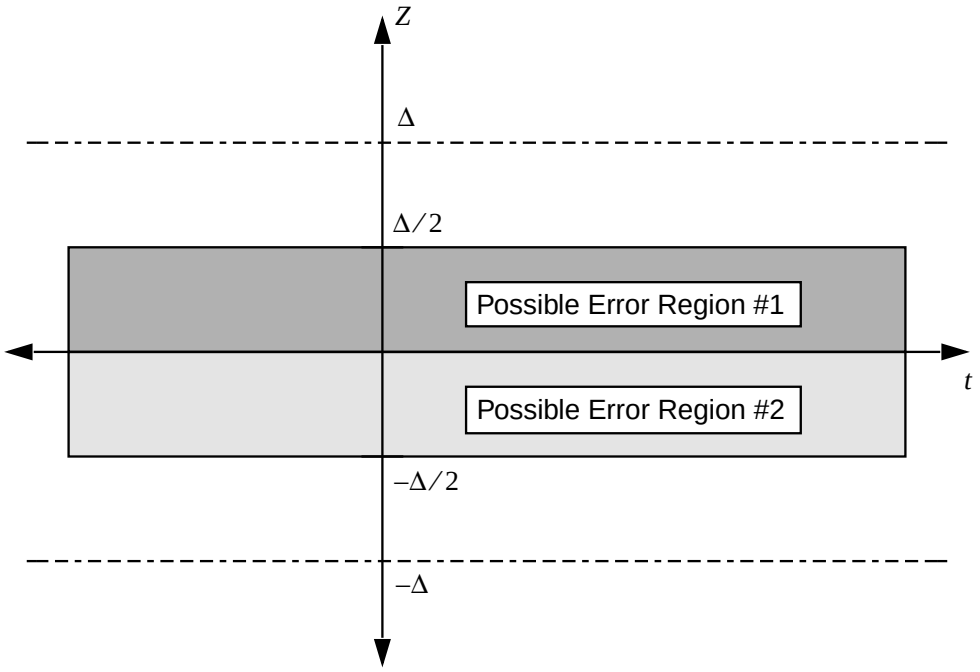

Figure 7.24: Inaccuracies in the Uniform Noise Model

violated under certain conditions in the multistage receiver. As the number of quantization bits decreases, we increase the probability that the two interference estimation routines for users k and $k+1$ will be quantizing to the same level. If the users have the same power levels, then we would expect the decision statistic to be at roughly the same level since the difference will be in that they are correlating with different signature sequences and that each will have attempted to cancel the other's interference. If each estimate is similar in amplitude, then the overall correlation should be similar in amplitude. As the bin spacing gets coarser, they become more likely to be quantized identically and thus are no longer independent in the error they produce. This implies that we cannot simply convolve their distributions together and expect the Central Limit Theorem to hold.

A similar effect holds when comparing the quantization noise from stage s to stage $s+1$ for user k. As the bin spacing gets larger, the probability increases that the same quantization level will be chosen at stages s and $s+1$. If the same level is chosen, the error will be the same at each stage and thus the noise sources are not independent in any sense, but in fact identical.

The net effect of assuming independence of noise sources is that we ignore the cross-

Table 7.6: Lumped Estimation Quantization Noise

# of Bits	**Stage 2 μ**	**Stage 2 σ**	**Stage 3 μ**	**Stage 3 σ**
4	-1.3878	44.2960	-0.2470	31.1220
6	-0.2601	11.2362	-0.2056	9.0660
8	-0.1111	2.8302	-0.0036	2.1325
12	-0.0051	0.1763	-0.0013	0.1423

product terms that must be accounted for when computing the overall noise distribution. Simply ignoring these terms leaves out a significant portion of the noise term when the bin spacings are large, and so the net effect is to underestimate the effect of the noise and subsequently underestimate the corresponding bit error rate. As we have seen, this optimism in predicting the BER is quite severe when the bin spacing is large.

Determining how the noise sources are correlated is a non-trivial task and best accomplished by simulation. Here, we simply determine the total noise caused by all of the quantizers in the estimation blocks, and then use this lumped noise source to represent the degradation in the decision statistic. This lumped source inherently accounts for any non-independence of noise sources, but has the drawback in that it is only strictly valid for the number of users used in the simulation and thus is not as widely applicable as our previous model. However, as seen in Fig. 7.31, using such a model for the case of 4 quantization bits provides a close match between simulation and predicted BER performance. The lumped parameters are summarized in Table 7.6 for bits 4 through 12 when there are 10 active users and $E_b/N_o = 5$ dB.

The Degradation in BER Due to Quantization

Summarizing the results from the previous section, we see from Figs. 7.19 and 7.20 that there is little to no degradation in performance when using 8 or 12 bits for quantization, there is some dropoff for the interference cancellers when using 6 bits, and performance is unacceptable in all cases when using 4 bits. We can draw several conclusions from these results.

First, the fact that, for the case considered here, the receiver is performing well even with only 8 bits (and possibly acceptably well with 6 bits) implies that the multistage architecture is well-adapted to a fixed-point implementation, *provided that the received signal $r(t)$ has a limited dynamic range.* The results presented above assume that all users are received with the same power level, and thus the possible range of values for

the magnitude of $r(t)$ is fairly limited. This is important, because one of the principal drawbacks to a fixed-point implementation is that signals with a wide dynamic range cannot be represented accurately. If all users are being received with the same power level, this implies that power control is being employed. We saw in Chapter 4 that open-loop power control techniques are useful in minimizing the interference from unsynchronized users and thus improving acquisition time. Here, we see that stringent power control techniques (in other words, closed-loop techniques) can limit the dynamic range of the received signal and thus improve the performance of the multistage receiver when implemented with fixed-point arithmetic.

Next, it becomes clear that changing the number of quantization bits by only 1 or 2 bits can have a significant impact on system performance. This can occur because the number of bins used for quantization is exponentially related to the number of bits. This exponential relationship implies that the performance degradation when using fewer bits will not be linear. Thus, we would expect that going from 6 to 4 bits will have a much more significant impact than going from 12 to 10 bits, and the results clearly support this. As evidenced by the comparisons, the falloff is rather rapid when below 8 bits, implying that care needs to be taken when choosing the minimum number of bits to be used.

7.6.6 Alternative Quantization Strategies

There are different quantization strategies that can be employed in an effort to improve the system performance. First, a smaller quantization range can be chosen, and thus, for the same number of bits, the bin width will decrease. The drawback is that overflow may be more likely to occur, and the system designer will have to tradeoff the increase in BER due to overflow against the decrease in BER because of the increased ability to accurately quantize the interference estimates. A second strategy would be to employ non-uniform quantizers in an attempt to take advantage of the signal characteristics. Finally, different quantizers can be employed at different stages of the receiver, so that one quantizer (with a given range and number of bits) could be used to quantize the received signal and another quantizer (with a different range and/or number of bits) could be used when quantizing the interference estimates. This type of flexibility is particularly amenable to the reconfigurable computing architecture being employed for the prototype multistage receiver (the hardware platform and system specifications are discussed in more detail in Chapter 8).

Decreasing the Quantization Range

First, we consider the case where we decrease the quantization range, allowing more overflow in the hope that the increased resolution in the quantization of the interference esti-

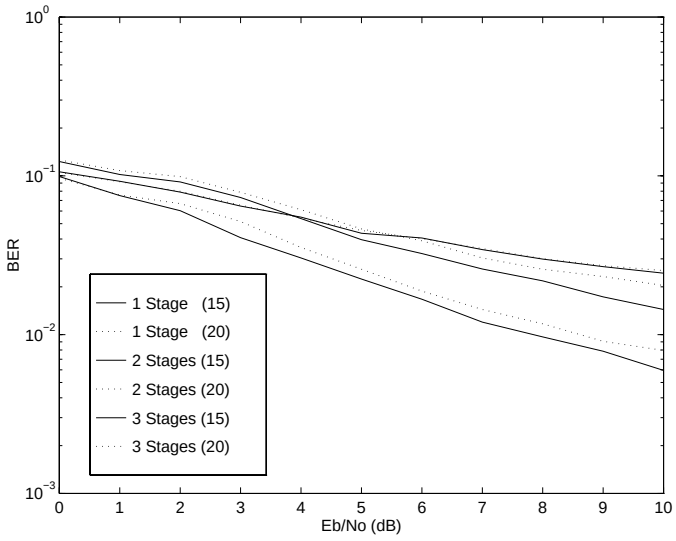

Figure 7.25: BER vs. E_b/N_o for 6 bits and Limit=15

mates will yield an overall decrease in BER. We must turn to simulation to examine the performance difference, since *all* analytical techniques are based on the assumption that overflow does not occur, and thus they cannot account for the case when overflow occurs. In Fig. 7.25, the simulated BER vs. E_b/N_o is shown when 6 quantization bits are used, but the quantization range is now from -15 to 15 instead of from -20 to 20. The performance is compared to the original case when 6 bits were used over the range of [-20, 20]. Overflow occurred for every value of E_b/N_o. As can be seen from this graph, the net effect is a slight decrease in the BER when interference cancellation is employed (stages 2 and 3). The bin width for this case is given by

$$\begin{aligned} \Delta_6 &= \frac{15-(-15)}{64} \\ &= 0.46875. \end{aligned} \tag{7.40}$$

The maximum error due to quantization is thus $\Delta/2 = 0.2344$ (it was 0.3125 for the larger range).

In Fig. 7.26, the BER vs. E_b/N_o for a 3 stage receiver is shown, where three cases are compared: six bits with a range of [-20,20], six bits with a range of [-15,15], and eight bits with a range of [-20,20]. Using six bits with a range of [-15,15] falls between the other two cases, so we see that by using this smaller range we can gain back much of the degradation

caused by going from 8 bits to 6 bits. In Fig. 7.27, a 2 stage receiver is shown for the same bit levels and quantization ranges. A similar effect is seen, although there is more of a difference between the 6 bit, [-15, 15] case and the 8 bit, [-20, 20] case at higher values of E_b/N_o.

Non-uniform Quantization

Another alternative would be to use non-uniform quantization when computing the interference estimates. Non-uniform quantization allows the bins to be non-uniformly distributed across the quantization range. Thus if we have some *a priori* knowledge of the signal characteristics, we can design the quantizer to maximize system performance. For the multistage receiver, there are two key types of signals we need to be able to quantize: the received signal and the interference estimates. The received signal is fairly strong and random, so we expect that a uniform quantizer is most appropriate here. The interference estimates, however, are constant over a bit period and expected to be in the neighborhood of a single user's signal's amplitude. Therefore, using a non-uniform quantizer here, we could concentrate bins at the smaller signal levels and thus more accurately model the individual interference estimates. The problem here is that once we begin summing the estimates to perform interference cancellation, the resulting sum will increase its dynamic range and thus require a different quantization strategy. After all K estimates have been summed, the result will have approximately the same dynamic range as the received signal $r(t)$ and therefore should be quantized in the same way. The drawback to this technique is that the non-uniform quantization will have to match the strength of each estimate, and overflow in any intermediate sums may cause overflow in the final result since we are changing quantization strategies with each sum. Since the appropriate pattern for the non-uniform bin distribution will depend upon the amplitude of the estimate, the pattern will also have to be dynamic and able to change over time. In general, the uniform quantizer may well provide a much more reasonable and practical solution from an implementation standpoint.

Using Different Quantizers At Different Points

In a similar fashion to employing non-uniform quantizers at the interference estimates, we could use uniform quantizers but with a much smaller range or a higher number of bits, thus decreasing the bin width and increasing the overall resolution of the quantizer. The reconfigurable computing platform will allow a great deal of flexibility in using different quantization types at different places. As before, however, the difficulty with this technique is that when the interference estimates are summed, the resulting signal has a similar dynamic range to the received signal, and will require a similar quantization range and

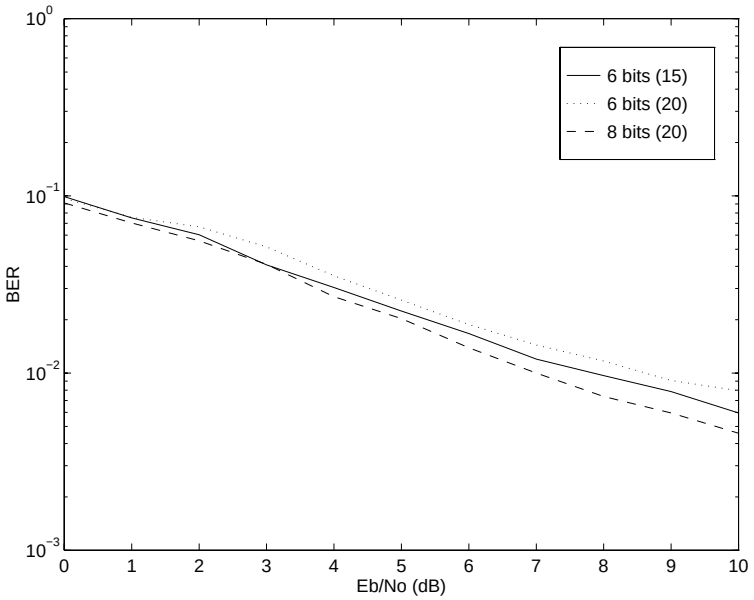

Figure 7.26: BER vs. E_b/N_o for 3 Stage Receiver

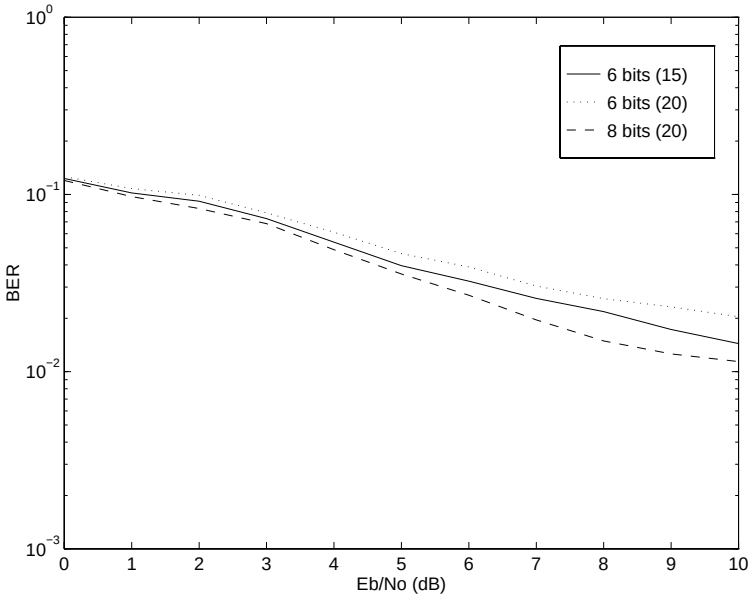

Figure 7.27: BER vs. E_b/N_o for 2 Stage Receiver

number of bits. For the cases studied here, such a complex technique is not required. If a different system was being studied with a higher spreading coefficient N and a higher number of users (and thus increased dynamic range of $r(t)$), using these different strategies may be more beneficial.

7.6.7 A Semi-Analytic Approach

We have seen that the analysis can be optimistic, and that this effect can be quite severe as the number of quantization bits decreases. This suggests that simulation must be used to determine an accurate representation of the BER performance in some cases. However, simulation runs take much longer than the analysis (for the typical BER graph above, running on a Sparc 20, the analysis takes a few seconds, whereas the simulations take two or three days). We would like a technique which has the accuracy of the simulations but with the speed of the analysis. A semi-analytic model could provide the answer, where we use the analytic model developed previously but now calibrate our noise sources based on simulation results. This technique will also try to compensate for the effects of the bias, although we will be assuming that our noise sources have zero means and the only parameter we will be adjusting is the variance of the decision statistic.

We can adjust the variance of the noise so that the resulting BER calculation more closely follows the BER of the simulation results. In so doing, we can select several simulation points and calibrate the variance of the noise in the semi-analytic model to yield a close match in BER. We thus only require a few simulation runs, greatly reducing the amount of time it takes to determine the BER performance. In addition, once calibrated, the noise sources can be used in analyzing other similar situations without requiring any new simulation runs.

In Figs. 7.28-7.31, we see the performance of the semi-analytic model compared to the simulation results. The standard deviations used for each of the estimation noise sources are summarized in Table 7.7 and compared with the analytic values. These values are then used in the variance calculation of 7.34. These values were chosen to give a good match across the entire range of E_b/N_o and for all stages. The system designer may wish to optimize the values to match only a specified range or a specified stage (or both). A least-squares linear regression technique could also be employed to obtain the values. It is assumed that these noise sources are Gaussian (and not uniform as before), so the fourth moment is given by $3\sigma^2$. Clearly, these semi-analytic curves follow the simulation curves much more closely than did the analytic curves. There are still some places where some deviation is noted, but it has been greatly reduced and thus this approach can be a useful tool for predicting the performance of the multistage receiver when fixed-point implementation is used. The values used for 4 bits are simply the values derived from the

Table 7.7: Semi-Analytic Characterization of ϵ_s

	Semi-Analytic σ_{ϵ_s}	**Semi-Analytic σ_{ϵ_s}**
Quantization Bits	**Stage 2**	**Stage 3**
12	15	12
8	15	12
6	20	15
4	44.2960	31.1220

lumped parameters, there was no need to develop them based on comparisons with BER curves (this is due to the negligible effect the bias has at this quantization level).

7.7 Conclusions

We have presented an analytic, semi-analytic, and simulation model for the multistage receiver when implemented using fixed-point arithmetic. Gaussian noise sources based on simulation results are used to model all correlated quantization noise. When compared with simulation results, the analytic model can be optimistic, and quite severely optimistic in certain circumstances. Semi-analytic models were then developed that retain much of the accuracy of the simulation model but with much of the speed of the analytic model.

The BER curves show that, as long as the dynamic range of the input signal is constrained, the multistage receiver performs quite well when using fixed-point arithmetic. Almost no degradation is noticed when 8 bits are used and overflow is allowed only rarely at low E_b/N_o, and only small degradation is noticed when 6 bits are used and overflow is allowed more frequently. Since these bit levels are easily achievable in practice, the multistage receiver can be implemented in hardware using fixed-point arithmetic and still retain nearly all of the performance of the receiver when quantization is not used.

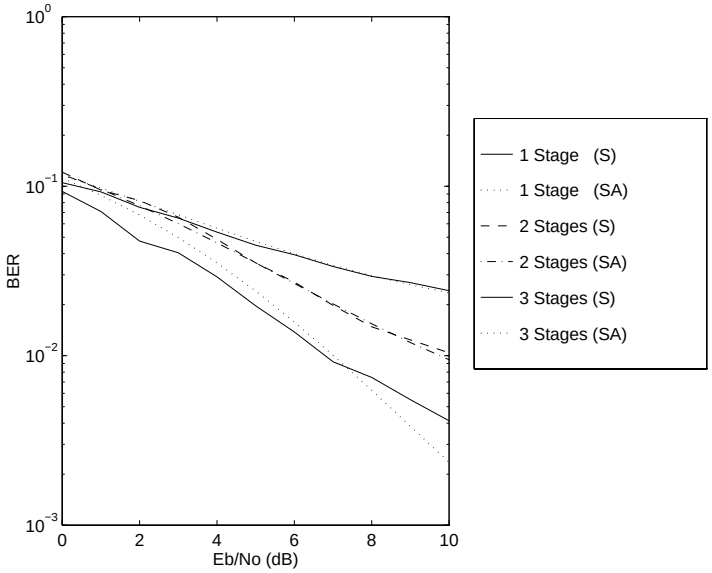

Figure 7.28: BER Using Semi-analytic Model for 12 bits

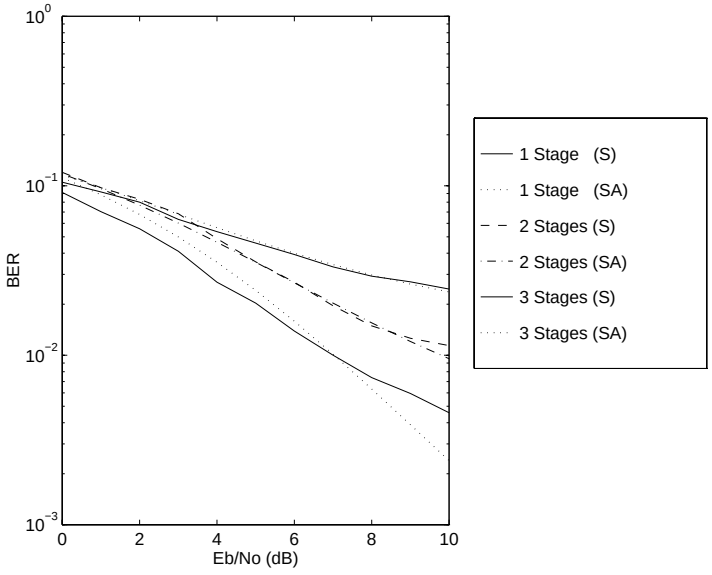

Figure 7.29: BER Using Semi-analytic Model for 8 bits

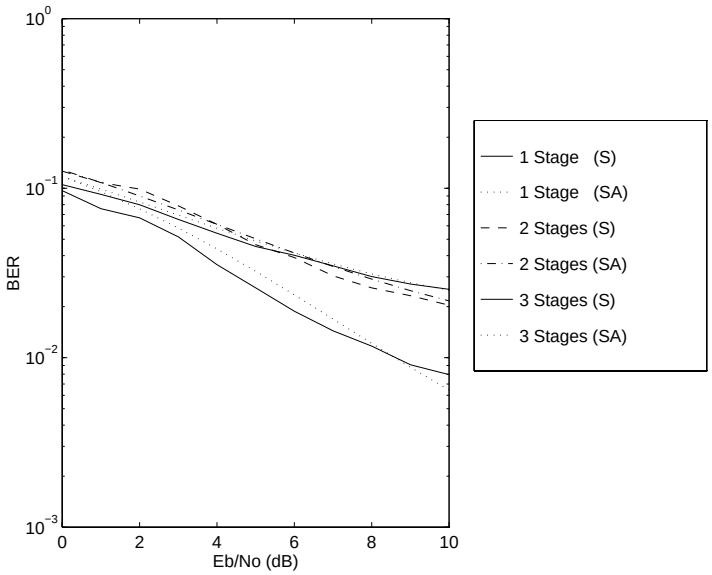

Figure 7.30: BER Using Semi-analytic Model for 6 bits

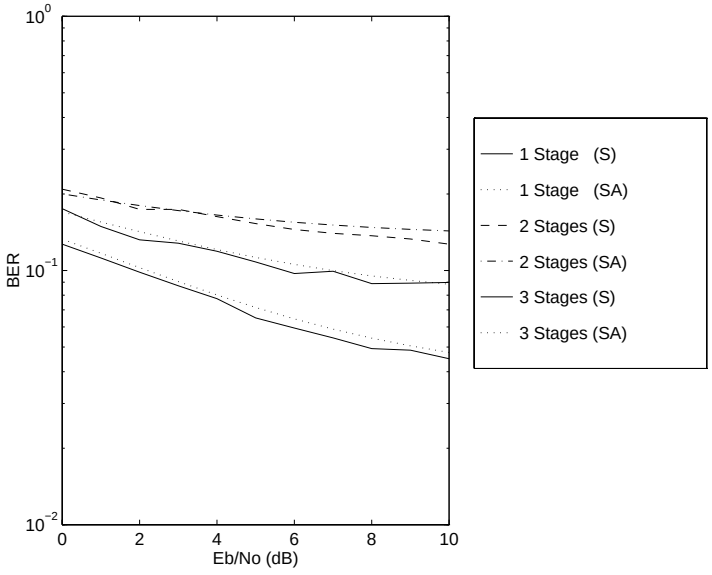

Figure 7.31: BER Using Semi-analytic Model for 4 bits

Chapter 8

Hardware Implementation

The prototype hardware implementation of the multistage receiver is one portion of an ongoing multiple year project[1] and involves four key research areas that will eventually be integrated into a single unified system: adaptive antennas, adaptive filtering, multistage receivers, and a reconfigurable DSP computing platform.

This chapter is organized as follows. First, the original proposed air interface is discussed. Next, a rough draft of the air protocol interface (API) that is currently being developed is discussed. Next, the problem of phase estimation is discussed, including a maximum likelihood phase estimator that attempts to estimate the phase of the received signal from each user. Finally, the hardware prototype is discussed with a focus on eventual integration of the four principal technologies.

8.1 Original Air Interface Standard

In the first year of the project, a basic air interface was jointly specified by the researchers. The goal of the project is to show how these various technologies can be used together to provide a high-capacity, high data rate, bandwidth-efficient wireless communications system. In support of those goals, the following parameters were specified:

- Binary Phase Shift Keying (BPSK) Modulation
- Data rate of $r_b = 128$ kbps

[1] the DARPA sponsored Glomo project, of which Virginia Tech is one of a group of universities pursuing mobile communications projects

- Spreading code length of $N = 15$
- 4 samples per chip on the reverse link
- RF carrier frequency near 2 GHz

The data rate was chosen to provide a higher data rate than typically seen in cellular telephony (data rates in the neighborhood of 10 kbps [33]). This would allow for a variety of different information sources to be transmitted, including ISDN channels, low-bandwidth video, computer data files such as MPEG movie clips, etc. The number of samples per chip on the reverse link was set to 4 to ensure that the PN codes could be aligned with enough precision to allow for accurate interference cancelation (Mike Buehrer studied the effects of timing offsets in [18]). The short spreading code length was chosen both to demonstrate and showcase the capabilities of the mobile and base station receivers, and also to keep the overall sample rate as low as possible given the high data rate. Based on the above parameters, the overall chipping rate is 1.92 Mcps and the overall sample rate is 7.68 Msps.

The carrier frequency was chosen not only because the research group has an experimental license in this range, but also to showcase the RF technology near the new unlicensed PCS band near 2.4 GHz. The RF hardware at 2.4 GHz is significantly more expensive than at 2.0 GHz, and so the decision was made to go with the lower frequency. This still provides a higher carrier frequency than the 900 MHz unlicensed band (the ISM band) and the current cellular telephony frequencies.

The synchronization analysis of Chapter 5 is not based on these system specifications, but instead uses a data rate of 9600 bps and a spreading code length of 31. The number of samples per chip is the same at 4. This approach was taken to generalize the synchronization results, since an active correlation approach is analyzed. The short spreading code length of the hardware prototype allows a simple matched filter technique to be used. The quantization results in Chapter 7 are based on these proposed system specifications.

While not specifically specified as such, the multistage research to date has assumed that the receiver will have knowledge of the carrier phase. This information could either be provided by a coherent phase reference (such as a pilot tone used in the forward link of the IS-95 standard [33]) or by a phase estimation technique. Phase estimation is discussed in more detail in Section 8.3.

8.2 The Multiuser API

The project team is beginning to design a multiuser air protocol interface (API) that can be used by other researchers. It is hoped that this API will be general enough that it will

contribute to the eventual common API that is being developed in conjunction with the various research teams in the entire project effort[2]. The API is a work-in-progress and the air interface is being modified somewhat from the original specifications to account for limitations of the RF hardware and to aid in the development time. A rough draft of the API has been fleshed out and tabulated in Table 8.1, although it must be stressed that this is a work-in-progress and the result of some preliminary discussions only. The API is being designed to be general enough to encompass all multiple user systems, not just multistage implementations.

The modulation format has been selected as differential BPSK to allow for noncoherent demodulation. BPSK cannot be noncoherently demodulated (although it can be noncoherently acquired). It is not practical to have the mobiles transmit pilot signals to provide a coherent phase reference. Estimation techniques are also not a robust solution to the problem as discussed in Section 8.3. Therefore, using a differential scheme will allow the use of a noncoherent approach such as that discussed in [18].

Frequency division duplexing (FDD) will be used to accommodate the transmit (TX) and receive (RX) channels. This will require separate RF bandwidths for the TX and RX channels, although the exact bandwidth allocations have not been specified pending further research. The other alternative would have been time division duplexing (TDD), which would have utilized the same RF front end for TX and RX, and switched in time to accommodate TX and RX. This would require more system overhead, and so the familiar FDD approach has been taken.

The data and channel rates are the most notable components that have been downgraded from the initial specifications. The nominal rates are 33.33 kbps and 500 kcps for the data and channel (chipping) rates, respectively. The maximum values are 66.66 kbps and 1 Mcps. The filters used in the current RF design were a direct motivation for reducing the bit rate. This also has the added benefit of reducing the overall computational load on the DSP processors, which will be particularly beneficial during the phase in which the prototype is being developed using traditional DSP processors. The reconfigurable implementation will allow for higher computational loads, and will also allow for computations to be computed in parallel pipelines whenever possible.

The issues of forward error correction (FEC) and interleaving warrant further study and so their exact parameters have not yet been specified. The use of error correction in the multistage receiver is a particularly interesting problem [104]. Typically, error correction

[2]DARPA is attempting to develop a common Glomo API that can be used by all of the research teams in the Glomo effort. Some research teams are contributing individual API's that stress what features are important to their particular system. It is hoped that eventually a common API can be developed that will resolve the differences in the various systems, although it has not been determined at this stage exactly how this will be accomplished.

Table 8.1: Multiuser API (Draft)

	Multiuser Receiver	**Adaptive Array**	**Adaptive Receiver**
Modulation	DBPSK	DBPSK	DBPSK
Multiplexing	FDD	FDD	FDD
RF Band	TBD	TBD	TBD
TX Power	10mw-1W	10mw-1W	10mw-1W
TX Power Step	1 dB	1 dB	1 dB
RX Sensitivity	-100 to -90 dBm	-100 to -90 dBm	-100 to -90 dBm
Channel Rate	500 kcps (nom) 1 Mcps (max)	500 kcps (nom) 1 Mcps (max)	500 kcps (nom) 1 Mcps (max)
Info Rate	33.33 kbps (nom) 66.66 kbps (max)	33.33 kbps (nom) 66.66 kbps (max)	33.33 kbps (nom) 66.66 kbps (max)
Proc. Gain	15 (variable)	15 (variable)	15 (variable)
FEC	TBD	TBD	TBD
Control	RSSI Available Power Control	RSSI Available Power Control	RSSI Available Power Control
Antenna Div.	Switched Beam	Array	Selection
Multipath	2 Finger Rake	2D-Rake	-
Modes of Operation	Active TX, RX Parallel TX Sleep Standby Jamming	Active TX, RX Parallel TX Sleep Standby Jamming	Active TX, RX Parallel TX Sleep Standby Jamming

is used to allow a system to operate with a lower E_b/N_o for an equivalent BER. In the multistage receiver, however, if we do not perform error correction after each stage, then operating at a lower E_b/N_o has simply increased the noise in the estimates and thus the performance of the receiver will be degraded. For maximum performance, error correction must be performed after each stage. However, this increases both the computational complexity and the time delay before a bit estimate can be made.

If error correction is only to be performed once, it then becomes imperative to determine after which stage the decoding should be performed. Perhaps the most obvious location is after the last stage, where error correction is used in making the actual bit estimate. Another approach would be to use error correction after the first stage, in order to get as strong an estimate as possible early on in the receiver and thus cancel as much interference as quickly as possible. In this case error correction is not used before making the actual bit estimate at the final stage.

A Rake receiver is chosen to combat multipath fading. Because of the relatively low bandwidth of the spread signal, at 500 kcps multipath components must be 2 μs apart for the receiver to be able to resolve them. This will only happen in some outdoor scenarios. Only 2 fingers are proposed for the Rake to minimize the overall computational complexity (Qualcomm's cellular system uses 3 or 4 fingers [33]).

8.3 Estimating the Phase

Most of the research that has been performed on multistage receivers has assumed that the receiver has knowledge of the coherent phase of each user. This presumes that either the mobile unit is providing a coherent phase reference (such as a pilot tone) or that the receiver is either able to track or estimate the phase of each user's received signal at the receiver. Tracking or estimating the phase is particularly difficult in the multistage receiver, because we must know each user's phase relative to all of the other users. Many techniques which track the phase use a closed-loop approach such as some variant of the phase locked loop, in which a local carrier replica is adjusted until an error is minimized when compared with the received signal. This closed loop cannot provide relative phase information, however, since each loop requires a separate oscillator, and each oscillator will have its own phase ambiguity.

8.3.1 The Source of Phase Error

We would like to use a single RF front end at the receiver and downconvert all of the user's signals with a single oscillator. If we do not compensate for the frequency offset in each carrier frequency, then the actual phase of the signal will drift over time from the expected value. When attempting to reconstruct the interference estimates in their I and Q form, we will be using the wrong phase. In addition, the wrong phase will be used in the complex correlation in the correlation receiver. Therefore, we need to be able to compensate for this frequency offset at the receiver.

While the carrier frequency may be nominally at 2.0 GHz, each of the oscillators will have some tolerance within which the actual frequency will fall. Manufacturers usually specify this tolerance in parts per million. For example, for the case considered here, a tolerance of +/- 2.5 parts per million is assumed, which is the tolerance allowed in oscillators for the TDMA cellular standard. At 2.0 GHz, this allows a deviation of +/- 5 kHz. Therefore, each of the oscillators in the mobile units will be slightly different based on this frequency offset. For each modulator, instead of modulating by $\cos(\omega_c t)$, we are instead modulating by $\cos[(\omega_c + 2\pi\Delta_k)t]$, where Δ_k is the frequency offset in Hz for user k.

Doppler shift will also cause some phase ambiguity if the mobile is moving relative to the base station. Doppler effects are likely to be much smaller in magnitude than the phase offsets due to the oscillator variations, and so they are not considered directly here. The amount of the Doppler shift will vary with time, however, whereas the oscillator drift will tend to be constant as long as the operating temperature does not vary significantly.

The channel will also introduce a phase ambiguity. This is typically modeled as being a uniform random variable over the range $[0, 2\pi]$. This will change over time as the channel changes and the mobiles move relative to each other and the base station. This can be particularly problematic if we use interleaving in an attempt to randomize burst errors (this is important when using decoders for forward error correction such as Viterbi decoders). If we have a block of bits at the transmitter that all have a similar phase due to the frequency offset, then interleave them and transmit them over the channel, we have to deinterleave before we can estimate the phase. However, if the phase of the channel has changed, it is quite possible that the bits that have the most similar phase due to the frequency offset will have very different phase offsets due to the channel. This suggests that if the dynamic phase of the channel is corrupting the interleaved bits differently, the estimation routine will best track either the frequency offset or the channel phase offset, but not both.

8.3.2 Determining the Phase

The most straightforward way of obtaining the phase is to use a pilot signal like that of the forward link of the IS-95 system [33]. The pilot signal will be affected by the channel in the same fashion as the data signal, and thus provides a coherent phase reference. The use of a pilot tone is simply not practical on the reverse link. This would require that each mobile transmit two signals, one of which is not conveying any information but is simply a drain on battery power and occupies bandwidth. Qualcomm's cellular system does not use pilot signals on the reverse link but instead performs non-coherent demodulation. In addition, for the interference canceler, the phases will not be obtained relative to some common reference and thus will not be useful for cancelation purposes.

If a coherent phase reference cannot be provided, the next alternative is to attempt to estimate the received signal. Since the received signal can be broken down into its I and Q components, where the I channel is weighted by $\cos\phi$ and the Q by $\sin\phi$, we can make an estimate of the phase by use of the inverse tangent. Buehrer shows how the phase can be estimated in this fashion in [18], and in particular that averaging can be used to decrease the variance of the noise in this estimate. It was assumed, however, that the receiver knew the correct bit information, which allows the receiver to resolve the ambiguity of π in the signal.

Another approach is the maximum likelihood estimator [105, 106]. This detector was designed for a land mobile satellite system employing differential PSK (DPSK). The differential nature of the modulation allows for the phase output to be limited between -$\pi/2$ and $\pi/2$. Since the original goal for the hardware prototype was to estimate the phase for a coherent phase system, the actual phase is needed without any phase ambiguity and over the full range from 0 to 2π. A block diagram of the SPW model is shown in Fig. 8.1, and the file is stored as *phase_est*.

An example of the operation of the maximum likelihood phase estimator is shown in Fig. 8.2, where no noise or interference is added to the received signal. The top plot is the actual phase, based on a frequency offset of 5 kHz and a random phase which is allowed to change in the simulation every 20 bits and is uniform over $[0, 2\pi]$. The middle plot is the estimated phase based on the technique of Divsalar and Simon [106] without any compensation for the phase ambiguity. The output is constrained by the estimator between -90 and 90 degrees. The bottom plot is the estimated phase with the phase ambiguity removed; it estimates the phase almost perfectly.

The performance of the estimator begins to degrade when noise is added, particularly in resolving the phase ambiguity. This implies that pilot symbols would have to be sent more frequently to keep the estimator predicting the correct phase. The ambiguity of π in the phase particularly degrades the bit error rate performance when the output of the

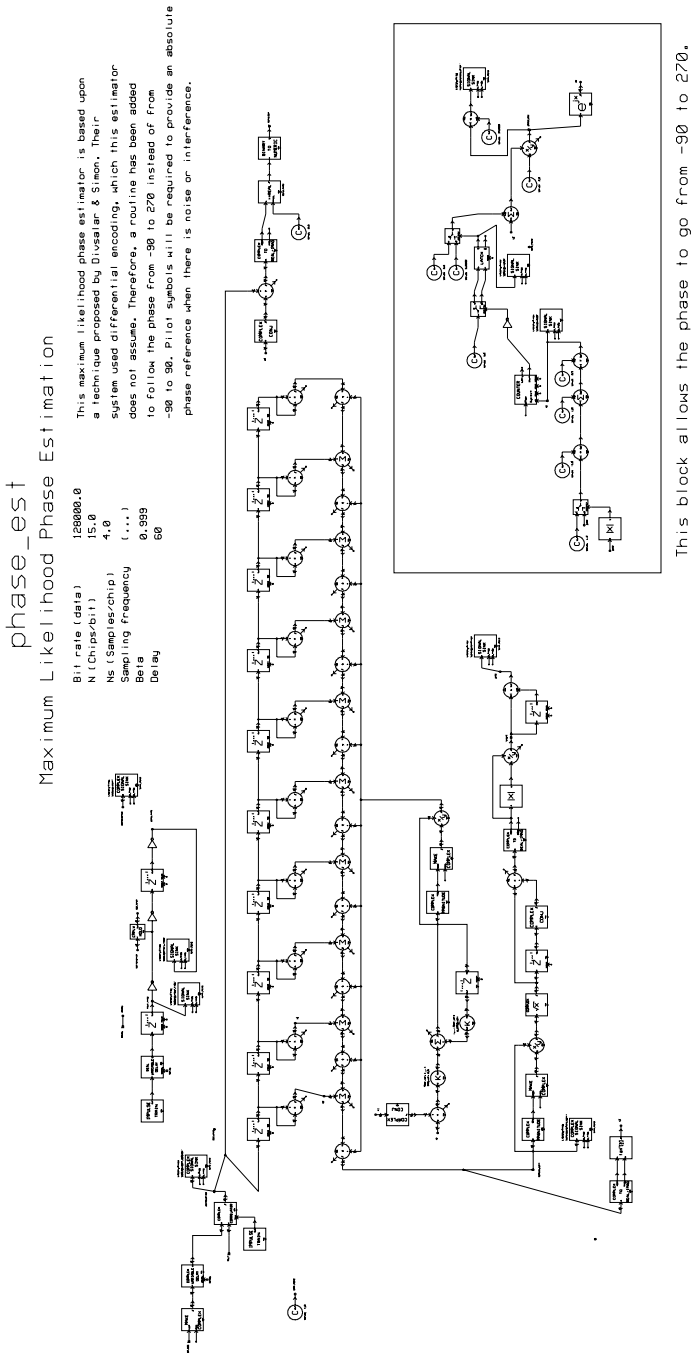

Figure 8.1: SPW Model of Maximum Likelihood Phase Estimator

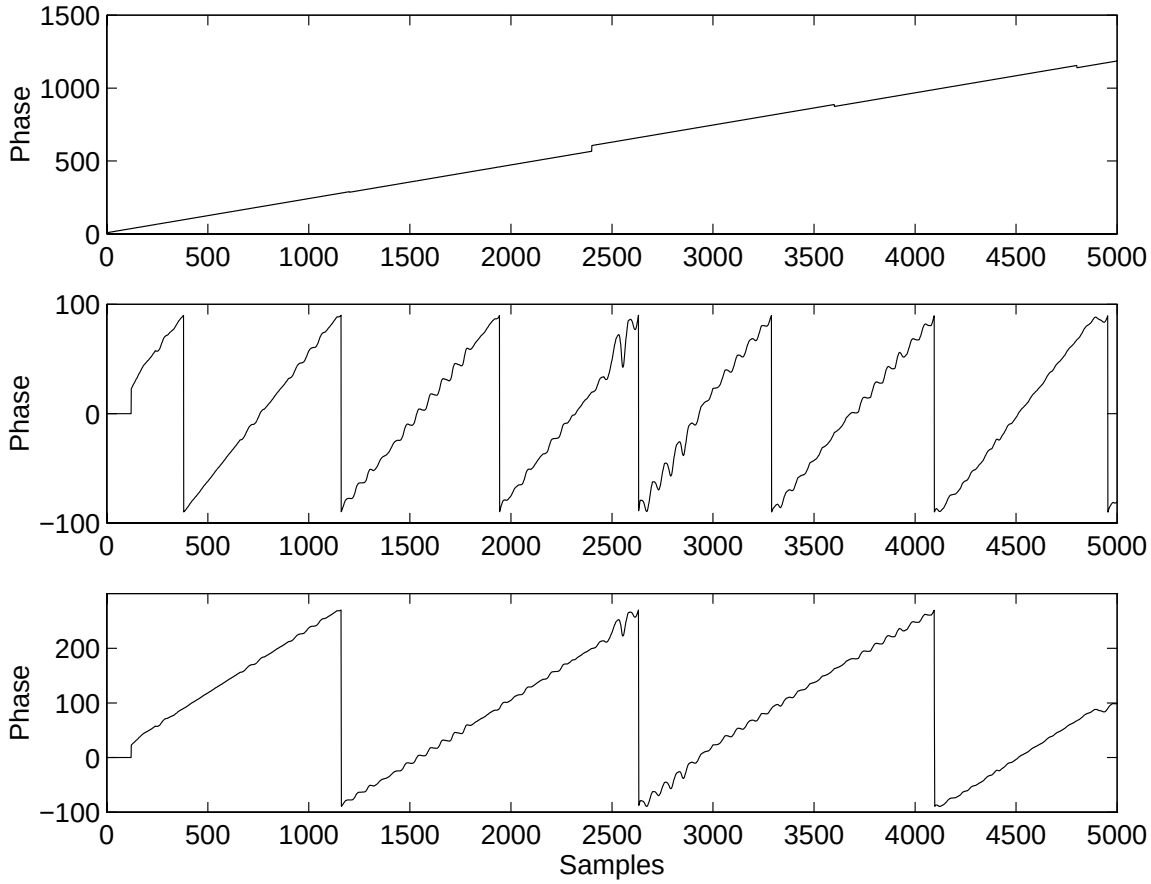

Figure 8.2: Example of Phase Estimation (No Noise or Interference)

correlator is strong, as it is the confusion over the phase ambiguity causing the wrong bit decision to be made and so a significant amount of interference will be added when we attempt to cancel the interference. The receiver will continue adding this interference until it encounters another phase change that puts the estimated phase back in the same half-plane as the true phase. The addition of interference degrades the estimation process even further. Therefore, it is recommended that differential modulation be used and that the receiver be based on a noncoherent scheme, so that the phase need not be estimated. Although a non-coherent scheme has poorer performance than a coherent scheme, the error in the phase estimate will degrade the coherent performance to the point that the noncoherent scheme may be preferable. In addition, this is a simpler implementation that will allow the associated computing cycles to be used elsewhere in the receiver design.

8.4 Computational Complexity

One of the factors that determines what DSP chips must be chosen is the computational complexity of the proposed multistage architecture. This discussion will concentrate on a fairly high level description of the computations required, as the specific number of clock cycles required to compute these instructions varies from platform to platform. The rated performance figures of the chip are typically peak figures which cannot be maintained due to communication requirements. The true operational performance can be as low as half of the peak figures. Another important consideration is how parallelizable the algorithm is. This is particularly important for the reconfigurable platform, where the ability to compute in parallel is an important feature of the architecture. The GloMo specifications are designed with the reconfigurable architecture in mind, since this will be the DSP architecture used for the final prototype. The DSP testbed, which will be used in the intermediate stages, should come as close as possible to being able to support the project specifications.

An advantage of the multistage receiver is that there are no complex algorithms that must be computed: the main operations are addition, subtraction and multiplication. Many of the multiplies are trivial, requiring at most a possible sign change. Most of this discussion will assume baseband operation and determines the number of operations required to make a bit decision, and is therefore a conservative estimation of the number of operations per bit.

The first major operation is the correlation of the received signal with the locally generated PN code replica. This will require NN_s multiplications, although the PN code chip values are +1 or -1 and therefore the multiplications are trivial. The accumulation process will require $NN_s - 1$ additions. This must be done for the I and the Q channels, so the overall requirement is $2NN_s$ multiplications and $2NN_s - 1$ additions per correlator. Each of the I and Q correlations can be done in parallel, and if the NN_s values of the received sequence are stored in memory, the multiplications may be done in parallel as well, and many of the additions. The decision statistic is then compared to the threshold and passed to the estimation routine. Since there are LK correlation receivers, where L is the number of fingers in the Rake receiver, the total number of operations for this stage are $2LKNN_s$ multiplications (all +1 or -1 multiplies) and $2LKNN_s - LK$ additions.

In the estimation stage, the first operation is the multiplication of the PN replica with the data bit estimate. Since the estimate will be +1 or -1, this amounts to, at most, flipping the bit of every sample in the PN code. This yields a possibility of NN_s multiplies, all trivial. The next stage is the multiplication of these chip values by the weighting factor, which is the decision statistic divided by NN_s. This is a non-trivial multiplication and requires NN_s multiplies to reconstruct the bit. To reconstruct the I and Q channels, this product is then multiplied by the cosine and sine of the phase estimate, for a total of $2NN_s$

non-trivial multiplies. The I and Q estimates can obviously be computed in parallel. The cosine and sine of the phase will also have to be calculated, although this will only need to be recalculated as the phase changes. The received estimate has now been reconstructed using $4NN_s$ multiplies, NN_s of which are trivial. Since this must be done for K users and L Rake fingers, this requires a total of $4LKNN_s$ multiplies to construct all users' estimates.

The next stage is the interference cancellation process, in which all users' estimates are subtracted from a delayed version of the received signal. Many of these cancellations can be done in parallel. The first two estimates will require NN_s additions, with each additional estimate adding an additional NN_s additions, for a total of $(LK-1)NN_s$ additions. This must be subtracted from the received signal, so obtaining the residual signal will require an additional NN_s subtractions, for a total of $(LK-1)NN_s$ additions and NN_s subtractions. At the input to the next receiver stage, each user's estimate is added back to the residual signal, which will require $KLNN_s$ additions to do this for all K users and L Rake fingers. Therefore the total estimation process requires $(2LK-1)NN_s$ additions and NN_s subtractions. Since this must be done for the I and Q channels, the operations double to $(4LK-2)NN_s$ additions and $2NN_s$ subtractions.

The next correlation process will use $2LKNN_s$ multiplies and $2LKNN_s - LK$ additions, as mentioned above. Therefore, the total stage requires the sum of the operations for the estimation, cancellation, and the correlation process, or $(6LK-2)NN_s - LK$ additions, $2NN_s$ subtractions, and $6LKNN_s$ multiplies. Assuming that all of these operations can be accomplished in an identical number of clock cycles, typically one, this is a total of $12LKNN_s - LK$ operations. There will be some final addition at the last stage of the receiver, where the L decision statistics in the Rake receiver are weighted and summed, which will require LK multiplications and $LK-1$ additions. The LK terms are much smaller than the $LKNN_s$ terms, however, and can be neglected. Therefore, each stage that performs cancellation will require on the order of $12LKNN_s$ operations per bit period. The last stage of the receiver only performs a correlation and thus only requires on the order of $4LKNN_s$ operations per bit. Therefore, for an s stage receiver, the total number of operations required per bit is on the order of $12LK(s-1)NN_s + 4LKNN_s$.

Even though some of these operations are trivial multiplies, this is still a large number of operations per second. To illustrate this, the numbers from the proposed GloMo air interface can be used. The total number of users K is not part of the air interface, but $K = 10$ can be used for purposes of illustration. If we assume there are $L = 2$ fingers in the Rake receiver (the cellular CDMA system uses 3 on the forward channel and 2 on the reverse channel) and 2 stages in the receiver, then using $N = 15$ and $N_s = 4$, the total number of operations per bit is 19,200 operations per bit. For a data rate of 128 kbps, each bit takes 7.8125 μs, or a total of $2.4576 * 10^9$ operations per second, which is an extremely high number. As mentioned previously, this number is not quite as extreme as

it might seem, since there is a good deal of parallel operations and some of the operations are trivial. In addition, this decodes *all* users in the system, so we effectively require $0.24576 * 10^9$ operations per second per user. This suggests that a DSP testbed can be constructed using off-the-shelf hardware for a small number of active transmitters, perhaps with some reduction in the sampling rate.

8.4.1 Choosing the DSP Chips

These high computational requirements meant that the DSP chip chosen as the basis for the DSP testbed would have to be state of the art chips. Another PhD student supporting the multistage portion of this project, Mike Buehrer, studied the available options in the industry today and settled on the Analog Devices 2106x (SHARC) chip [18]. Analog Devices and Bittware offer a plug-in board for a single chip that can be integrated into an IBM compatible personal computer (PC). In addition, Bittware offers expansion modules that allow a multiple processor configuration using either board. LSI is creating boards using the SHARC chip, but they are not currently available. The SHARC chips can be programmed using either assembly or C language. Hyperception, Inc. has a program that programs the chip using a block diagram editor approach. The multiprocessing capability will allow higher throughput if additional modules are purchased.

8.5 Developing the Hardware Prototype

The hardware development of the multistage receiver is currently being developed by other members of the multistage receiver team. At this stage in the project, the receiver is being built using the traditional Analog Devices DSP chips, with the eventual goal being to port the design to the reconfigurable computing platform when it is available. The RF portion is being developed in conjunction with the entire project team because of the similarities in requirements and design. At this point, it is not envisioned that the adaptive antenna array will be used in conjunction with the multistage receiver. Due to the low spreading code length, it is not expected that the system will support enough users to make the use of both technologies at the base station a viable concept.

8.6 Conclusion

A multiuser API is being developed that is a modification of the original proposed air interface for the entire hardware prototype. The API is being developed to apply to all

multiuser systems, not just the system being developed for this project. The hardware prototype is currently in development using traditional DSP processors and will eventually be ported to the reconfigurable computing platform.

The hardware version of the multiuser receiver will not have knowledge of the coherent phase of each user, and it is impractical to obtain a coherent reference from the mobile. Therefore, a maximum likelihood phase estimator has been investigated that could provide relative phase estimates for each user. However, it is seen that the estimator performance degrades in the presence of heavy interference, and frequent pilot symbols will be required to resolve the phase ambiguity which can arise. It is recommended that a noncoherent scheme such as that discussed in [18] be pursued instead for use in the hardware prototype.

Chapter 9

Conclusions

9.1 Contributions

In this report, we have described the research supporting the development of a baseband multistage receiver in DSP hardware. The following contributions have been made:

- survey of multiuser receiver designs, spread spectrum synchronization techniques, and quantization analysis
- derivation of near-far resistance of multistage receiver
- analysis and discussion of the mean of interference estimates and the use of a backoff factor to improve system performance when the estimates are noisy. In situations where the predominant source of errors is caused by heavy system loading, the non-zero mean of the interference estimates can cause a signficant number of errors. The use of a backoff factor can be used any time the interference estimates are noisy, as multiplying the estimates by this factor reduces both the mean and standard deviation of the estimates by the backoff factor is well. This allows for conservative interference cancellation when the accuracy of the estimate is questionable.
- analysis and simulation of bit error rate in presence of both cancelled and uncancelled interference components. Unsynchronized users cannot be canceled, and thus the multistage receiver provides no near-far resistance against the interference they cause. If the power in these users is significant relative to the power in the residual signal after cancellation, then even a small number of unsynchronized users can dominate and greatly increase the BER of synchronized users. For a spreading gain of $N = 128$ and a four stage receiver, even one unsynchronized user that had a 6 dB increase in

power over the synchronized users caused over a 10% drop in capacity at a BER of 10^{-3}.

- analysis and simulation of mean acquisition time for single dwell time synchronization. The less noisy residual received signal can be acquired more quickly, although there is an inherent time delay associated with each stage. Furthermore, the optimum threshold setting may decrease as the number of stages increases, although this is dependent upon the penalty time.
- development of SPW simulation model for multistage receiver. The SPW block diagram approach produces a basic multistage receiver design similar to that of a physical system. Here, the model was adapted for synchronization, quantization, and phase estimation.
- analysis and simulation of quantization effects. Due to the limited dynamic range of an input signal in a tightly power controlled environment, a fixed-point implementation can be used with a relatively low number of bits and still not show signficant performance degradation from the ideal case. If the allowable level of overflow is increased, even smaller number of bits may be used. The multistage receiver is well-suited to a fixed-point implementation. For the parameters studied here, there was no noticeable dropoff in performance with 8 bits, and little with 6 bits if overflow is allowed.
- simulation of frequency offsets and a maximum likelihood phase estimator to estimate the phase of each user. Each user's transmitter will have a unique phase offset. If a coherent phase reference cannot be provided (as is usually the case on the reverse link), an estimate of the phase can be generated. For this case, a maximum likelihood estimator was simulated, although performance was poor due to the high inteference levels. A phase ambiguity could cause the receiver to choose the opposite of the correct bit.

9.2 Future Work

This thesis has provided several contributions towards the multistage hardware effort at Virginia Tech. There are still issues that remain to be solved however. Some examples include:

- A more detailed study of error correction in the multistage receiver to build on the work of [104]. In particular, the effect of performing error correction at differing stages needs to be investigated.

- An extension of the semi-analytic model and analytic model presented in this thesis to allow directly for a non-zero mean in the interference estimates. The model as it has been developed for zero-mean random variables only. This would allow the mean of the interference estimates to be modeled more precisely, with parameters based on simulation results to overcome the difficulty in obtaining a value analytically.

- An investigation into practical methods of determing an appropriate backoff factor at a given time and channel condition. Current research has focused on choosing a backoff factor in the AWGN channel based on system loading, but practical systems will need to determine this factor in a variety of channels and loading conditions.

- A thorough performance evaluation of a non-coherent multistage receiver. Most multistage receiver research to date has focused on the coherent implementation; reverse links will often need to be non-coherent, as the mobile cannot be expected to transmit pilot tones, and because phase estimation can be problematic in mobile communications systems.

- An optimization of the multistage DSP implementation to take advantage of the highly parallel nature of the reconfigurable computing platform.

- Consideration of system-to-chip design, to maximize efficiency of a hardware implementation.

- Consideration of network level issues, including further development and refinement of the API and network performance under loading conditions.

Appendix A

Derivation of Variance of Effective Signal Power

In this section, we develop a definition for the variance of the effective interference power, $(\sigma_{P_k}^{(s+1)})^2$, as discussed in Sec. 5.3.4. The variance by definition is given by

$$(\sigma_{P_k}^{(s+1)})^2 = E\left[\left(\nu_k^{(s+1)}\right)^2\right] - \left(\mu_{P_k}^{(s+1)}\right)^2. \tag{A.1}$$

Since we found $\mu_{P_k}^{(s+1)}$ in Section 5.3.3, we need to find an expression for $E[(\nu_k^{(s+1)})^2]$.

By using the definition for $\nu_k^{(s)}$ given in (5.25), we find

$$\begin{aligned} E\left[\left(\nu_k^{(s+1)}\right)^2\right] &= E\left[P_k^2 - 2\sqrt{8P_k}P_k\frac{Z_k^{(s)}}{T}b_{k,i} + 12P_k\left(\frac{Z_k^{(s)}}{T}\right)^2\right. \\ &\quad \left. -4\sqrt{8P_k}\left(\frac{Z_k^{(s)}}{T}\right)^3 b_{k,i} + 4\left(\frac{Z_k^{(s)}}{T}\right)^4\right]. \end{aligned} \tag{A.2}$$

In [21], it is shown that if we take the expectation conditioned on P_k, we can solve this to be

$$\begin{aligned} E\left[\left(\nu_k^{(s+1)}\right)^2\right] &= E_{P_k}\left[\frac{3N_o^2}{4T^2} + \frac{6N_o}{T^3}E\left[\left(\sum_{l=1,l\neq k}^{K} I_{l,k}^{(s)}\right)^2 \mid P_k\right]\right. \\ &\quad \left. +\frac{4}{T^4}E\left[\left(\sum_{l=1,l\neq k}^{K} I_{l,k}^{(s)}\right)^4 \mid P_k\right]\right]. \end{aligned} \tag{A.3}$$

The first term is constant, and therefore we only need to derive expressions for the second and third terms. From [21], these terms can be derived to be

$$\begin{aligned} E_{P_k}\left[E\left[\left(\sum_{l=1,l\neq k}^{K} I_{l,k}^{(s)}\right)^2 \mid P_k\right]\right] &= E\left[var\left\{\sum_{l=1,l\neq k}^{K} I_{l,k}^{(s)}\right\}\right] \\ &= E[\Psi^{(s)}] \\ &= \mu_{\Psi^{(s)}} \end{aligned} \tag{A.4}$$

and

$$\begin{aligned} E_{P_k}\left[E\left[\left(\sum_{l=1,l\neq k}^{K} I_{l,k}^{(s)}\right)^4 \mid P_k\right]\right] &= E\left[\sum_{l=1,l\neq k}^{K}\left(I_{l,k}^{(s)}\right)^4\right. \\ &\quad \left. +3\sum_{l=1,l\neq k}^{K}\sum_{m=1,m\neq l\neq k}^{K}\left(I_{l,k}^{(s)}\right)^2\left(I_{m,k}^{(s)}\right)^2\right]. \end{aligned} \tag{A.5}$$

The first term of (A.5) can be evaluated by

$$\begin{aligned} E\left[\sum_{l=1,l\neq k}^{K}\left(I_{l,k}^{(s)}\right)^4\right] &= E\left[\sum_{l=1,l\neq k}^{K_1}\left(I_{l,k}^{(s)}\right)^4\right] + E\left[\sum_{l=K_1+1}^{K_2}\left(I_{l,k}^{(s)}\right)^4\right] \\ &= E\left[\sum_{l=1,l\neq k}^{K_1}\left(T_c\sqrt{\frac{\nu_l^{(s)}}{2}}cos(\phi_l-\phi_k)W_l\right)^4\right] + E\left[\sum_{l=K_1+1}^{K_2}\left(T_c\sqrt{\frac{P_l}{2}}cos(\phi_l-\phi_k)W_l\right)^4\right] \\ &= \frac{3T_c^4}{32}\left\{\sum_{l=1,l\neq k}^{K_1} E\left[\left(\nu_l^{(s)}\right)^2\right]E[W_l^4] + \sum_{l=K_1+1}^{K_2} E[P_l^2]E[W_l^4]\right\}. \end{aligned} \tag{A.6}$$

We can solve for $E[(\nu_l^{(s)})^2]$ from (A.1) as

$$E\left[\left(\nu_l^{(s)}\right)^2\right] = (\sigma_{P_l}^{(s)})^2 + \left(\mu_{P_l}^{(s)}\right)^2 \tag{A.7}$$

and by definition

$$E\left[(P_l)^2\right] = (\sigma_{P_l}^{(1)})^2 + \left(\mu_{P_l}^{(1)}\right)^2. \tag{A.8}$$

Therefore, (A.6) reduces to

$$E\left[\sum_{l=1,l\neq k}^{K}\left(I_{l,k}^{(s)}\right)^4\right] = \frac{3T_c^4}{32}\sum_{l=1,l\neq k}^{K}\left[(\sigma_{P_l}^{(s)})^2 + \left(\mu_{P_l}^{(s)}\right)^2\right]E[W_l^4]. \tag{A.9}$$

It is shown in [21] that

$$E[W_l^4] = \frac{12N^2 - 9N}{5}. \tag{A.10}$$

Therefore, we can finally reduce (A.9) to

$$E\left[\sum_{l=1,l\neq k}^{K}\left(I_{l,k}^{(s)}\right)^4\right] = \frac{3T_c^4}{32}\frac{12N^2-9N}{5}\sum_{l=1,l\neq k}^{K}\left[(\sigma_{P_l}^{(s)})^2 + \left(\mu_{P_l}^{(s)}\right)^2\right]. \tag{A.11}$$

The second term of (A.5) can be evaluated by

$$\begin{aligned} E\left[3\sum_{l=1,l\neq k}^{K}\sum_{m=1,m\neq l\neq k}^{K}\left(I_{l,k}^{(s)}\right)^2\left(I_{m,k}^{(s)}\right)^2\right] &= 3E\left[\sum_{l=1,l\neq k}^{K}\left\{\sum_{m=1,m\neq l\neq k}^{K_1}\left(I_{l,k}^{(s)}\right)^2\left(I_{m,k}^{(s)}\right)^2\right.\right. \\ &\qquad \left.\left. + \sum_{m=K_1+1,m\neq l}^{K_2}\left(I_{l,k}^{(s)}\right)^2\left(I_{m,k}^{(s)}\right)^2\right\}\right] \\ &= 3E\left[\sum_{l=1,l\neq k}^{K_1}\left\{\sum_{m=1,m\neq l\neq k}^{K_1}\left(I_{l,k}^{(s)}\right)^2\left(I_{m,k}^{(s)}\right)^2 + \sum_{m=K_1+1}^{K_2}\left(I_{l,k}^{(s)}\right)^2\left(I_{m,k}^{(s)}\right)^2\right\}\right. \\ &\qquad \left. + \sum_{l=K_1+1}^{K_2}\left\{\sum_{m=1}^{K_1}\left(I_{l,k}^{(s)}\right)^2\left(I_{m,k}^{(s)}\right)^2 + \sum_{m=K_1+1,m\neq l}^{K_2}\left(I_{l,k}^{(s)}\right)^2\left(I_{m,k}^{(s)}\right)^2\right\}\right]. \end{aligned} \tag{A.12}$$

Using (5.26), this can be shown to reduce to

$$E\left[3\sum_{l=1,l\neq k}^{K}\sum_{m=1,m\neq l\neq k}^{K}\left(I_{l,k}^{(s)}\right)^2\left(I_{m,k}^{(s)}\right)^2\right] = \frac{T_c^4(4N^2-9N+13)}{48}\sum_{l=1,l\neq k}^{K}\sum_{m=1,m\neq l\neq k}^{K}\mu_{P_l}^{(s)}\mu_{P_l}^{(s)}. \tag{A.13}$$

Therefore, we have now derived all the terms necessary to explicitly solve (A.3). Using (A.4), (A.11), and (A.13), we find

$$\begin{aligned} E\left[\left(\nu_k^{(s+1)}\right)^2\right] &= \frac{3N_o^2}{4T^2} + \frac{6N_o}{T^3}\mu_{\Psi^{(s)}} + 9\frac{4N^2-3N}{40N^4}\sum_{l=1,l\neq k}^{K}\left[(\sigma_{P_l}^{(s)})^2 + \left(\mu_{P_l}^{(s)}\right)^2\right] \\ &\quad + \frac{4N^2-9N+13}{12N^4}\sum_{l=1,l\neq k}^{K}\sum_{m=1,m\neq l\neq k}^{K}\mu_{P_l}^{(s)}\mu_{P_m}^{(s)}. \end{aligned} \tag{A.14}$$

Next, we note that by modifying (5.14) for stages 2 and beyond as

$$\mu_{\Psi}^{(s)} = \frac{T_c^2 N}{6}\sum_{l=1,l\neq k}^{K}\mu_{P_l}^{(s)} \tag{A.15}$$

and combining it with (5.32), we get that for $1 \leq k \leq K_1$,

$$\mu_{P_k}^{(s+1)} = \frac{N_o}{2T} + \frac{2\mu_{\Psi}^{(s)}}{T^2}. \tag{A.16}$$

Finally, by substituting (A.14) and (A.16) into (A.1), the expression for the variance of the effective interference power at stage $s+1$ caused by user k, $1 \leq k \leq K_1$, is given by

$$\begin{aligned}(\sigma_{P_k}^{(s+1)})^2 &= \frac{N_o^2}{2T^2} + \frac{4N_o}{T^3}\mu_{\psi}^{(s)} - \frac{4}{T^4}\left(\mu_{\Psi}^{(s)}\right)^2 + \frac{9(4N^2-3N)}{40N^4}\sum_{l=1,l\neq k}^{K}\left[(\sigma_{P_l}^{(s)})^2 + \left(\mu_{P_l}^{(s)}\right)^2\right] \\ &\quad + \frac{4N^2-9N+13}{12N^4}\sum_{l=1,l\neq k}^{K}\sum_{m=1,m\neq l\neq k}^{K}\mu_{P_l}^{(s)}\mu_{P_m}^{(s)}. \end{aligned} \tag{A.17}$$

Appendix B

Effective Signal Power Variance for Quantization

In this section, we develop a definition for the variance of the effective interference power, $(\sigma_{P_k,\epsilon}^{(s+1)})^2$, when fixed-point quantization is used as discussed in Chapter 7. The variance by definition is given by

$$(\sigma_{P_k,\epsilon}^{(s+1)})^2 = E\left[\left(\nu_{k,\epsilon}^{(s+1)}\right)^2\right] - \left(\mu_{P_k,\epsilon}^{(s+1)}\right)^2. \tag{B.1}$$

Since we found $\mu_{P_k,\epsilon}^{(s+1)}$ in Section 7.4.3, we need to find an expression for $E[(\nu_{k,\epsilon}^{(s+1)})^2]$.

By using the definition for $\nu_{k,\epsilon}^{(s)}$ given in (5.25), we find

$$\begin{aligned} E\left[\left(\nu_{k,\epsilon}^{(s+1)}\right)^2\right] &= E\left[P_k^2 - 2\sqrt{8P_k}P_k\left(\frac{Z_k^{(s)}}{T}+\frac{\epsilon_s}{2}\right)b_{k,i} + 12P_k\left(\frac{Z_k^{(s)}}{T}+\frac{\epsilon_s}{2}\right)^2\right. \\ &\quad \left. -4\sqrt{8P_k}\left(\frac{Z_k^{(s)}}{T}+\frac{\epsilon_s}{2}\right)^3 b_{k,i} + 4\left(\frac{Z_k^{(s)}}{T}+\frac{\epsilon_s}{2}\right)^4\right]. \end{aligned} \tag{B.2}$$

We can take the expectation on P_k to solve the parenthetical terms:

$$E\left[\frac{Z_k^{(s)}}{T}+\frac{\epsilon_s}{2}|P_k\right] = E\left[\frac{Z_k^{(s)}}{T}\right] \tag{B.3}$$

$$E\left[\left(\frac{Z_k^{(s)}}{T}+\frac{\epsilon_s}{2}\right)^2|P_k\right] = E\left[\frac{(Z_k^{(s)})^2}{T^2}+\frac{Z_k^{(s)}\epsilon_s}{T}+\frac{\epsilon_s^2}{4}\right] \tag{B.4}$$

$$E\left[\left(\frac{Z_k^{(s)}}{T}+\frac{\epsilon_s}{2}\right)^3|P_k\right]=E\left[\frac{(Z_k^{(s)})^3}{T^3}+\frac{3(Z_k^{(s)})^2\epsilon_s}{2T^2}+\frac{3Z_k^{(s)}\epsilon_s^2}{4T}+\frac{\epsilon_s^3}{8}\right] \tag{B.5}$$

$$E\left[\left(\frac{Z_k^{(s)}}{T}+\frac{\epsilon_s}{2}\right)^4|P_k\right]=E\left[\frac{(Z_k^{(s)})^4}{T^4}+\frac{2(Z_k^{(s)})^3\epsilon_s}{T^3}+\frac{3(Z_k^{(s)})^2\epsilon_s^2}{2T^2}+\frac{Z_k^{(s)}\epsilon_s^3}{2T}+\frac{\epsilon_s^4}{16}\right] \tag{B.6}$$

We therefore need to derive the first through fourth moments of both $Z_k^{(s)}$ and ϵ_s.

B.0.1 Moments of $Z_k^{(s)}$

From the definition of $Z_k^{(s)}$ given in Chapter 8, we can expand these terms as follows:

$$E\left[Z_k^{(s)}\right]=\sqrt{\frac{P_k}{2}}Tb_k \tag{B.7}$$

$$E\left[\left(Z_k^{(s)}\right)^2\right]=\frac{N_oT}{4}+E[\epsilon_r^2]+\frac{P_kT^2}{2}+E\left[\left(\sum_{j=1,j\neq k}^{K}I_{j,k}^{(s)}\right)^2|P_k\right] \tag{B.8}$$

$$\begin{aligned}E\left[\left(Z_k^{(s)}\right)^3\right] &= \left(\sqrt{\frac{P_k}{2}}\right)^3T^3b_k^3+3\left(\frac{N_oT}{4}+E[\epsilon_r^2]\right)\sqrt{\frac{P_k}{2}}Tb_k \\ &\quad +3\sqrt{\frac{P_k}{2}}Tb_kE\left[\left(\sum_{j=1,j\neq k}^{K}I_{j,k}^{(s)}\right)^2|P_k\right]\end{aligned} \tag{B.9}$$

$$\begin{aligned}E\left[\left(Z_k^{(s)}\right)^4\right] &= 3\left(\frac{N_oT}{4}\right)^2+E[\epsilon_r^4]+\left(\frac{P_k}{2}\right)^2T^4+6\left(\frac{N_oT}{4}+E[\epsilon_r^2]\right)\frac{P_k}{2}T^2 \\ &\quad +6\left(\frac{N_oT}{4}+E[\epsilon_r^2]+\frac{P_k}{2}T^2\right)E\left[\left(\sum_{j=1,j\neq k}^{K}I_{j,k}^{(s)}\right)^2|P_k\right] \\ &\quad +E\left[\left(\sum_{j=1,j\neq k}^{K}I_{j,k}^{(s)}\right)^4|P_k\right]+6\frac{N_oT}{4}E[\epsilon_r^2]\end{aligned} \tag{B.10}$$

B.0.2 Moments of ϵ_s

We now need to develop the first through fourth moments of the uniform quantizer noise source ϵ_s. We know that ϵ_s has a uniform distribution between $[-\Delta/2, \Delta/2]$. We can find the moments from the characteristic function $\Psi_{\epsilon_s}(\omega)$ which is given by [103]

$$\begin{aligned} \Psi_{\epsilon_s}(\omega) &= E[exp(j\omega\epsilon_s)] && \text{(B.11)} \\ &= \int_{-\infty}^{\infty} f_{\epsilon_s}(\epsilon_s) exp(j\omega\epsilon_s) d\epsilon_s. && \text{(B.12)} \end{aligned}$$

where $j = \sqrt{-1}$. If we solve this in general for a continuous uniform random variable x that is uniform over the interval $[a, b]$, then the characteristic function is given by

$$\Psi_{\epsilon_s}(\omega) = \frac{e^{j\omega b} - e^{j\omega a}}{j\omega(b-a)}. \tag{B.13}$$

We can then find the kth moment by taking the kth derivative of $\Psi_X(\omega)$ and evaluating the result at $\omega = 0$, or

$$E\left[X^k\right] = \frac{1}{j^k}\left[\frac{d^k\Psi_X(\omega)}{d\omega^k}\right] \text{ at } \omega = 0. \tag{B.14}$$

Since we need the first four moments of ϵ_s, we need to find the first four derivatives of the uniform characteristic function, which can be shown to be

$$\begin{aligned} \frac{d\Psi_X(\omega)}{d\omega} &= \frac{1}{j(b-a)} \frac{(j\omega b - 1)e^{j\omega b} - (j\omega a - 1)e^{j\omega a}}{\omega^2} && \text{(B.15)} \\ \frac{d^2\Psi_X(\omega)}{d\omega^2} &= \frac{1}{j(b-a)} \frac{(\omega^2 a^2 + 2j\omega a - 2)e^{j\omega a} - (\omega^2 b^2 + 2j\omega b - 2)e^{j\omega b}}{\omega^3} && \text{(B.16)} \\ \frac{d^3\Psi_X(\omega)}{d\omega^3} &= \frac{1}{j(b-a)} \left\{ \frac{(j\omega^3 a^3 - 3\omega^2 a^2 - 6j\omega a + 6)e^{j\omega a}}{\omega^4} \right. \\ &\quad \left. - \frac{(j\omega^3 b^3 - 3\omega^2 b^2 - 6j\omega b - 2)e^{j\omega b}}{\omega^4} \right\} && \text{(B.17)} \\ \frac{d^4\Psi_X(\omega)}{d\omega^4} &= \frac{1}{j(b-a)} \left\{ \frac{(\omega^4 b^4 + 4j\omega^3 b^3 - 12\omega^2 b^2 - 24j\omega b + 24)e^{j\omega b}}{\omega^5} \right. \\ &\quad \left. - \frac{(\omega^4 a^4 + 4j\omega^3 a^3 - 12\omega^2 a^2 - 24j\omega a + 24)e^{j\omega a}}{\omega^5} \right\}. && \text{(B.18)} \end{aligned}$$

Although we now have the four expressions we need, when we set $\omega = 0$ as specified in (B.14), all four terms reduce to the indeterminate form of $0/0$. Thus we must apply

L'Hôpital's rule to find the derivatives when evaluated at this point. L'Hôpital's rule states that [107]

$$\lim_{x\to c}\frac{f(x)}{g(x)}=\lim_{x\to c}\frac{f'(x)}{g'(x)}, \tag{B.19}$$

provided that both $f(x)$ and $g(x)$ are differentiable over an open interval (x_1, x_2) that contains point c (although they need not be differentiable at c itself). By applying this rule once to each of the four derivatives, we find that these expressions, when evaluated at $\omega = 0$ and multiplied by $1/j^k$ as specified in (B.14), are given by

$$E[X] = \frac{a+b}{2} \tag{B.20}$$

$$E\left[X^2\right] = \frac{(b-a)^2}{12} \tag{B.21}$$

$$E\left[X^3\right] = \frac{b^4-a^4}{4(b-a)} \tag{B.22}$$

$$E\left[X^4\right] = \frac{b^5-a^5}{5(b-a)}. \tag{B.23}$$

Finally, we can apply these expressions to our specific case where ϵ_s is uniformly distributed over $[\Delta/2, \Delta/2]$. These moments then reduce to

$$E[X] = 0 \tag{B.24}$$

$$E\left[X^2\right] = \frac{\Delta^2}{12} \tag{B.25}$$

$$E\left[X^3\right] = 0 \tag{B.26}$$

$$E\left[X^4\right] = \frac{\Delta^4}{80}. \tag{B.27}$$

We now have the terms we need to proceed to evaluate the expressions in (B.3) - (B.6).

B.0.3 Evaluating the Variance

By direct substitution of these moments into B.2, it can be shown that if we take the expectation conditioned on P_k, we can solve this to be

$$E\left[\left(\nu_k^{(s+1)}\right)^2\right] = E_{P_k}\left[\frac{3N_o^2}{4T^2}+4\frac{E[\epsilon_r^4]}{T^4}+\frac{E[\epsilon_s^4]}{4}+6\frac{N_oE[\epsilon_r^2]}{T^3}+\frac{3N_oE[\epsilon_s^2]}{2T}+6\frac{E[\epsilon_r^2]E[\epsilon_s^2]}{T^2}\right.$$

$$+\left(6\frac{N_o}{T^3}+24\frac{E[\epsilon_r^2]}{T^4}+6\frac{E[\epsilon_s^2]}{T^2}\right)E\left[\left(\sum_{l=1,l\neq k}^{K}I_{l,k}^{(s)}\right)^2\mid P_k\right]$$
$$+\frac{4}{T^4}E\left[\left(\sum_{l=1,l\neq k}^{K}I_{l,k}^{(s)}\right)^4\mid P_k\right]\Bigg]. \quad \text{(B.28)}$$

The first six terms are constant, and therefore we only need to derive expressions for the final two terms. From [21], these terms can be derived to be

$$\begin{aligned}E_{P_k}\left[E\left[\left(\sum_{l=1,l\neq k}^{K}I_{l,k}^{(s)}\right)^2\mid P_k\right]\right] &= E\left[var\left\{\sum_{l=1,l\neq k}^{K}I_{l,k}^{(s)}\right\}\right]\\ &= E[\Psi^{(s)}]\\ &= \mu_{\Psi^{(s)}} \quad \text{(B.29)}\end{aligned}$$

and

$$\begin{aligned}E_{P_k}\left[E\left[\left(\sum_{l=1,l\neq k}^{K}I_{l,k}^{(s)}\right)^4\mid P_k\right]\right] &= E\left[\sum_{l=1,l\neq k}^{K}\left(I_{l,k}^{(s)}\right)^4\right.\\ &\quad \left.+3\sum_{l=1,l\neq k}^{K}\sum_{m=1,m\neq l\neq k}^{K}\left(I_{l,k}^{(s)}\right)^2\left(I_{m,k}^{(s)}\right)^2\right]. \quad \text{(B.30)}\end{aligned}$$

The first term of (B.30) can be evaluated by

$$\begin{aligned}E\left[\sum_{l=1,l\neq k}^{K}\left(I_{l,k}^{(s)}\right)^4\right] &= E\left[\sum_{l=1,l\neq k}^{K}\left(T_c\sqrt{\frac{\nu_l^{(s)}}{2}}cos(\phi_l-\phi_k)W_l\right)^4\right]\\ &= \frac{3T_c^4}{32}\left\{\sum_{l=1,l\neq k}^{K}E\left[\left(\nu_l^{(s)}\right)^2\right]E[W_l^4]\right\}. \quad \text{(B.31)}\end{aligned}$$

We can solve for $E[(\nu_l^{(s)})^2]$ from (B.1) as

$$E\left[\left(\nu_l^{(s)}\right)^2\right]=(\sigma_{P_l}^{(s)})^2+\left(\mu_{P_l}^{(s)}\right)^2 \quad \text{(B.32)}$$

and by definition

$$E\left[(P_l)^2\right]=(\sigma_{P_l}^{(1)})^2+\left(\mu_{P_l}^{(1)}\right)^2. \quad \text{(B.33)}$$

Therefore, (B.31) reduces to

$$E\left[\sum_{l=1,l\neq k}^{K}\left(I_{l,k}^{(s)}\right)^4\right]=\frac{3T_c^4}{32}\sum_{l=1,l\neq k}^{K}\left[(\sigma_{P_l}^{(s)})^2+\left(\mu_{P_l}^{(s)}\right)^2\right]E[W_l^4] \tag{B.34}$$

It is shown in [21] that

$$E[W_l^4]=\frac{12N^2-9N}{5}. \tag{B.35}$$

Therefore, we can finally reduce (B.34) to

$$E\left[\sum_{l=1,l\neq k}^{K}\left(I_{l,k}^{(s)}\right)^4\right]=\frac{3T_c^4}{32}\frac{12N^2-9N}{5}\sum_{l=1,l\neq k}^{K}\left[(\sigma_{P_l}^{(s)})^2+\left(\mu_{P_l}^{(s)}\right)^2\right] \tag{B.36}$$

The second term of (B.30) can be evaluated using (5.26) and can be shown to reduce to

$$E\left[3\sum_{l=1,l\neq k}^{K}\sum_{m=1,m\neq l\neq k}^{K}\left(I_{l,k}^{(s)}\right)^2\left(I_{m,k}^{(s)}\right)^2\right]=\frac{T_c^4(4N^2-9N+13)}{48}\sum_{l=1,l\neq k}^{K}\sum_{m=1,m\neq l\neq k}^{K}\mu_{P_l}^{(s)}\mu_{P_m}^{(s)}. \tag{B.37}$$

Therefore, we have now derived all the terms necessary to explicitly solve (B.28). Using (B.29), (B.36), and (B.37), we find

$$\begin{aligned}E\left[\left(\nu_k^{(s+1)}\right)^2\right] &= \frac{3N_o^2}{4T^2}+4\frac{E[\epsilon_r^4]}{T^4}+\frac{E[\epsilon_s^4]}{4}+6\frac{N_oE[\epsilon_r^2]}{T^3}+\frac{3N_oE[\epsilon_s^2]}{2T}+6\frac{E[\epsilon_r^2]E[\epsilon_s^2]}{T^2}\\ &\quad+\left(6\frac{N_o}{T^3}+24\frac{E[\epsilon_r^2]}{T^4}+6\frac{E[\epsilon_s^2]}{T^2}\right)\mu_{\Psi^{(s)}}\\ &\quad+9\frac{4N-3}{40N^3}\sum_{l=1,l\neq k}^{K}\left[(\sigma_{P_l}^{(s)})^2+\left(\mu_{P_l}^{(s)}\right)^2\right]\\ &\quad+\frac{4N^2-9N+13}{12N^4}\sum_{l=1,l\neq k}^{K}\sum_{m=1,m\neq l\neq k}^{K}\mu_{P_l}^{(s)}\mu_{P_m}^{(s)}.\end{aligned} \tag{B.38}$$

Next, we note that by modifying (5.14) for stages 2 and beyond as

$$\mu_{\Psi}^{(s)}=\frac{T_c^2N}{6}\sum_{l=1,l\neq k}^{K}\mu_{P_l}^{(s)} \tag{B.39}$$

and combining it with (5.32), we get that for $1\leq k\leq K$,

$$\mu_{P_k}^{(s+1)}=\frac{N_o}{2T}+\frac{2E[\epsilon_r^2]}{T^2}+\frac{E[\epsilon_s^2]}{2}+\frac{2\mu_{\Psi}^{(s)}}{T^2}. \tag{B.40}$$

Finally, by substituting (B.38) and (B.40) into (B.1), the expression for the variance of the effective interference power at stage $s+1$ caused by user k, $1 \leq k \leq K$, is given by

$$\begin{aligned}(\sigma_{P_k}^{(s+1)})^2 &= \frac{N_o^2}{2T^2} + 4\frac{E[\epsilon_r^4]}{T^4} + \frac{E[\epsilon_s^4]}{4} + \frac{N_o E[\epsilon_s^2]}{T} + 4\frac{E[\epsilon_r^2]E[\epsilon_s^2]}{T^2} + 4\frac{N_o E[\epsilon_r^2]}{T^3} \\ &\quad + \left(\frac{4N_o}{T^3} + 16\frac{E[\epsilon_r^2]}{T^4} + 4\frac{E[\epsilon_s^2]}{T^4}\right)\mu_\psi^{(s)} - 4\frac{E^2[\epsilon_r^2]}{T^4} - \frac{E^2[\epsilon_s^2]}{4} \\ &\quad - \frac{4}{T^4}\left(\mu_\Psi^{(s)}\right)^2 + \frac{9(4N-3)}{40N^3}\sum_{l=1,l\neq k}^{K}\left[(\sigma_{P_l}^{(s)})^2 + \left(\mu_{P_l}^{(s)}\right)^2\right] \\ &\quad + \frac{4N^2-9N+13}{12N^4}\sum_{l=1,l\neq k}^{K}\sum_{m=1,m\neq l\neq k}^{K}\mu_{P_l}^{(s)}\mu_{P_m}^{(s)}. \end{aligned} \tag{B.41}$$

Appendix C

Publications

The following papers have been submitted or published in support of this research.

- R. A. Cameron, "Performance analysis of CDMA in multipath channels," Master's thesis, Virginia Polytechnic Institute and State University, May 1993.
- R. A. Cameron and B.D. Woerner, "An analysis of CDMA with imperfect power control," in *Proc. of the 1992 Veh. Tech. Conf.*, (Denver, CO), pp. 977-980, May 1992.
- R. A. Cameron and B.D. Woerner, "Measurement-based performance analysis of CDMA systems in multipath fading," in *Proc. of the 1993 Veh. Tech. Conf.*, (Piscataway, NJ), pp. 81-84, May 1993.
- B. D. Woerner and R. A. Cameron, "A comparison of performance analysis techniques for Code Division Multiple Access," *Proc. of the International Symposium on Wireless Communications*, July 1993.
- R. A. Cameron and B. D. Woerner, "Performance analysis of CDMA with imperfect power control," *IEEE Trans. Comm.*. vol. 44., no. 7, pp. 777-781, July 1996.
- R. A. Cameron and B. D. Woerner, "Performance analysis of CDMA in multipath channels", submitted to the *IEEE Trans. Veh. Tech.*.
- R. A. Cameron and B. D. Woerner, "Synchronization of CDMA systems employing interference cancellation," *Proc. of 1996 Veh. Tech. Conf.*, (Atlanta, GA), June 1996.

Appendix D

SPW Models

The SPW design and system files are stored under the library name *camlib*. All signal files are stored under the library name *camsigs*.

D.1 Multiuser Receiver

The basic multiuser receiver system in an AWGN channel is stored in *gauss71, gauss72, gauss73* for 7 users and 1, 2, and 3 stage receivers, respectively. In *gauss103*, all 3 stages are modeled concurrently and 10 users are modeled. These files assume a spreading code length of 31 and a data rate of 9600 bps. The system file *glomo* is based on the original air interface and has a spreading code length of 15 and a data rate of 128 kbps. These can be changed by simply changing the appropriate parameter. There are 10 users and up to 3 stages in the receiver.

The basic transmitter block is *ss_tx_iq*. This produces the random transmitter phase, the PN code (a random sequence of chips), the information bits, and the complex (I and Q) spread signal. The block *cplx_dlay_unif* adds the complex uniform time delay to the transmitted signal.

The block *corr_rcvr* is the correlation receiver used in the first stage of the receiver. The block *estimator* is used in stages 2 and above to estimate the received signal from each user. The block *corr_rx_2a* is the correlation receiver used in stages 2 and above (it requires additional delays not needed in the first stage).

D.2 Synchronization

The system files used to determine the BER of synchronized users in the presence of an unsynched interferer are *synch1a1* and *synch1a2* for a 1 and 2 stage receiver, respectively. There are 6 synched users and 1 unsynched interferer.

For analyzing acquisition time, the files *synch2a* and *synch2a2* are used for a 1 and 2 stage receiver, respectively. The files *synchbox* and *synchbox2* are used to model the single dwell time acquisition technique for the 1 and 2 stage receiver, respectively. They replace the correlation receiver in the desired user's stage.

D.3 Quantization

The effects of uniform quantization are modeled in *glomo_q*. The system parameters are based upon the original air interface for the hardware prototype. The systems *int_q_calc* and *int_q_calc2* are used to compute the parameters of the correlated quantization noise sources of the estimates in the analytic model. The parameters for the correlated quantization noise source from the received signal is computed in *glomo_g* itself.

The quantized estimates are calculated in *estimator_q*.

D.4 Frequency Offsets

The effects of frequency offset and the maximum likelihood phase estimator are modeled in *glomo_foff2*. The transmitters are modeled in *ss_tx_foff*. This block takes as an input the desired frequency offset for that user. It can be constant or it can vary with time. The estimate of the phase is calculated via *phase_est*.

The correlation receiver used in the first stage is *corr_rx_foff*. The estimator used in stage 2 is *estimator_foff*. No attempt is made to compensate for the frequency offsets in the receivers in stages 2 and 3 due to the poor performance of the phase estimator.

Bibliography

[1] K. S. Gilhousen, I. M. Jacobs, R. Padovani, A. J. Viterbi, L. A. Weaver, and C. E. Wheatley, "On the capacity of a cellular CDMA system", *IEEE Trans. Veh. Technol.*, vol. 40, no. 2, pp. 303–312, May 1991.

[2] Rick A. Cameron and Brian D. Woerner, "An analysis of CDMA with imperfect power control", in *Proc. 1992 Veh. Technol. Conf.*, Denver, CO, May 1992, pp. 977–980.

[3] Rick A. Cameron and Brian D. Woerner, "Performance analysis of CDMA with imperfect power control", *IEEE Trans. Commun.*, vol. 44, no. 7, pp. 777–781, July 1996.

[4] Jeffrey H. Reed and Tien. C. Hsia, "The performance of time-dependent optimal filtering for interference rejection", *IEEE Trans. Acoustics, Speech, and Signal Processing*, vol. 38, no. 8, pp. 1373–1385, Aug. 1990.

[5] Sergio Verdú, "Minimum probability of error for asynchronous Gaussian multiple-access channels", *IEEE Trans. Info. Theory*, vol. IT-32, no. 1, pp. 85–96, Jan. 1986.

[6] Sergio Verdú, "Computational complexity of optimum multiuser detection", *Algorithmica*, vol. 4, no. 3, pp. 303–312, 1989.

[7] Kenneth S. Schneider, "Optimum detection of code division multiplexed signals", *IEEE Trans. Aerospace and Electronic Systems*, vol. AES-15, no. 1, pp. 181–185, Jan. 1979.

[8] Ruxandra Lupas and Sergio Verdú, "Linear multiuser detectors for synchronous code-division multiple-access channels", *IEEE Trans. Info. Theory*, vol. 35, no. 1, pp. 123–136, Jan. 1989.

[9] Ruxandra Lupas and Sergio Verdú, "Near-far resistance of multiuser detectors in asynchronous channels", *IEEE Trans. Commun.*, vol. 38, no. 4, pp. 496–508, Apr. 1990.

[10] Pulin Patel and Jack Holtzman, "Analysis of a simple successive interference cancellation scheme in a DS/CDMA system", *IEEE J. Select. Areas Commun.*, vol. 12, no. 5, pp. 796–807, June 1994.

[11] Mahesh K. Varanasi and Behnaam Aazhang, "Multistage detection in asynchronous code-division multiple-access communications", *IEEE Trans. Commun.*, vol. COM-38, no. 4, pp. 509–519, Apr. 1990.

[12] Stavros Striglis, Ashish Kaul, Ning Yang, and Brian D. Woerner, "A multistage RAKE receiver for improved capacity of CDMA systems", in *Proc. 1994 IEEE Veh. Technol. Conf.*, Stockholm, Sweden, June 1994, pp. 789–793.

[13] Ashish Kaul and Brian D. Woerner, "An analysis of adaptive multistage interference cancellation for CDMA", in *Proc. 1995 IEEE Veh. Technol. Conf.*, Rosemont, IL, July 1995.

[14] Mahesh K. Varanasi and Behnaam Aazhang, "Near-optimum detection in synchronous code-division multiple-access systems", *IEEE Trans. Commun.*, vol. 39, no. 5, pp. 725–736, May 1991.

[15] Paul Dent, Bjorn Gudmundson, and Magnus Ewerbring, "CDMA-IC: A novel code division multiple access scheme based on interference cancellation", in *Proc. 1992 Int. Symposium on Personal, Indoor, and Mobile Radio Commun.*, Boston, MA, 1992, pp. 98–102.

[16] Alexandra Duel-Hallen, "Decorrelating decision-feedback multiuser detector for synchronous code-division multiple-access channel", *IEEE Trans. Commun.*, vol. 41, no. 2, pp. 285–290, Feb. 1993.

[17] Dao Sheng Chen and Sumit Roy, "An adaptive multiuser receiver for CDMA systems", *IEEE J. Select. Areas Commun.*, vol. 12, no. 5, pp. 808–816, June 1994.

[18] R. Michael Buehrer, *The Application of Multiuser Detection to Cellular CDMA*, PhD thesis, Virginia Polytechnic Institute and State University, June 1996.

[19] Ashish Kaul, "An adaptive multistage interference cancellation receiver for CDMA", Master's thesis, Virginia Polytechnic Institute and State University, Mar. 1995.

[20] Stavros Striglis, "A multistage RAKE receiver for CDMA systems", Master's thesis, Virginia Polytechnic Institute and State University, Aug. 1994.

[21] R. Michael Buehrer, "Analysis of adaptive multistage interference cancellation for CDMA using an improved Gaussian approximation", in *Proc. of 1995 Mil. Conf. Commun. (MILCOM)*, San Diego, CA, Nov. 1995, pp. 1195–1199.

[22] Jay E. Padgett, Christoph G. Günther, and Takeshi Hattori, "Overview of wireless personal communications", *IEEE Commun. Mag.*, vol. 33, no. 1, pp. 28–41, Jan. 1995.

[23] Ryuji Kohno, Reuven Meidan, and Laurence B. Milstein, "Spread spectrum access methods for wireless communications", *IEEE Commun. Mag.*, vol. 33, no. 1, pp. 58–67, Jan. 1995.

[24] Andrew. J. Viterbi, "Spread spectrum communications - myths and realities", *IEEE Commun. Mag.*, pp. 11–18, May 1979.

[25] George L. Turin, "Introduction to spread-spectrum antimultipath techniques and their application to urban digital radio", *Proc. IEEE*, vol. 68, no. 3, pp. 328–353, Mar. 1980.

[26] C. L. Weber, G. K. Huth, and B. H. Batson, "Performance considerations of code division multiple-access systems", *IEEE Trans. Veh. Technol.*, vol. VT-30, no. 1, pp. 3–10, Feb. 1981.

[27] E. A. Geraniotis and Michael B. Pursley, "Performance of coherent direct-sequence spread-spectrum communications over specular multipath fading channels", *IEEE Trans. Commun.*, vol. COM-33, pp. 502–508, June 1985.

[28] James S. Lehnert and Michael B. Pursley, "Error probabilities for binary direct-sequence spread-spectrum communications with random signature sequences", *IEEE Trans. Commun.*, vol. COM-35, pp. 87–97, Jan. 1987.

[29] James S. Lehnert and Michael B. Pursley, "Multipath diversity reception of spread-spectrum multiple-access communications", *IEEE Trans. Commun.*, vol. COM-35, pp. 1189–1198, Nov. 1987.

[30] James S. Lehnert, "An efficient technique for evaluating direct-sequence spread-spectrum multiple-access communications", *IEEE Trans. Commun.*, vol. 37, no. 8, pp. 851–858, Aug. 1989.

[31] Donald L. Schilling, Raymond L. Pickholtz, and Laurence B. Milstein, "Spread spectrum goes commercial", *IEEE Spectrum*, pp. 40–45, Aug. 1990.

[32] Andrew. J. Viterbi and R. Padovani, "Implications of mobile cellular CDMA", *IEEE Commun. Mag.*, vol. 30, no. 12, pp. 38–41, Dec. 1992.

[33] "IS-95 interim standard".

[34] Dilip V. Sarwate and Michael B. Pursley, "Crosscorrelation properties of pseudorandom and related sequences", *Proc. IEEE*, vol. 68, no. 5, pp. 593–619, May 1980.

[35] A. J. Viterbi, A. M. Viterbi, and E. Zehavi, "Performance of power-controlled wideband terrestrial digital communication", *IEEE Trans. Commun.*, vol. 41, no. 4, pp. 559–569, Apr. 1993.

[36] Rick A. Cameron, "Performance analysis of CDMA systems in multipath channels", Master's thesis, Virginia Polytechnic Institute and State University, May 1993.

[37] R. Price and P.E. Green, "A communication technique for multipath channels", *Proc. IRE*, pp. 555–570, Mar. 1958.

[38] Rick A. Cameron and Brian D. Woerner, "Measurement-based performance analysis of CDMA systems in multipath fading", in *Proc. 1993 Veh. Technol. Conf.*, Piscataway, NJ, May 1993, pp. 81–84.

[39] Alexandra Duel-Hallen, Jack Holtzman, and Zoran Zvonar, "Multiuser detection for cdma systems", *IEEE Personal Commun. Mag.*, pp. 46–57, Apr. 1995.

[40] D. Horwood and R. Gagliardi, "Signal design for digital multiple access communications", *IEEE Trans. Commun.*, vol. COM-23, no. 3, pp. 378–383, Mar. 1975.

[41] W. Van Etten, "Maximum likelihood receiver for multiple channel transmission systems", *IEEE Trans. Commun.*, vol. COM-24, no. 2, pp. 276–283, Feb. 1976.

[42] Zhenhua Xie, Robert T. Short, and Craig K. Rushforth, "A family of suboptimum detectors for coherent multiuser communications", *IEEE J. Select. Areas Commun.*, vol. 8, no. 4, pp. 683–690, May 1990.

[43] Ryuji Kohno and Mitsutoshi Hatori, "Cancellation techniques of co-channel interference in asynchronous spread spectrum multiple access systems", Electronics and Commun. in Japan, vol. 66-A, no. 5, pp. 20–29, May 1983.

[44] William L. Brogan, *Modern Control Theory*, Prentice Hall, Englewood Cliffs, NJ, 1991.

[45] Fu-Chun Zheng and Stephen K. Barton, "On the performance of near-far resistant cdma detectors in the presence of synchronization errors", *comm*, vol. 43, no. 12, pp. 3037–3045, Dec. 1995.

[46] R. Michael Buehrer, Ashish Kaul, Stavros Striglis, and Brian D. Woerner, "Analysis of DS-CDMA parallel interference cancellation with phase and timing errors", *IEEE J. Select. Areas Commun.*, vol. 14, no. 8, pp. 1522–1535, Oct. 1996.

[47] Alexandra Duel-Hallen, "Equalizers for multiple input/multiple output channels and PAM systems with cyclostationary input sequences", *IEEE J. Select. Areas Commun.*, vol. 10, no. 3, pp. 630–639, Apr. 1992.

[48] Anja Klein and Paul W. Baier, "Linear unbiased data estimation in mobile radio systems applying CDMA", *IEEE J. Select. Areas Commun.*, vol. 11, no. 7, pp. 1058–1066, Sep. 1993.

[49] Andrew. J. Viterbi, "Very low rate convolutional codes for maximum theoretical performance of spread-spectrum multiple-access channels", *IEEE J. Select. Areas Commun.*, vol. 8, no. 4, pp. 641–649, May 1990.

[50] Magnus Ewerbring, Bjorn Gudmundson, Paul Teder, and Per Willars, "CDMA-IC: A proposal for future high capacity digital cellular systems", in *Proc. 1993 IEEE Veh. Technol. Conf.*, Seacaucus, NJ, May 1993, pp. 440–443.

[51] Paul Teder and Per Willars, "Capacity simulations of a CDMA system with interference cancellation", in *Proc. 1992 Nordic Seminar on Digital Mobile Radio Commun.*, Helsinki, FI, 1992, pp. 229–235.

[52] Magnus Ewerbring, Bjorn Gudmundson, Gustav Larsson, and Paul Teder, "CDMA with interference cancellation: A technique for high capacity wireless systems", in *Proc. 1993 Int. Conf. Commun.*, 1993, pp. 1901–1906.

[53] Hermann Kremer, "On theory of fast walsh transform algorithms", in *Proc. 1973 Theory and Applications of Walsh and Other Non-Sinusoidal Functions Conf.*, Hatfield, UK, June 1973, pp. 1–25.

[54] Don Breslin, Mike Buehrer, and Rick Cameron, "Interference cancellation via Walsh transforms", Class Project for EE 5624, Virginia Tech, May 1995.

[55] Ryuji Kohno, Hideki Imai, Mitsutoshi Hatori, and Subbarayan Pasupathy, "An adaptive canceller of cochannel interference for spread-spectrum multiple-acess communication networks in a power line", *IEEE J. Select. Areas Commun.*, vol. 8, no. 4, pp. 691–699, May 1990.

[56] Ashish Kaul and Brian D. Woerner, "Analytic limits on performance of adaptive multistage interference cancellation for CDMA", *Electron. Lett.*, vol. 30, no. 25, pp. 2093–2095, 8 Dec. 1994.

[57] R. Michael Buehrer and Brian D. Woerner, "Analysis of adaptive multistage interference cancellation for CDMA using an improved Gaussian approximation", *IEEE Trans. Commun.*, vol. 44, no. 10, pp. 1308–1321, Oct. 1996.

[58] Rodger E. Ziemer and Roger L. Peterson, *Introduction to Digital Communication*, Macmillan Publishing Company, New York, 1992.

[59] Robert K. Morrow and James S. Lehnert, "Bit-to-bit error dependence in slotted DS/SSMA packet systems with random signature sequences", *IEEE Trans. Commun.*, vol. COM-37, pp. 1052–1061, Oct. 1989.

[60] Jack M. Holtzman, "A simple, accurate method to calculate spread spectrum multiple access error probabilities", *IEEE Trans. Commun.*, vol. 40, no. 3, pp. 461–464, Mar. 1992.

[61] Joseph C. Liberti Jr., *CDMA Cellular Communication Systems Employing Adaptive Antennas*, PhD thesis, Virginia Polytechnic Institute and State University, 1995.

[62] Parag Agashe and Brian D. Woerner, "Analysis of interference cancellation for a multicellular CDMA environment", in *Proc. 1995 Personal, Indoor, and Mobile Radio Conf.*, Toronto, Canada, Sep. 1995.

[63] Parag Agashe, "Selective cancellation of multipath and multicell interference in CDMA", Master's thesis, Virginia Polytechnic Institute and State University, Dec. 1995.

[64] Ryuji Kohno, Hideki Imai, Mitsutoshi Hatori, and Subbarayan Pasupathy, "Combination of an adaptive array antenna and a canceller of interference for direct-sequence spread-spectrum multiple-access system", *IEEE J. Select. Areas Commun.*, vol. 8, no. 4, pp. 675–682, May 1990.

[65] R. Michael Buehrer, Neiyer S. Correal, and Brian D. Woerner, "A comparison of multiuser receivers for cellular CDMA", in *Proc. of the 1996 Global Commun. Conf. (GLOBECOM)*, London, Nov. 1996.

[66] Andreas Polydoros and Charles W. Weber, "A unified approach to serial search spread-spectrum code acquisition - part I: General theory", *IEEE Trans. Commun.*, vol. COM-32, no. 5, pp. 542–549, May 1984.

[67] Gerald F. Sage, "Serial synchronization of pseudonoise systems", *IEEE Trans. Commun. Technol.*, vol. COM-12, pp. 123–127, Dec. 1964.

[68] Marvin K. Simon, Jim K. Omura, Robert A. Scholtz, and Barry K. Levitt, *Spread Spectrum Communications Handbook*, chapter Pseudonoise Code Acquisition in Direct-Sequence Receivers, pp. 751–833, McGraw-Hill, Inc., New York, 1994.

[69] Jack K. Holmes and Chang C. Chen, "Acquisition time performance of PN spread-spectrum systems", *IEEE Trans. Commun.*, vol. COM-25, no. 8, pp. 778–784, Aug. 1977.

[70] Stephen S. Rappaport and Donald M. Grieco, "Spread-spectrum signal acquisition: Methods and technology", *IEEE Commun. Mag.*, vol. 22, no. 6, pp. 6–21, June 1984.

[71] Robert C. Dixon, *Spread Spectrum Systems*, chapter Synchronization, pp. 214–260, John Wiley & Sons, New York, 1984.

[72] Andreas Polydoros and Charles W. Weber, "A unified approach to serial search spread-spectrum code acquisition - part II: A matched-filter receiver", *IEEE Trans. Commun.*, vol. COM-32, no. 5, pp. 550–560, May 1984.

[73] David M. DiCarlo and Charles L. Weber, "Statistical performance of single dwell serial synchronization systems", *IEEE Trans. Commun.*, vol. COM-28, no. 8, pp. 1382–1388, Aug. 1980.

[74] David M. DiCarlo and Charles L. Weber, "Multiple dwell serial search: Performance and application to direct sequence code acquisition", *IEEE Trans. Commun.*, vol. COM-31, no. 5, pp. 650–659, May 1983.

[75] A. Wald, *Sequential Analysis*, Wiley, New York, 1947.

[76] Walter R. Braun, "Performance analysis for the expanding search PN acquisition algorithm", *IEEE Trans. Commun.*, vol. COM-30, no. 3, pp. 424–435, Mar. 1982.

[77] R. B. Ward, "Acquisition of pseudonoise signals by sequential estimation", *IEEE Trans. Commun. Technol.*, vol. COM-13, no. 4, pp. 474–483, Dec. 1965.

[78] Zhen-Liang Shi, Peter F. Driessen, and Weixiu Du, "PN code acquisition for asynchronous CDMA communications based on interference cancellation", in *Proc. 1993 IEEE Pacific Rim Conf.*, 1993, pp. 778–781.

[79] Zhen-Liang Shi and Peter F. Driessen, "Automatic threshold control for acquisition in spread spectrum packet radio communication", in *Proc. 1993 IEEE Int. Conf. Commun.*, Geneva, Switzerland, May 1993.

[80] Stephen S. Rappaport and Donald L. Schilling, "A two-level coarse code acquisition scheme for spread spectrum radio", *IEEE Trans. Commun.*, vol. COM-28, no. 9, pp. 1734–1742, Sep. 1980.

[81] Yu T. Su, "Rapid code acquisition algorithms employing PN matched filters", *IEEE Trans. Commun.*, vol. 36, no. 6, pp. 724–733, June 1988.

[82] Essam A. Sourour and Someshwar C. Gupta, "Direct-sequence spread-spectrum parallel acquisition in a fading mobile channel", *IEEE Trans. Commun.*, vol. 38, no. 7, pp. 992–998, July 1990.

[83] Essam A. Sourour and Someshwar C. Gupta, "Direct-sequence spread-spectrum parallel acquisition in nonselective and frequency-selective fading channels", *IEEE Trans. Commun.*, vol. 10, no. 3, pp. 535–544, Apr. 1992.

[84] Alan V. Oppenheim and Ronald W. Schafer, *Discrete-Time Signal Processing*, chapter Structures for Discrete-Time Systems, pp. 290–402, Prentice Hall, Englewood Cliffs, NJ, 1989.

[85] A. G. Clavier, P. F. Panter, and D. D. Grieg, "PCM distortion analysis", *Electrical Engineering*, vol. 66, pp. 1110–1122, Nov. 1947.

[86] A. G. Clavier, P. F. Panter, and D. D. Grieg, "Distortion in a pulse code modulation system", *Trans. American Institute of Electrical Engineers*, vol. 66, pp. 989–1005, 1947.

[87] W. R. Bennett, "Spectra of quantized signals", *Bell System Technical Journal*, vol. 27, pp. 446–472, July 1948.

[88] Robert M. Gray, "Quantization noise spectra", *IEEE Trans. Info. Theory*, vol. 36, no. 6, pp. 1220–1244, Nov. 1990.

[89] Donald E. Knuth, *The Art of Computer Programming*, Addison-Wesley Publishing Company, Reading, Mass., 1969.

[90] Joseph F. Cavanagh, *Digital Computer Arithmetic: Design and Implementation*, McGraw-Hill Book Company, New York, 1984.

[91] Bernard Widrow, "A study of rough amplitude quantization by means of nyquist sampling theory", *IRE Trans. Circuit Theory*, vol. CT-3, pp. 266–276, Dec. 1956.

[92] Anekal B. Sripad and Donald L. Snyder, "A necessary and sufficient condition for quantization errors to be uniform and white", *IEEE Trans. Acoustics, Speech, and Signal Processing*, vol. ASSP-25, no. 5, pp. 442–448, Oct. 1977.

[93] Leland B. Jackson, "On the interaction of roundoff noise and dynamic range in digital filters", *Bell System Technical Journal*, vol. 49, no. 2, pp. 159–184, Feb. 1970.

[94] Casper W. Barnes, Bon N. Tran, and Shu H. Leung, "On the statistics of fixed-point roundoff error", *IEEE Trans. Acoustics, Speech, and Signal Processing*, vol. ASSP-33, no. 3, pp. 595–606, June 1985.

[95] H. Stark and J.W. Woods, *Probability, Random Processes, and Estimation Theory for Engineers*, Prentice Hall, Englewood Cliffs, NJ, 1986.

[96] Isao Tokaji and Casper W. Barnes, "Roundoff error statistics for a continuous range of multiplier coefficients", *IEEE Trans. Circuits and Systems*, vol. CAS-34, no. 1, pp. 52–59, Jan. 1987.

[97] Ping Wah Wong, "Quantization noise, fixed-point multiplicative roundoff noise, and dithering", *IEEE Trans. Acoustics, Speech, and Signal Processing*, vol. 38, no. 2, pp. 286–300, Feb. 1990.

[98] David Slepian, "On delta modulation", *Bell System Technical Journal*, vol. 51, no. 10, pp. 2101–2137, Dec. 1972.

[99] Joel Max, "Quantizing for minimum distortion", *IRE Transactions on Information Theory*, vol. IT-6, pp. 7–12, Mar. 1960.

[100] S. P. Lloyd, "Least squares optimization in PCM", *IEEE Trans. Info. Theory*, vol. IT-28, pp. 129–137, Mar. 1982.

[101] John G. Proakis, *Digital Communications*, McGraw-Hill Book Company, New York, 1989.

[102] N. S. Jayant and P. Noll, *Digital Coding of Waveforms*, Prentice Hall, Englewood Cliffs, NJ, 1984.

[103] K. S. Shanmugan and A. M. Breipohl, *Random Signals: Detection, Estimation, and Data Analysis*, John Wiley & Sons, New York, 1988.

[104] Ning Yang, "Multiuser detection for CDMA systems with convolutional coding", Master's thesis, Virginia Polytechnic Institute and State University, Oct. 1995.

[105] Andrew. J. Viterbi and Audrey M. Viterbi, "Nonlinear estimation of PSK-modulated carrier phase with application to burst digital transmission", *IEEE Trans. Info. Theory*, vol. IT-29, no. 4, pp. 543–551, July 1983.

[106] Dariush Divsalar and Marvin K. Simon, "Pseudocoherent demodulation of DPSK radio signals", NASA Tech Brief Vol. 19, No. 5, Item #44, June 1995.

[107] Earl W. Swokowski, *Calculus with Analytic Geometry*, Prindle, Weber, and Schmidt, Boston, MA, 1983.

Vita

Rick A. Cameron

Rick Cameron was born in La Grange, IL on August 26, 1968. He received his Bachelor of Science (BS) degree from Virginia Polytechnic Institute and State University in May 1990. He joined the Mobile and Portable Radio Research Group (MPRG) in 1991. He received his Master of Science (MS) degree from Virginia Polytechnic Institute and State University in May 1993.

During the summer of 1991, he worked for the Department of Defense in Fort Meade, MD, in the telecommunications area. During the summers of 1992 and 1993, he worked for Grayson Electronics in Lynchburg, VA, simulating communications systems. During the summer of 1994, he worked for Motorola Paging Products in Boynton Beach, FL, simulating spread spectrum paging systems. He is currently employed with Tektronix Inc. in Beaverton, OR.

Mr. Cameron is a member of the IEEE and Eta Kappa Nu.